AD-A080 846 WEIZMANN INST OF SCIENCE REHOVOTH (ISRAEL) DEPT OF --ETC F/G 16/4
APPLICATION OF SYNTHESIS TECHNIQUE FOR NONLINEAR UNCERTAIN SYST--ETC(U)
JUN 79 B GOLUBEV, I HOROWITZ, Y KATZ DA-ERO-77-G-096

UNCLASSIFIED NL

1 OF 2
AD A080846

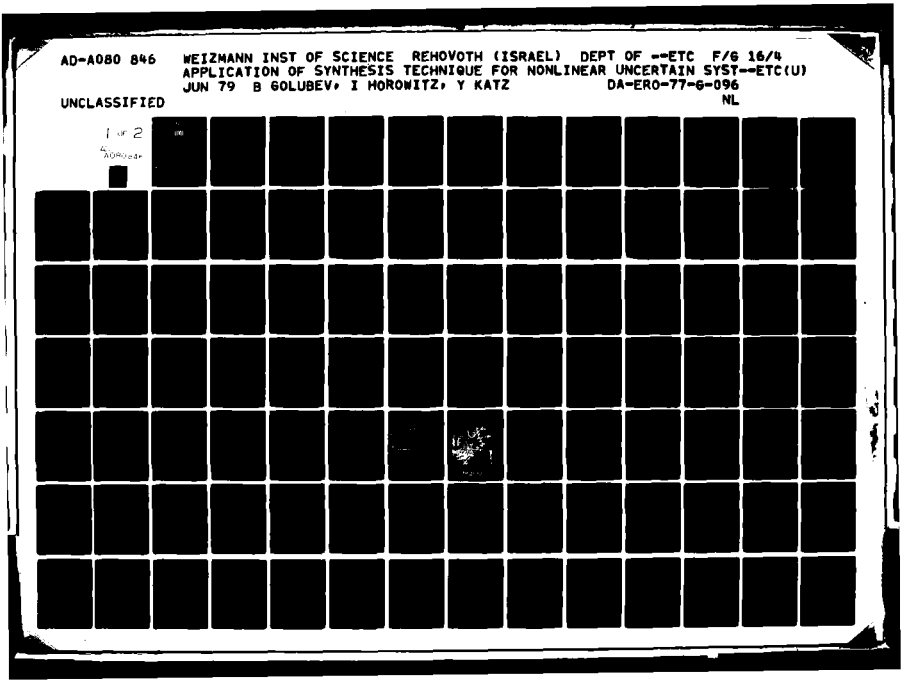

מכון ויצמן למדע
THE WEIZMANN INSTITUTE OF SCIENCE
REHOVOT · ISRAEL רחובות · ישראל

DEPARTMENT OF APPLIED MATHEMATICS המחלקה למתמטיקה שמושית

LEVEL II

APPLICATION OF SYNTHESIS TECHNIQUE FOR NONLINEAR UNCERTAIN SYSTEMS TO FLIGHT CONTROL OF ADVANCED MISSILES

Final Technical Report

by

Boris Golubev, Isaac Horowitz, Yizhar Katz

EUROPEAN RESEARCH OFFICE
United States Army
London, England

GRANT NUMBER DA-ERO-77-G-096

Department of Applied Mathematics
The Weizmann Institute of Science
Rehovot, Israel

19 Jun 79 | 160

June 1, 1979

Approved for Public Release; distribution unlimited.

CABLE ADDRESS: WEIZINST (Israel) מען למברקים: PHONE: (054)82111-83111 טלפון: TELEX: 31934 טלקס:

400 763

ABSTRACT

A simplified but nonlinear model is used for the autopilot in the single-axis missile interceptor problem. A recent exact design technique for uncertain nonlinear feedback systems, is used to design the autopilot. A large number of target initial range, position, velocity and acceleration values were used. Also, uncertainty in the aerodynamic missile parameters was allowed. The objective was to guarantee that the autopilot response satisfied specified tolerances over the above ranges. This was satisfactorily achieved. This autopilot design was then used in the simulation of the single-axis interceptor system, over the above set of target trajectories. The results were highly satisfactory.

FIGURE TITLES

TABLE OF CONTENTS

APPLICATION OF SYNTHESIS TECHNIQUE FOR NONLINEAR UNCERTAIN SYSTEMS TO FLIGHT CONTROL OF ADVANCED MISSILES

1. INTRODUCTION

1.1. In many control systems there is a given constrained part, denoted here as the Plant, whose output is the system output of interest. Mathematically, the plant is represented by nonlinear differential equations. Often, the parameters of the differential equations are not precisely known and/or may change in time. Also, there may be external disturbances, such as wind gusts, not known in advance. Generally, it is desired that the system output satisfy given performance specifications, despite the parameter uncertainty and the external disturbances, so a feedback structure is necessary.

There have not been available exact techniques for designing feedback systems around nonlinear uncertain plants, so a variety of approximate techniques have emerged. These are usually supplemented by considerable testing and experimentation. However, there has recently appeared an exact synthesis procedure for a large class of nonlinear plant (even nonlinear time-varying) with significant parameter uncertainty [1,2]. The specialty of this technique is synthesis to satisfy assigned performance specifications. In fact, the assignment of such performance specifications is essential — which is generally not an unreasonable demand. But even in those cases where there is uncertainty as to what constitutes reasonable performance, one may use his best judgement to formulate them anyhow and proceed with the design technique. If the performance specifications are unreasonable, the design which emerges will reveal this, typically by signal levels at some points which exceed the saturation values of plant elements. The specifications can then be suitably modified.

1.2. The Nonlinear Design Philosophy

To simplify the presentation, consider a nonlinear, time-invariant plant set $W = \{w\}$ (a set because of uncertainty). Each parameter combination gives a different w. The basic idea is to convert this set into a linear time-invariant (denoted by ℓti) plant set $P = \{p(s)\}$, such that P is

precisely equivalent to the nonlinear set W providing the output of any $P(s)$ in P belongs to the set of acceptable outputs. To help grasp this idea, consider a black box B_1 which contains a nonlinear element w_0. Let the input be x_1 and the resulting output be $y_1 = w_0(x_1)$. Now one could (in most cases) build another black box B_2 containing a linear element p such that for this same input x_1 the output is $y_1 = p(x_1)$. If you are not allowed to apply any other input except x_1, it is impossible for you to determine which is the linear and which the nonlinear box. The following is a simple technique for finding p. Obtain the Laplace transforms of $y_1(t)$, $x_1(t)$: $Y_1(s) = Ly_1(t)$, $X_1(s) = Lx_1(t)$ and let $P(s) = Y_1(s)/X_1(s)$. Then $p(t) = L^{-1}P(s)$ and $y_1(t) = p(t)*x_1(t)$, where $*$ indicates linear convolution of signals. Hence two necessary conditions for this equivalence of lti p to nonlinear w_0 are:

1. The output $y_1 = w_0(x_1)$ is unique or equivalently given y_1, the input $x_1 = w_0^{-1}(y_1)$ is unique.
2. The signals $y_1(t)$, $x_1(t)$ are Laplace transformable. This condition is difficult to violate.

Condition 1 excludes a large nonlinear class, e.g. hard saturation. Nevertheless, this technique has been applied to the latter case, by replacing the hard saturation by very low gain over the applicable intervals [2]. But obviously, it is then essential that the specified set of desired system outputs, be consistent with the limitation due to saturation. Actually, a good argument can be made for the violation of Condition 1, providing (a) the single output y_1 can be associated with a compact set $X_1 = \{x\}$, i.e. a set which can be approximated as accurately as desired by a finite number of elements and (b) a small enough change in output y_1 results in a small change in the associated x_1. But this has not as yet been rigorously proven.

In any case, in the above, only one nonlinear plant w_0 and one output $y_1(t)$ were considered. The idea can be extended to uncountable sets $W = \{w\}$ and $Y = \{y(t)\}$, as follows. We work backwards from the output of the nonlinear plant, because in a synthesis problem one generally knows what kind of outputs he would like to have in response to the command input (not the plant input — for example the latter could be the elevator control surface while the former is the pilot stick motion). Due to uncertainty, there is a

set of nonlinear plants $W = \{w\}$. Take any pair $y^i \in Y$, $w_j \in W$ and find $x_j^i(t) = w_j^{-1}(y^i(t))$. Then find p_j^i , the lti equivalent of w_j (with respect to y^i), as shown above e.g., by finding $Y^i(s) = Ly^i(t)$, $X_j^i(s) = Lx_j^i(t)$ and setting $Y^i(s)/X_j^i(s) \triangleq P_j^i(s) = Lp_j^i(t)$. This is repeated over the $w_j \in W$ and the $y^i \in Y$ giving a set $P = \{P_j^i\}$. The set P is the lti equivalent of W , with respect to the set Y . If W has 10 elements and Y has 20, then P has 200 elements. In practice, both W and Y are in general infinite and so is P . Of course, in the execution of the design technique a finite number of W and Y elements are taken.

The above lti equivalence idea is the heart of the method. Once we have a linear time-invariant plant set P , we have a purely lti problem. It is essential that we be able to solve this lti problem. For only then it is guaranteed that the actual output is indeed a member of the acceptable set Y , no matter which $w \in W$ happens to be the actual plant. Thus, the solution ($F(s)$, $G(s)$ in Figure 1 if lti compensation is used), to the lti problem is guaranteed to also be the solution of the nonlinear uncertainty problem. It is important to emphasize that there are no approximations involved here. The procedure is exact and theoretically rigorous.

In the above, only a single command input $r = r_a$ in Figure 1 was assumed, and the output set Y_a is the set of acceptable responses to $r_a(t)$ i.e. in Figure 1 it is required that $c(t) \in Y$. This is a highly exceptional case. Usually one has a set $R = \{r\}$ of typical inputs. Suppose one wants the closed-loop system to essentially behave like a lti one, in response to these inputs, with transfer function $T(s) \in T$, the set of acceptable transfer functions. Note that a set of acceptable $\{T(s)\}$ must be specified when there is plant uncertainty, because invariance is impossible to achieve. Then the overall total set $Y = \{Y_a\}$ is obtained by generating $Y_a^b(s) = R_a(s)T^b(s)$ for the $R_a \in R$, $T^b \in T$. One then finds the lti equivalent of this total Y set.

It is worth emphasizing that the synthesis technique has even greater flexibility. Suppose an overall closed-loop nonlinear system is desired, in the following sense: For input r_a one wants system response characterized by $T_a = \{T^a(s)\}$, but for input r_b one wants system response characterized by set $T_b = \{T^b(s)\}$. For example, suppose r_a is a unit step and its

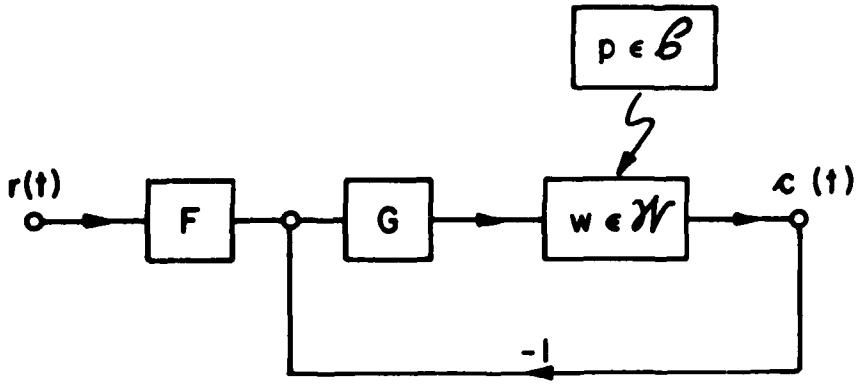

FIGURE 1 Nonlinear set W is replaced by lti equivalent set $\mathcal{P}$.

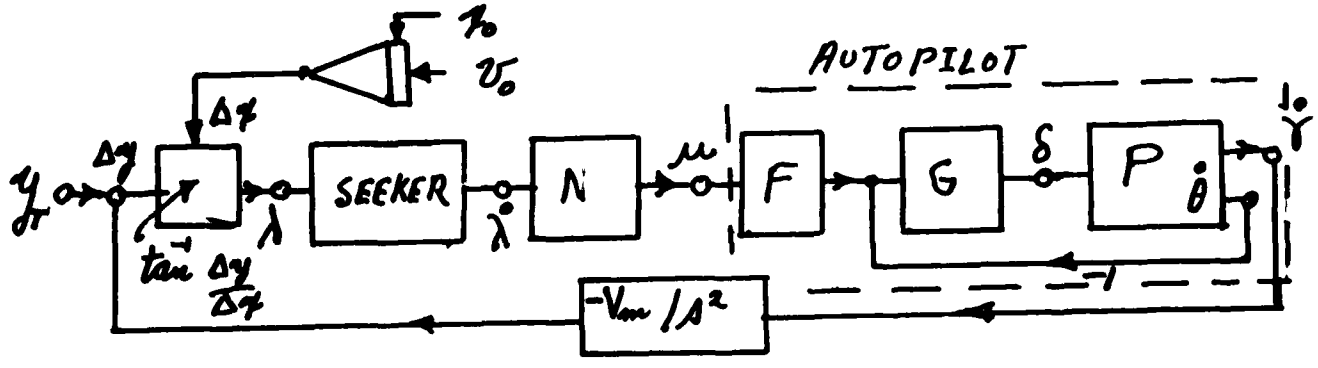

FIGURE 2 Problem structure.

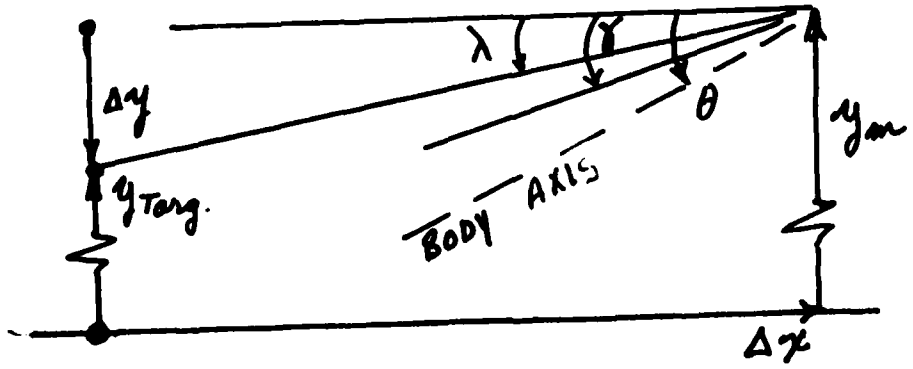

FIGURE 3 Missile-target geometry.

acceptable response function set is T_a . Suppose r_b is a unit ramp but one does not want the system response to be the integral of its response when the input was a unit step, but of a different nature entirely. This can be done. The F in Figure 1 must then be nonlinear. See Reference 2 for an example of such design. The output c(t) due to a two-value step need not be twice that of a unit-valued step etc., if one does not want it so.

It is worth reemphasizing the importance of the synthesis approach. One must formulate the set of desired plant outputs or alternatively its desired set of inputs. Otherwise it is not possible to find the ℓti equivalent set P , which is the basis of the technique. It is also worth including here, as Appendix I, the design results for an application of this design technique, recently done for the U.S. Air Force. Here, the set of acceptable plant outputs was very clearly apriori specified at the very beginning. Unfortunately, in our present case, however, a great deal of work was required to obtain the set of acceptable outputs.

2. STATEMENT OF THE PROBLEM

2.1. The problem considered is the single-axis missile interceptor problem, shown in Figure 2. Feedback around the body pitch-rate is usually used. The nonlinear missile equations of motion are usually linearized. But if the missile has a large flight envelope, then such linearization may be inadequate. The objective here is to use nonlinear equations of motion and the ℓti plant-equivalent method described in Section 1, to perform the design of the auto-pilot in Figure 2.

The equations describing Figure 2, are

Autopilot (Figure 3).

α = angle of attack (radians), $\dot{\theta} = q$ = body axis pitch rate (r/s, s = seconds),
λ = line of sight angle (r), γ = velocity angle tangent to trajectory (r),
δ = elevator deflection (r).

$$\left.\begin{aligned} \dot{\gamma} &= C_4[K_{L\alpha}(\alpha)\alpha + K_{L\delta}(\delta)\delta] \\ \ddot{\theta} &= C_3[K_{m\alpha}(\alpha)\alpha + K_{m\delta}(\delta)\delta + C_2\dot{\theta}] \\ \alpha &= \theta - \gamma \end{aligned}\right\} \qquad (1a\text{-}c)$$

$$\left.\begin{aligned} &C_4 = gQ/MV_m \text{ per sec.} \;,\; C_3 = QD/A \text{ per sec}^2. \;,\; C_2 = K_{mq}D/2V \text{ sec.} \\ &g = 9.81 \text{ m/s}^2 \text{ (meters/sec}^2\text{)} \;,\; Q = 176 \text{ kgm} \;,\; K_{mq} = -1000 \\ &M = 70 \text{ k (kgm)} \;,\; V_m = 200 \text{ m/s} \;,\; D = .17 \;,\; A = 3.8 \end{aligned}\right\} \qquad (2)$$

$$\left.\begin{aligned} K_{L\alpha} &= C_{L\alpha}(17 + 1.3\alpha) \;,\; K_{L\delta} = C_{L\delta}(15 + 1.1\delta) \\ K_{m\alpha} &= C_{m\alpha}(-8.6 - 2\alpha) \;,\; K_{m\delta} = C_{m\delta}(25 + .8\alpha) \end{aligned}\right\} \qquad (3a\text{-}d)$$

In (3a-d), the coefficients are independently uncertain.

$$C_{L\alpha}, C_{L\delta}, C_{m\alpha}, C_{m\delta} \in [0.8\,,\,1.2] \qquad (4)$$

Geometry: $\hat{y}_m = \hat{\dot{\gamma}} V_m / s^2 \;,\; V_m = 200 \text{ m/s}$ (5)

(the hat over the time function represents its Laplace transform).

Input: The target position $y_{Targ} = y_0 + v_0 t + \frac{a_0 t^2}{2}$ (6)

$$\begin{aligned} &y_0 \in [0,200]\text{m} \;,\; v_0 \in [0,10]\text{m/s} \\ &a_0 \in [0,2]\text{m/s}^2 \end{aligned} \qquad (7)$$

These give the range of target position (initial), velocity and acceleration values, constants in a specific run.

Feedback equations:

$$\lambda = \arctan \frac{\Delta y}{\Delta x} \;,\; \Delta y = y_{Targ} - y_m \;,\; \Delta x = R - V_m t \cos\gamma \qquad (8)$$

$$R \text{ (range)} \in [1500,3000]\text{m} \qquad (9)$$

$$N \text{ (Fig. 2)} \in [2,4] \qquad (10)$$

Initial conditions:

$$\dot{\gamma}(0) = \gamma(0) = \theta(0) = \dot{\theta}(0) = \alpha(0) = \delta(0) = 0 \;. \qquad (11)$$

3. APPLICATION OF NONLINEAR SYNTHESIS TECHNIQUE

3.1. The Set of Acceptable Outputs Y. It was emphasized in Section 1, that it is imperative that a set of acceptable plant outputs Y, be specified, in order to obtain the lti equivalent set P. The latter set is guaranteed to be the correct equivalent of the nonlinear plant set W, only for the set Y (although it may and usually is so, for a larger set than Y). Hence, it is essential that Y contain the true typical nonlinear plant outputs which are desired under actual working conditions, including the extreme cases. Here, the nonlinear synthesis technique is to be applied to the portion labelled A/P (autopilot), in Figure 2 and the nonlinear plant (w of Section 1) is the portion from δ to $\dot{\gamma}$. So the set Y refers to the set of desirable $\dot{\gamma}$ that exist over the range of conditions described by Equations (1-10), with particular attention paid to the parameter uncertainty spread given in Equations (4,7,9,10).

To achieve such a Y in the present case, the autopilot in Figure 2 was modelled as a second order system with transfer function (for $\hat{\dot{\gamma}}/\hat{\dot{\lambda}}$, where the hat over a time function represents its Laplace transform).

$$\frac{\hat{\dot{\gamma}}}{\hat{\dot{\lambda}}} = \frac{N\omega_n^2}{s^2 + 2\zeta\omega_n s + \omega_n^2} \quad , \quad N \text{ of Eq. (10)} \tag{12}$$

$$\omega_n \in [1,4] \; ; \quad \zeta = .7 \quad . \tag{13}$$

This second-order simulation of the autopilot replaced the autopilot in Figure 2. Several hundred runs were made of this simplified Figure 2 system. The fictitious $\dot{\gamma}(t)$ values so obtained, i.e. the output of this second order simulation, provided the acceptable set Y. Each $y \in Y$ was then used as a known signal in Equations (1a-c), to solve for $\dot{\theta}(t)$, $\delta(t)$, giving an lti equivalent $P(s)$.

3.2. The LTI Equivalent Set P

Several hundred random combinations were used of the 10 parameters of Equations (4,7,9,10,13) in the above manner. For each combination, the time functions $\delta(t)$, $\dot{\theta}(t)$ were obtained to give the lti plant equivalent. Note that $\dot{\theta}(t)$ rather than $\dot{\gamma}(t)$ is used at this stage for the nonlinear plant output, because the feedback is taken from $\dot{\theta}$. A representative

number of these time function pairs is shown in Figures 4a-q. In these and later figures:

$$\begin{aligned} &XN = N \quad \text{(Eq. 10)} \quad , \quad AT = a_0 \quad \text{(Eq. 7)} \quad , \\ &VW = v_0 \quad \text{(Eq. 7)} \quad , \quad XMO = y_0 \quad \text{(Eq. 7)} \quad , \\ &R = R \quad \text{(Eq. 9)} \quad , \quad WN = \omega_n \quad \text{(Eq. 13)} \quad , \\ &CLA = C_{L\alpha} \quad \text{(Eq. 3a)} \quad , \quad CLD = C_{L\delta} \quad \text{(Eq. 3b)} \quad , \\ &CMA = C_{m\alpha} \quad \text{(Eq. 3c)} \quad , \quad CMD = C_{m\delta} \quad \text{(Eq. 3d)} \quad . \end{aligned} \tag{14}$$

The ℒti equivalent $P(j\omega)$

$$P(j\omega) = \hat{\ddot{\theta}}(j\omega)/\hat{\delta}(j\omega) \quad . \tag{15}$$

3.3. The Frequency-Response Calculation Problem

At first, attempts were made to find $\hat{\ddot{\theta}}(j\omega)$, $\hat{\delta}(j\omega)$ separately and perform the division in (15). Adaptive numerical integration, of $\int_0^\infty f(t) \begin{matrix}\cos \omega t \\ \sin \omega t\end{matrix} dt$ was made, in the sense that the time increment for numerical integration was shortened as ω was increased. For many cases, good results were obtained. For many others, the results were quite poor in the high-frequency range. Other computer library techniques, including "Fast Fourier Transform", were tried and found to be highly inadequate in the high-frequency range. These routines are adequate for communication-oriented problems, where good accuracy over the signal bandwidth, is usually sufficient. However, in a feedback-oriented problem such as the present one, with significant parameter uncertainty, good accuracy is needed for a very much larger frequency range. It is especially important to have clean results for several octaves in the high-frequency asymptotic region. Thus, given a signal $x(t)$ and its transform $X(s)$, as $s \to \infty$, $X(s) \to k/s^{e_p}$, where e_p is the excess of $X(s)$ poles over zeros. In feedback problems of the present type, it is essential to have good results for several octaves in this range.

In our problem, it turned out eventually that $P(j\omega)$, the ratio in (15), was relatively simple. However, each of $\hat{\ddot{\theta}}$, $\hat{\delta}$ was very complex, with the complexity cancelling out in the division. After numerical integration was found inadequate at high frequencies, it was thought to use a separate

representation for $\dot{\theta}(t)$, $\delta(t)$, for small t , since the latter corresponds to large ω values in the signal transforms. The Taylor series expansion was used. A computer program was prepared which used a large number of time samples and an optimization routine, to find the best Taylor series fit for some range $t \in [0,T/m]$, m a fraction of the run time. Numerical integration was also used. If there was an overlapping frequency range where the two techniques gave very similar values, then the results were considered satisfactory. The numerical integration results were then used in the low frequency range, and the Taylor series results in the high-frequency range. This approach was helpful for a significant number of runs, but there still remained a substantial number of cases where it too failed. Figures 5a,b are illustrative of the $|P(j\omega)|$ of Equation (15) obtained in such cases.

Finally, a new technique, original (to the best of our knowledge), was developed in which $P(j\omega)$ was found directly, without first finding $\hat{\dot{\theta}}(j\omega)$, $\hat{\delta}(j\omega)$ of Equation (15). In this way, there is avoided the problem of finding the very complex $\hat{\dot{\theta}}(j\omega)$, $\hat{\delta}(j\omega)$. This technique is described in Appendix 2, and is a valuable byproduct of the research effort. Some results are shown in Figures 6a-f. To check the results, numerous runs were made in which the $\delta(t)$ signal was the input to lti network with the transfer function $P(j\omega)$ gotten by the above. Numerical inverse transform integration was used to find the resulting output. Representative results are shown in Figures 7a-c. In each of these figures, the first part gives the $\dot{\theta}(t)$, $\delta(\hat{t})$ signals obtained from the original simulation described in 3.1. The second part shows $|P(j\omega)|$ obtained by the new method. Arg $P(j\omega)$ was obtained but is not shown. The third part gives $L^{-1}P(j\omega)\hat{\delta}(j\omega) = \dot{\theta}^*(t)$, which should be checked against $\dot{\theta}(t)$ of the first figure. It is seen that excellent agreement was obtained.

3.4. Review of LTI Synthesis Technique

Once C , the lti plant equivalent of the nonlinear plant set W has been obtained, the problem becomes one of designing a lti feedback system to cope with uncertainty of a lti plant. A detailed synthesis technique for this purpose is described in Reference 3, which is briefly reviewed here.

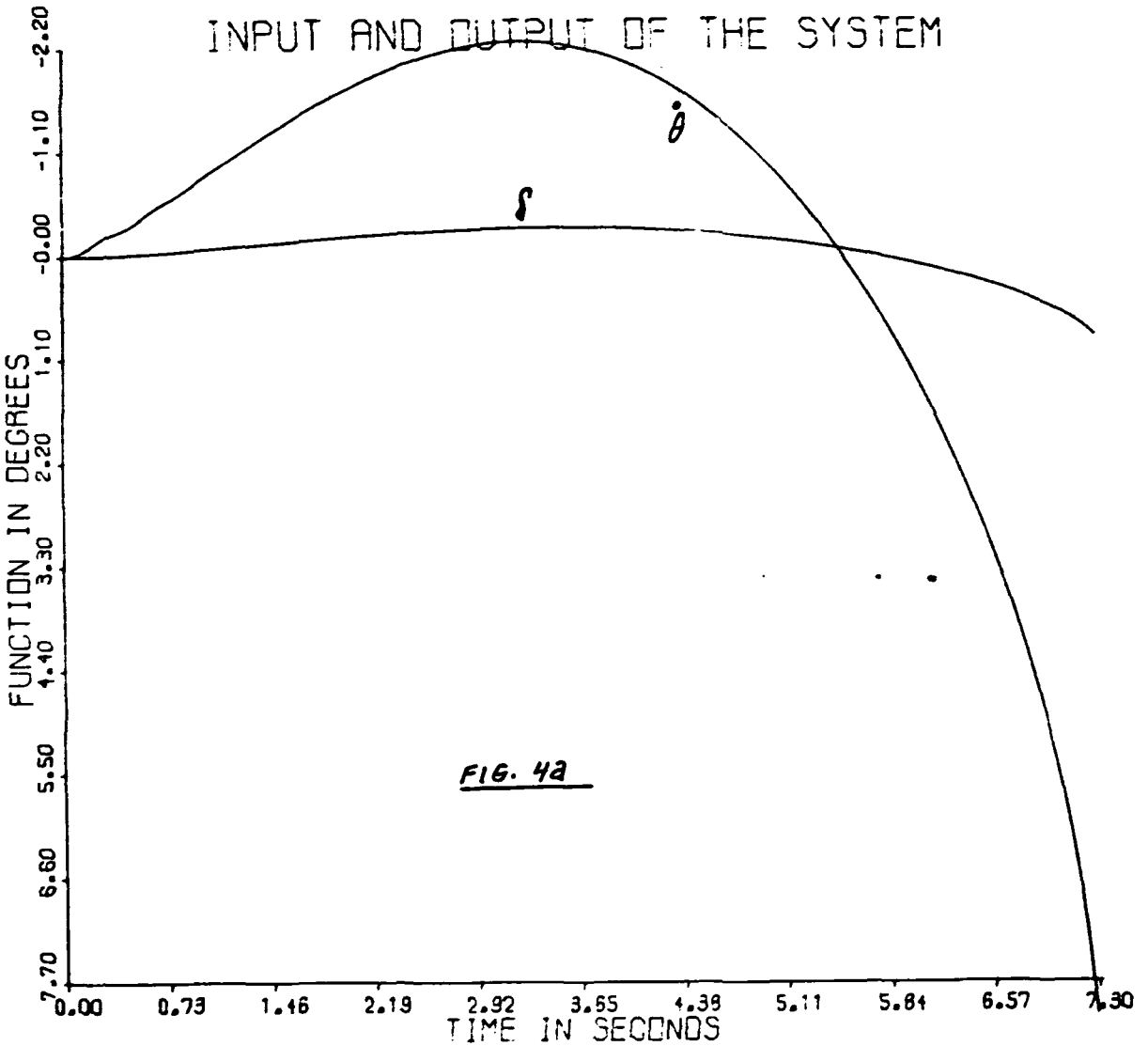

FIG. 42

XN=4.00

AT=1.00

VW=10.00

XMO=0.

R=1500.

WN=1.00

CLA=1.00

CLD=1.00

CMA=1.00

CMD=1.00

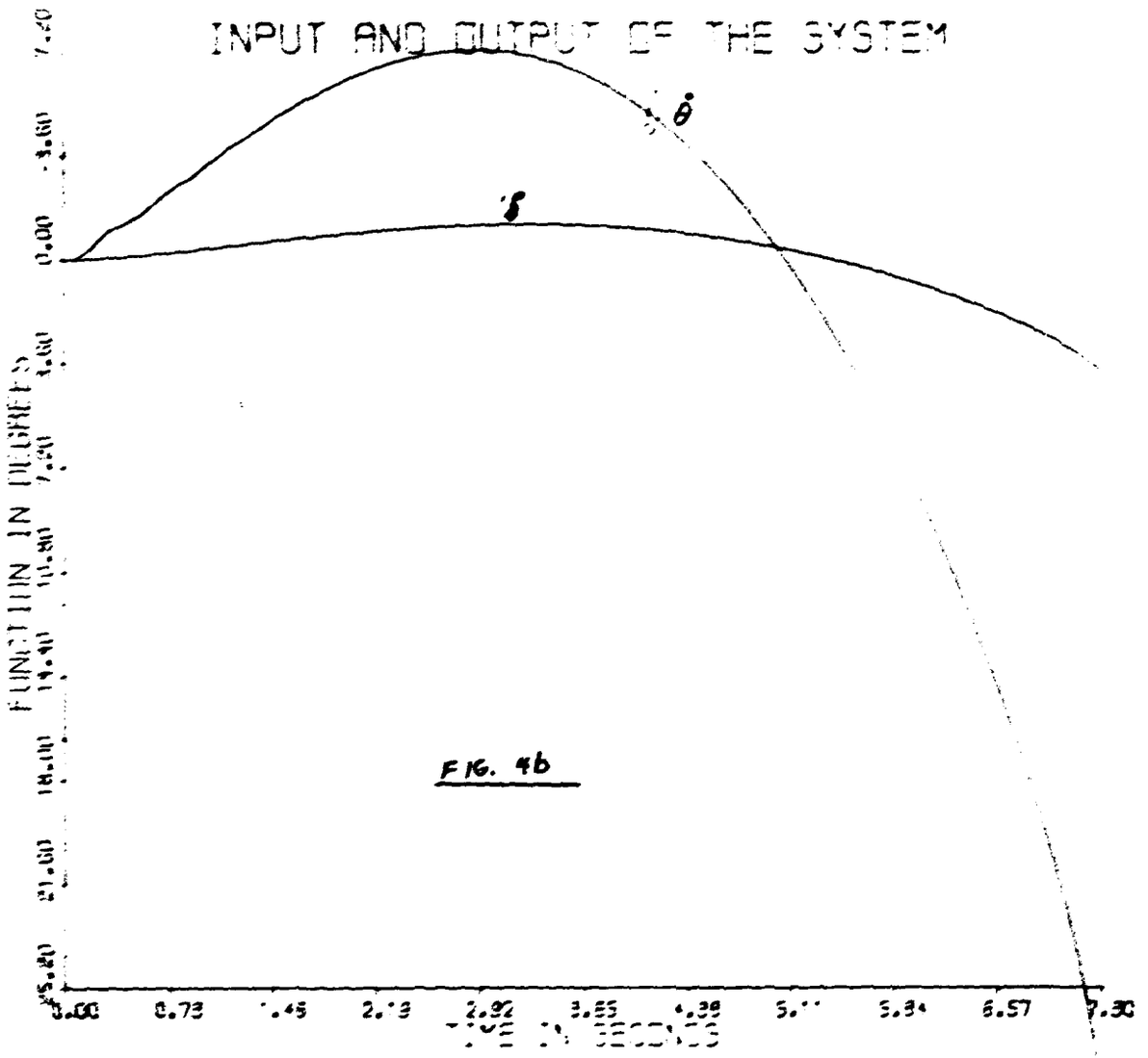
INPUT AND OUTPUT OF THE SYSTEM
θ
δ
FUNCTION IN DEGREES
0.00
0.73
1.46
2.19
2.92
3.65
4.38
5.11
5.84
6.57
7.30

FIG. 4b

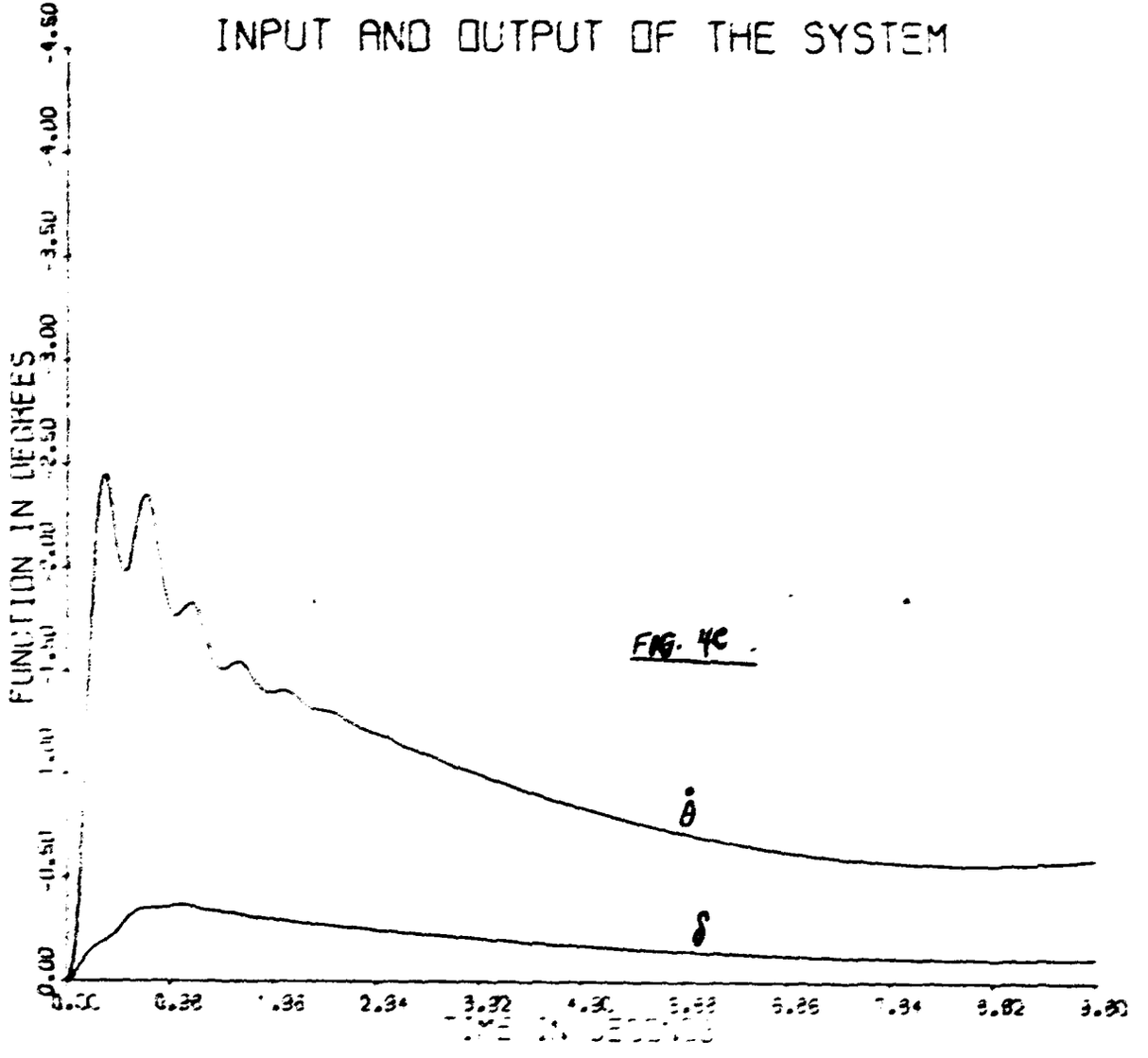
INPUT AND OUTPUT OF THE SYSTEM
FUNCTION IN DEGREES
-4.50
-4.00
-3.50
-3.00
-2.50
-1.50
-0.50
0.00
θ̇
δ
XN=4.00
RT=1.00
VW=5.00
XMO=100.
R=2000.
WN=4.00
CLA=0.80
CLD=1.20
CMA=1.20
CMD=0.80

FIG. 4C

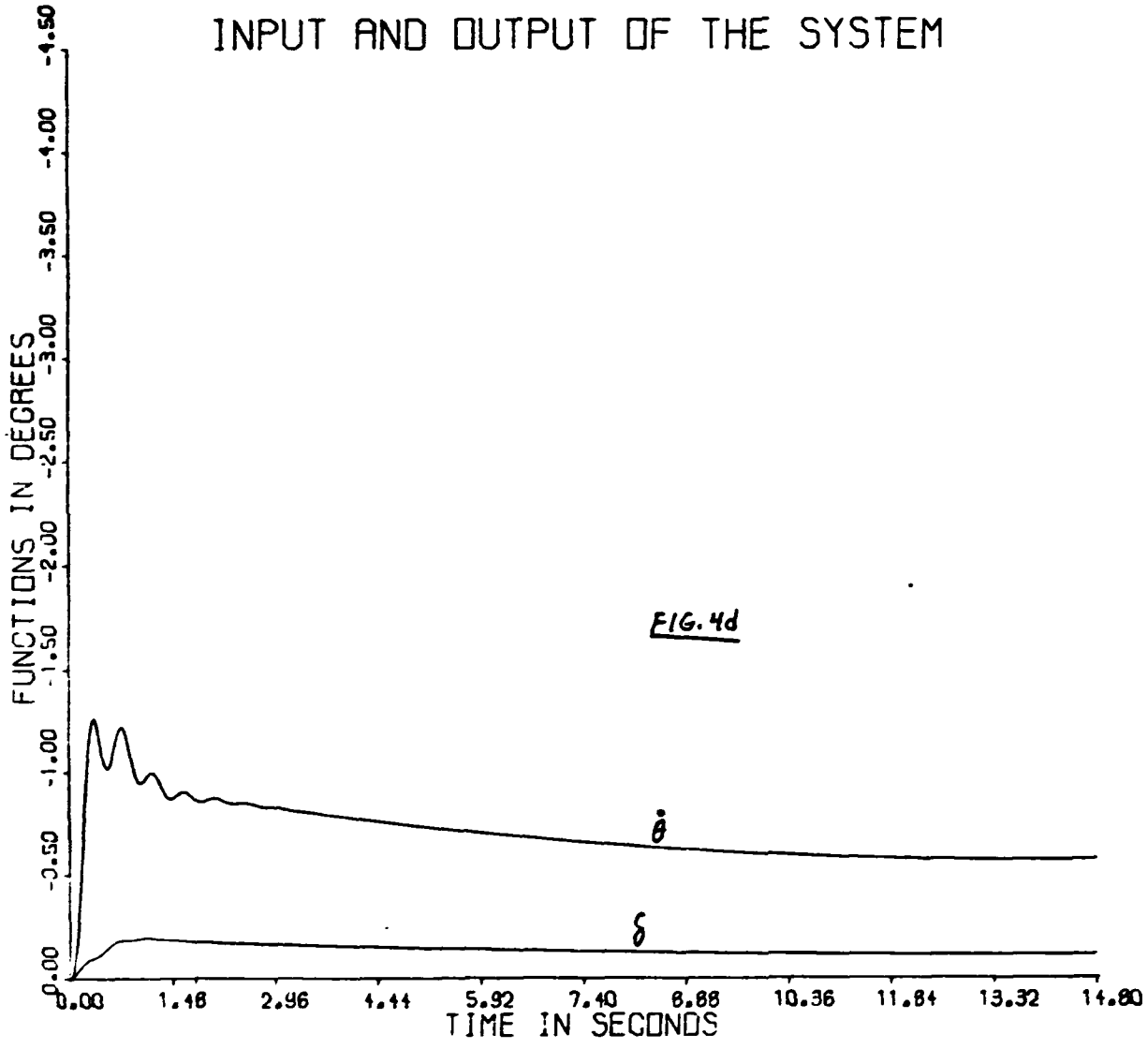

FIG. 4d

XN=4.00

AT=1.00

VW=5.00

XMO=100.

R=3000.

WN=4.00

CLA=0.80

CLD=1.20

CMA=1.20

CMD=-0.80

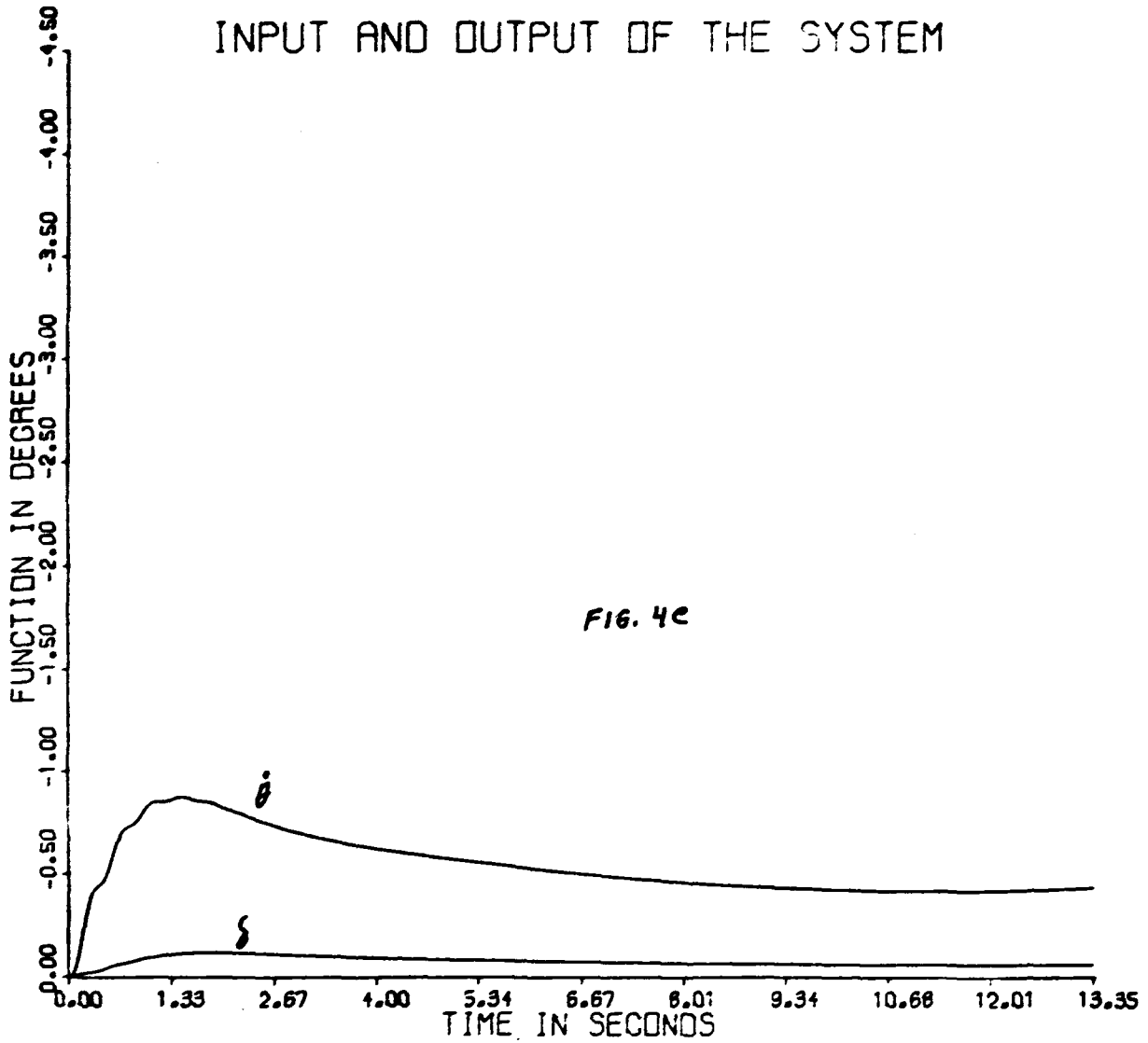

FIG. 4C

XN=4.00

AT=0.74

VW=1.13

XMO=98.

R=2709.

WN=2.16

CLA=0.96

CLD=0.95

CMA=0.88

CMD=0.89

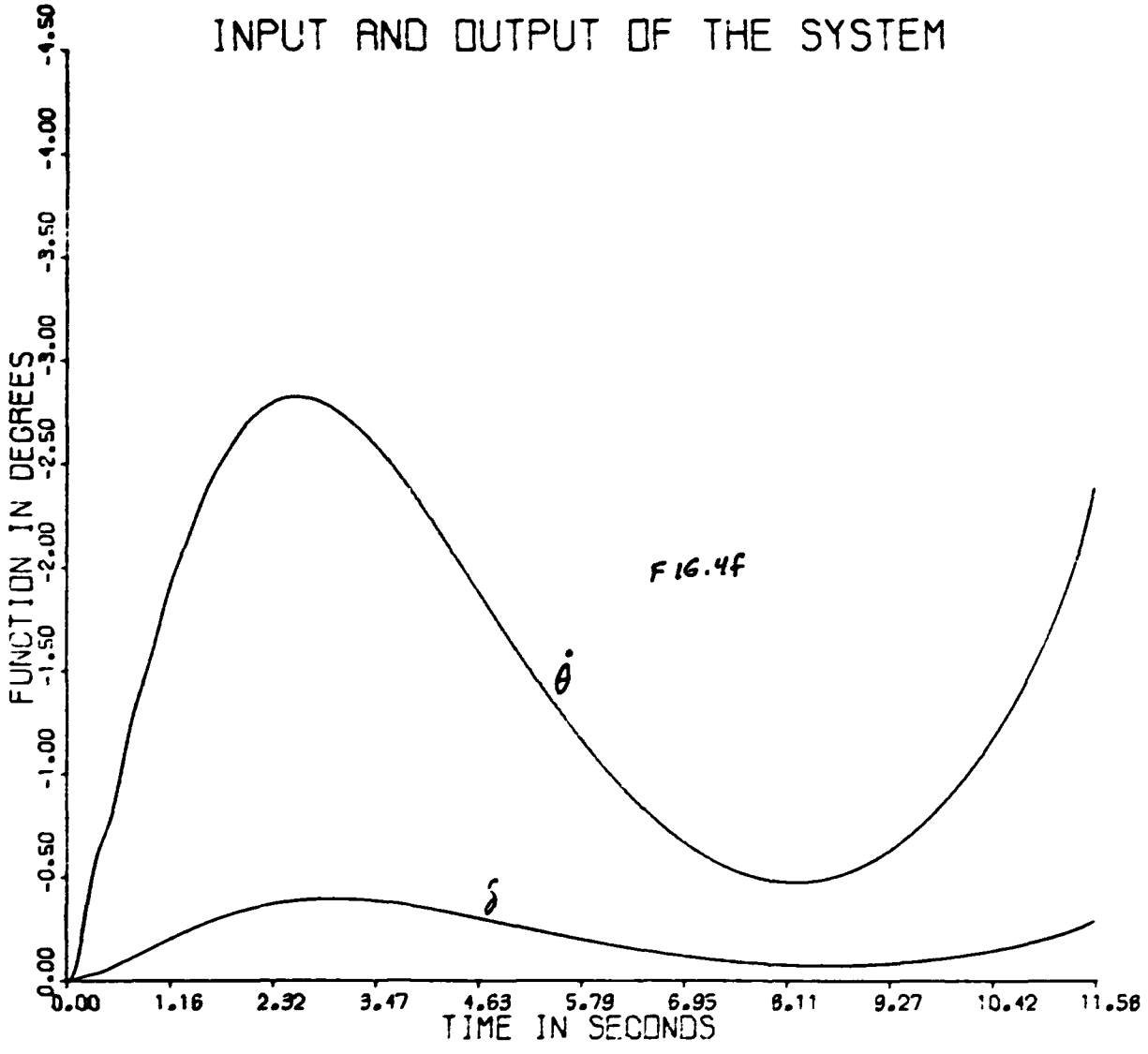

FIG.4f

XN=3.93

RT=1.41

VW=8.99

XMO=172.

R=2356.

WN=1.27

CLA=0.82

CLD=1.19

CMA=0.95

CMD=1.02

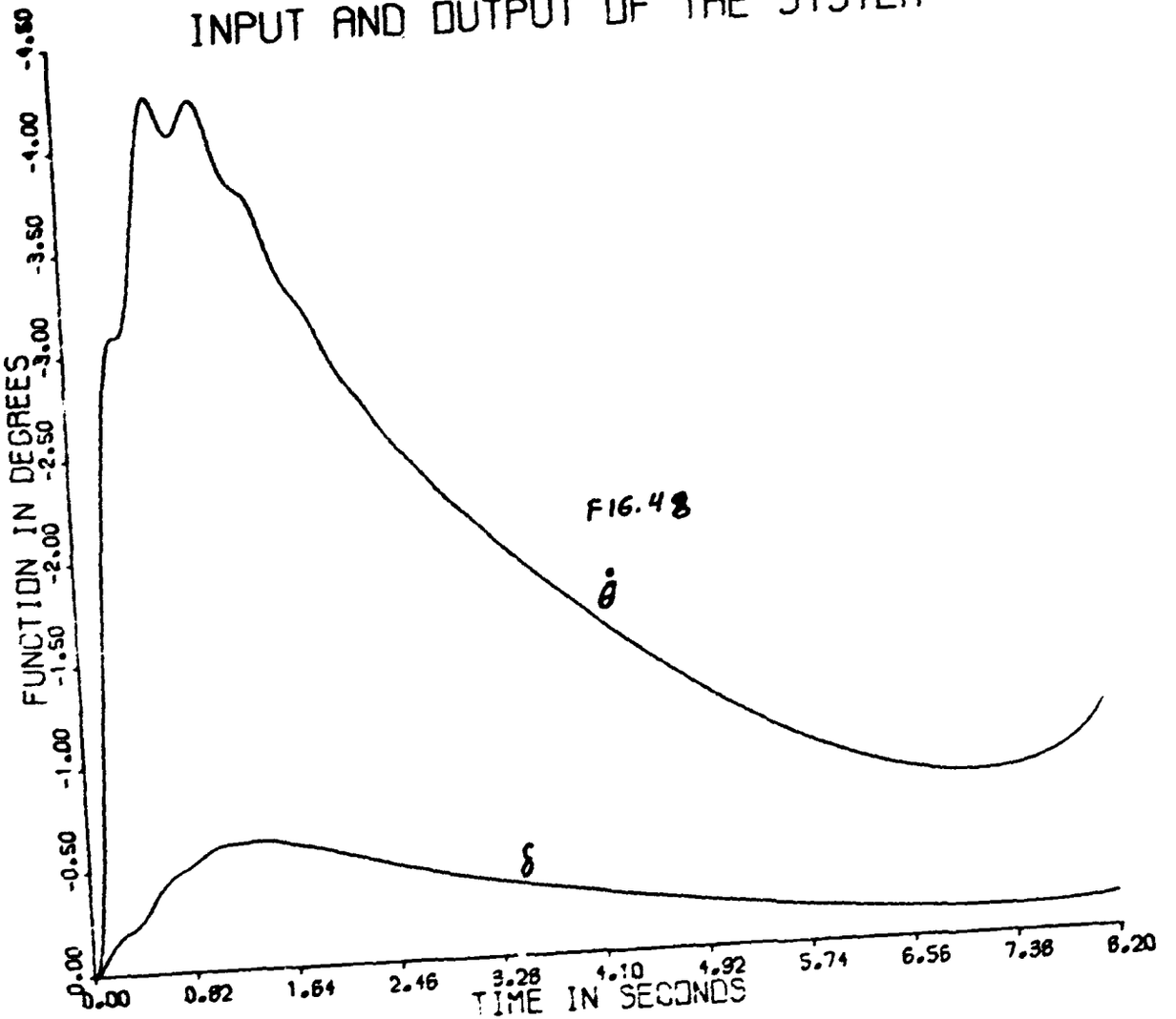

FIG. 4 B

XN=3.66

AT=1.38

VW=5.22

XMO=185.

R=1680.

WN=2.89

CLA=0.98

CLD=1.09

CMA=1.04

CMD=0.83

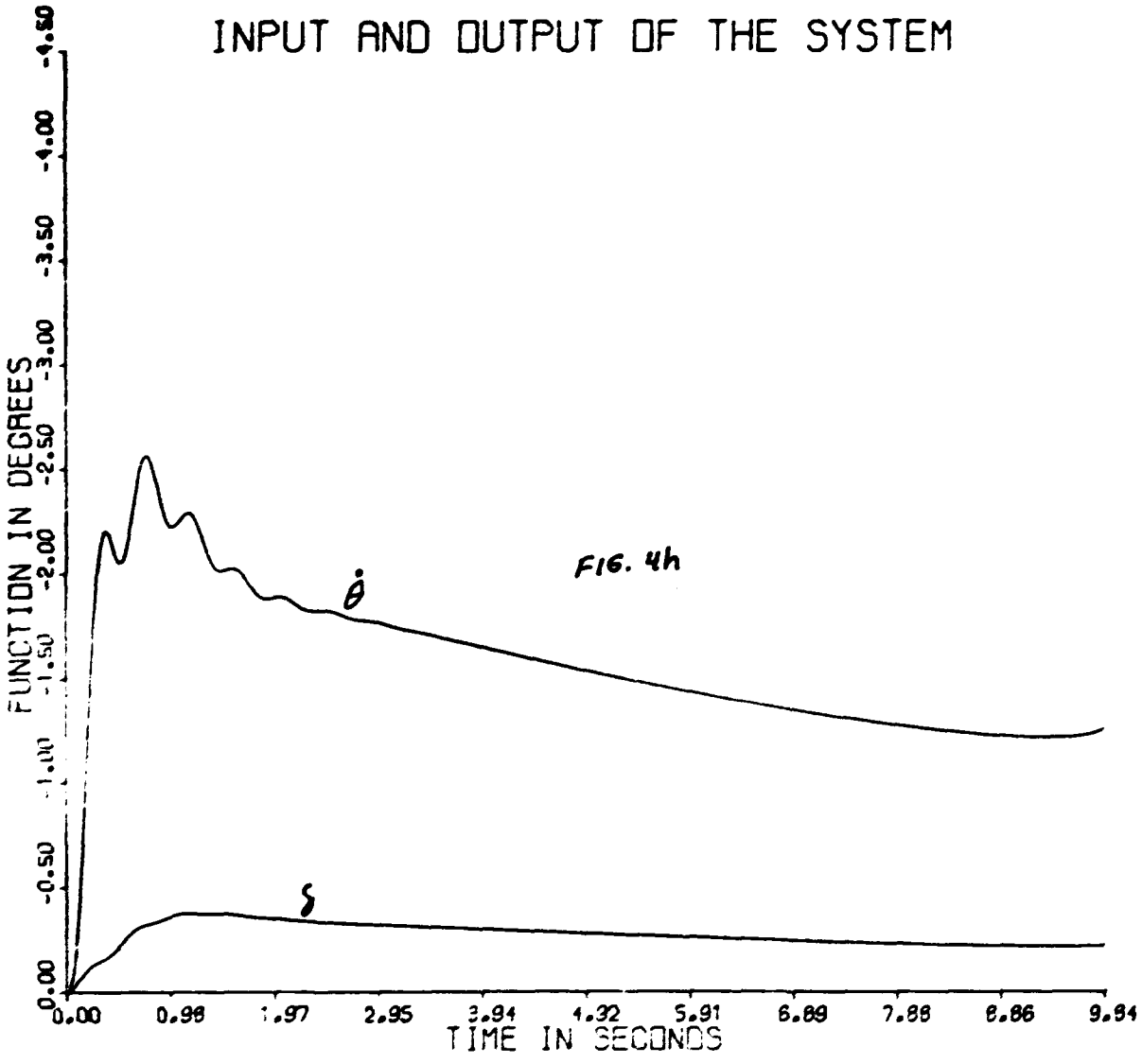

FIG. 4h

XN=3.34

AT=1.74

VW=8.48

XMO=108.

R=2009.

WN=3.34

CLA=0.81

CLD=1.16

CMA=1.10

CMD=0.87

INPUT AND OUTPUT OF THE SYSTEM

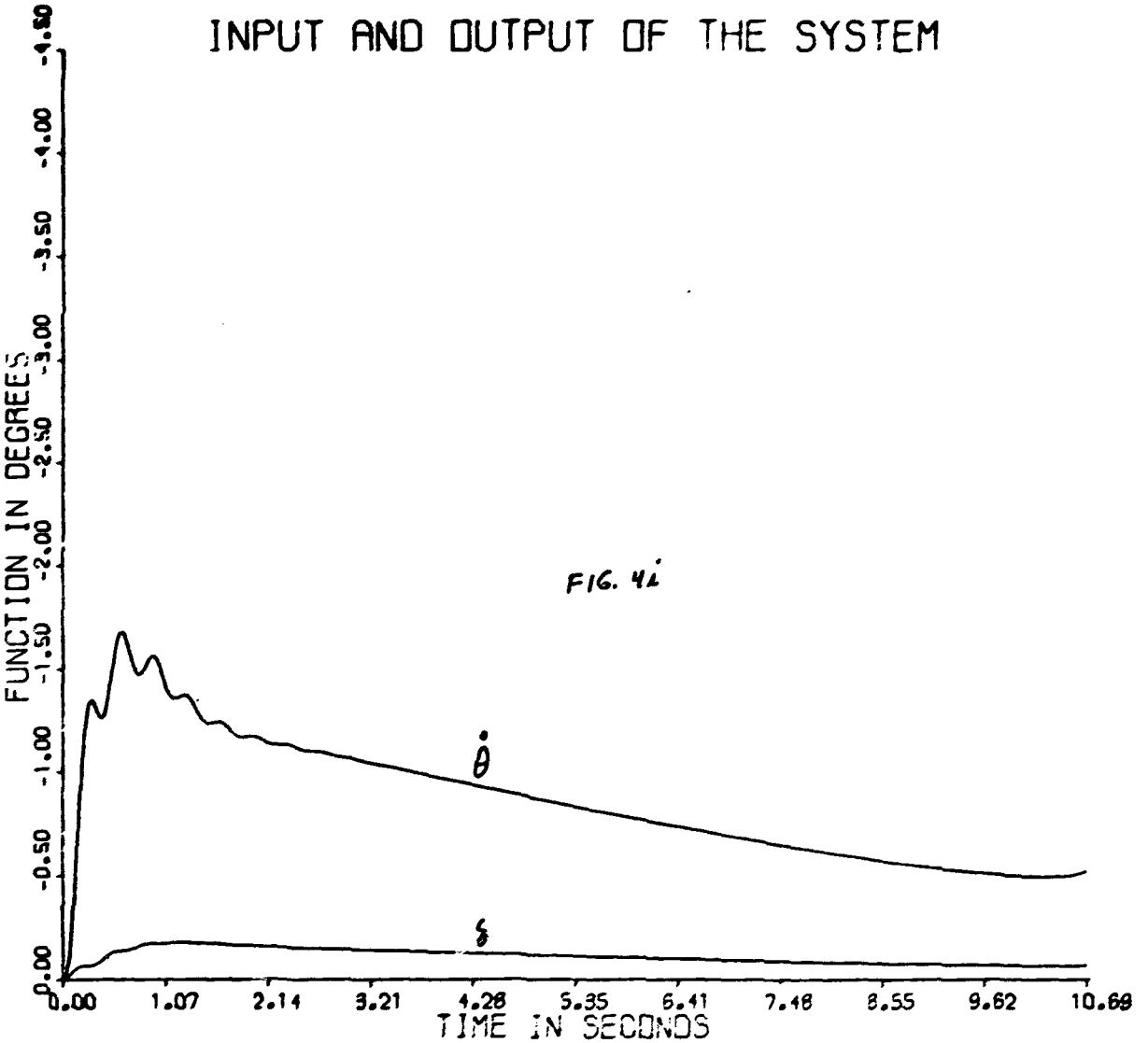

FIG. 4i

XN=3.27

AT=0.71

VW=5.14

XMO=98.

R=2178.

WN=3.46

CLA=0.98

CLD=0.93

CMA=0.97

CMD=1.10

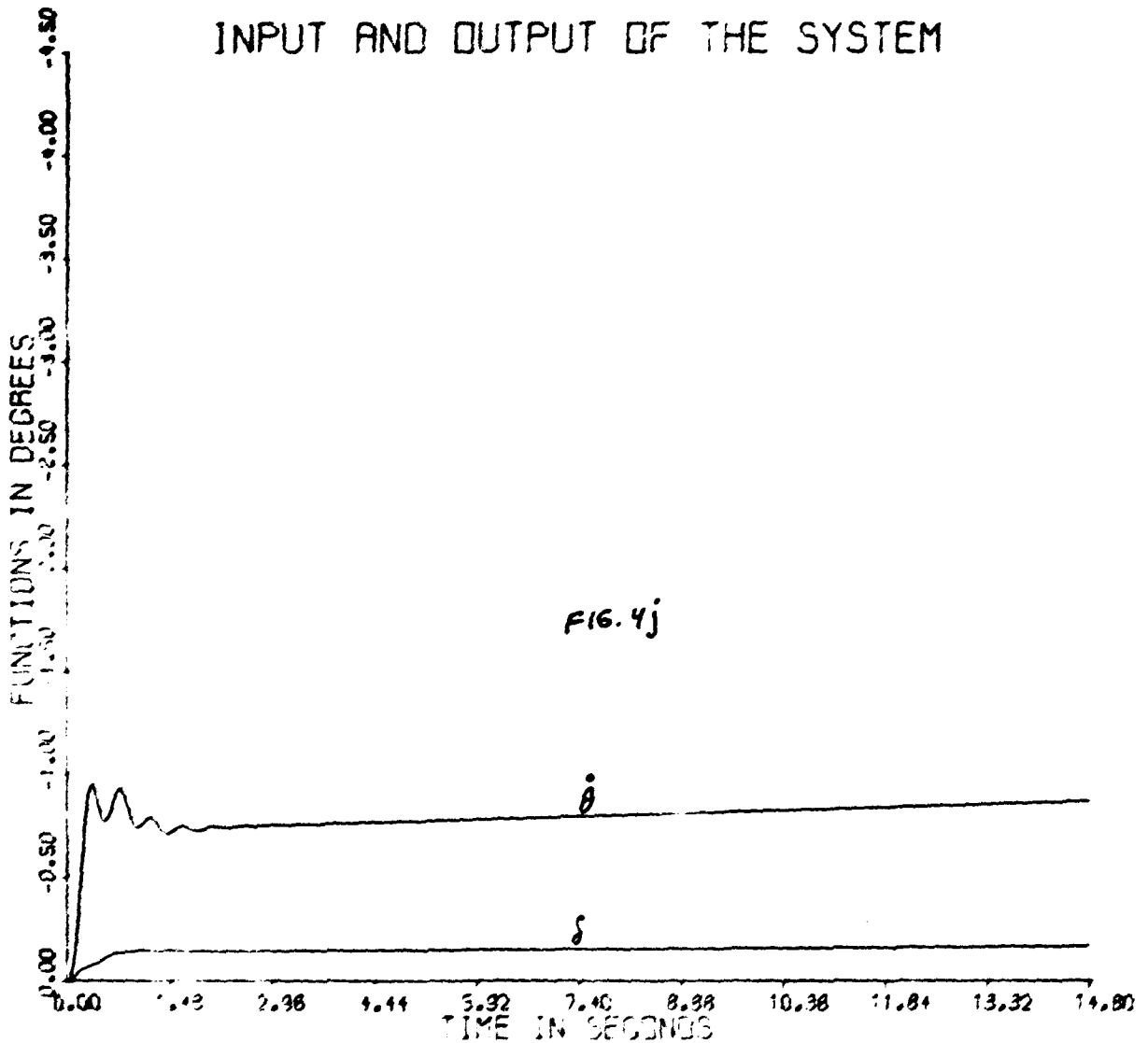
INPUT AND OUTPUT OF THE SYSTEM
FUNCTIONS IN DEGREES
-4.50
-4.00
-3.50
-3.00
-2.50
-0.50
0.00
$\dot{\theta}$
δ
0.00
2.36
4.44
5.92
7.40
8.88
10.36
11.84
13.32
14.80
TIME IN SECONDS
XN=3.00
AT=1.00
VW=5.00
XMO=100.
R=3000.
WN=4.00
CLA=0.80
CLD=1.20
CMA=1.20
CMD=0.80

FIG. 4j

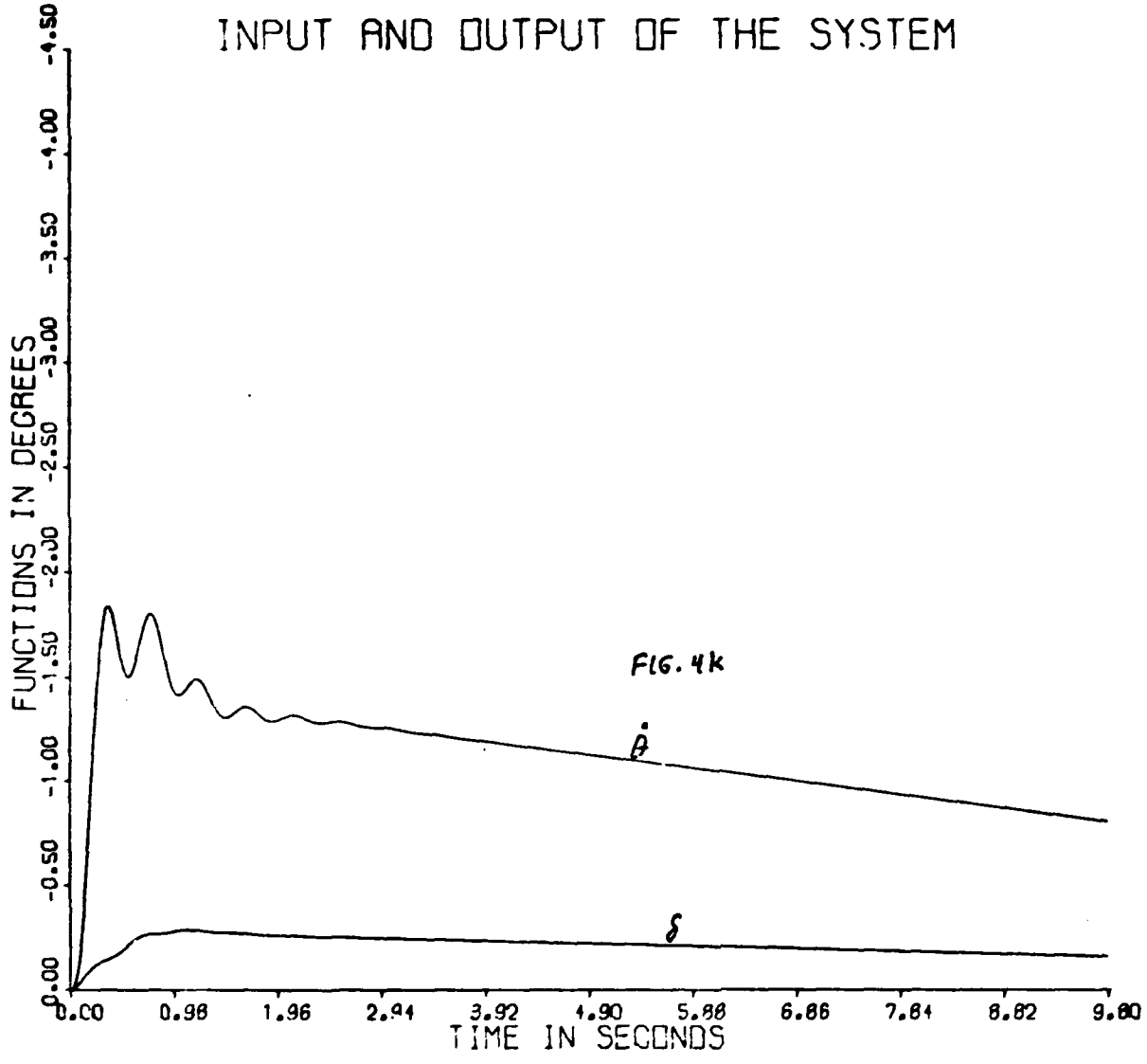

FIG. 4k

XN=3.00

AT=1.00

VW=5.00

XMO=100.

R=2000.

WN=4.00

CLA=0.80

CLD=1.20

CMA=1.20

CMD=0.80

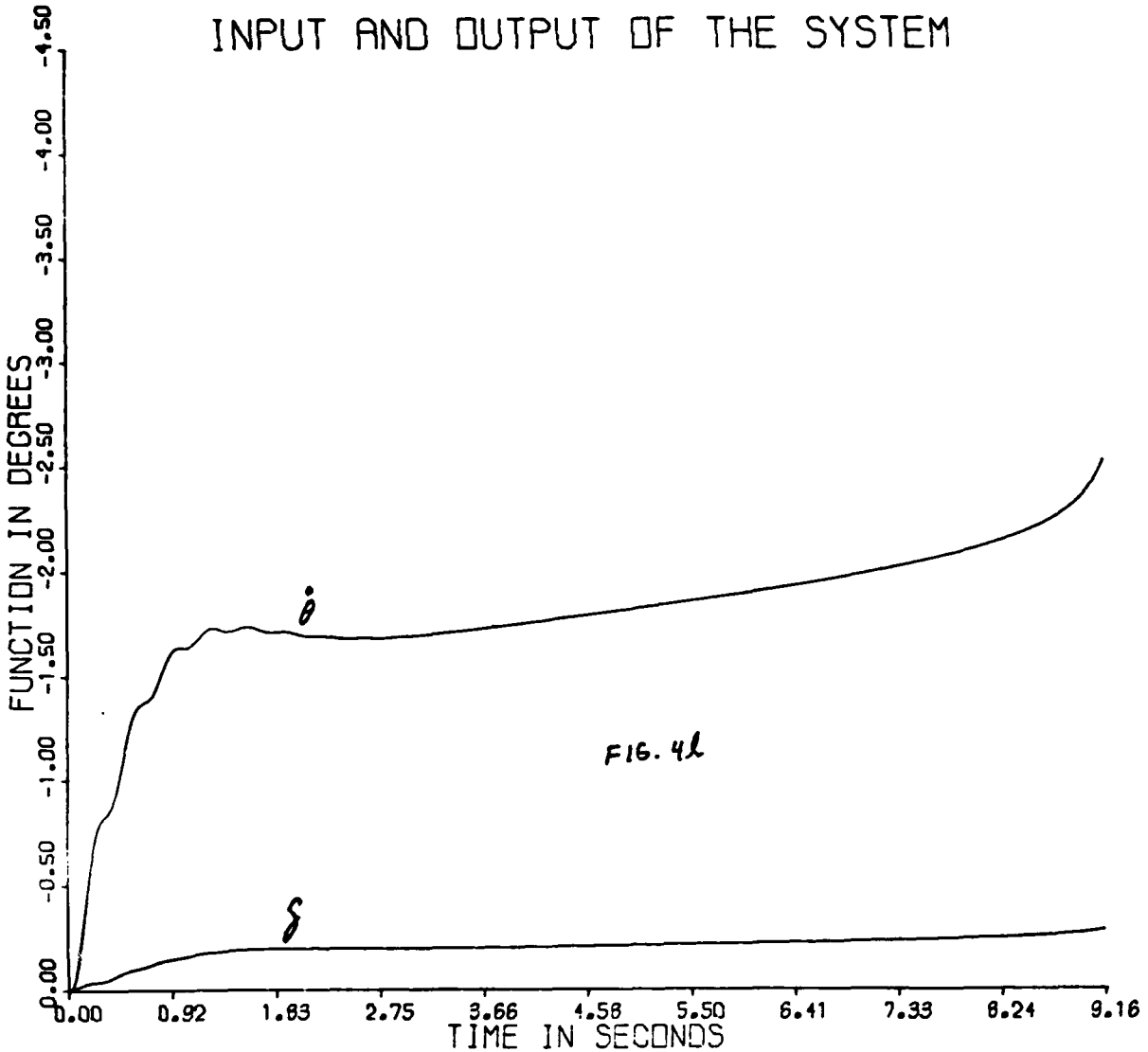
INPUT AND OUTPUT OF THE SYSTEM
FUNCTION IN DEGREES
0.00
-0.50
-1.00
-1.50
-2.00
-2.50
-3.00
-3.50
-4.00
-4.50
0.00
0.92
1.83
2.75
3.66
4.58
5.50
6.41
7.33
8.24
9.16
TIME IN SECONDS
$\dot{\theta}$
δ
XN=2.60
AT=1.78
VW=1.25
XMO=140.
R=1872.
WN=2.51
CLA=1.14
CLD=1.08
CMA=1.10
CMD=1.17

FIG. 4l

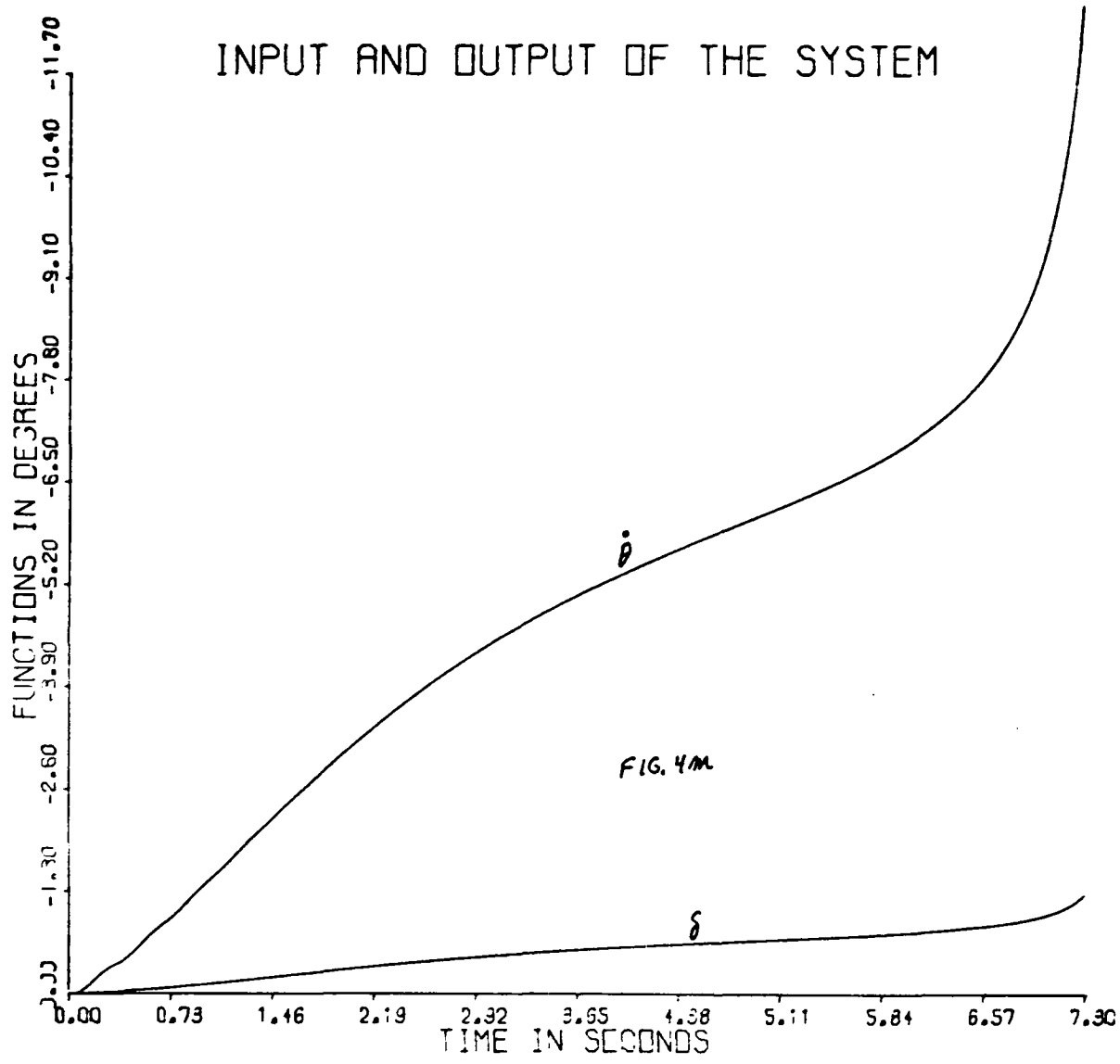
INPUT AND OUTPUT OF THE SYSTEM
FUNCTIONS IN DEGREES
-11.70
-10.40
-9.10
-7.80
-6.50
-5.20
-3.90
-2.60
-1.30
0.00
0.00
0.73
1.46
2.19
2.92
3.65
4.38
5.11
5.84
6.57
7.30
TIME IN SECONDS
$\dot{\theta}$
δ
XN=2.00
AT=1.00
VW=10.00
XMO=200.
R=1500.
VN=1.00
CLA=1.20
CLD=1.20
CMA=1.20
CMD=1.20

FIG. 4M

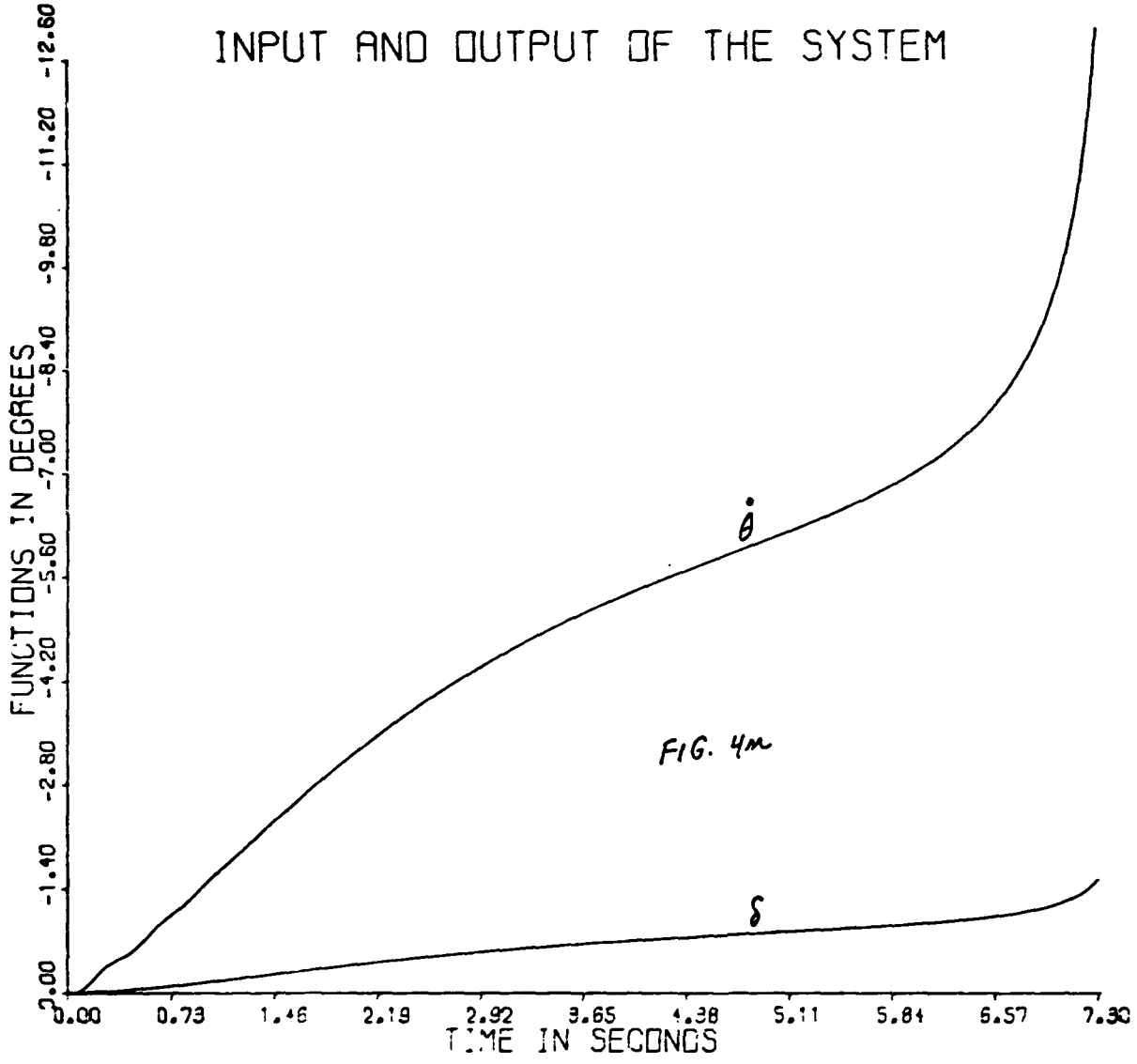

FIG. 4m

XN=2.CO

RT=1.00

VW=10.00

XMO=200.

R=1500.

WN=1.0C

CLA=1.0C

CLD=1.CO

CMA=1.CO

CMD=1.CO

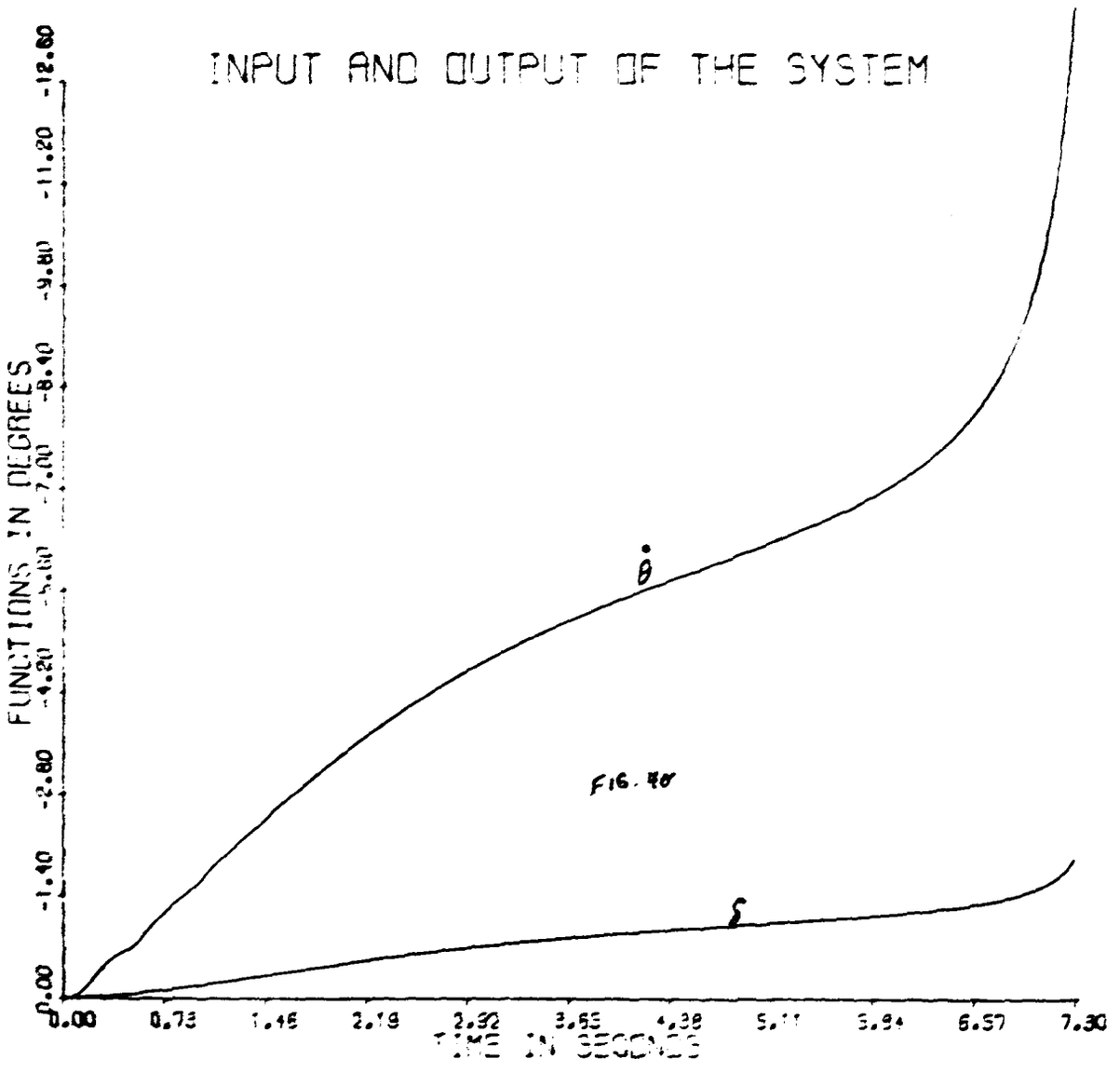

FIG. 4a

XN=2.00

AT=1.00

VW=10.00

XMO=200.

R=1500.

WN=1.00

CLA=0.80

CLD=0.80

CMA=0.80

CMD=0.80

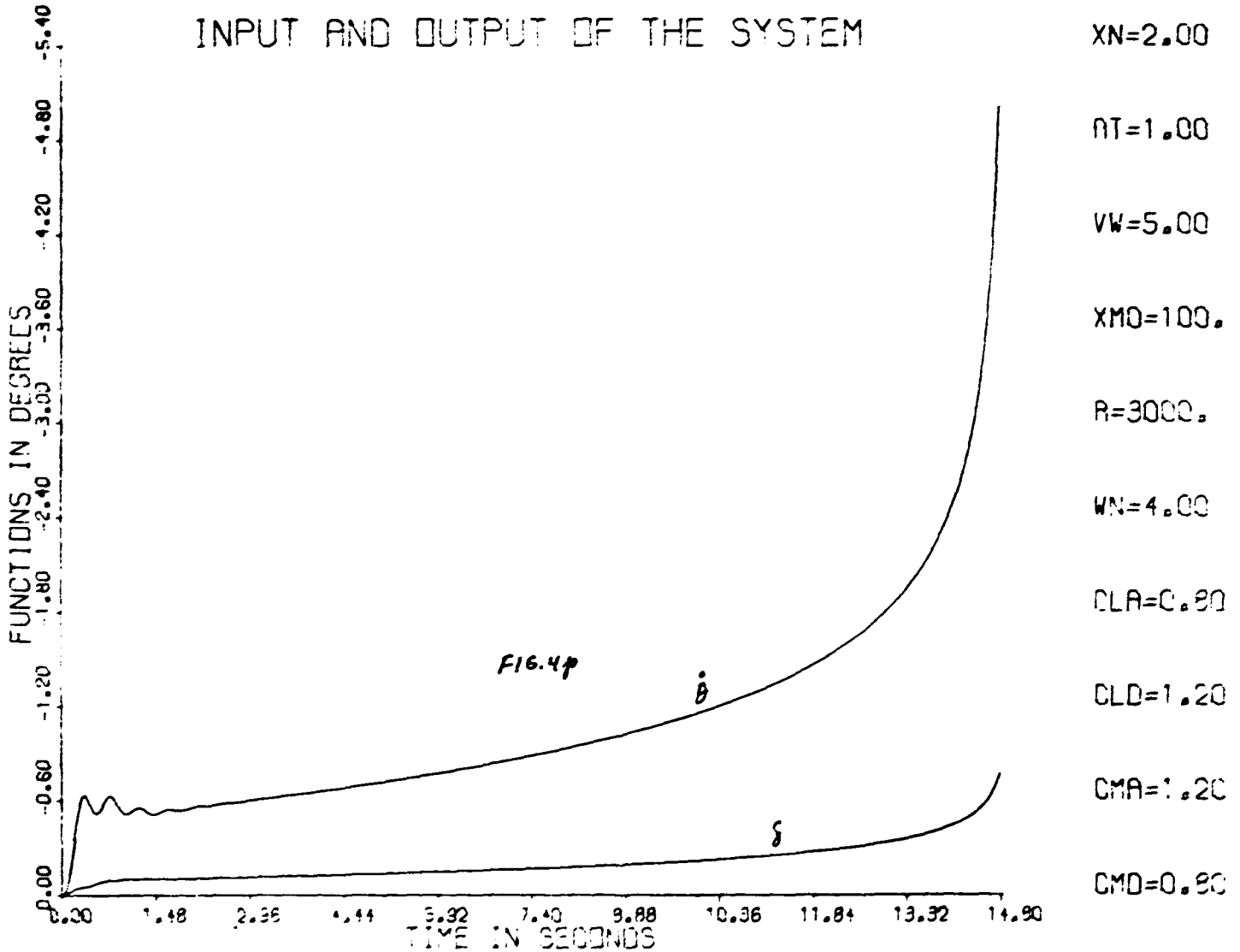
INPUT AND OUTPUT OF THE SYSTEM
FUNCTIONS IN DEGREES
-5.40
-4.80
-4.20
-3.60
-3.00
-2.40
-1.80
-1.20
-0.60
0.00
0.30
1.48
2.36
4.44
6.32
7.40
9.88
10.36
11.84
13.32
14.90
TIME IN SECONDS
$\dot{\beta}$
δ
XN=2.00
NT=1.00
VW=5.00
XMO=100.
R=3000.
WN=4.00
CLA=0.80
CLD=1.20
CMA=-.20
CMD=0.80

FIG. 4p

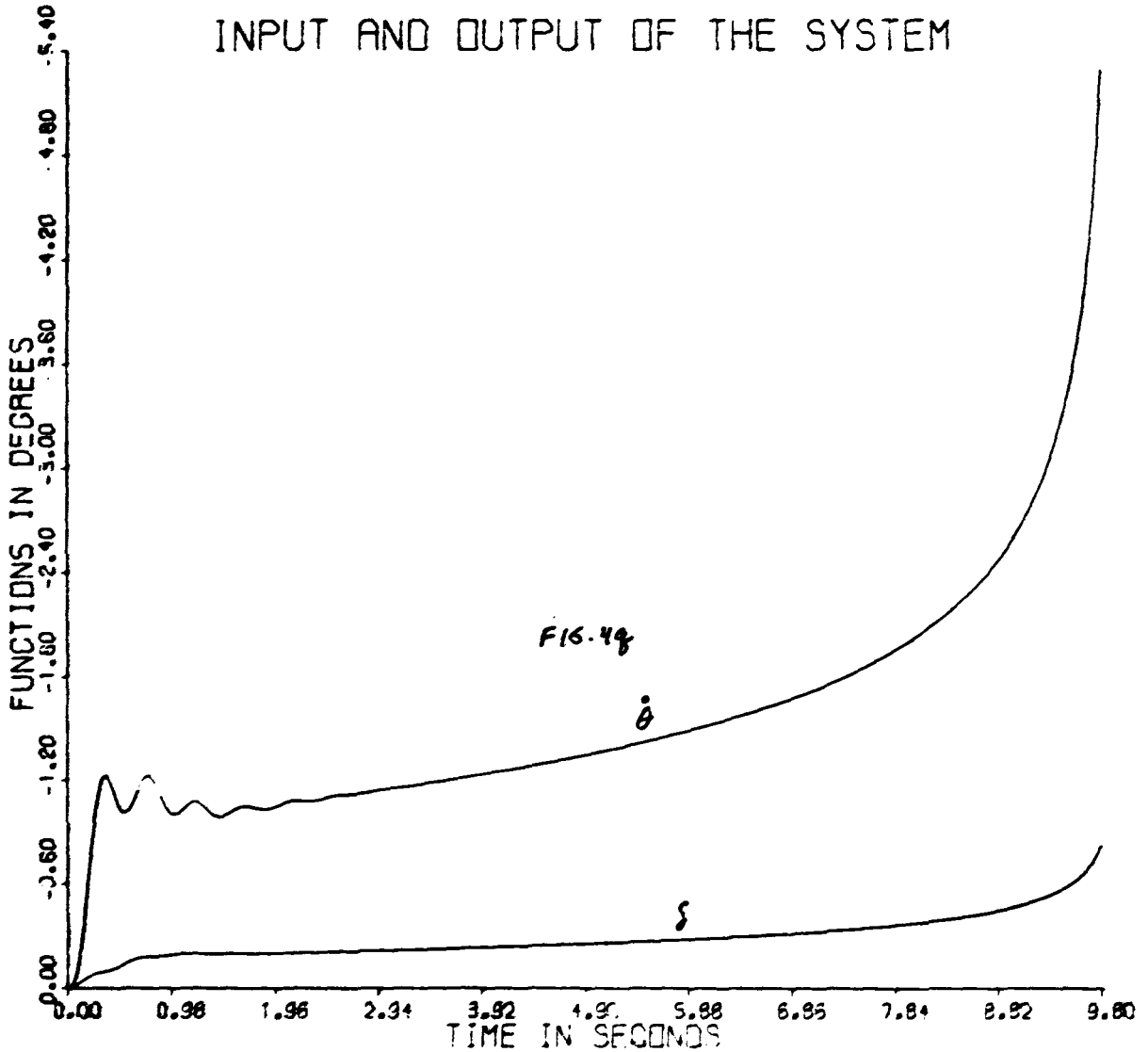

FIG. 4g

XN=2.00

AT=1.00

VW=5.00

XMO=100.

R=2000.

WN=4.00

CLA=0.80

CLD=1.20

CMA=1.20

CMD=0.80

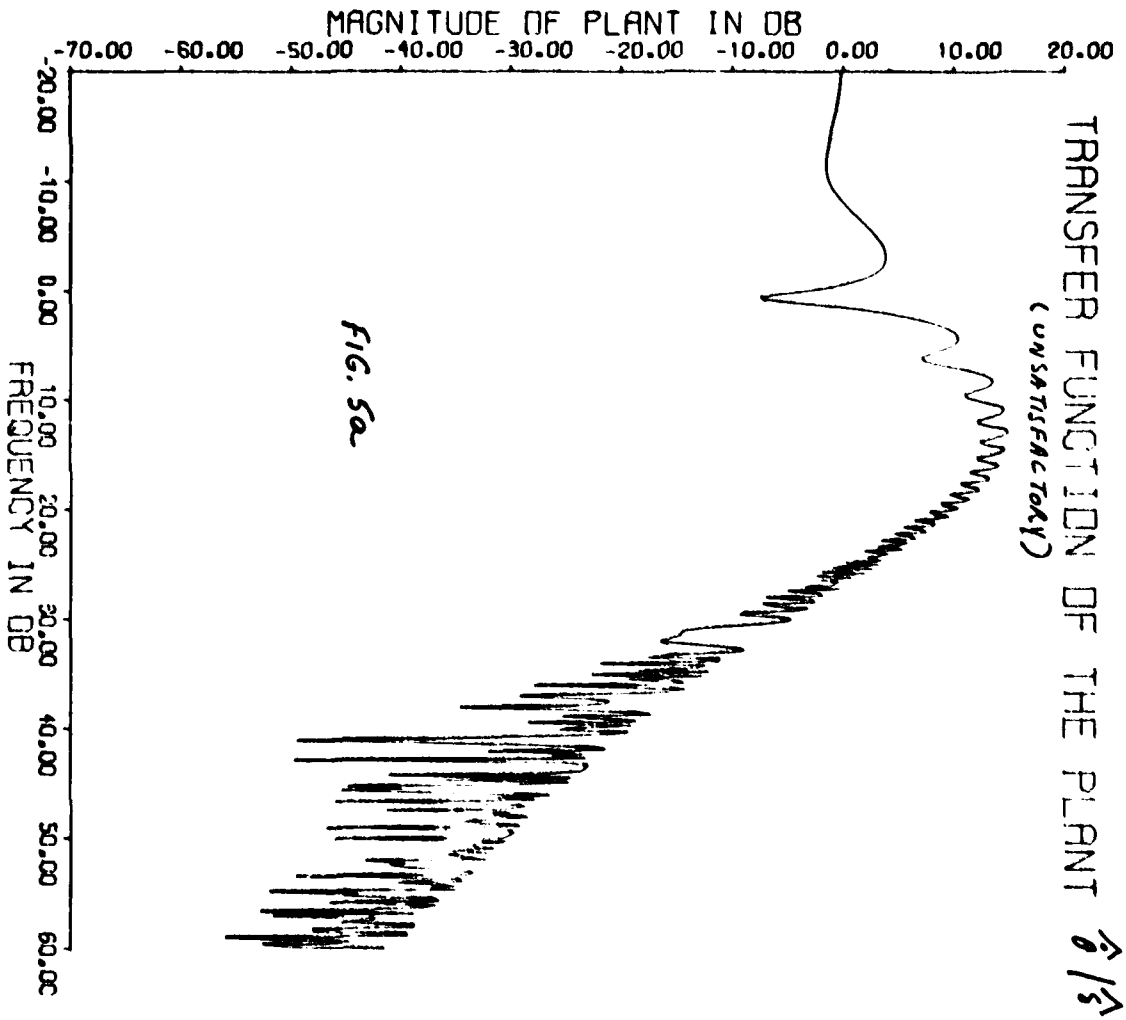
MAGNITUDE OF PLANT IN DB
-70.00
-60.00
-50.00
-40.00
-30.00
-20.00
-10.00
0.00
10.00
20.00
FREQUENCY IN DB
-20.00
-10.00
0.00
10.00
20.00
30.00
40.00
50.00
60.00
TRANSFER FUNCTION OF THE PLANT θ/δ
(UNSATISFACTORY)

FIG. 5a

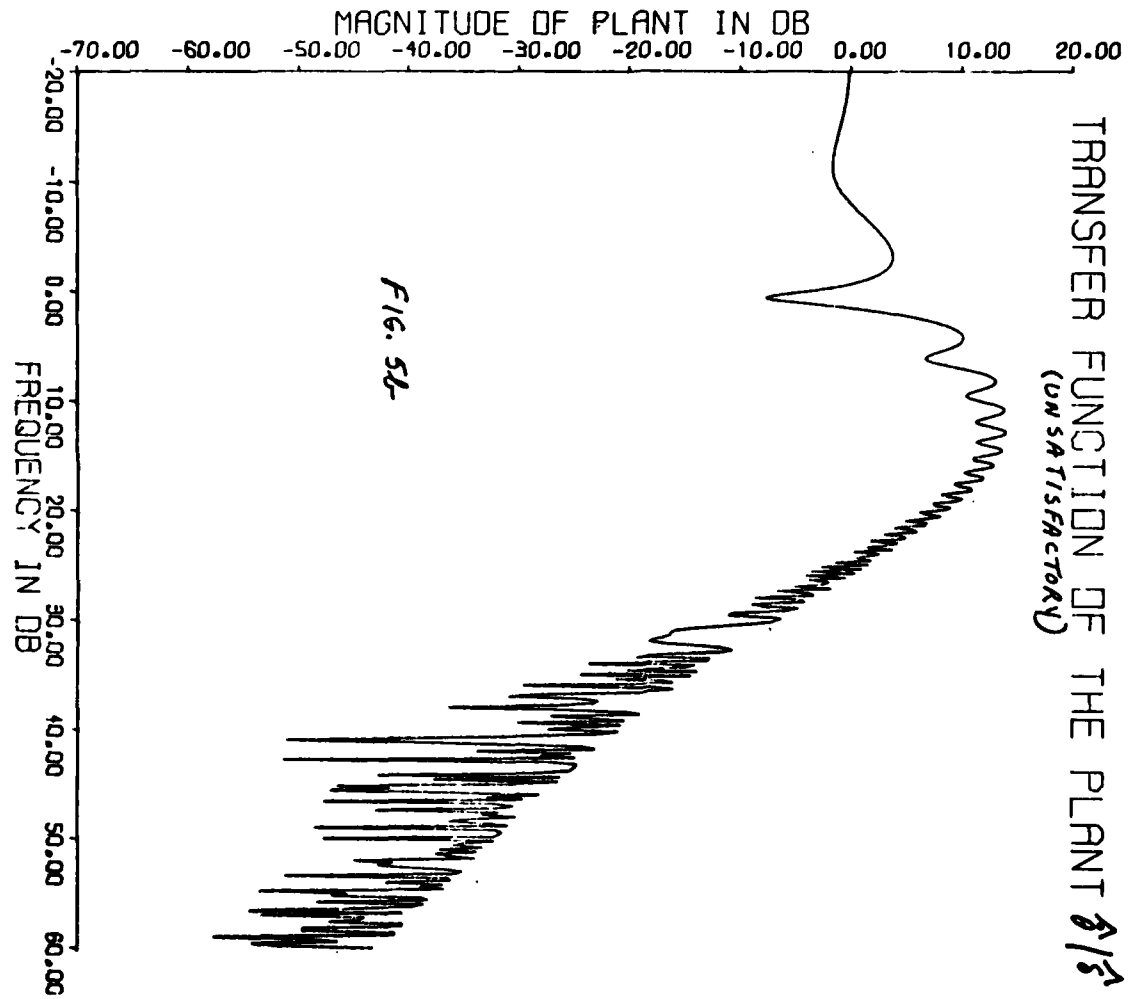

TRANSFER FUNCTION OF THE PLANT θ/δ
(UNSATISFACTORY)

FIG. 5A

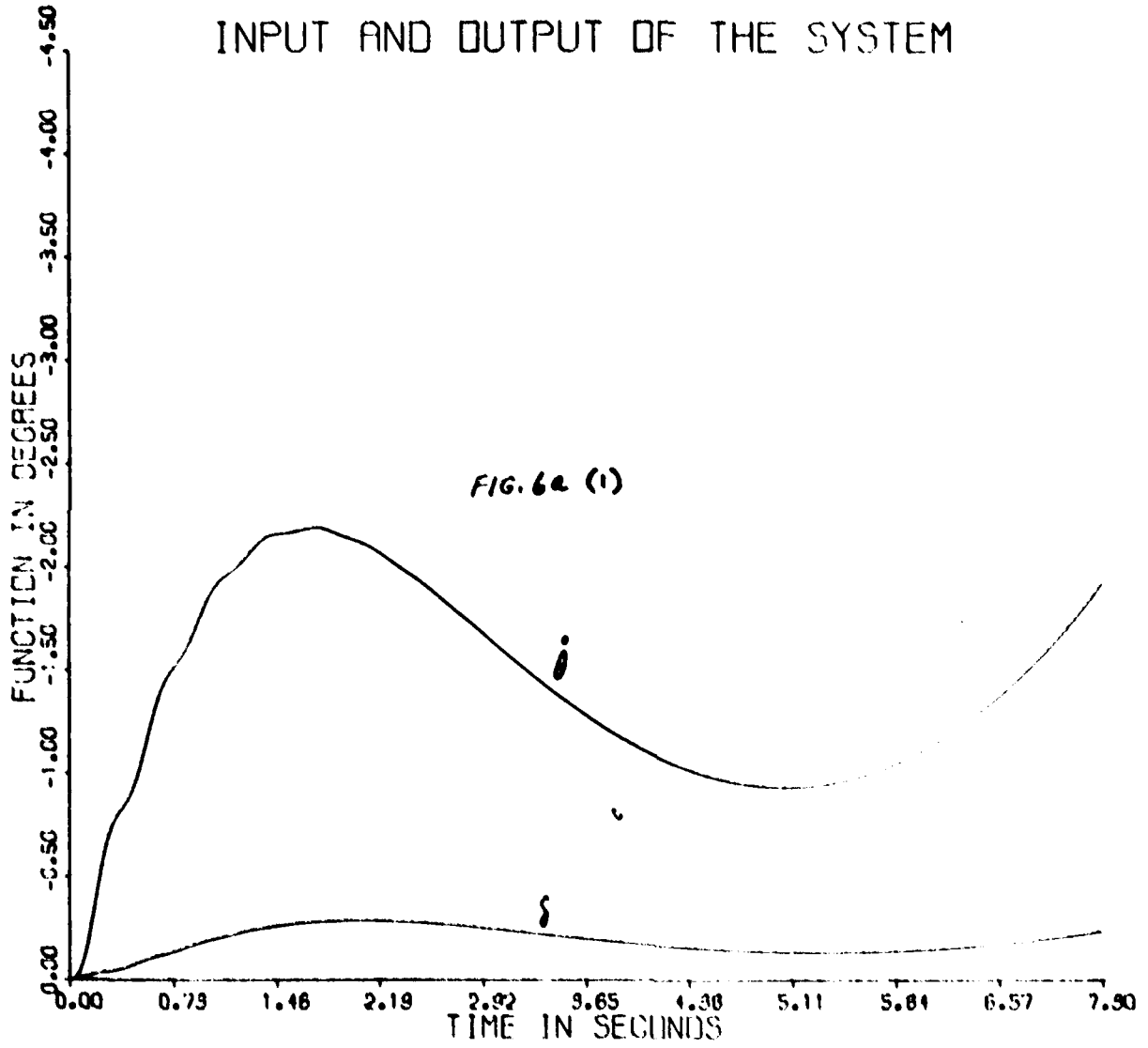
INPUT AND OUTPUT OF THE SYSTEM
FUNCTION IN DEGREES
-4.50
-4.00
-3.50
-3.00
-2.50
-2.00
-1.50
-1.00
-0.50
0.00
i
δ
0.00
0.73
1.46
2.19
2.92
3.65
4.38
5.11
5.84
6.57
7.30
TIME IN SECONDS

FIG. 6a (1)

,00
,00
).00
).
)0.
,00
.00
.00
.00
.00

TRANSFER FUNCTION OF THE PLANT

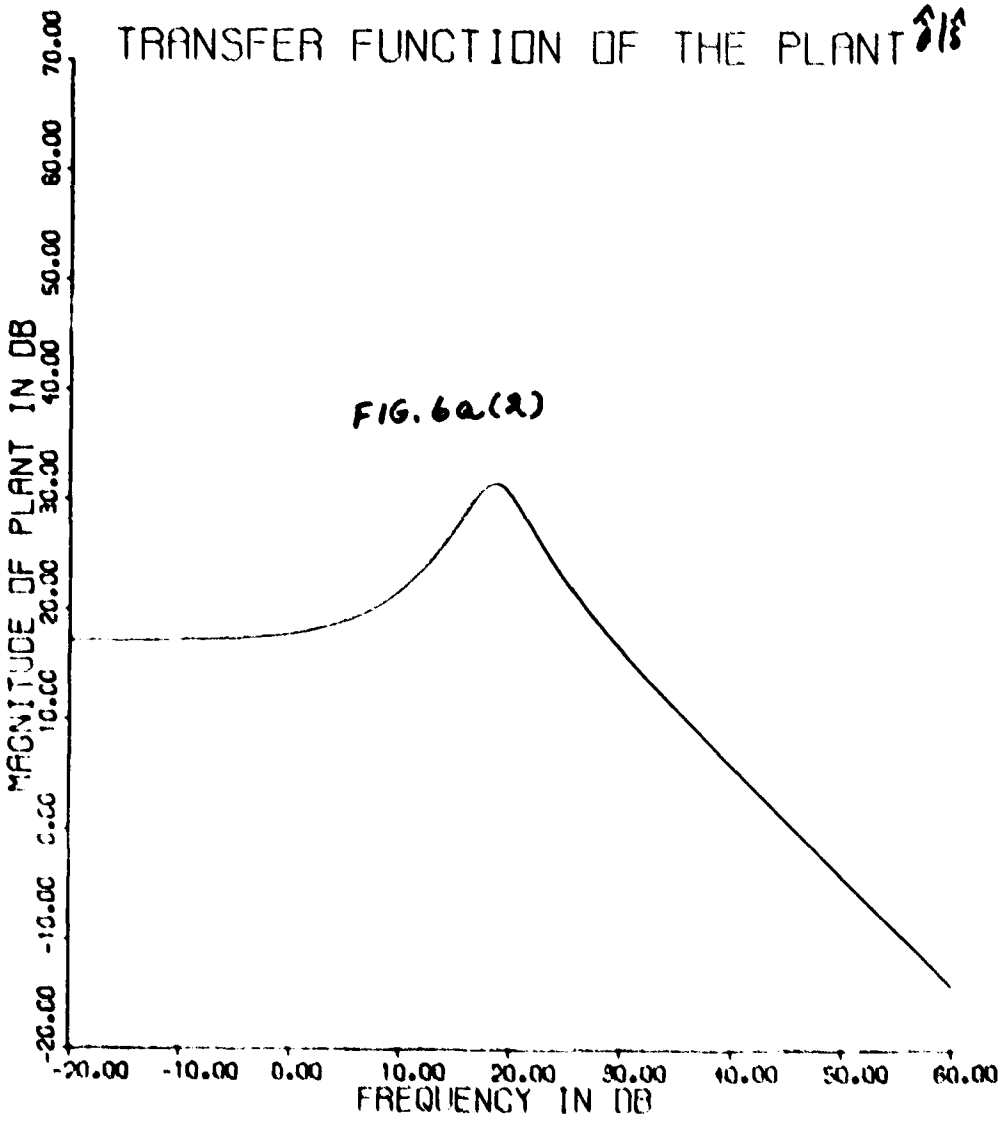

FIG. 6a(2)

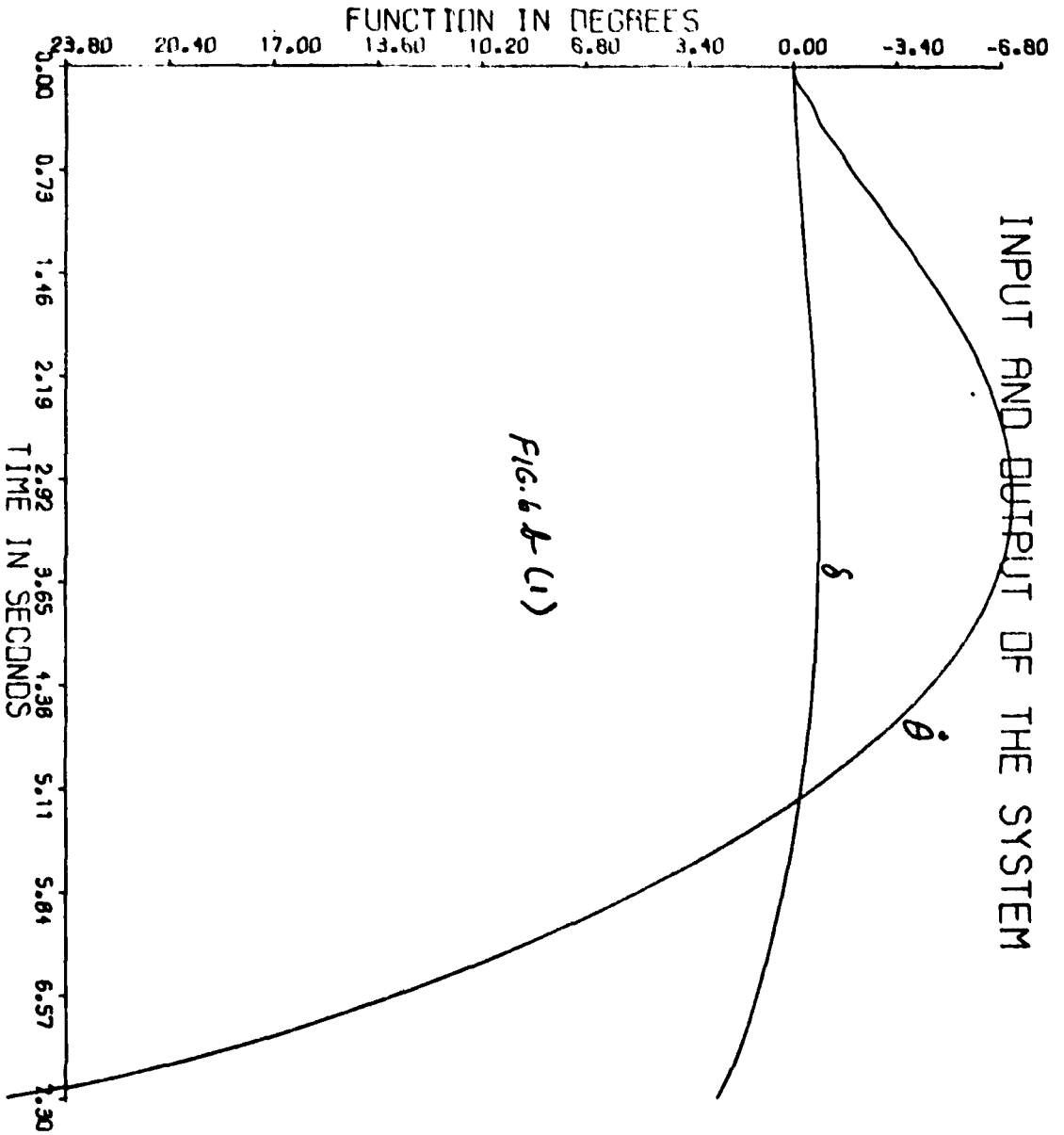
INPUT AND OUTPUT OF THE SYSTEM
FUNCTION IN DEGREES
23.80
20.40
17.00
13.60
10.20
6.80
3.40
0.00
-3.40
-6.80
TIME IN SECONDS
0.00
0.73
1.46
2.19
2.92
3.65
4.38
5.11
5.84
6.57
7.30
δ
θ̇

FIG. 6 & (1)

XN=4.00

RT=1.00

VW=10.00

XMO=200.

R=1500.

WN=1.00

CLA=1.20

CLD=1.20

CMA=1.20

CMD=1.20

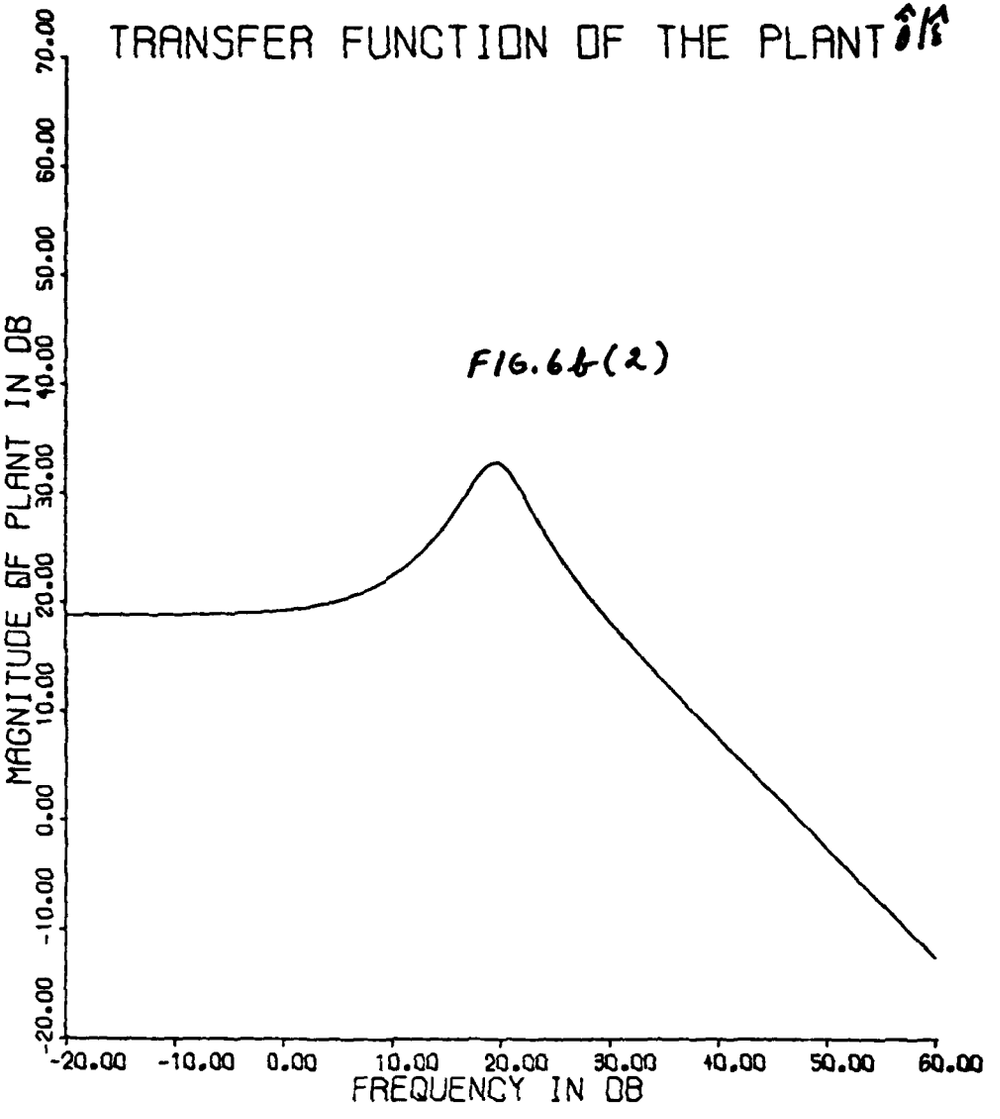

FIG. 6b(2)

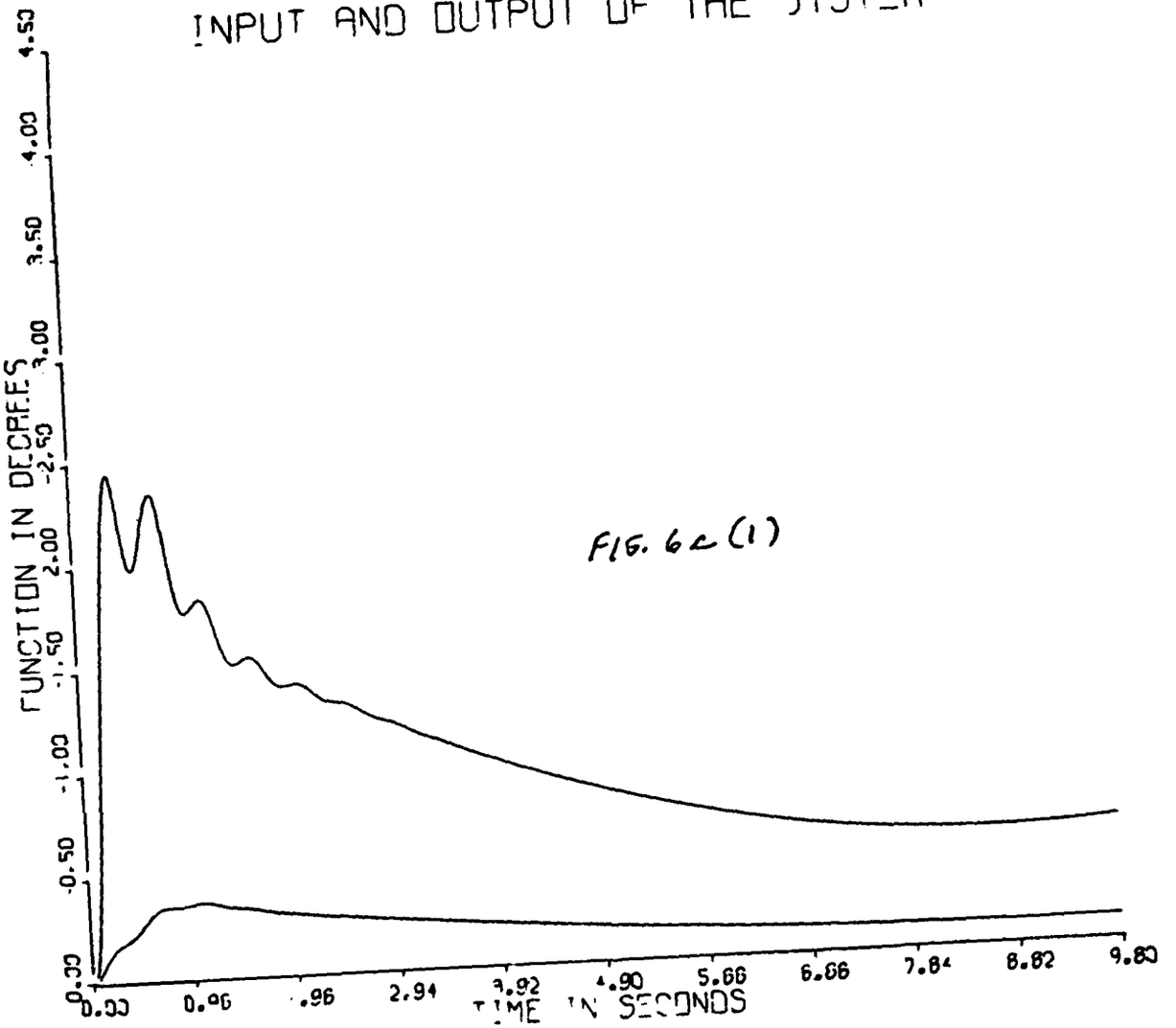
INPUT AND OUTPUT OF THE SYSTEM
FUNCTION IN DEGREES
4.50
4.00
3.50
3.00
2.50
2.00
1.50
1.00
0.50
0.00
-0.50
-1.00
0.00
0.98
1.96
2.94
3.92
4.90
5.88
6.86
7.84
8.82
9.80
TIME IN SECONDS

FIG. 6a (1)

XN=4.00

AT=1.00

VW=5.00

XMO=100.

R=2000.

WN=4.00

CLA=0.80

CLD=1.20

CMA=1.20

CMD=0.80

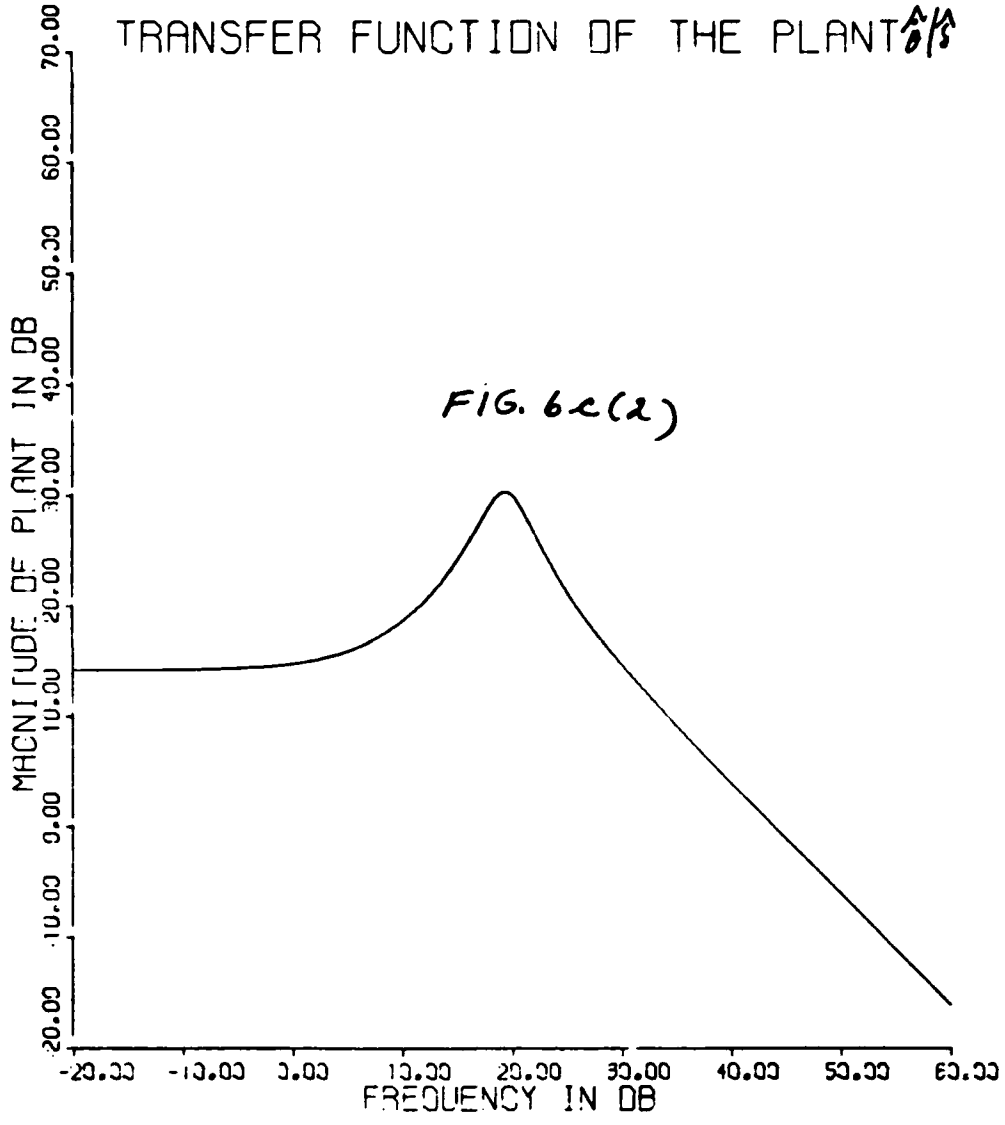

FIG. 6c(2)

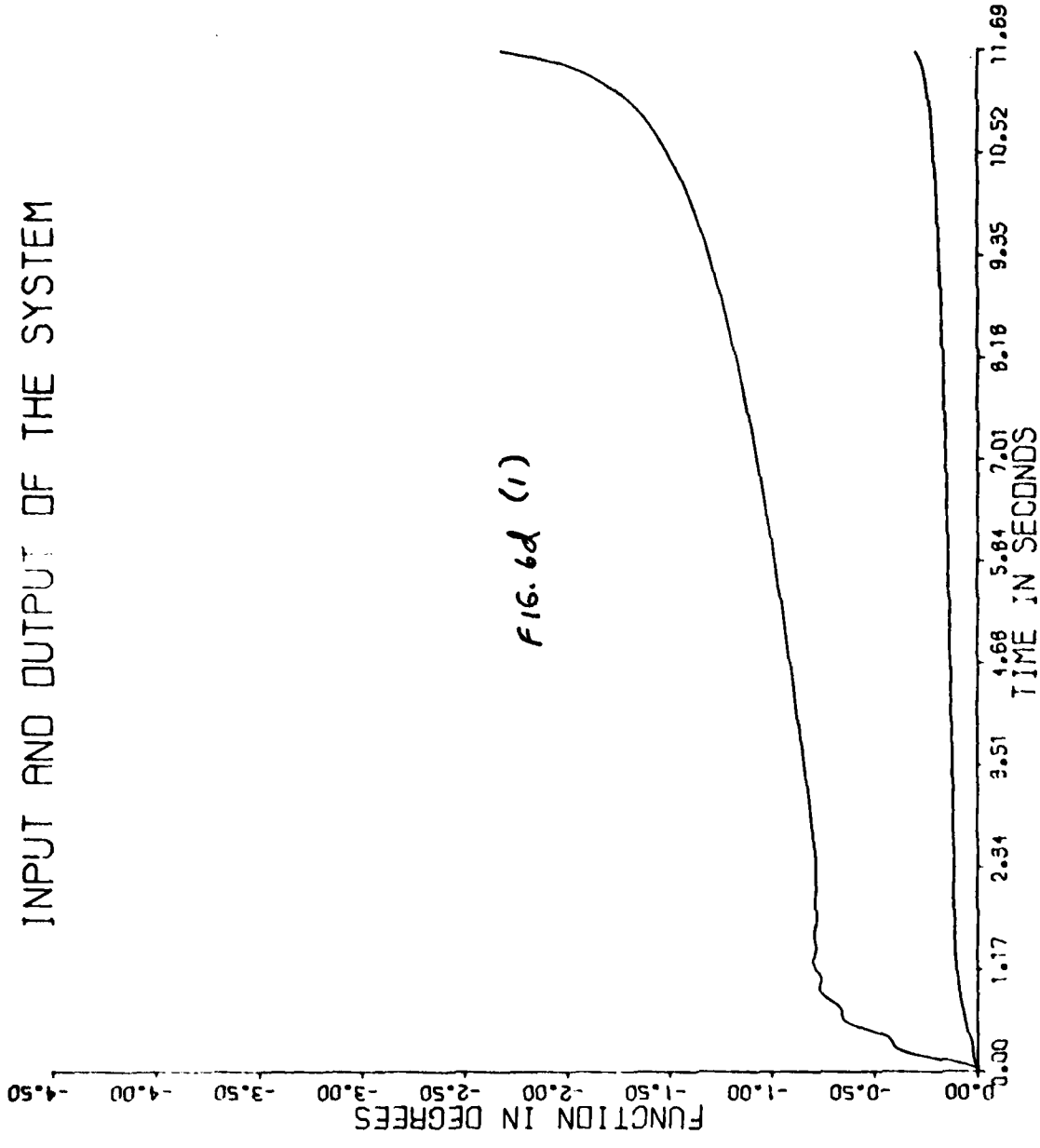
INPUT AND OUTPUT OF THE SYSTEM
FUNCTION IN DEGREES
0.00
-0.50
-1.00
-1.50
-2.00
-2.50
-3.00
-3.50
-4.00
-4.50
TIME IN SECONDS
0.00
1.17
2.34
3.51
4.68
5.84
7.01
8.18
9.35
10.52
11.69

FIG. 6d (1)

XN=2.42

AT=1.10

VW=7.67

XMO=31.

R=2378.

WN=2.63

CLA=1.10

CLD=0.83

CMA=1.08

CMD=0.98

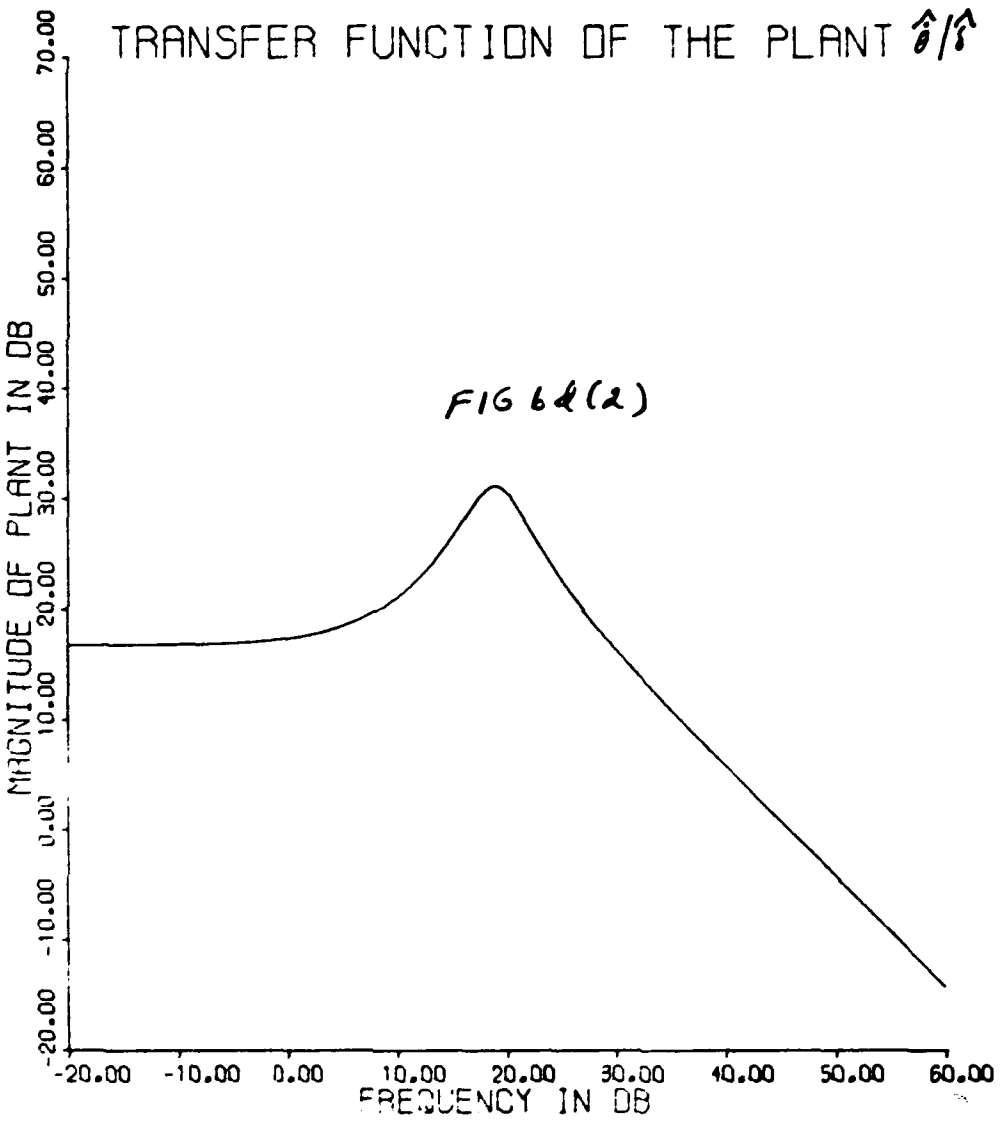

FIG 6.4(2)

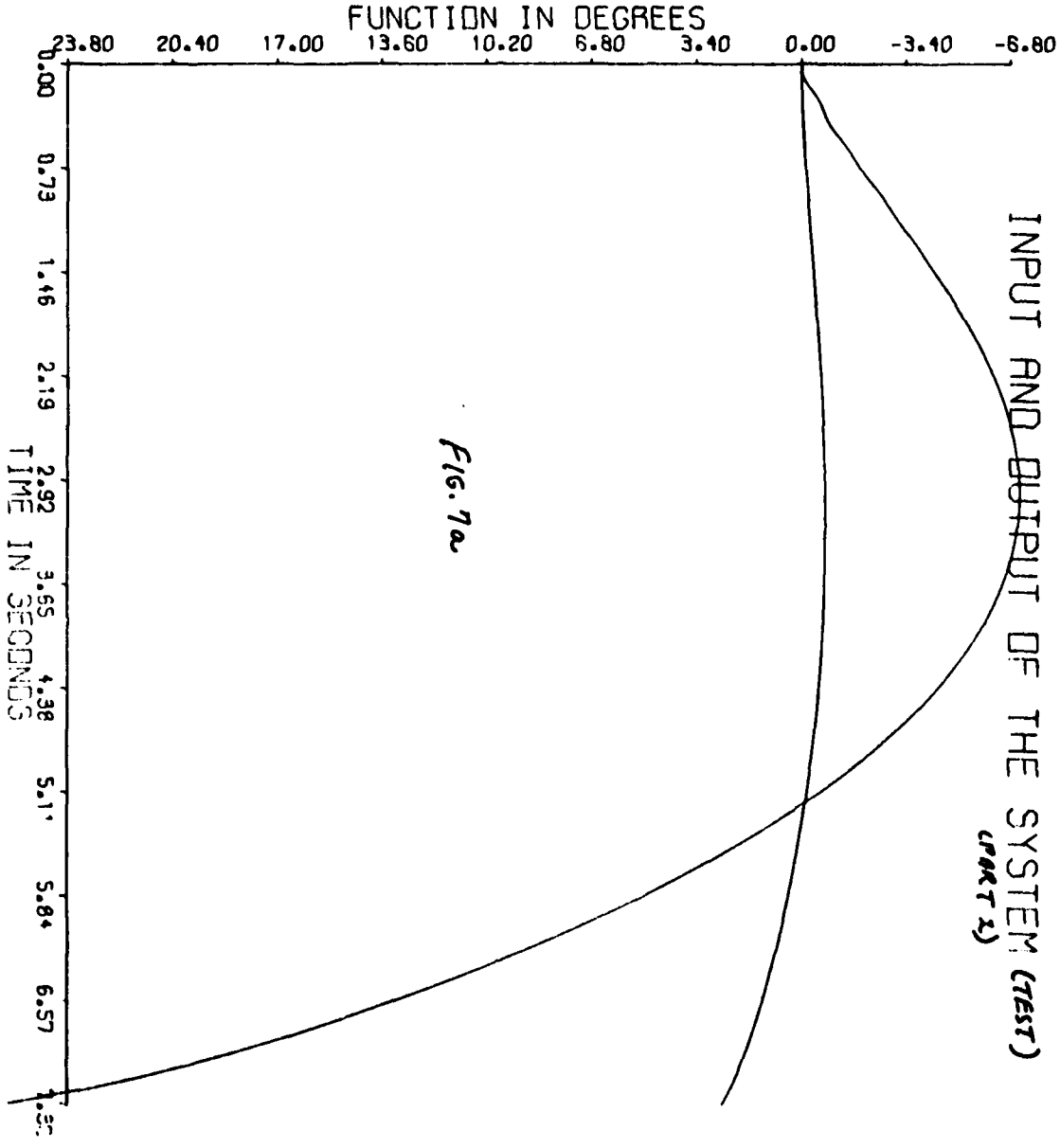
FUNCTION IN DEGREES
23.80
20.40
17.00
13.60
10.20
6.80
3.40
0.00
-3.40
-6.80
0.00
0.73
1.46
2.19
2.92
3.65
4.38
5.11
5.84
6.57
TIME IN SECONDS
INPUT AND OUTPUT OF THE SYSTEM (TEST)
(PART 2)

FIG. 7a

XN=4.00

AT=1.00

VW=10.00

XMO=200.

R=1500.

WN=1.00

CLF=1.20

CLO=1.20

CMF=1.20

CMO=1.20

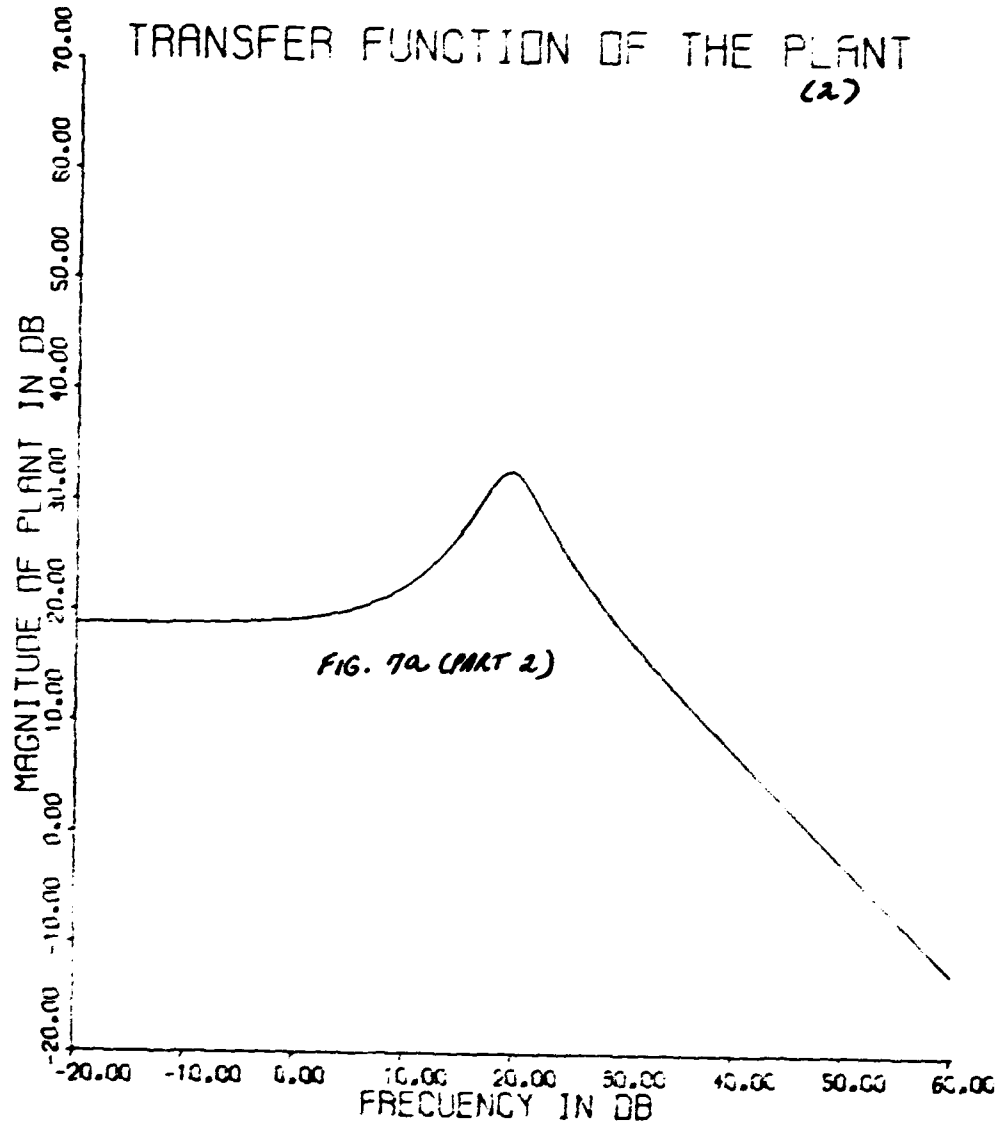

FIG. 7a (PART 2)

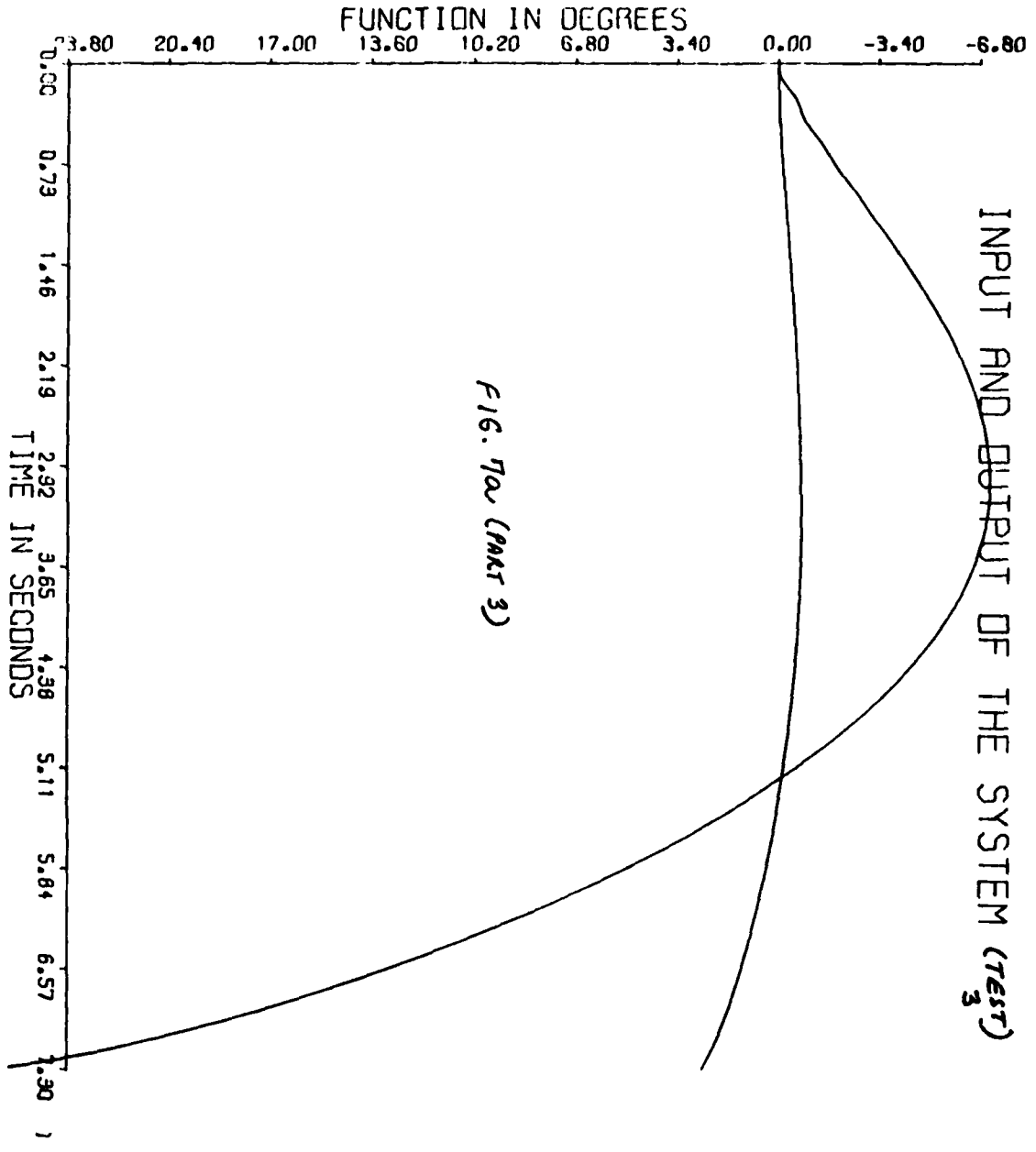
INPUT AND OUTPUT OF THE SYSTEM (TEST 3)
FUNCTION IN DEGREES
23.80
20.40
17.00
13.60
10.20
6.80
3.40
0.00
-3.40
-6.80
TIME IN SECONDS
0.00
0.73
1.46
2.19
2.92
3.65
4.38
5.11
5.84
6.57
7.30

FIG. 7a (PART 3)

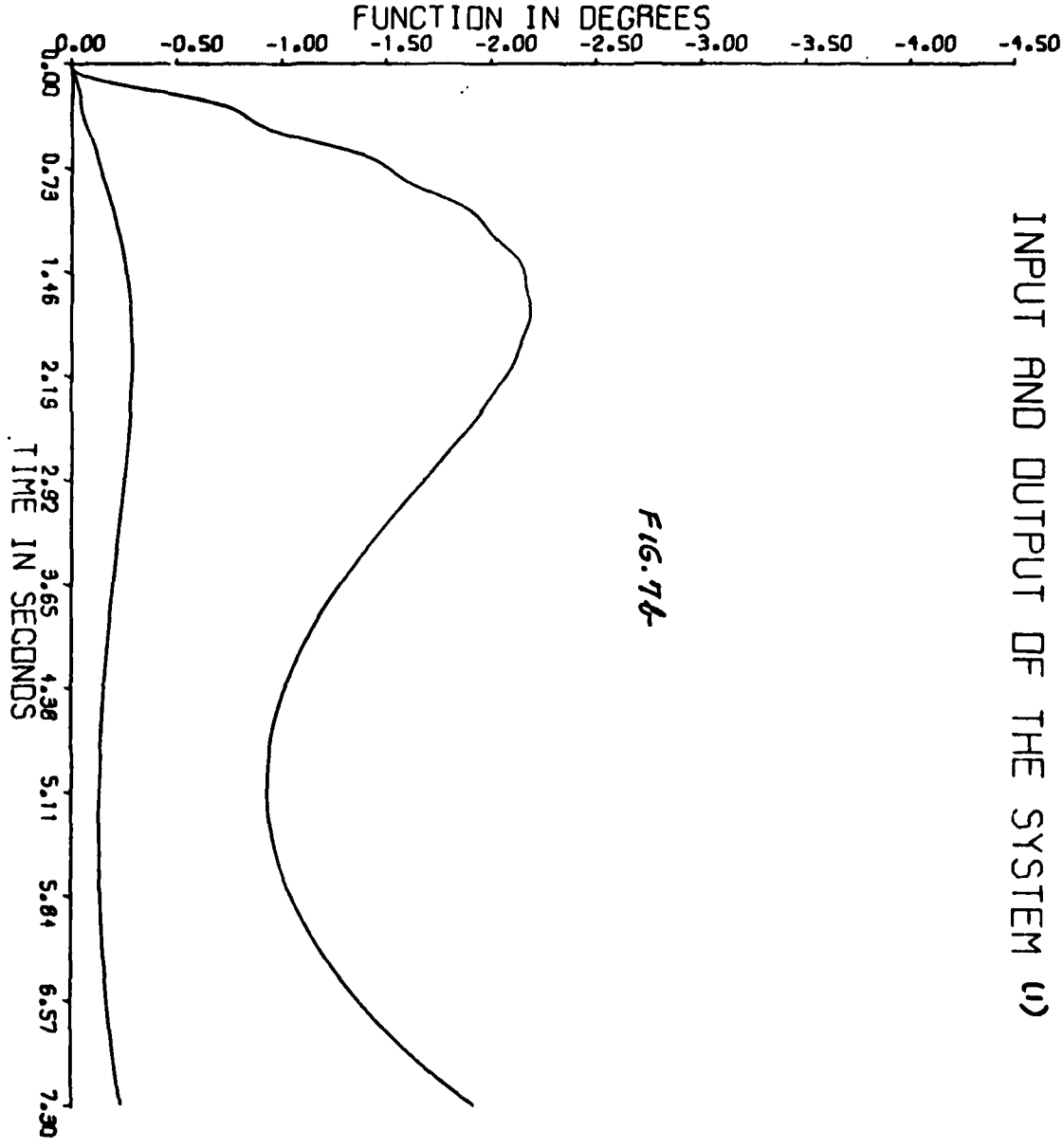

FIG. 7A

INPUT AND OUTPUT OF THE SYSTEM (1)

XN=4.00

AT=2.00

VW=10.00

XMO=0.

R=1500.

WN=2.00

CLA=1.00

CLD=1.00

CMA=1.00

CMD=1.00

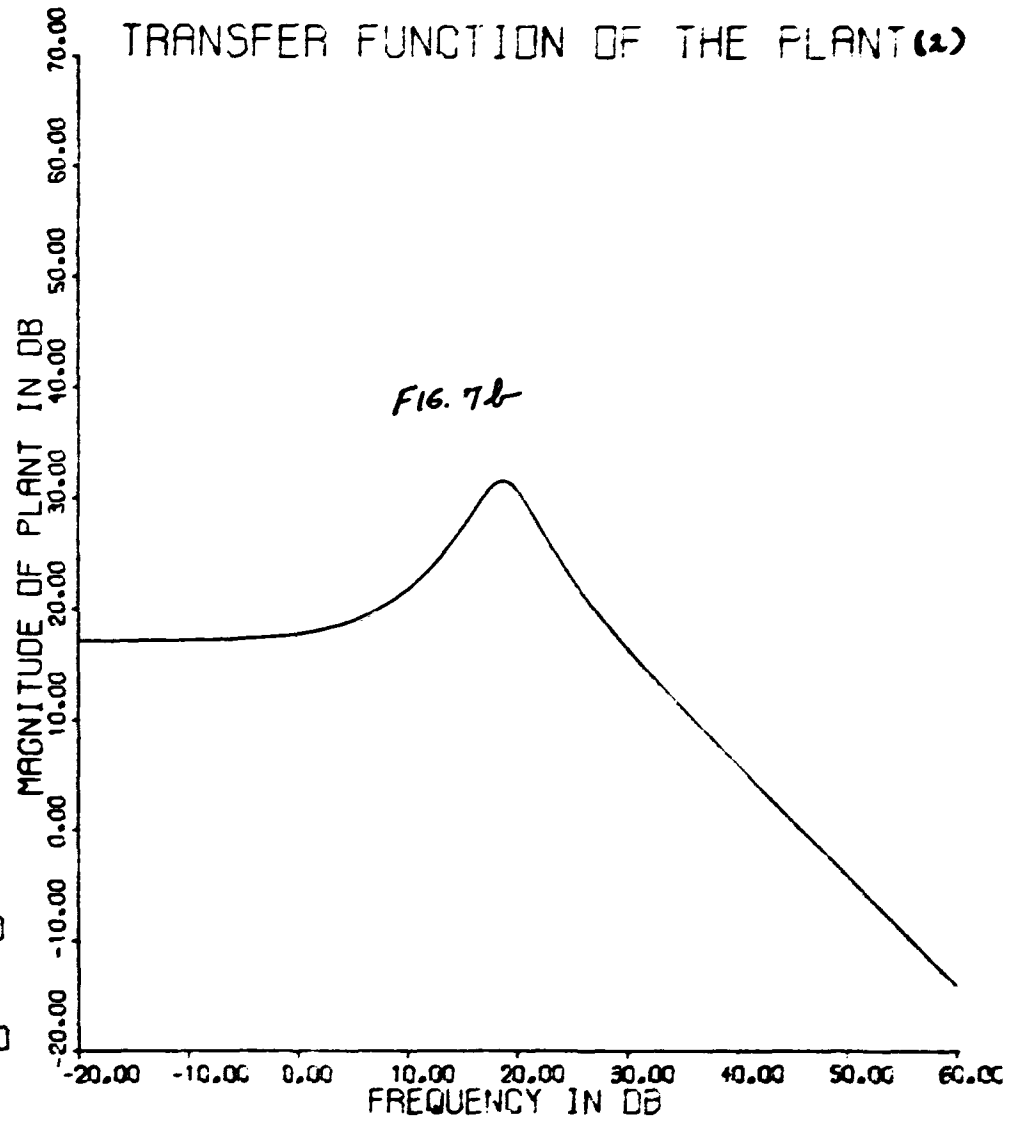

FIG. 7b

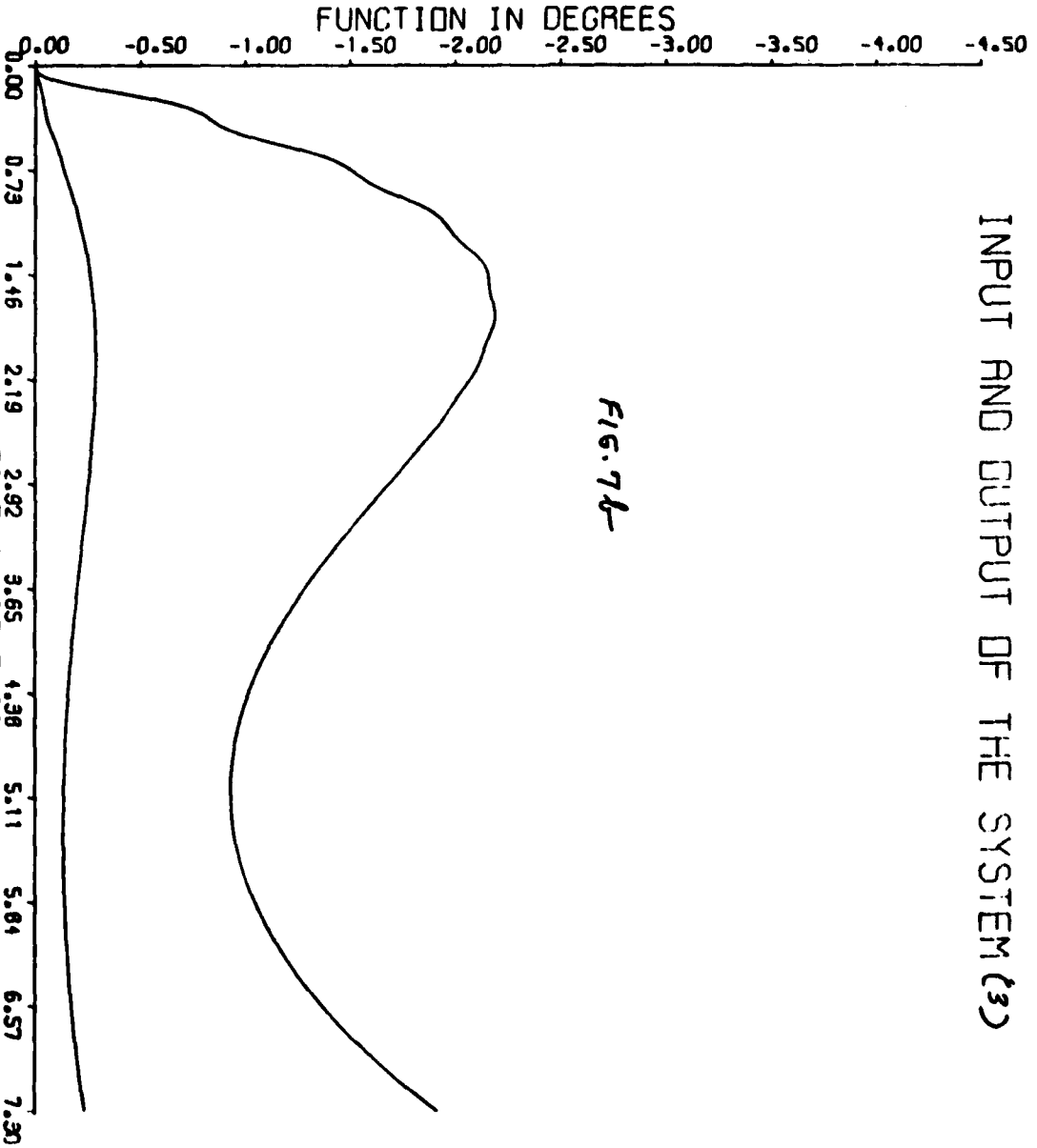

INPUT AND OUTPUT OF THE SYSTEM (3)

FIG. 7b

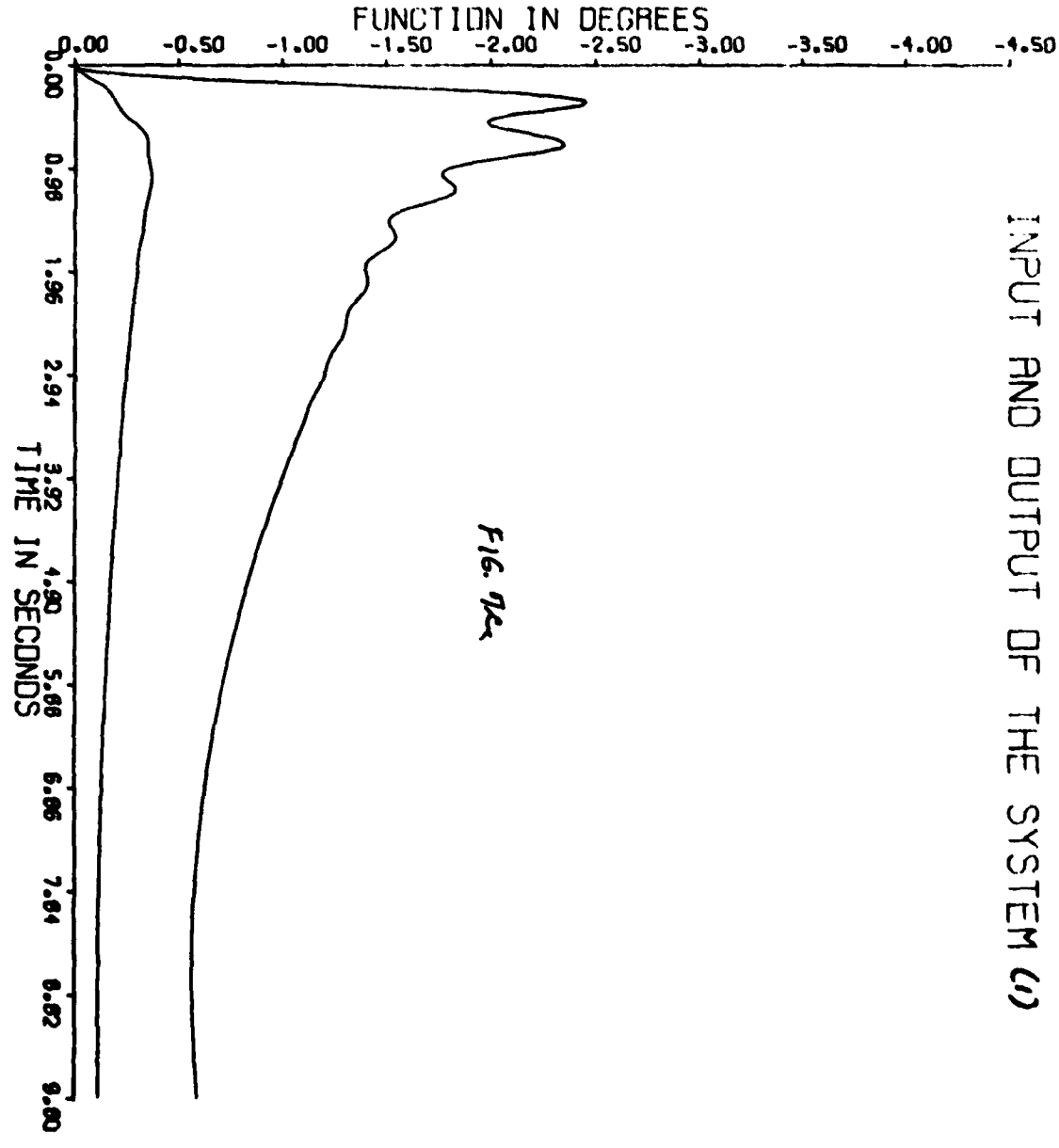

FIG. 11c

INPUT AND OUTPUT OF THE SYSTEM (1)

XN=4.00

AT=1.00

VW=5.00

XMO=100.

R=2000.

WN=4.00

CLA=0.80

CLD=1.20

CMA=1.20

CMD=0.80

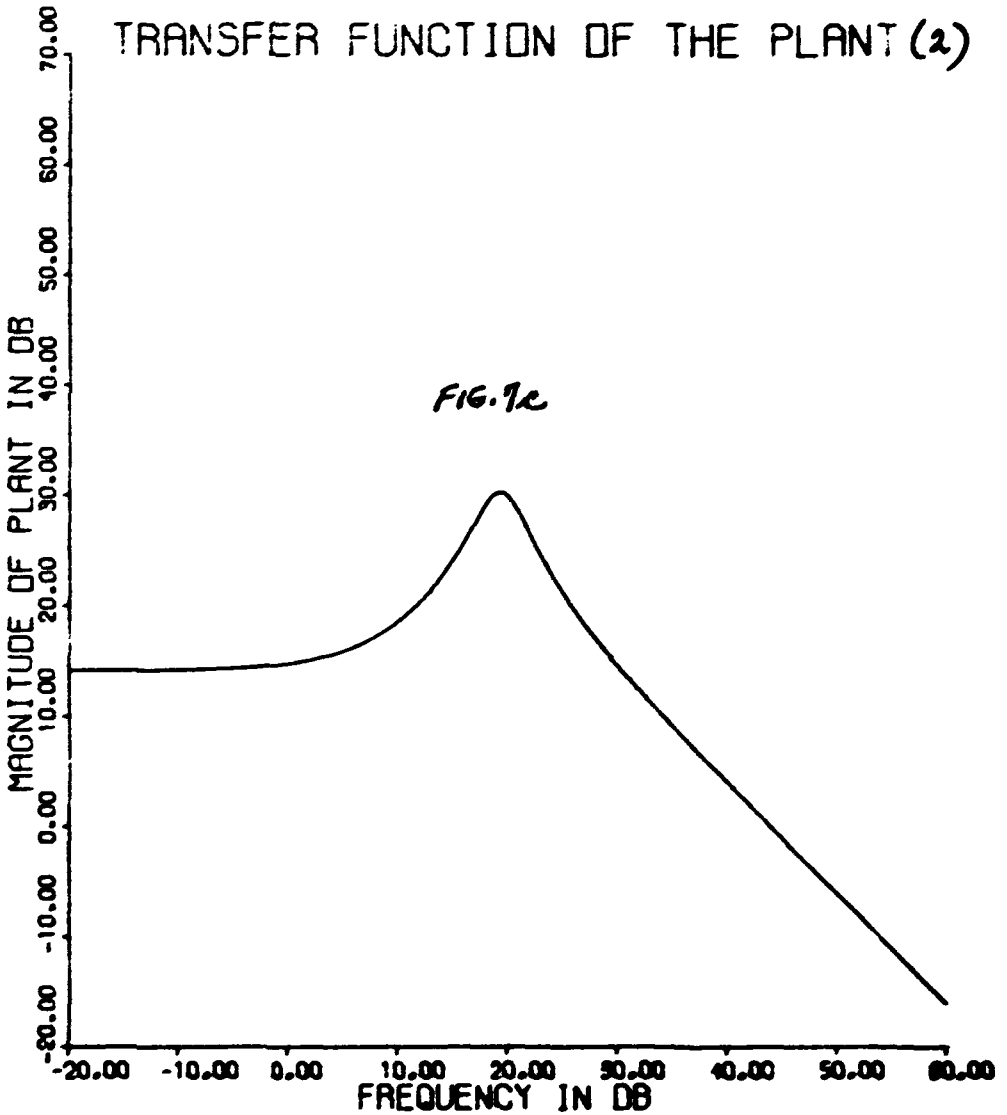

FIG. 7c

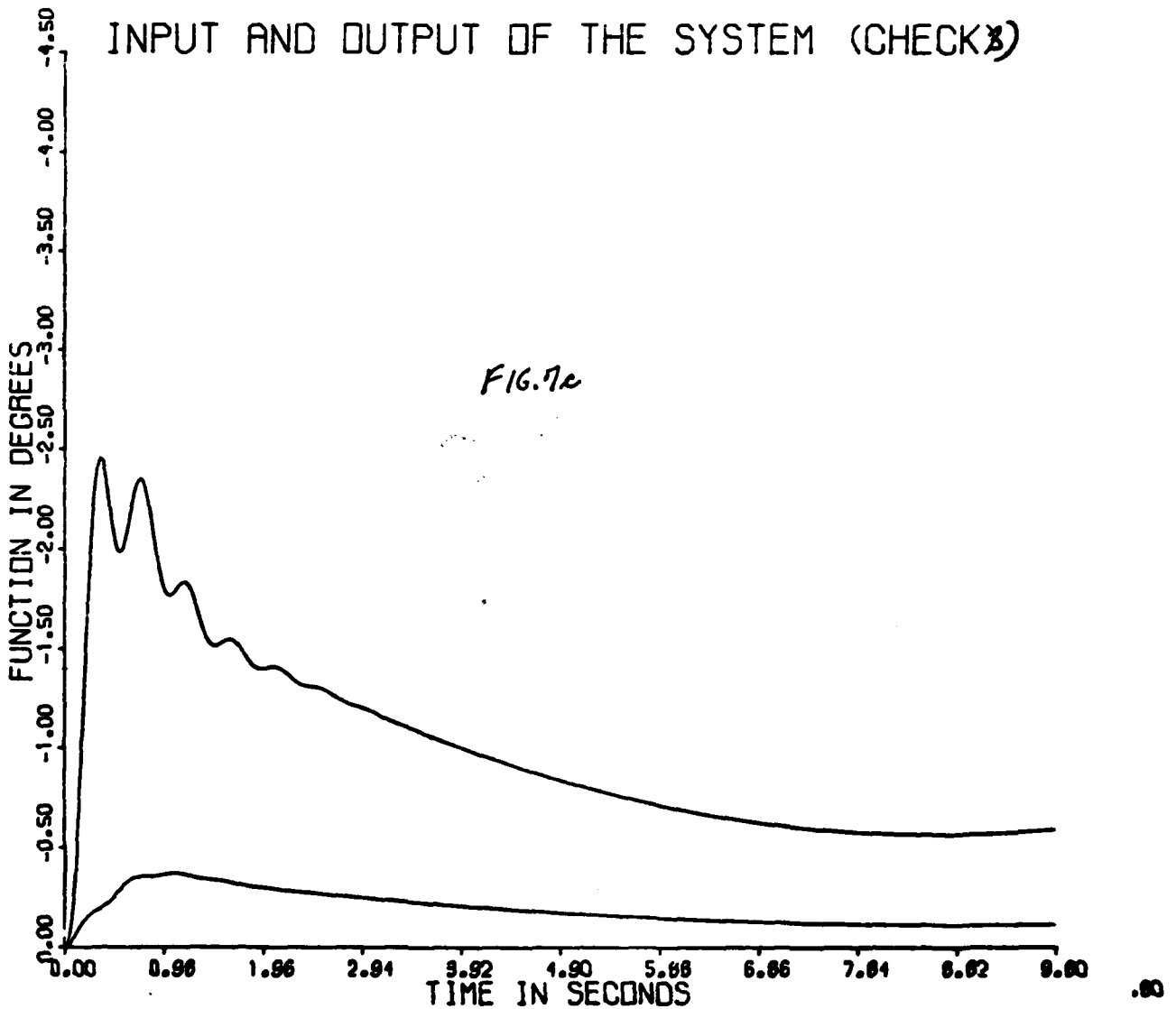
INPUT AND OUTPUT OF THE SYSTEM (CHECK)
FUNCTION IN DEGREES
0.00
-0.50
-1.00
-1.50
-2.00
-2.50
-3.00
-3.50
-4.00
-4.50
0.00
0.98
1.96
2.94
3.92
4.90
5.88
6.86
7.84
8.82
9.80
TIME IN SECONDS

FIG. 7c

.80

Figure 8 is used, in which the closed-loop transfer function is $T(s) = F(s)\frac{GP(s)}{1+GP(s)}$. It is assumed that the compensation networks F , G , whose power level can be very low (as the plant contains the power elements), can be constructed with negligible uncertainty in their transfer functions. Hence, due to the uncertainty in P ,

$$\Delta \ell n T = \Delta \ell n \frac{GP}{1+GP} = \Delta \ell n \frac{L}{1+L} \quad , \quad L = GP \tag{16}$$

and

$$\Delta \ell n |T(j\omega)| = \Delta \ell n \left| \frac{L(j\omega)}{1+L(j\omega)} \right| \quad . \tag{17}$$

There are given ω-domain specifications on $|T(j\omega)|$, as in Figure 9. Given that the maximum allowed change $\Delta \ell n |T(j\omega)| \leq \delta_1$ db for example at ω_1 in Figure 9 , what are the resulting constraints on $L(j\omega)$? It is convenient to pick a "nominal" plant $P_0(s)$, and derive the bounds on the resulting "nominal" loop function $L_0 = P_0 G$. These bounds can be found by means of a digital computer, but it is very useful for insight to see it done on the Nichols chart (logarithmic complex plane with abcissa in degrees, ordinate in decibels = 20 $\log_{10}$). The procedure is illustrated for the case

$$P(s) = \frac{ka}{s(s+a)} \quad ; \quad 1 \leq k \leq 10 \quad ; \quad 1 \leq a \leq 10 \quad . \tag{18}$$

At $\omega = 2$ rps , $P(j2)$ lies within the boundaries given by ABCD in Figure 10. Since $\ell nL = \ell nG + \ell nP$, the pattern outlined by ABCD may be translated, but not rotated, on the Nichols chart, the amount of translation being given by the value of $\ell nG(j2)$. For example, if a trial design of $L(j2)$ corresponds to the template $P(j2)$ at A'B'C'D' in Figure 10, then

$$\begin{aligned} |G(j2)|_{db} &= |L(j2)|_{db} - |P(j2)|_{db} \\ &= (-2.0) - (-13.0) = 11.0 \text{ db} \end{aligned} \tag{19a}$$

$$\begin{aligned} \text{Arg } G(j2) &= \text{Arg } L(j2) - \text{Arg } P(j2) \\ &= (-60°) - (-153.4°) = 93.4° \quad . \end{aligned} \tag{19b}$$

3.4.2. Bounds on $L(j\omega)$ in the Nichols chart

The templates of $P(j\omega)$ are manipulated to find the position of $L(j\omega)$ which results in the specifications of Figure 9 on $\ell n|T(j\omega)|$ being satisfied. Taking the $\omega = 2$ template, one tries, for example, positioning it, as shown

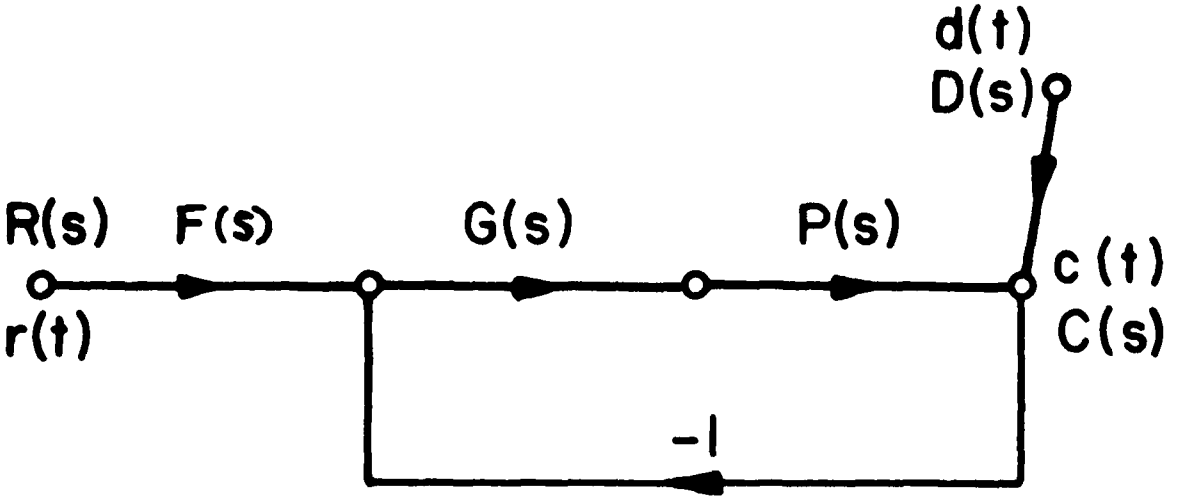

FIGURE 8 LTI two-degree-of-freedom structure.

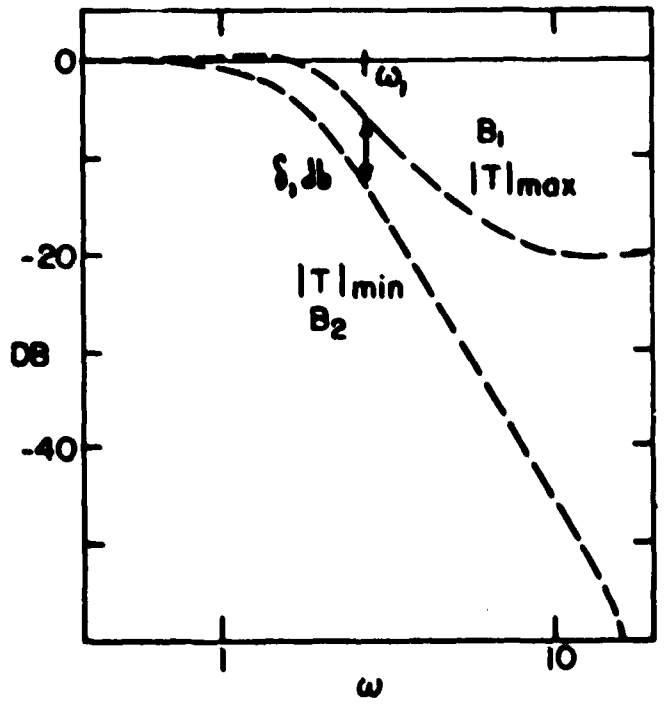

FIGURE 9 Bounds on $|T(j\omega)|$.

in Figure 10, at A'B'C'D'. Contours of constant $\ell n|L/(1+L)|$ are available on the Nichols chart. Using these contours, it is seen that the maximum change in $\ell n|L/(1+L)|$, which from (17) is the maximum change in $\ell n|T|$ is, in this case, very closely $(-0.49) - (-5.7) = 5.2$ db, the maximum being at point C', the minimum at point A'. Suppose that the specifications tolerate a change of 6.5 db at $\omega = 2$, so the above trial position of $|L(j2)|$ is in this case more than satisfactory. The template is lowered on the Nichols chart to A"B"C"D", where the extreme value of $\ell n|L/(1+L)|$ are at C" (-0.7 db), A" (-7.2 db). Thus if Arg $L_A(j2) = -60°$, then -4.2 db is the smallest magnitude of $L_A(j2)$ which satisfies the 6.5 db specification for $\Delta\ell n|T|$. Any larger magnitude is satisfactory but represents over-design at that frequency. The manipulation of the $\omega = 2$ template is repeated along a new vertical line, and a corresponding new minimum of $|L_A(j2)|$ found. Sufficient points are obtained in this manner to permit drawing a continuous curve of the bound on $L_A(j2)$, as shown in Figure 10. The above is repeated at other frequencies, resulting in a family of boundaries on $L_A(j2)$.

3.4.3. Nature of the bounds on $L(j\omega)$

A typical set of bounds is shown in Figure 11. The bounds tend to move down in the Nichols chart (become less onerous), obviously because as ω increases, greater change in $|T(j\omega)|$ is permitted, as in Figure 9. It is in fact essential that at large enough ω, the uncertainty in $|T(j\omega)|$ (i.e., the bounds on $|T(j\omega)|$) be greater than the uncertainty in $P(j\omega)$, because the net sensitivity reduction is always zero in any practical system as was long ago [4] shown by Bode,

$$\int_0^\infty \ell n|S_P^T(j\omega)|d\omega = -\int_0^\infty \ell n|1 + L(j\omega)|d\omega = 0 \qquad (20)$$

where $S_P^T = \frac{\partial T/T}{\partial P/P}$ is the sensitivity function.

In the above example, as $\omega \to \infty$, $P \to ka/s^2$, so $\Delta\ell n|P| \to \Delta\ell n(ka) = 40$ db. Note in Figure 9 that the permitted $\Delta\ell n|T(j\omega)| >> 40$ db for $\omega > 50$. Such large tolerances on $|T(j\omega)|$ at large ω are tolerable because $|T(j\omega)|$ is negligible at large ω, e.g., if $|P(j\omega)|$ can change at most by 40 db at large ω but $|T(j\omega)|$ changes by 52 db, who cares if this 52 db change is from $|T|_{min} = 10^{-6}$ to $|T|_{max}$ to 400×10^{-6}. In return, one can

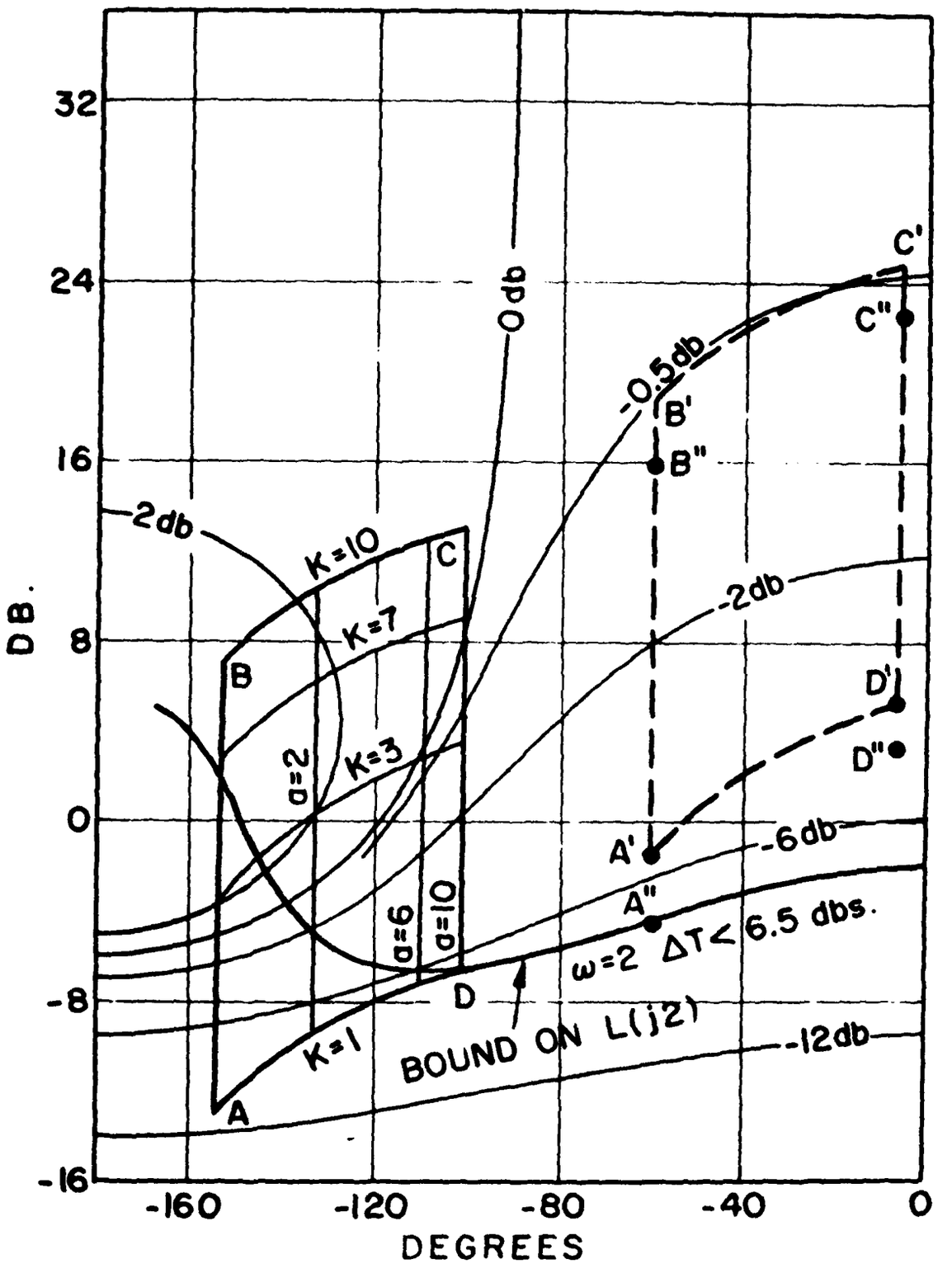

FIGURE 10 Derivation of bo[illegible] in Nichols chart.

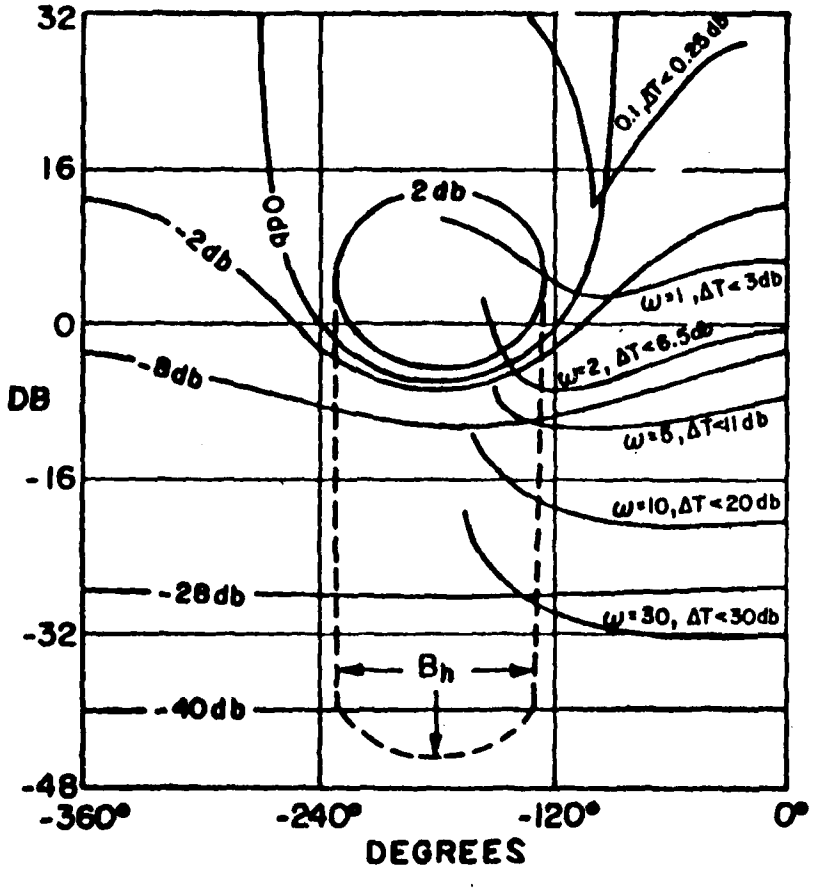

FIGURE 11 Typical bounds on $L_o(j\omega)$ at low and medium frequencies.

concentrate the sensitivity reduction over the bandwidth of $T(j\omega)$. Thus, although $|P(j\omega)|$ in this region vales by say 40 db, $|T(j\omega)|$ may be controlled to vary by only 4 db, or 0.04 db if desired.

3.4.4. Universal high-frequency boundary

As noted, in the high-frequency range $\Delta\ell n|T(j\omega)|$ must realistically be allowed to be $>> \Delta\ell n|P(j\omega)|$, and this is reflected in the bounds on $L_0(j\omega)$ tending to a very narrow pencil. In Figure 12, B_ν^P is drawn for the case $\Delta\ell nL = \Delta\ell nk = 20$ db , $\Delta\ell n|T(j\omega)| = \Delta\ell n|L/(1+L)| \leq 23$ db at ω_ν . However, the resulting peak value of $|L/(1+L)|$ is 23 db = 14.1 arithmetic at $k = k_{max}$, indicating a highly under-damped pole pair at the corresponding frequency with damping ratio $\zeta = 0.034$, when $k = k_{max}$. This tremendous peaking does not appear in the system response to the command inputs R , because it is filtered out by the pre-filter F in Figure 8. But the system response to a disturbance D is given by $T_d = C/D = (1+L)^{-1}$. Disturbance attenuation generates its own requirements on L , which may lead to more stringent bounds on L than those due to $T(j\omega)$. The final contours used in the design [3] must be the most stringent composite of the two. However, even if D is very small, it is usually certain that a peak $|T_d|$ of 14.1 is intolerable. It is reasonable to add a requirement $|T_d| \leq \gamma$ some constant, for all ω and over the whole range of P parameter values. The resulting constraining contours denoted by B_h^d are shown in Figure 12 for the case $\Delta\ell nk = 20$ db , and for $\gamma = 2.3, 3.5, 5$ db (all these contours are symmetrical with respect to the verical line Arg $L = -180°$ on the Nichols' chart). If $\gamma = 5$ db is used, then $B(\omega_\nu)$ indicates the composite contour shown in Figure 12. For $\omega > \omega_\nu$, $|\Delta T(j\omega)|$ increase while γ remains the same, so that sooner or later there is reached a frequency $\omega_\gamma \ni B(\omega)$ is a fixed boundary B_h^d , effective $\forall\, \omega > \omega_\gamma$.

3.4.5. The optimum $L(j\omega)$

It has been shown [5] a realistic definition of optimum in the lti system is the minimization of k , defined by $\lim_{s \to \infty} L(s) = ks^{-e}$, where e is the excess of poles over zeros assigned to $L(s)$.

It has been proven [5] that the optimum L lies on its boundary B_i at each ω_i and that such an optimum exists and is unique. Most important

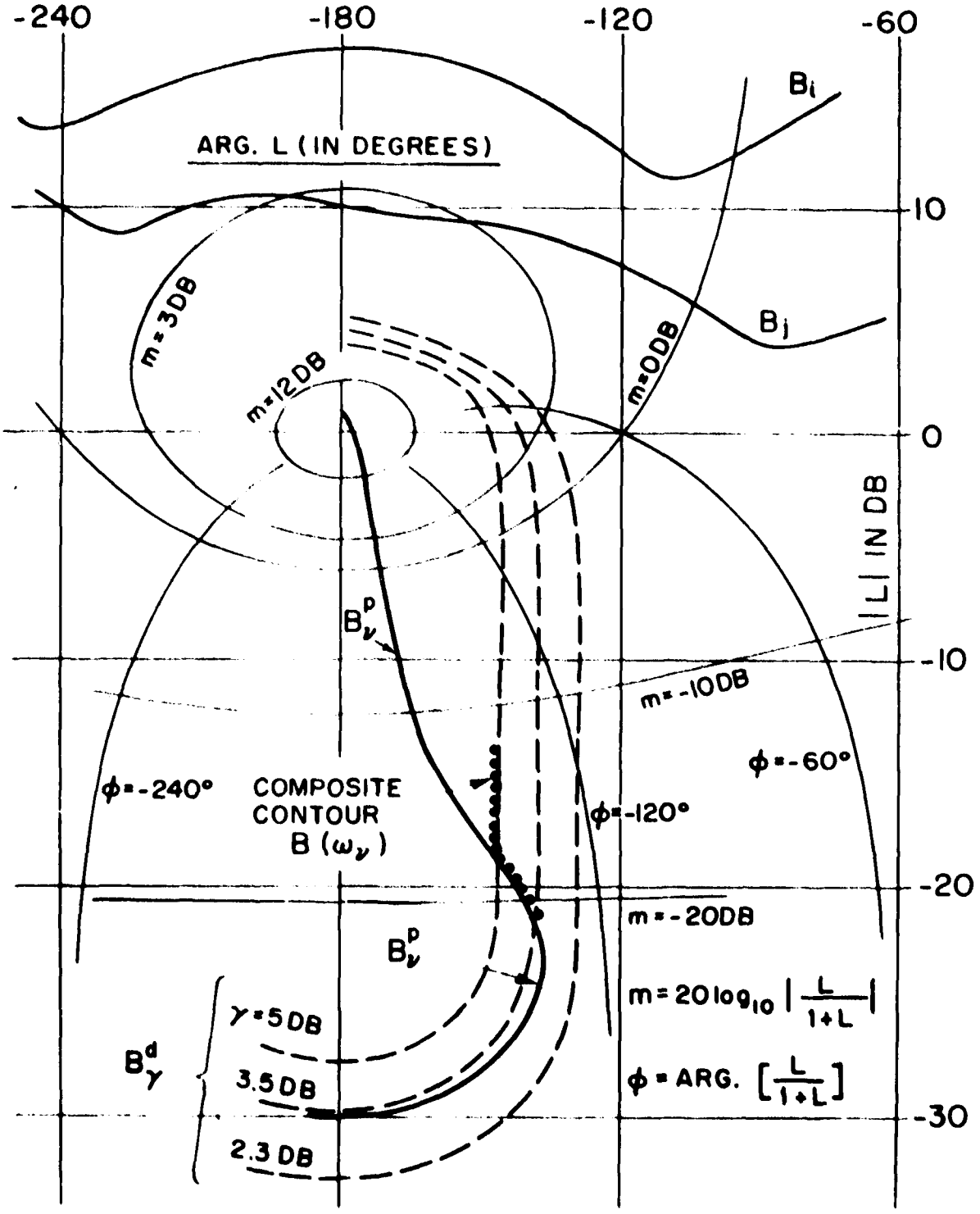

FIGURE 12 Typical bounds on $L_0(j\omega)$ in high frequency range.

for the present purpose, is that in significant plant ignorance problems the ideal optimal L has the properties shown in Figure 13, i.e., over a significant range it follows B_h along UV to the point J at which it abruptly jumps to infinity along WW'W'' and returns on the vertical line YZ, whose phase is $(-90°)\cdot e$. Such an ideal $L(j\omega)$ is, of course, impractical. A practical suboptimum L is shown in Figure 13.

Some results of a numerical design example are shown in Figure 14. They were derived for the following problem.

Numerical example. (Figure 14)

Plant:	$P = P_1 P_2$
Plant ignorance:	$P_1 = k_1/s \quad , \quad \sqrt{2} \leq k_1 \leq 10\sqrt{2}$
	$P_2 = k_2/s \quad , \quad \sqrt{2} \leq k_2 \leq 10\sqrt{2}$
Performance Specification:	Shown in Figure 9 were originally derived from time domain bounds [5].
Disturbance response:	$\gamma \leq 2.0$ db .

The derivation of a rational $L_0(s)$ which satisfies the bounds $B(\omega)$ on $L_0(j\omega)$, is somewhat of an art. For a given skill in the art, there is trade-off between design complexity and $L_0(j\omega)$ bandwidth reduction. Some computer programs have been prepared for automatic derivation of a practical optimum $L_0(j\omega)$, but complicated $B(\omega)$ patterns require human interaction.

3.4.6. Design of prefilter $F(s)$

The above only guarantees that $\Delta \log |T(j\omega)| \leq$ the relative change allowed by the tolerances in Figure 9. For example at ω_1 , say the allowed $|T|_{max} = -7.6$ db , and allowed $|T|_{min} = -22$ db , i.e. a maximum change of 14.4 db. A proper design of $L_0(s)$ in the manner described above only guarantees that the change of $|L/1+L| \leq 14.4$ db . But it is possible for $|L(j\omega_1)/1 + L(j\omega_1)|$ to actually be, for example, in the range 1.2 db to -8 db. The function of the prefilter $F(j\omega)$ in Figure 8, is to achieve the shift needed. In this example any $|F(j\omega_1)| \in [-8.8, -14]$ db is satisfactory, an allowance of 5.2 db because $L_0(j\omega_1)$ was overdesigned by 5.2 db.

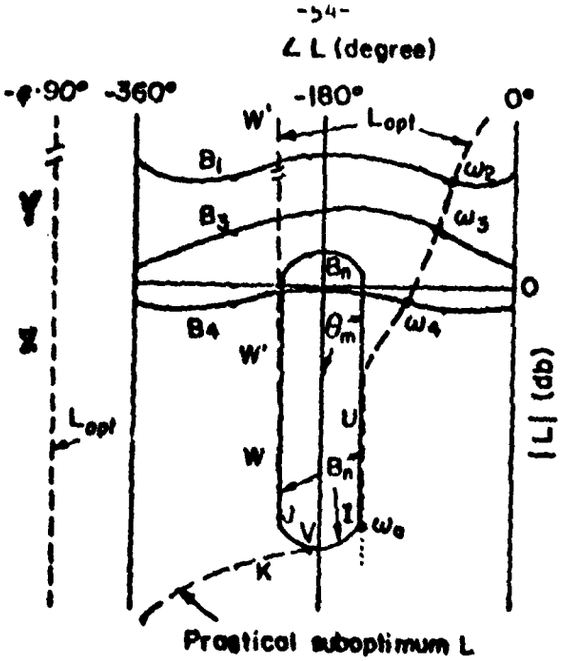

FIGURE 13 Optimum and "practical optimum" L.

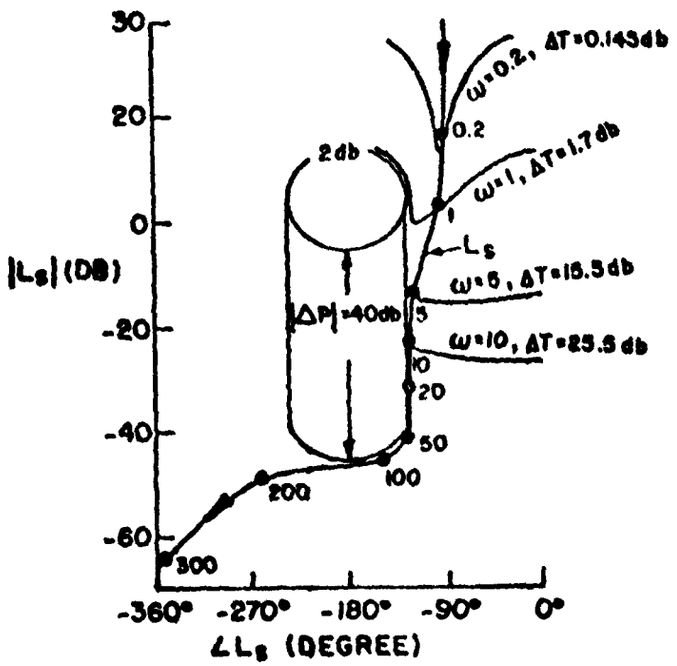

FIGURE 14 A design example.

We now turn to the application of the methods of Section 3.4 to our present problem.

3.5. Design of Autopilot

Section 3.3 described how the frequency response $P(j\omega)$ of the lti equivalent plant was obtained. Following 3.4.1, the next step is to find $Tp(\omega)$ templates of $P(j\omega)$, for a reasonable number of discrete ω values. $Tp(\omega_1)$ is simply the set $\{P(j\omega_1)\}$. A number of these are shown in Figure 15, in which the case marked by the large star is the chosen nominal plant function $P_0(j\omega)$. At very small ω, $Tp(\omega)$ is a vertical line because then $P(j\omega) \to$ a constant of zero phase but a different constant for different parameter combinations. At large ω, each $P(s) \to kp/s$ in the case, with kp a function of the parameter. Hence $Tp(\omega)$ is again a vertical line. Note the relatively small area of $Tp(\omega)$, indicating rather small uncertainty. Compare these $Tp(\omega)$ with those in the aircraft flight control problem of Appendix 1 (see Figures 6a-c, Appendix 1). In the latter some $P \in P$ are unstable (e.g. cases e,f in Figure 5 there). This is also seen from Appendix 1, Figure 6, where there are two verical line sub-templates 360° apart, due to the two groups of lti $P(j\omega)$, one stable and the other with two right half-plane poles. The uncertainty and nonlinearity in this missile problem are considerably less than in the aircraft problem of Appendix 1.

The bounds on $|T(j\omega)|$ (recall 3.4, Figure 9) are needed. These are determined by the model $T(s)$ in Equations (12,13), used for the autopilot. The resulting permissible spread in $|T(j\omega)|$, due to ω_n allowed to range $\in [1,4]$, is shown in Figure 16. The procedure described in 3.4.1 (Figure 10, etc.) is next followed to find the bounds on $L_0(j\omega)$. These are shown in Figure 17. The bounds are very moderate ones, due to the relatively small $Tp(\omega)$ sizes (small effective uncertainty in $P(j\omega)$), and generous $|T(j\omega)|$ tolerances. In view of these small demands, a very generous $L_0(j\omega)$ was chosen which satisfied the bounds $B(\omega)$, with much to spare — shown in Figures 17,18.

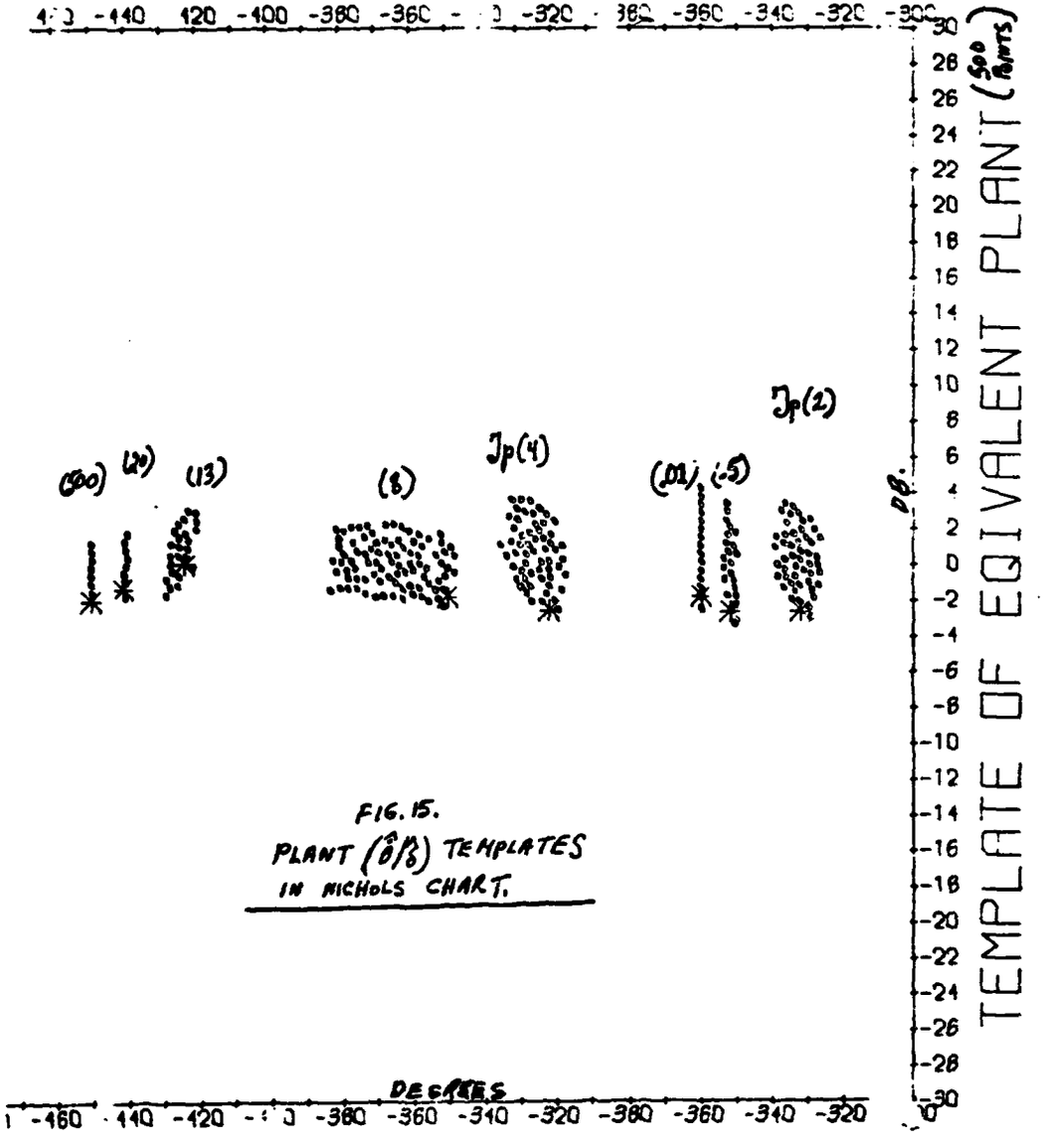

FIG. 15.
PLANT ($\hat{\theta}/\theta$) TEMPLATES
IN NICHOLS CHART.

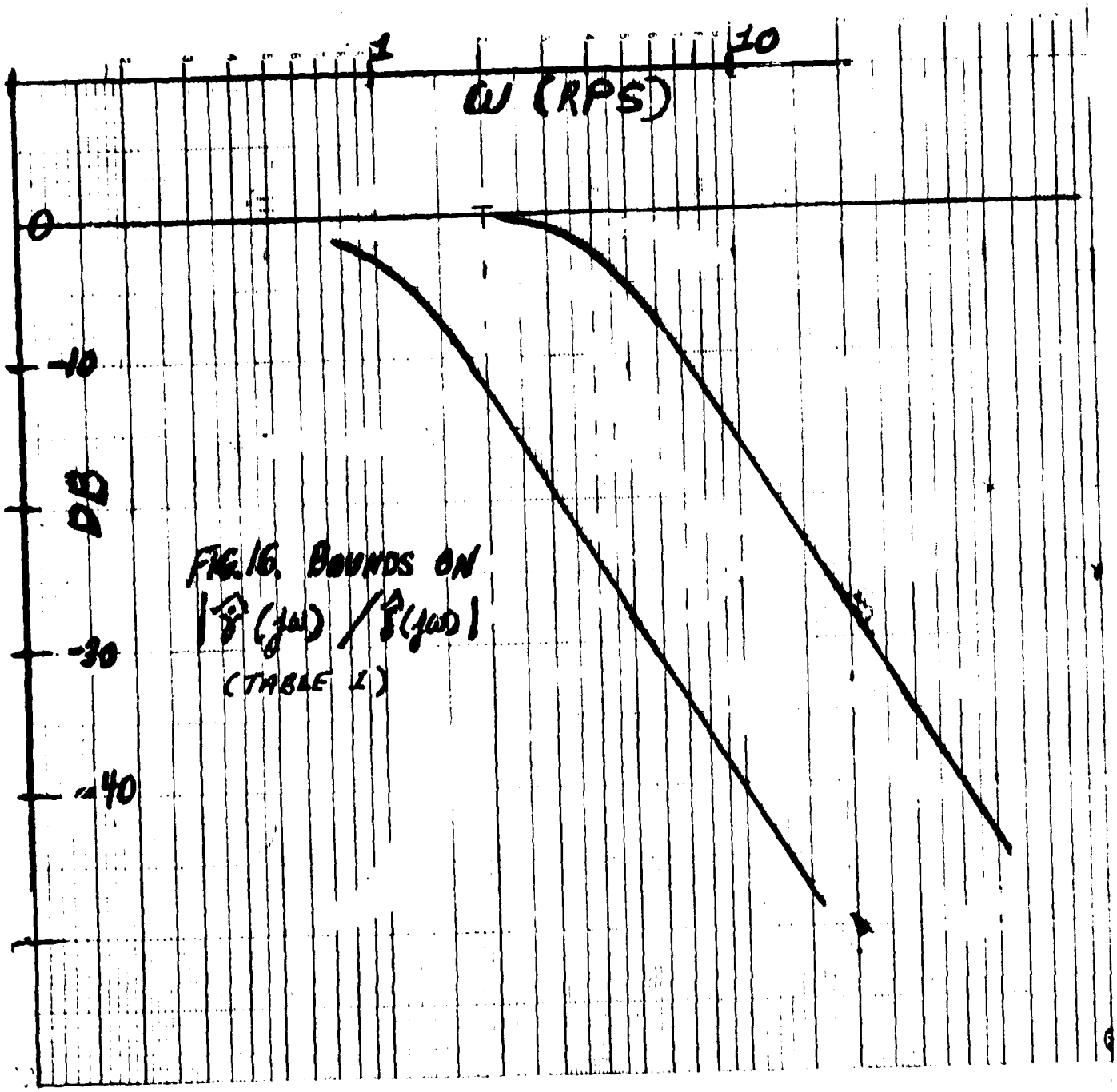

FIG. 16. BOUNDS ON $|\hat{\beta}(j\omega) / \beta(j\omega)|$ (TABLE I)

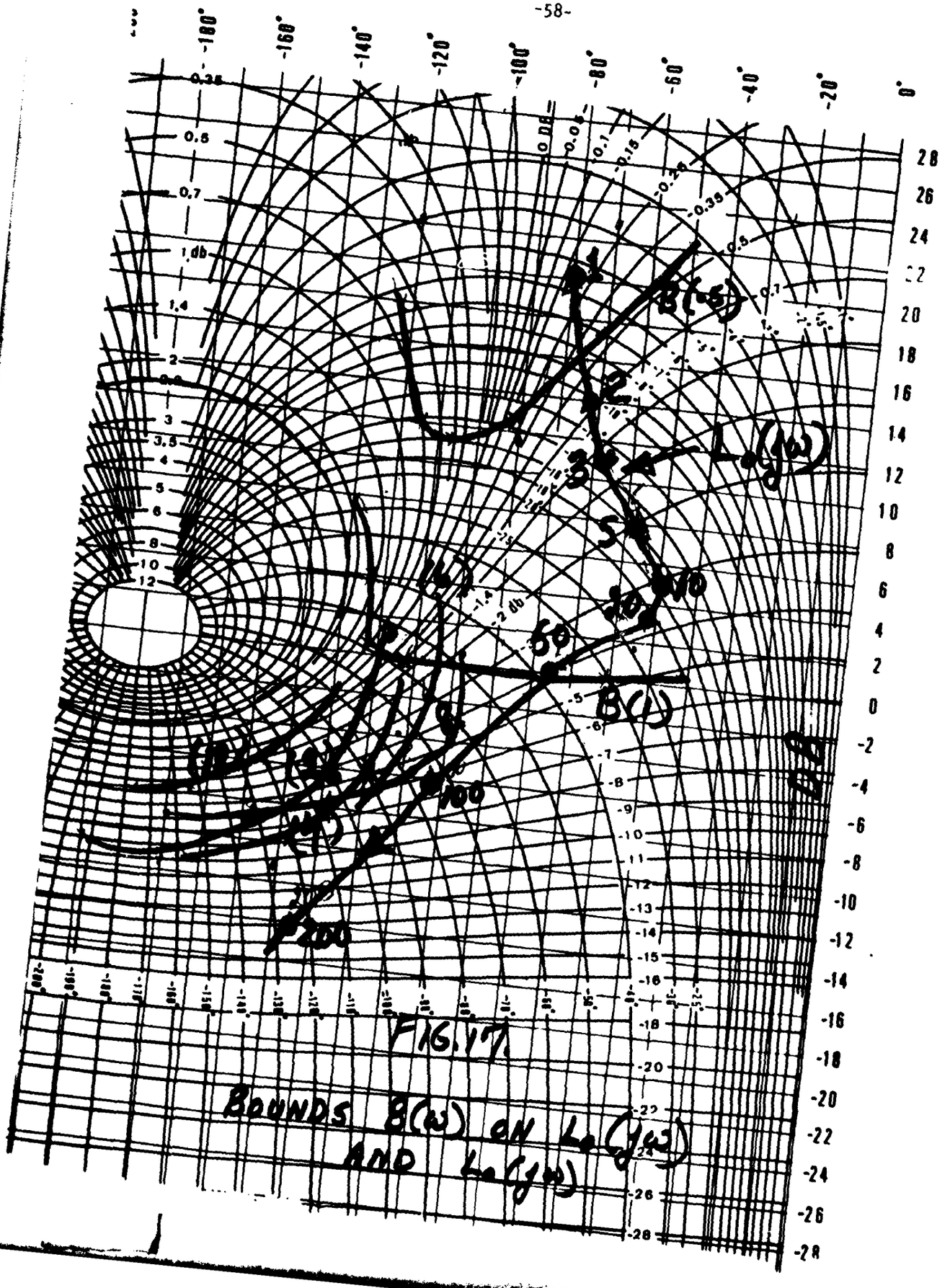
-180°
-160°
-140°
-120°
-100°
-80°
-60°
-40°
-20°
0°
0 DB
B(jω)
L(jω)
60
FIG. 17.
BOUNDS B(ω) ON L(jω)
AND L(jω)

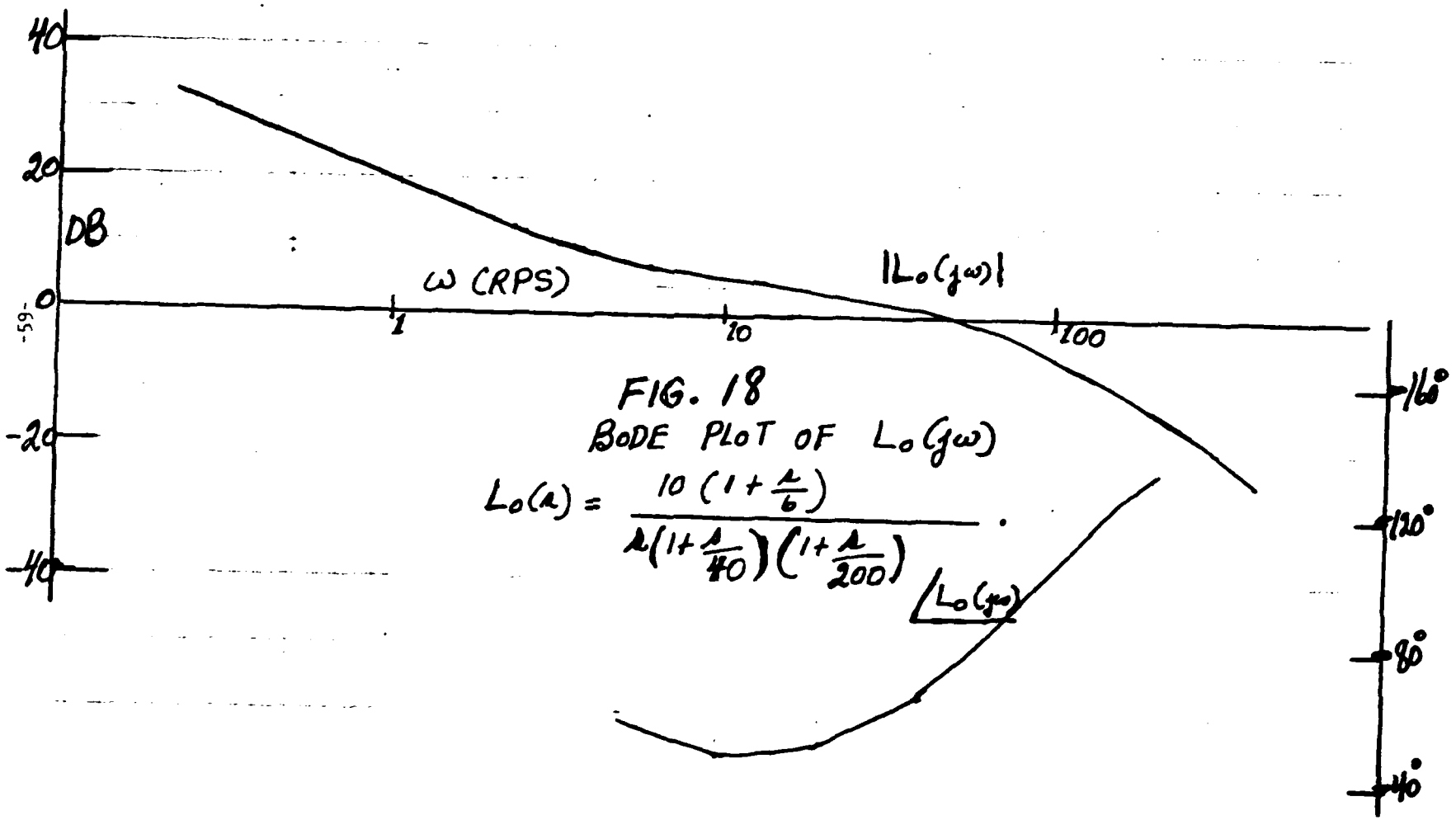

FIG. 18
BODE PLOT OF $L_o(j\omega)$

$$L_o(s) = \frac{10\left(1+\frac{s}{6}\right)}{s\left(1+\frac{s}{40}\right)\left(1+\frac{s}{200}\right)}$$

Design of Prefilter. The design of $F(s)$ of Figure 8, to satisfy the bounds on $|T(j\omega)|$ of Figure 9, has been described in 3.4.6. Our problem is more complicated because the feedback loop is around $\dot{\theta}$, while the tolerances are on the $\dot{\gamma}$ response in Figure 2. It is therefore necessary to derive $\hat{\dot{\theta}}/\hat{\dot{\gamma}}$ which multiplies the bounds on $\hat{\dot{\gamma}}$, to give the resulting bounds on $\hat{\dot{\theta}}$. A serious difficulty would arise if the uncertainty (spread) in $\hat{\dot{\theta}}/\hat{\dot{\gamma}}$ was of the same order of magnitude as that of $P(j\omega) = \hat{\dot{\theta}}/\hat{\delta}$. It is essential that the former be somewhat less than the latter. Fortunately, in this example there is little uncertainty in $\hat{\dot{\theta}}/\hat{\dot{\gamma}}$. Numerous runs (as described in 3.2), were made, giving $\dot{\theta}(t)$, $\dot{\gamma}(t)$. The new technique of Appendix 2 was used to find $\hat{\dot{\theta}}/\hat{\dot{\gamma}}$. Representative samples are shown in Figures 19a-f, and it is seen that there is little uncertainty in $\hat{\dot{\theta}}/\hat{\dot{\gamma}}$. In each of Figures 19a-f, the first part gives the time functions, and the second the frequency response $|\hat{\dot{\theta}}(j\omega)/\hat{\dot{\gamma}}(j\omega)|$. The new bounds on $|T(j\omega)|$, due to $\dot{\theta}$ being considered as the autopilot output, are given in Table 2. The old bounds, due to $\dot{\gamma}$ as output, are given in Table 1. The bounds on $|F(j\omega)|$ were then obtained, as explained in 3.4.6, resulting in

$$F(s) = \frac{48}{(s+1.5)(s+4)(s+8)}$$

3.6. Design Simulation — Local

It is important to recall that the nonlinear design technique has been applied only to the autopilot in Figure 2 — not to the entire closed-loop system of Figure 2. The proper verification of the design is then only for this autopilot portion. To effect this verification, the simulation of 3.2 was used to derive $\dot{\lambda}$ which became the input driving our above-designed autopilot. In the latter, there were used aerodynamic equations (1-3) and the $G(s)$, $F(s)$ of 3.5. Thus, only the autopilot as a self-contained closed-loop system was checked at this point — not as a part of the larger closed-loop structure of Figure 12. The results of the simulation for a representative number of runs, including the extreme (largest $\dot{\theta}$ values), are shown in Figures 20a-e, for $\dot{\theta}(t)$ and $\delta(t)$. Each figure has three parts. The first repeats the result obtained in the simulation of 3.2 with the second-order $T(s)$ model of Equations (12,13) (i.e. same as in

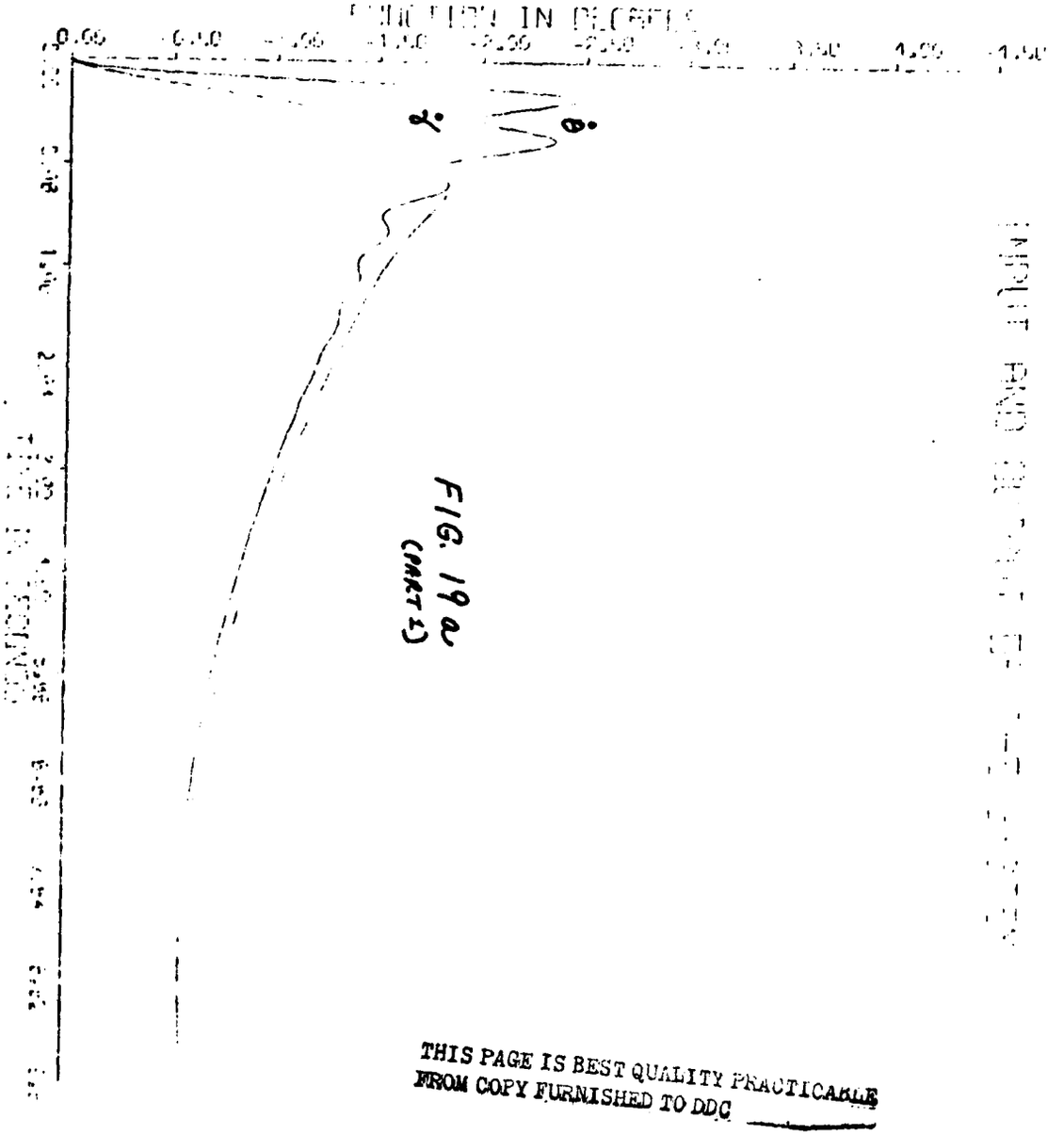

FIG. 19a
(PART 2)

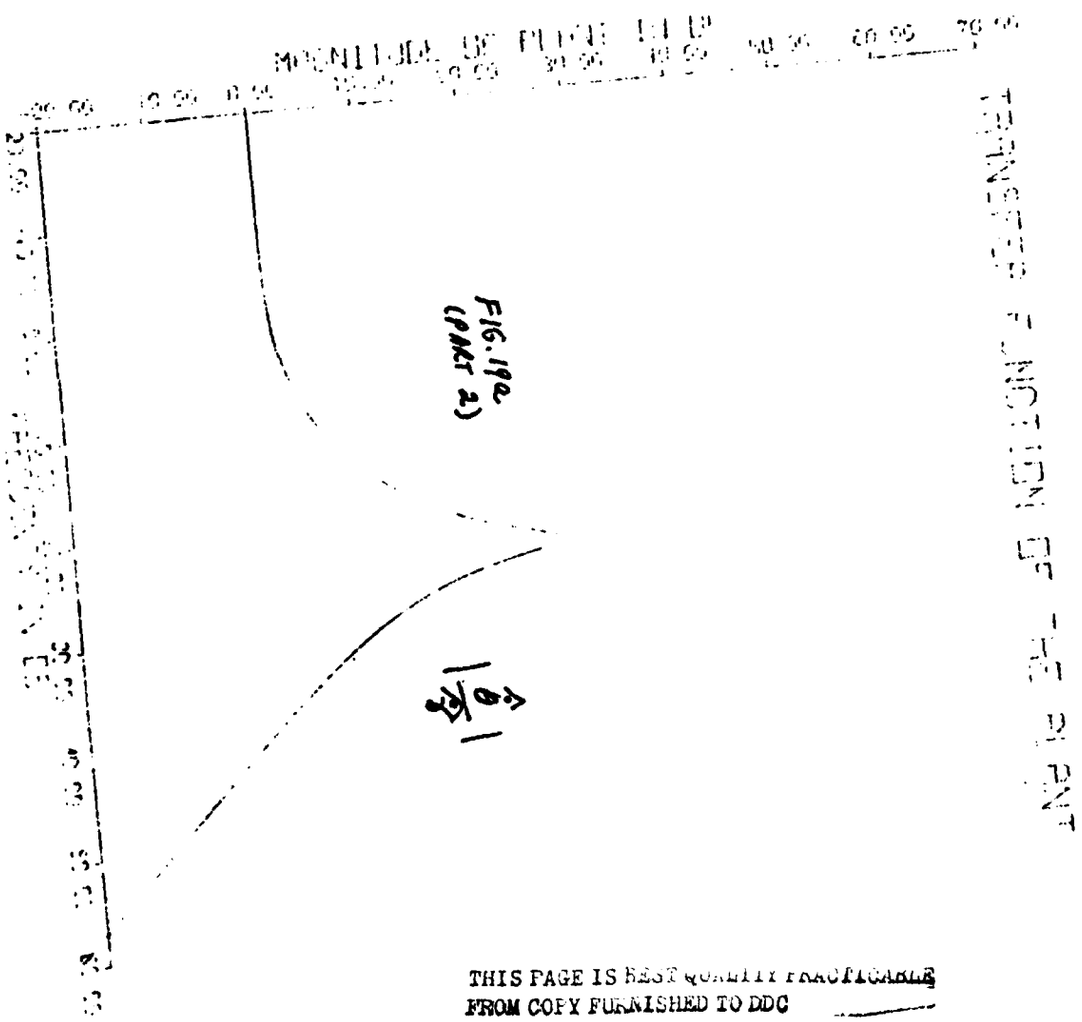

FIG. 19a
(PART 2)

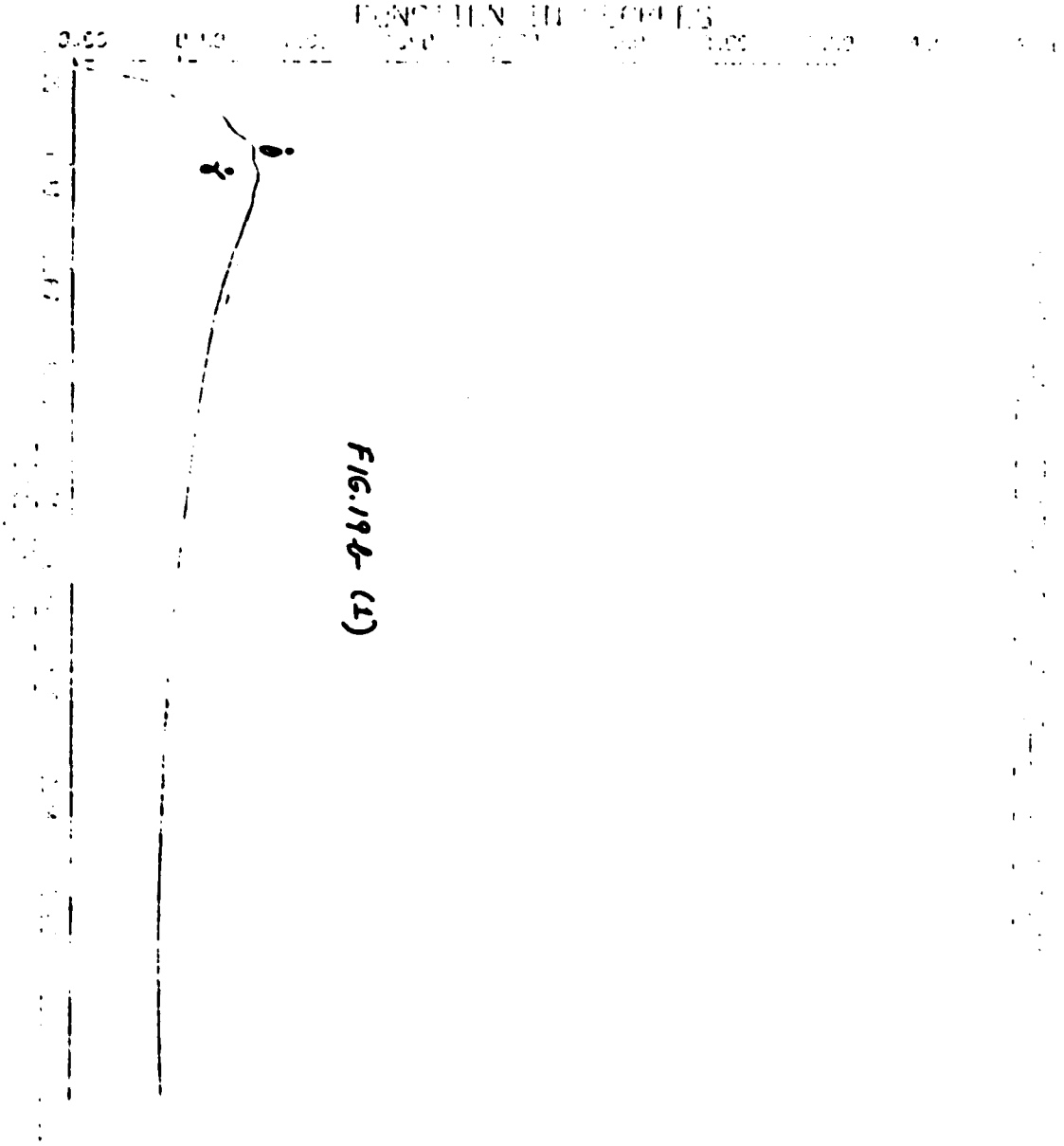

FIG. 19b (1)

XN=4.00

AT=0.74

VW=1.13

XMD=98.

R=2709.

WN=2.16

CLA=0.96

CLD=0.95

CMA=0.88

CMD=0.69

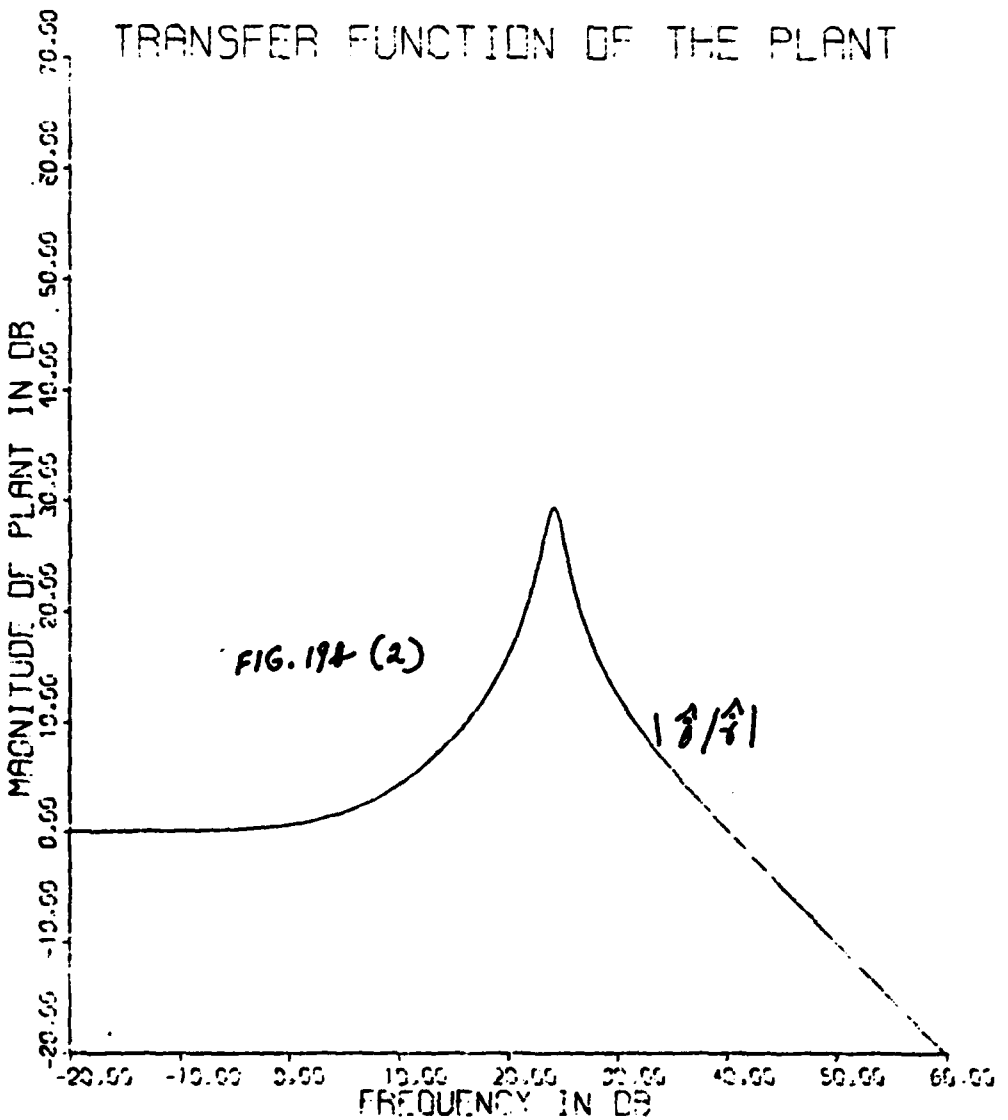

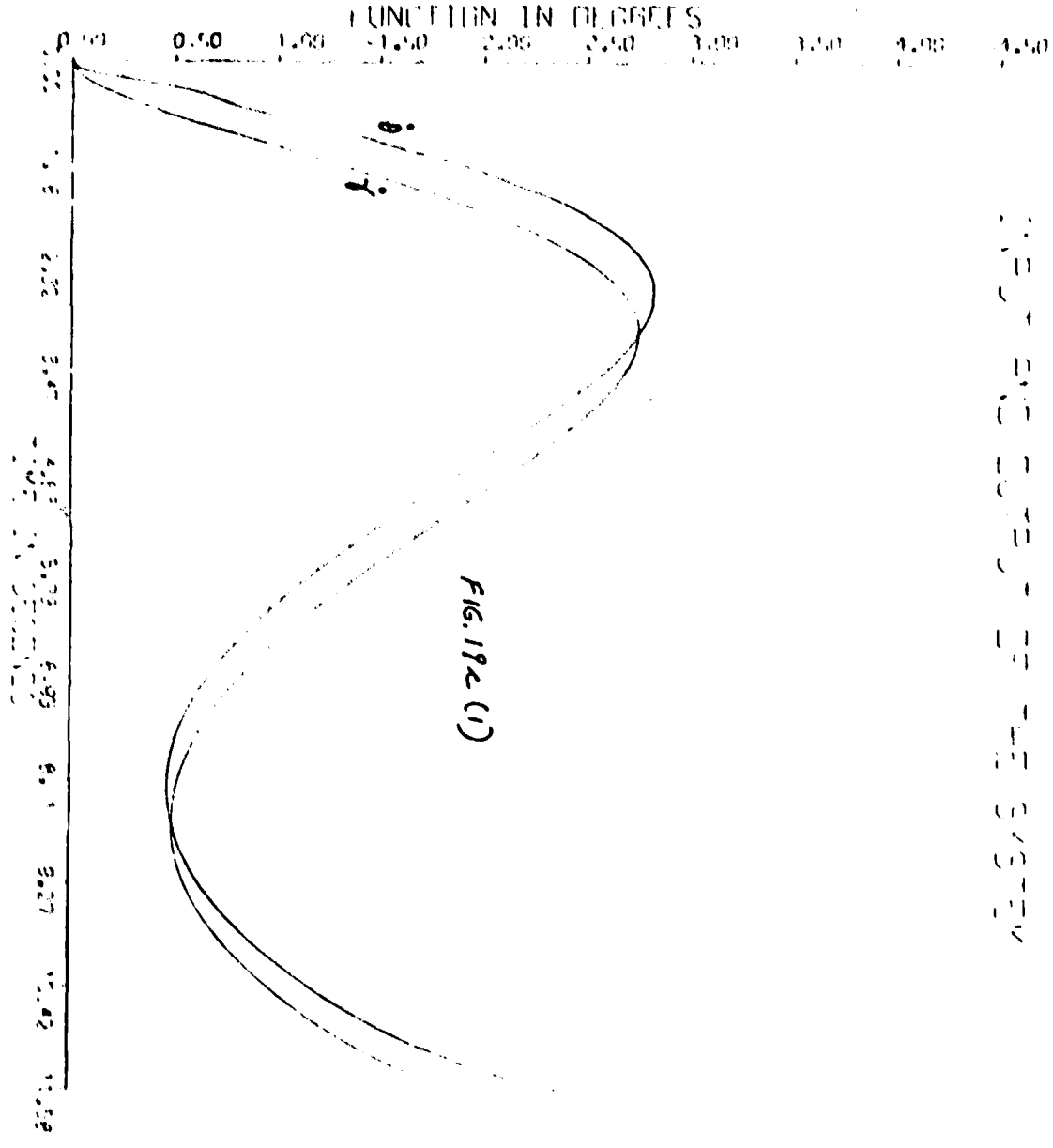

FIG. 19C (1)

ω_n=3.93

ζ=1.41

ω_n=0.99

ω_0=172.

K=2358.

ω_N=1.27

ζ_{LA}=0.82

ζ_{LD}=1.19

ζ_{MA}=0.95

ζ_{MD}=1.02

TRANSFER FUNCTION OF THE

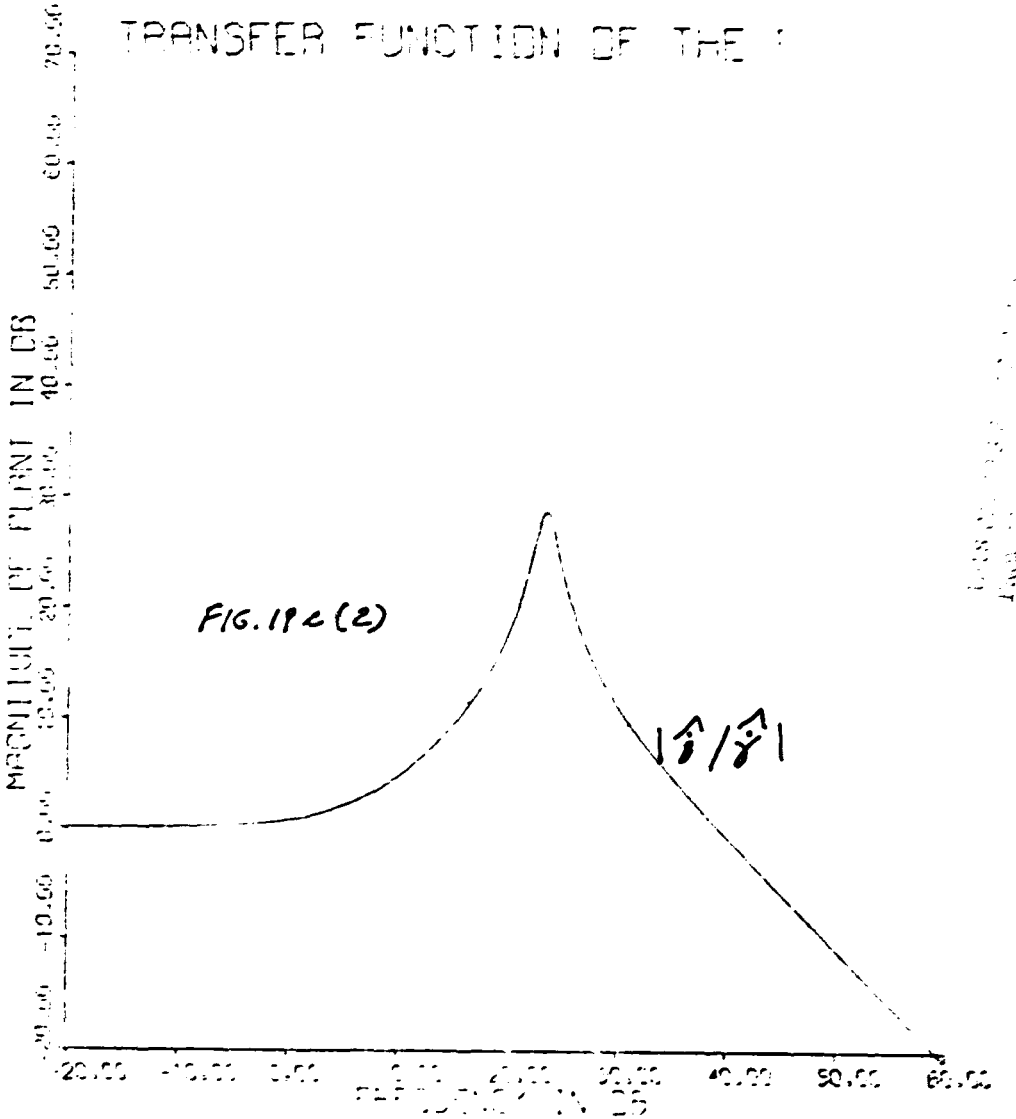

FIG. 19 c (2)

$|\hat{\delta}/\hat{\delta}|$

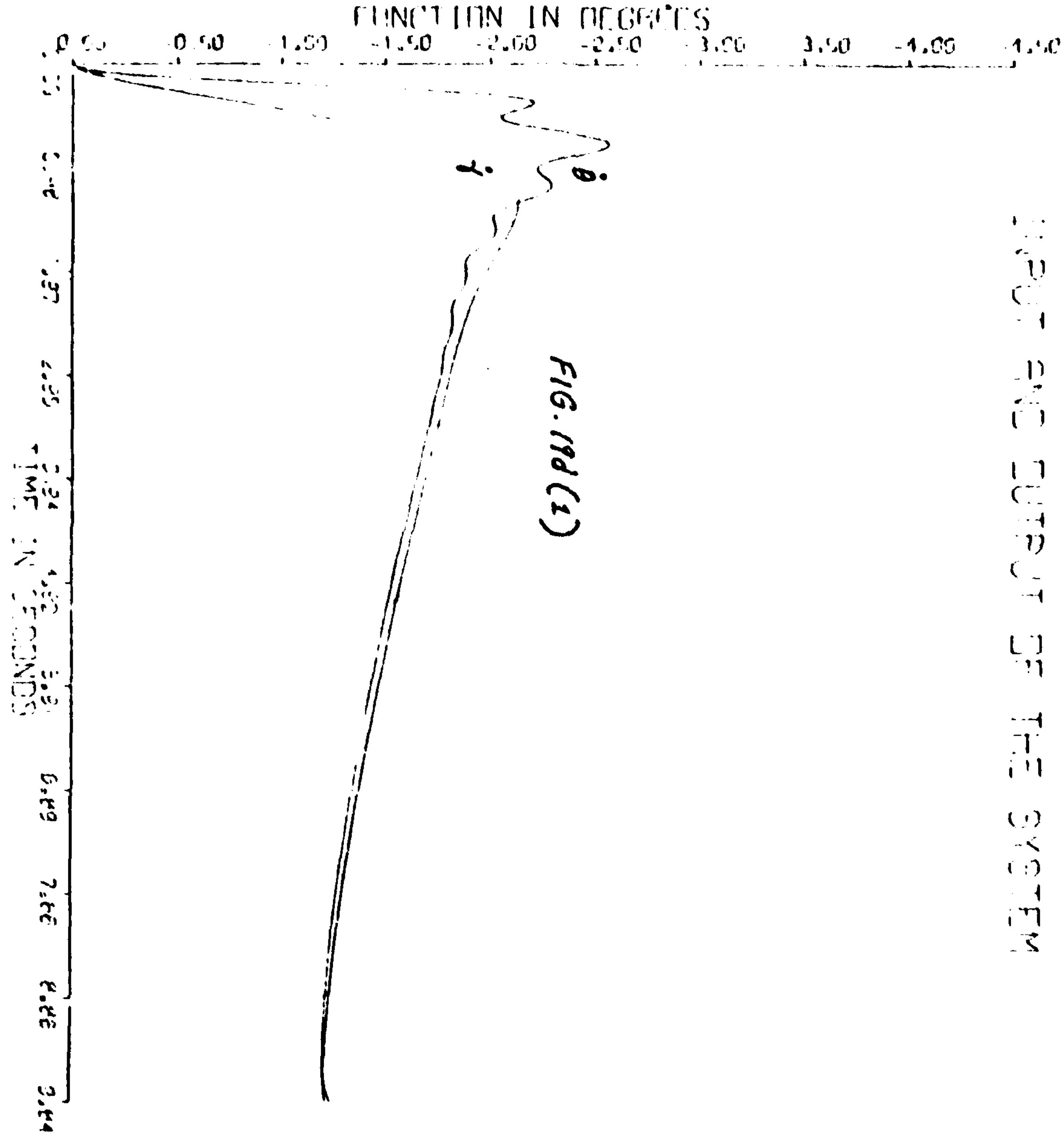
FUNCTION IN DEGREES
TIME IN SECONDS
INPUT AND OUTPUT OF THE SYSTEM
FIG. 19d(1)

XN=3.34

RT=1.74

VW=8.48

XMO=108.

R=2009.

WN=3.34

CLA=0.61

CLD=1.16

CMA=1.10

CMD=0.67

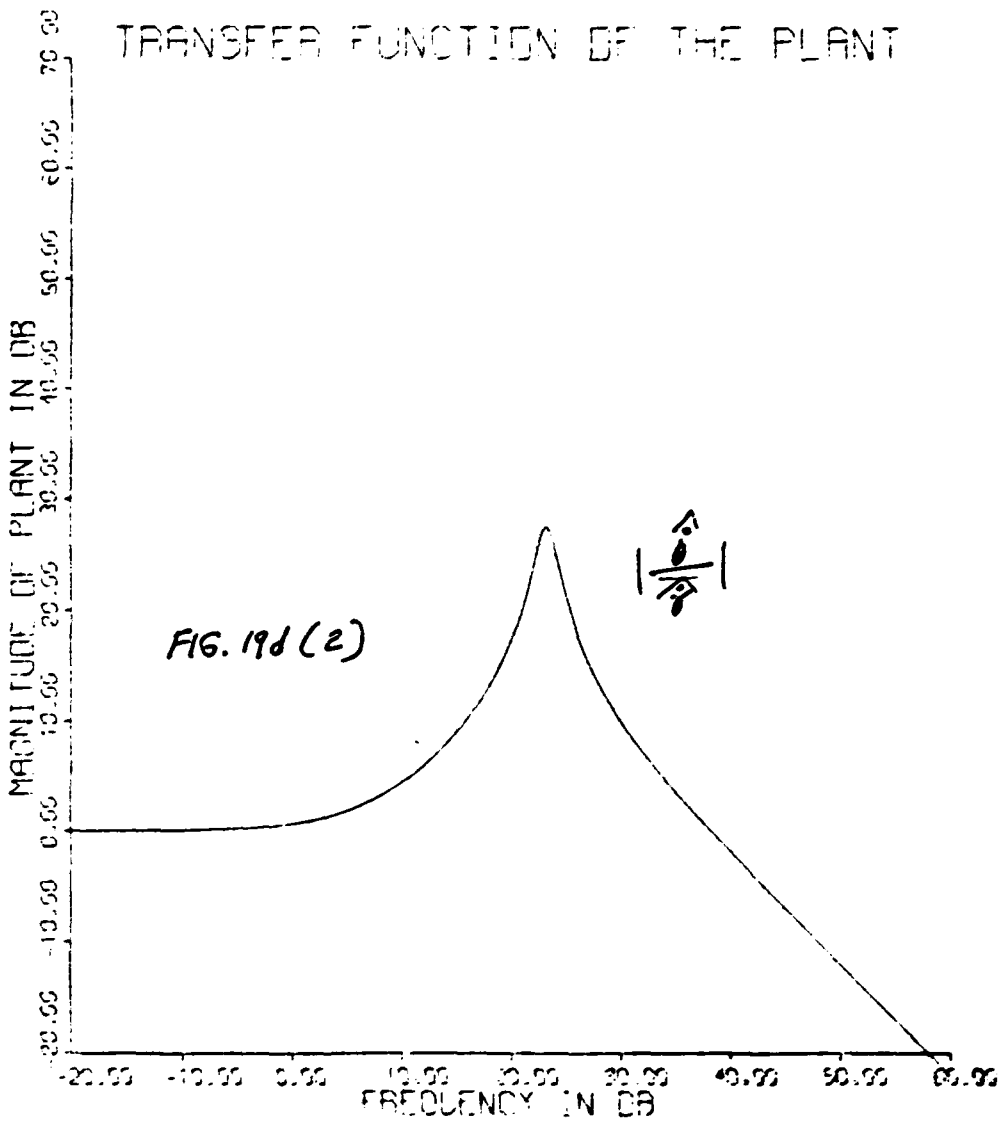

FIG. 19d (2)

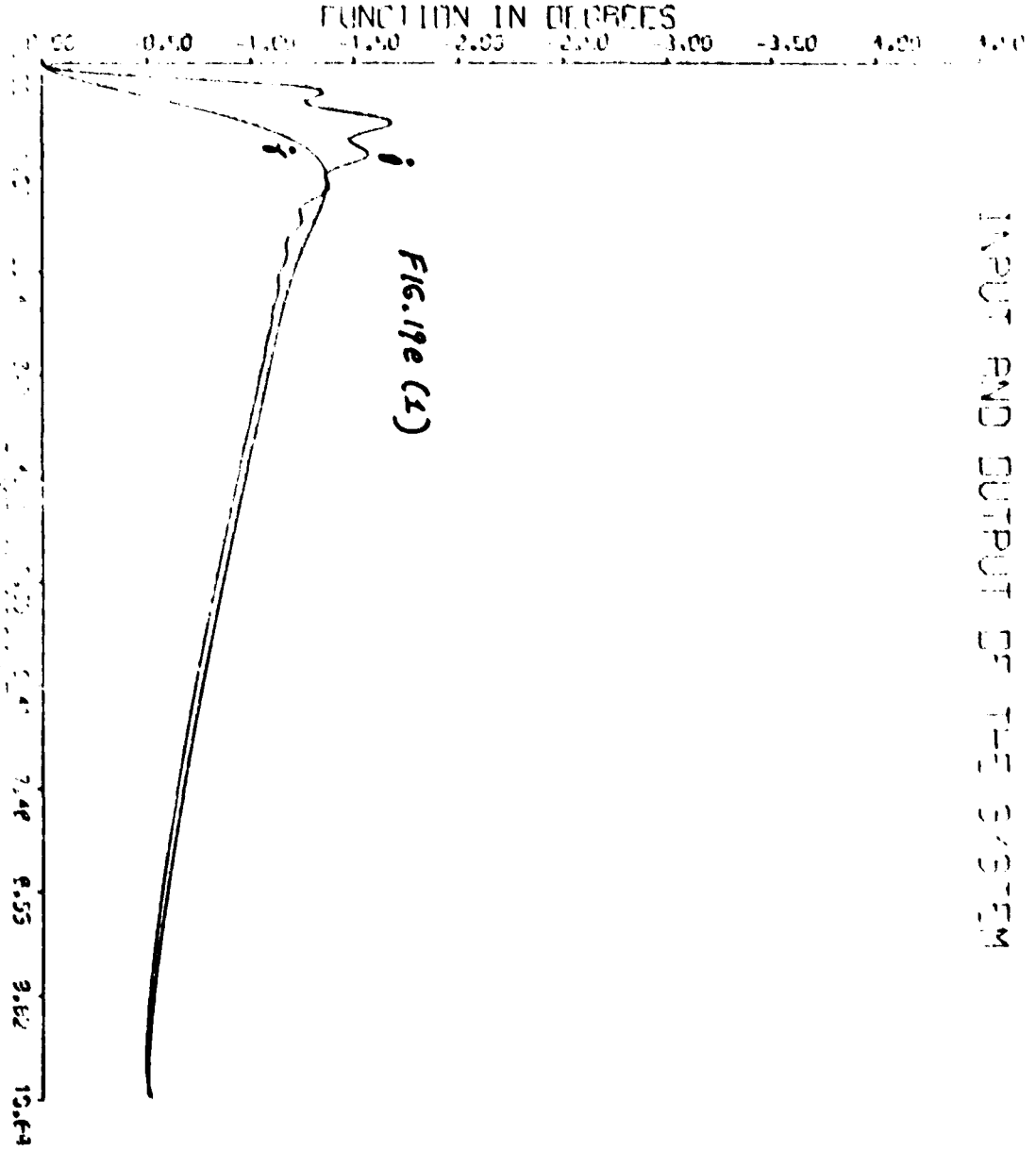

FIG. 18e (x)

XN=3.27

ZT=0.71

VW=5.14

XMD=98.

R=2178.

WN=3.46

CLA=0.98

CLD=0.93

CMA=0.97

CMD=1.10

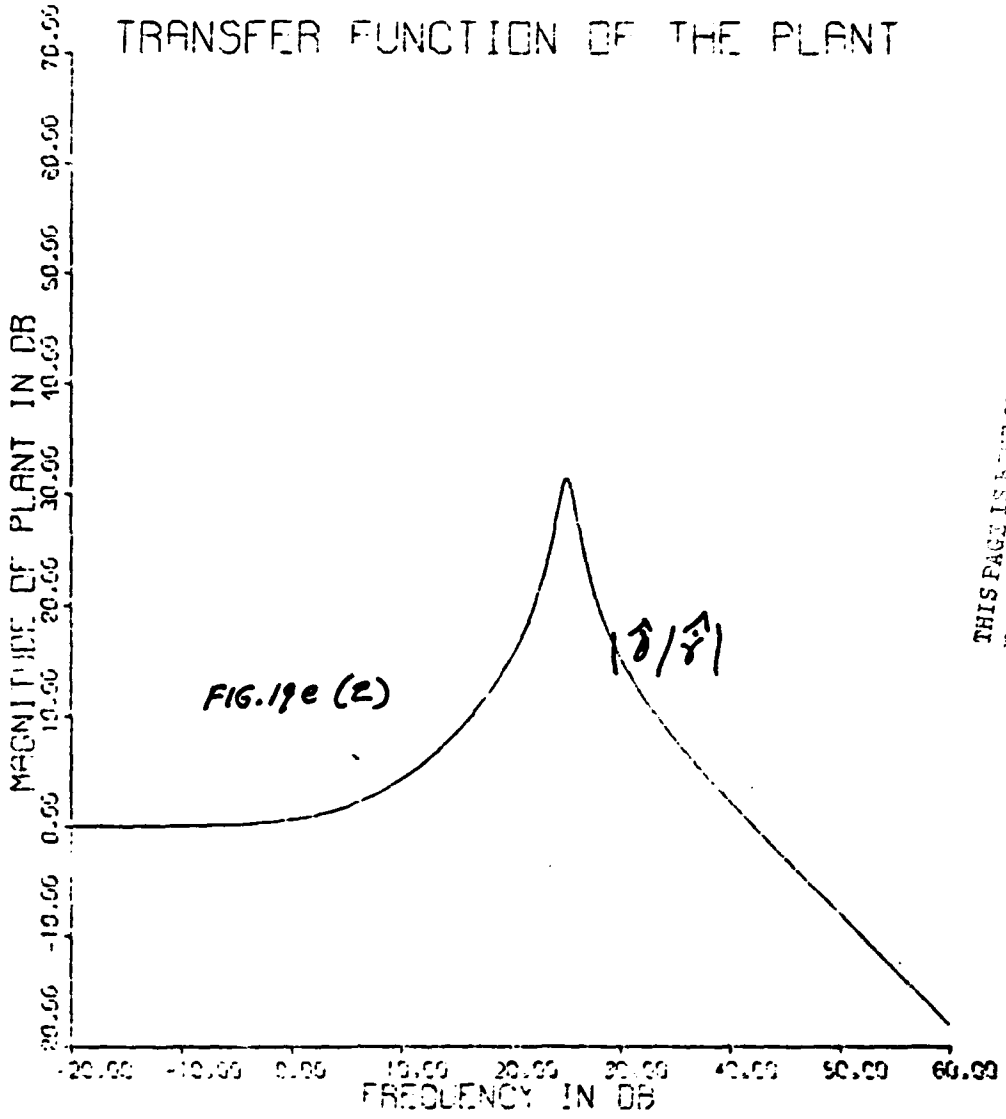

FIG. 19e (2)

Fig. 44 (2)

FREQ	IMAX	IMIN	DIFF
0.100E-01	0.165E-04	-0.517E-06	0.170E-04
0.100E+00	0.130E-02	0.107E-03	0.119E-02
0.500E+01	0.173E-02	-0.222E+00	0.223E+00
0.100E+01	-0.[illegible]E-02	-0.292E+01	0.291E+01
0.200E+01	-0.[illegible]E+00	-0.122E+02	0.120E+02
0.400E+01	-0.[illegible]E+01	-0.240E+02	0.211E+02
0.500E+01	-0.[illegible]E+01	-0.279E+02	0.226E+02
0.600E+01	-0.776E+01	-0.311E+02	0.233E+02
0.700E+01	-0.101E+02	-0.338E+02	0.236E+02
0.800E+01	-0.122E+02	-0.361E+02	0.238E+02
0.900E+01	-0.142E+02	-0.381E+02	0.239E+02
0.100E+02	-0.159E+02	-0.399E+02	0.239E+02
0.110E+02	-0.176E+02	-0.416E+02	0.240E+02
0.120E+02	-0.191E+02	-0.431E+02	0.240E+02
0.130E+02	-0.[illegible]E+02	-0.445E+02	0.240E+02
0.140E+02	-0.217E+02	-0.458E+02	0.240E+02
0.150E+02	-0.229E+02	-0.470E+02	0.240E+02
0.200E+02	-0.279E+02	-0.520E+02	0.240E+02
0.500E+02	-0.438E+02	-0.679E+02	0.240E+02
0.100E+03	-0.[illegible]E+02	-0.799E+02	0.240E+02
0.200E+03	-0.[illegible]E+02	-0.920E+02	0.240E+02
0.300E+03	-0.[illegible]E+02	-0.[illegible]E+02	0.240E+02
0.[illegible]E+03	-0.[illegible]E+02	-0.[illegible]E+02	0.240E+02

TABLE I.

BOUNDS ON $|T(j\omega)|$ FOR δ OUTPUT.

FREQ	TMAX	TMIN	DIFF
0.100E-01	0.691E-03	0.690E-0[illegible]	[illegible]
0.100E+00	0.551E-02	0.751E-02	[illegible]
0.500E+00	0.114E+00	0.615E-02	[illegible]
0.100E+01	0.430E+00	-0.206E+01	0.249E+0[illegible]
0.200E+01	0.134E+01	-0.950E+01	0.105E+0[illegible]
0.400E+01	[illegible]	-0.171E+0[illegible]	[illegible]
0.500E+01	[illegible]	-0.191E+02	[illegible]
0.600E+01	-0.579E-01	-0.205E+02	0.204E+0[illegible]
0.700E+01	[illegible]	-0.214E+02	[illegible]
0.800E+01	-0.153E+01	[illegible]	[illegible]
0.900E+01	-0.213E+01	[illegible]	[illegible]
0.100E+02	-0.257E+01	-0.223E+02	[illegible]
0.110E+02	-0.283E+01	[illegible]	[illegible]
0.120E+02	[illegible]	[illegible]	[illegible]
0.130E+02	[illegible]	[illegible]	[illegible]
0.140E+02	[illegible]	[illegible]	[illegible]
[illegible]	-0.191E+0[illegible]	[illegible]	[illegible]
[illegible]	-0.105E+01	[illegible]	[illegible]
[illegible]	[illegible]	[illegible]	[illegible]
[illegible]	-0.113E+0[illegible]	[illegible]	[illegible]
[illegible]	-0.151E+02	[illegible]	[illegible]
[illegible]	[illegible]	[illegible]	[illegible]
[illegible]	[illegible]	[illegible]	[illegible]
[illegible]	[illegible]	[illegible]	[illegible]
[illegible]	[illegible]	[illegible]	[illegible]
[illegible]	[illegible]	[illegible]	[illegible]
[illegible]	[illegible]	[illegible]	[illegible]
[illegible]	[illegible]	[illegible]	[illegible]
[illegible]	[illegible]	[illegible]	[illegible]

TABLE 2.
BOUNDS ON $|T(j\omega)|$
FOR β AS OUTPUT.

SECOND - ORDER SIMULATION

INPUT AND OUTPUT OF THE SYSTEM

FIG. 20 a

(1)

(a)

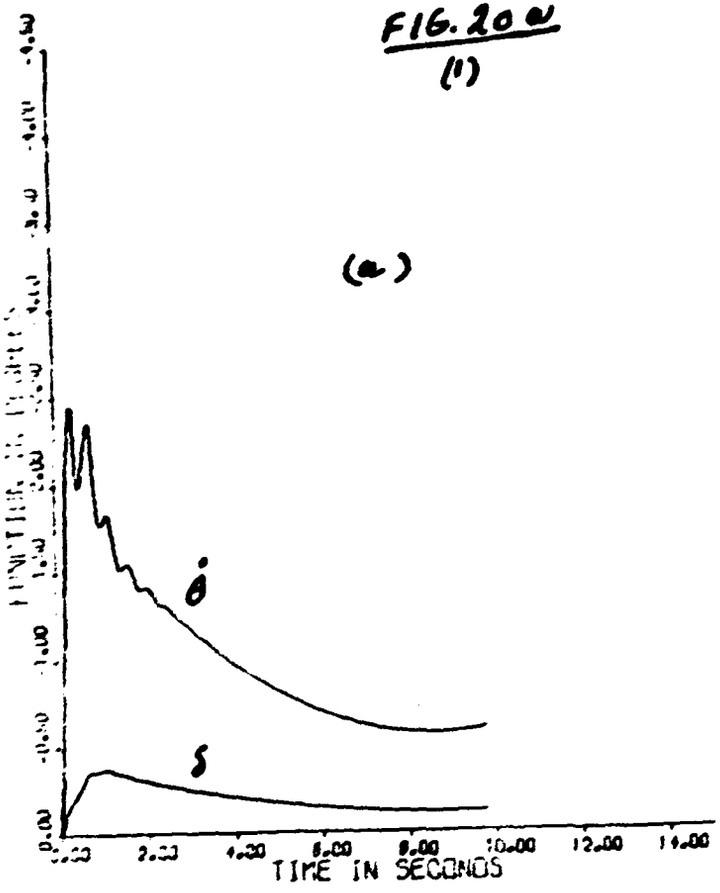

XN=4.00

AT=1.00

VW=5.00

XMO=100.

A=2000.

VN=4.00

CLA=0.80

CLO=1.20

CMA=1.20

CMO=0.80

LOCAL FEEDBACK SIMULATION

INPUT AND OUTPUT OF THE SYSTEM

(2)

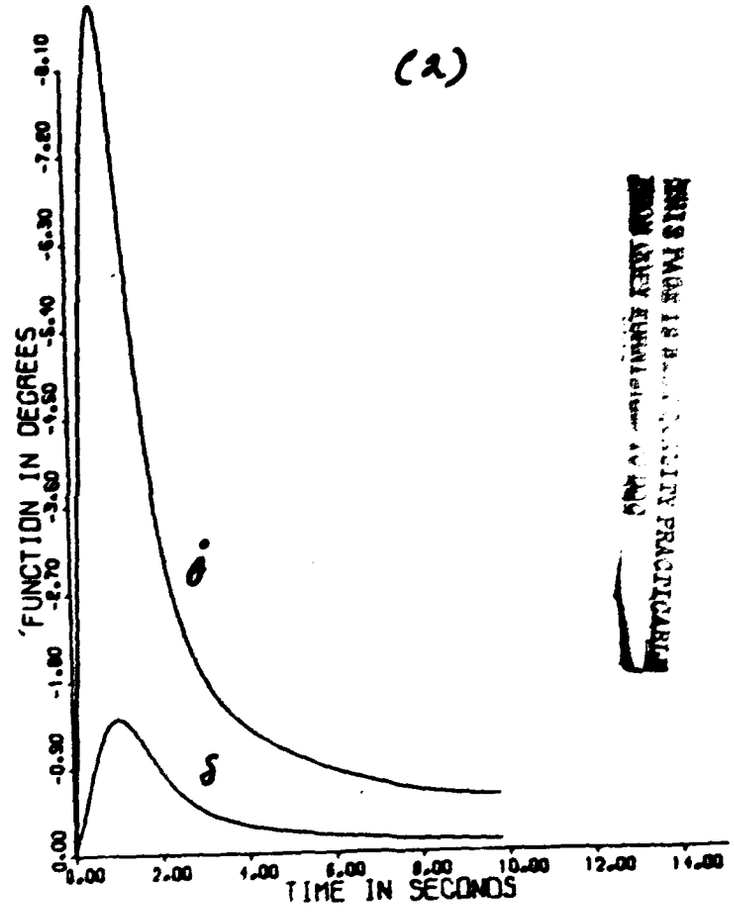

SECOND - ORDER SIMULATION

INPUT AND OUTPUT OF THE SYSTEM

FIG. 20a

(1)

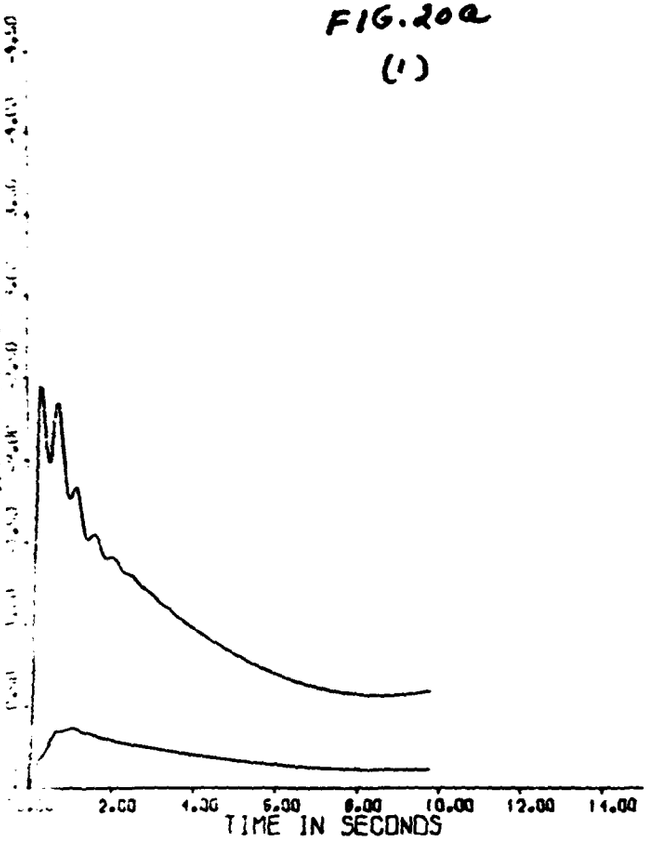

XN=4.00

RT=1.00

VW=5.00

XMO=100.

R=2000.

VN=4.00

CLA=0.80

CLD=1.20

CMA=1.20

CMO=0.80

GLOBAL FEEDBACK SIMULATION

INPUT AND OUTPUT OF THE SYSTEM

(3)

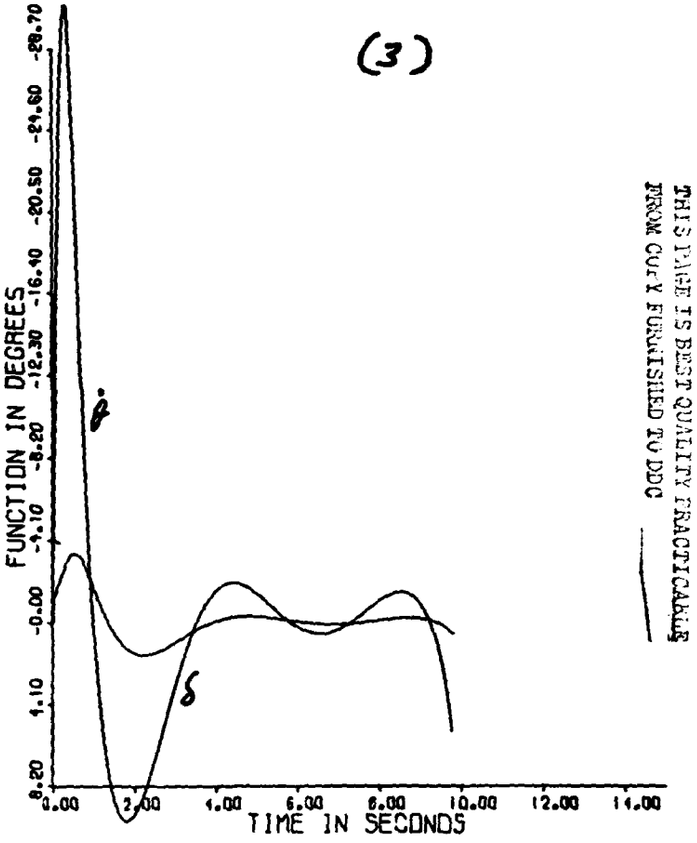

SECOND - ORDER SIMULATION

INPUT AND OUTPUT OF THE SYSTEM

FIG. 20b

(1)

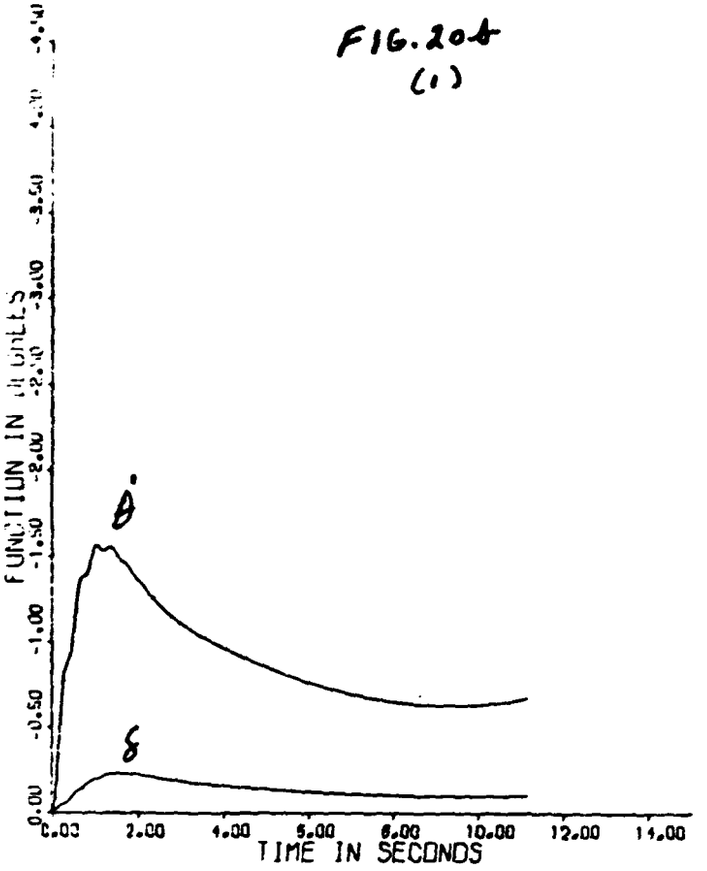

XN=3.96

AT=1.11

VW=6.36

XMO=71.

R=2271.

WN=2.47

CLA=0.98

CLD=0.98

CMA=1.13

CMD=0.97

LOCAL FEEDBACK SIMULATION

INPUT AND OUTPUT OF THE SYSTEM

(2)

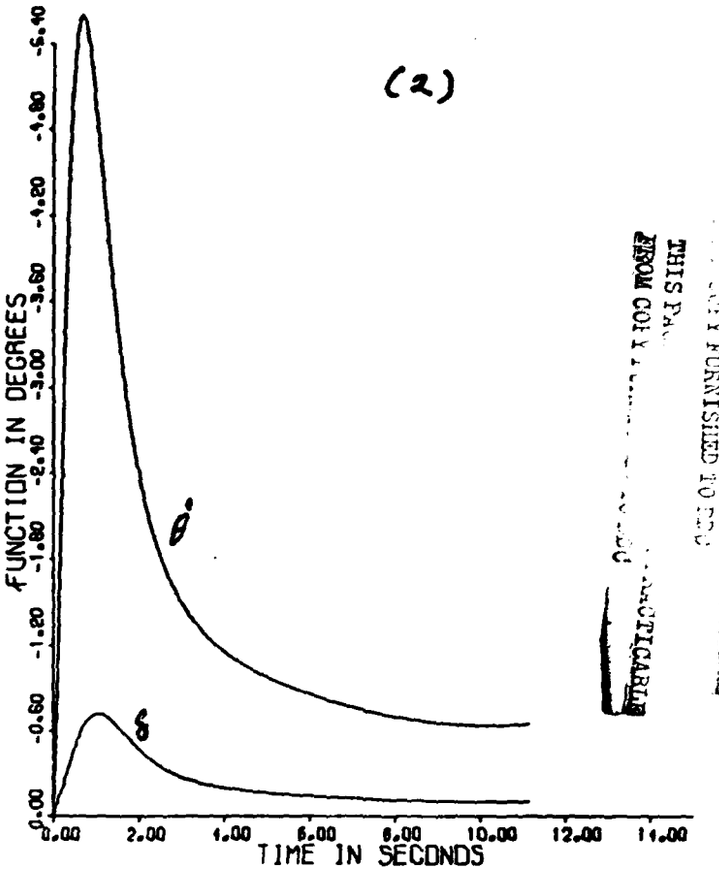

SECOND - ORDER SIMULATION

INPUT AND OUTPUT OF THE SYSTEM

FIG. 20b

(1)

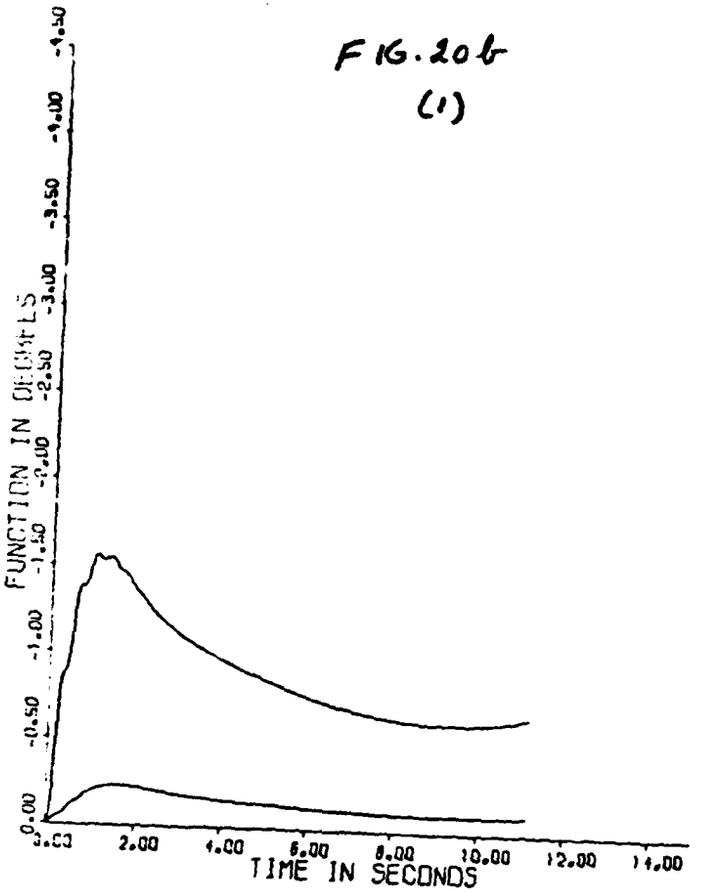

XN=3.96

RT=1.11

VW=6.36

XMO=71.

R=2271.

VN=2.47

CLA=0.98

CLD=0.98

CMA=1.13

CMD=0.97

GLOBAL FEEDBACK SIMULATION

INPUT AND OUTPUT OF THE SYSTEM

(3)

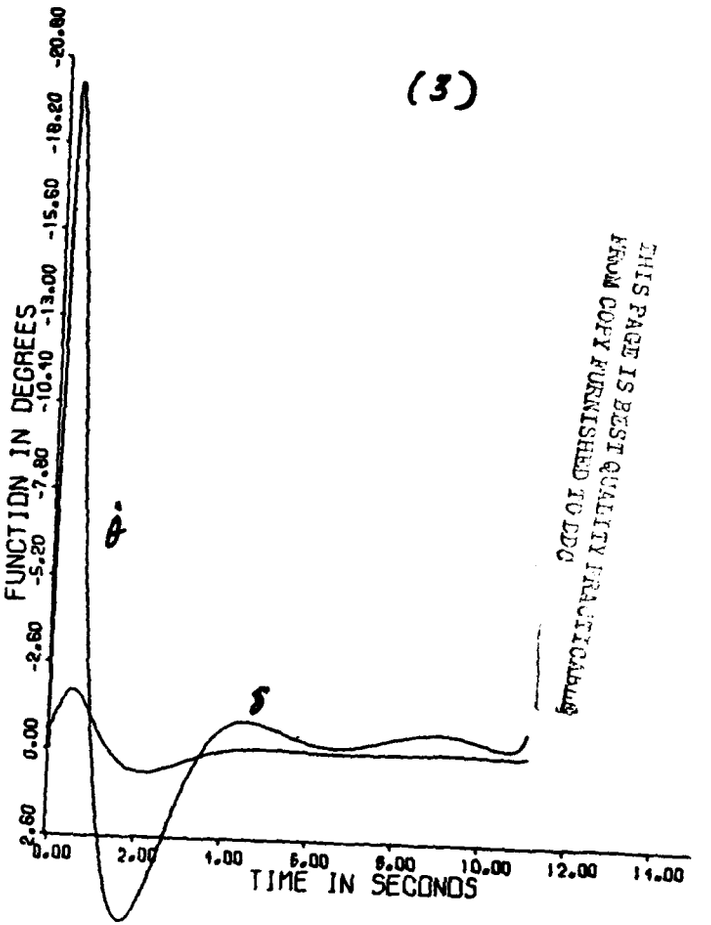

SECOND - ORDER SIMULATION

INPUT AND OUTPUT OF THE SYSTEM

FIG. 20a
(1)

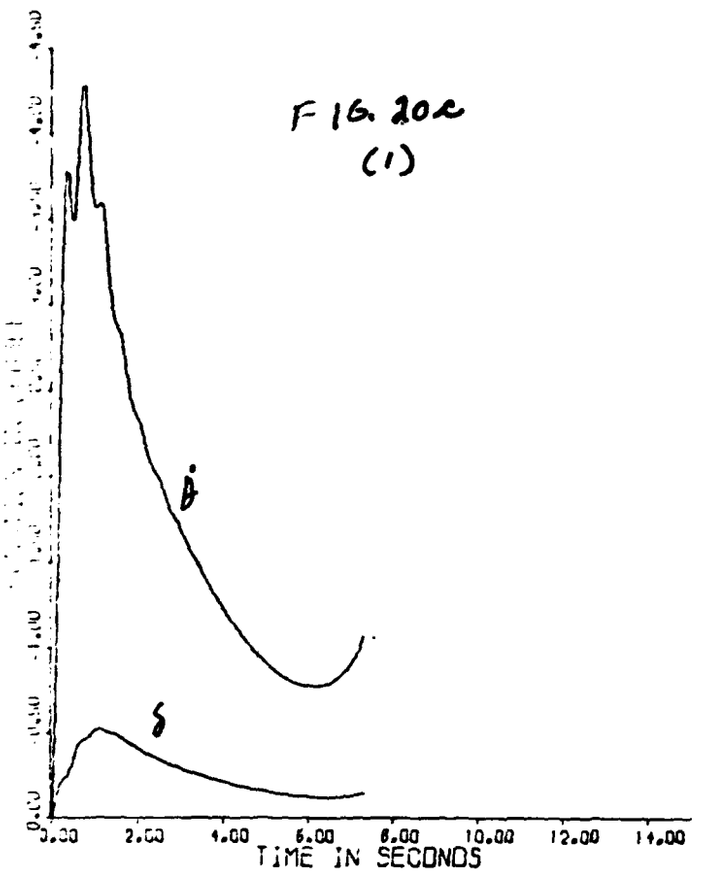

XN=3.79

AT=1.39

VW=7.14

XMO=104.

R=1505.

WN=3.29

CLA=0.62

CLD=1.19

CMA=0.92

CMD=0.91

LOCAL FEEDBACK SIMULATION

INPUT AND OUTPUT OF THE SYSTEM

(2)

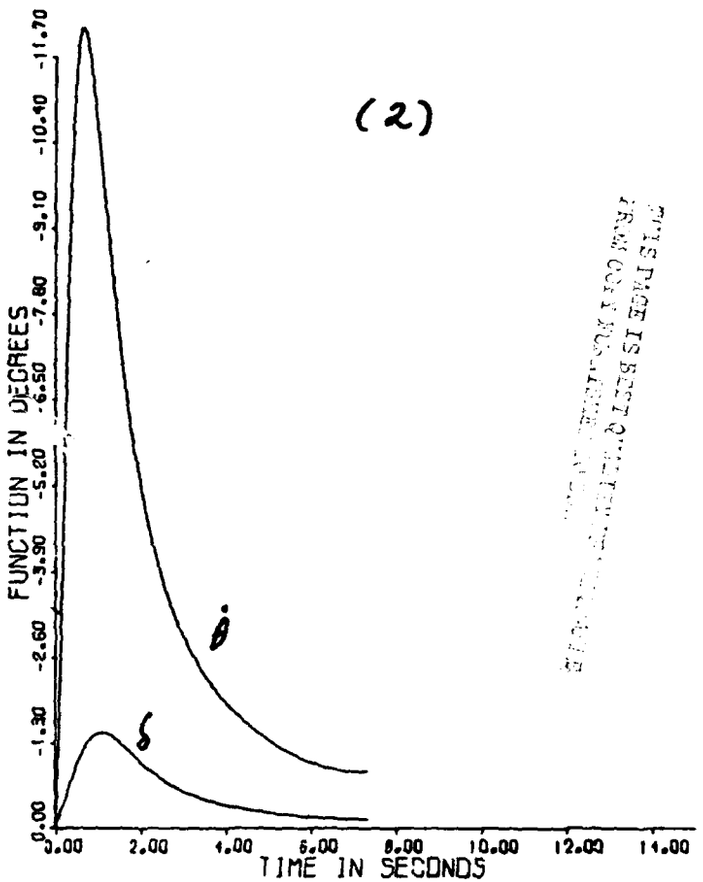

SECOND - ORDER SIMULATION

INPUT AND OUTPUT OF THE SYSTEM

FIG. 20c

(1)

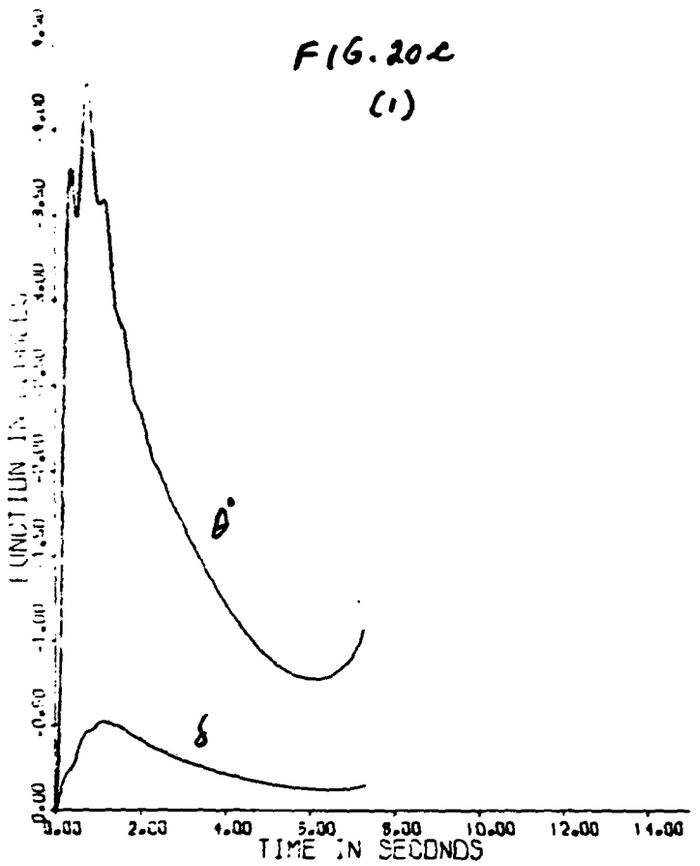

XN=3.79

AT=1.39

VW=7.14

XMO=104.

R=1505.

VN=3.29

CLA=0.82

CLD=1.19

CMA=0.92

CMD=0.91

GLOBAL FEEDBACK SIMULATION

INPUT AND OUTPUT OF THE SYSTEM

(3)

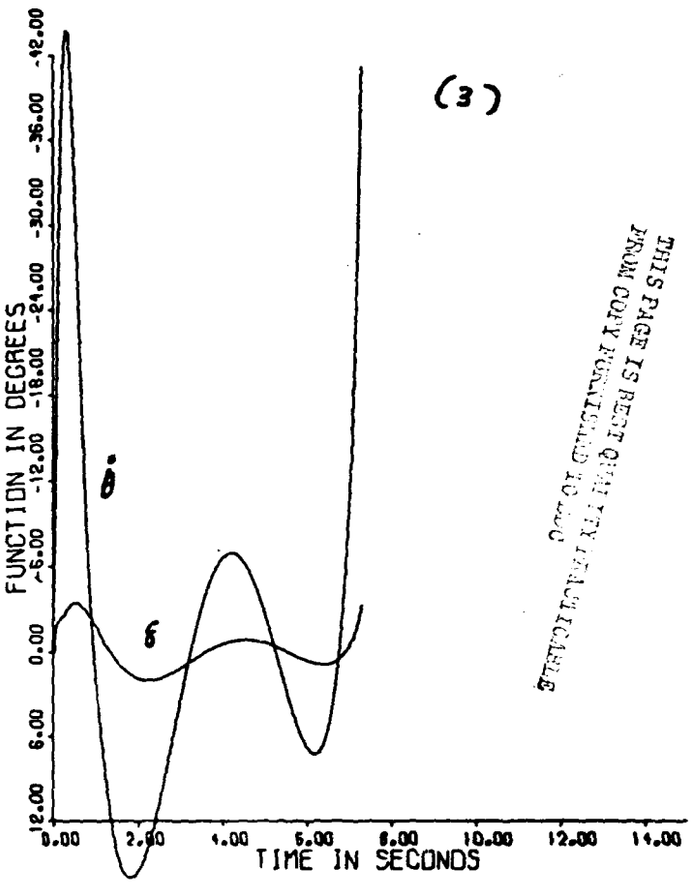

SECOND - ORDER SIMULATION

INPUT AND OUTPUT OF THE SYSTEM

FIG.20d
(1)

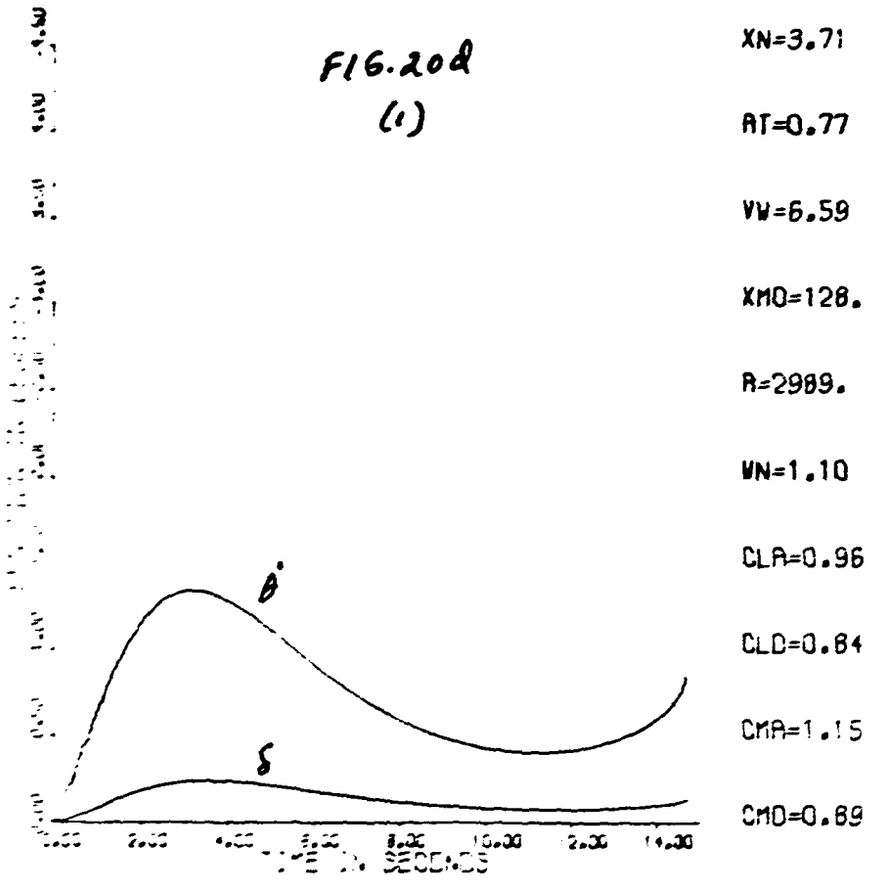

XN=3.71

RT=0.77

VW=6.59

XMO=128.

R=2989.

WN=1.10

CLA=0.96

CLD=0.84

CMA=1.15

CMO=0.89

LOCAL FEEDBACK SIMULATION

INPUT AND OUTPUT OF THE SYSTEM

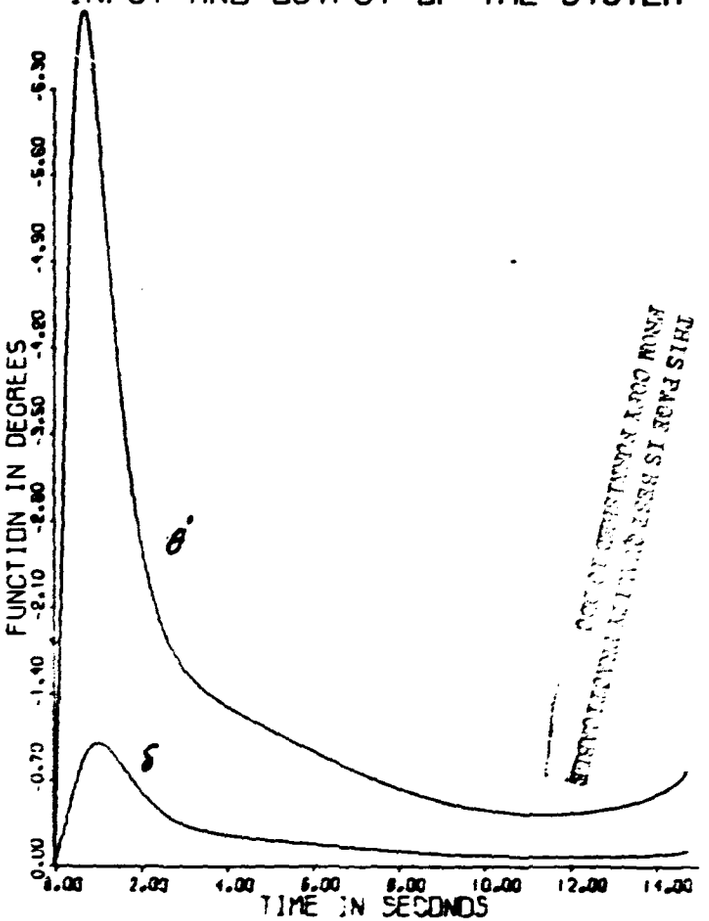

SECOND - ORDER SIMULATION

INPUT AND OUTPUT OF THE SYSTEM

FIG. 20A
(1)

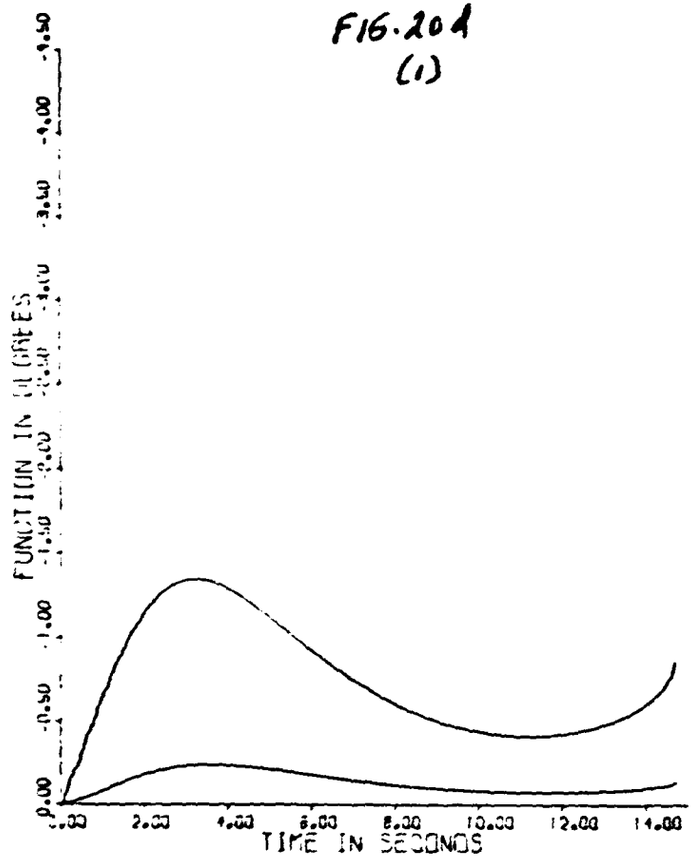

XN=3.71

AT=0.77

VW=6.59

XMD=128.

R=2989.

WN=1.10

CLA=0.96

CLD=0.84

CMA=1.15

CMD=0.89

GLOBAL FEEDBACK SIMULATION

INPUT AND OUTPUT OF THE SYSTEM

(3)

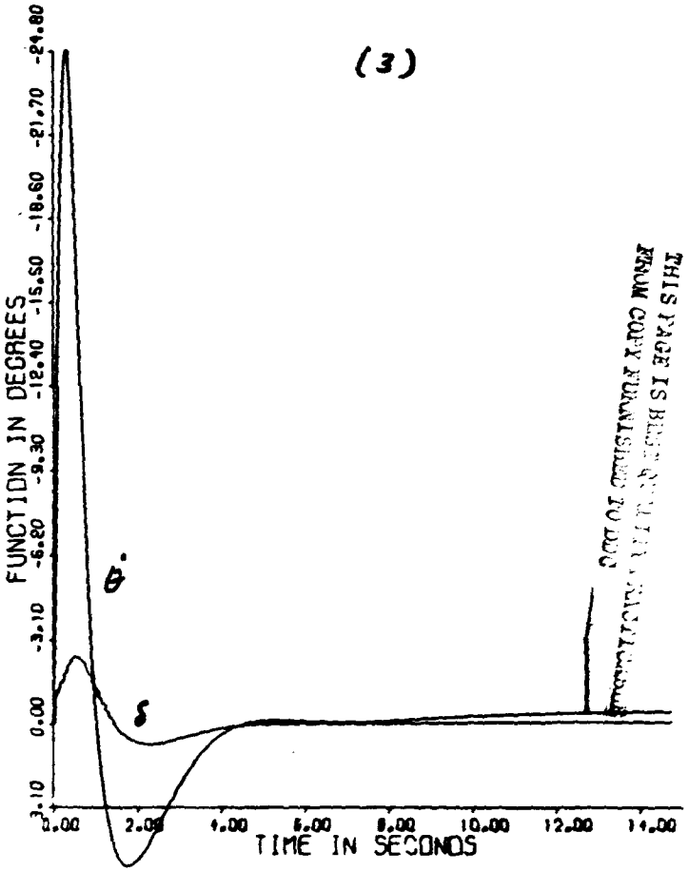

SECOND - ORDER SIMULATION

INPUT AND OUTPUT OF THE SYSTEM

FIG. 20e

(1)

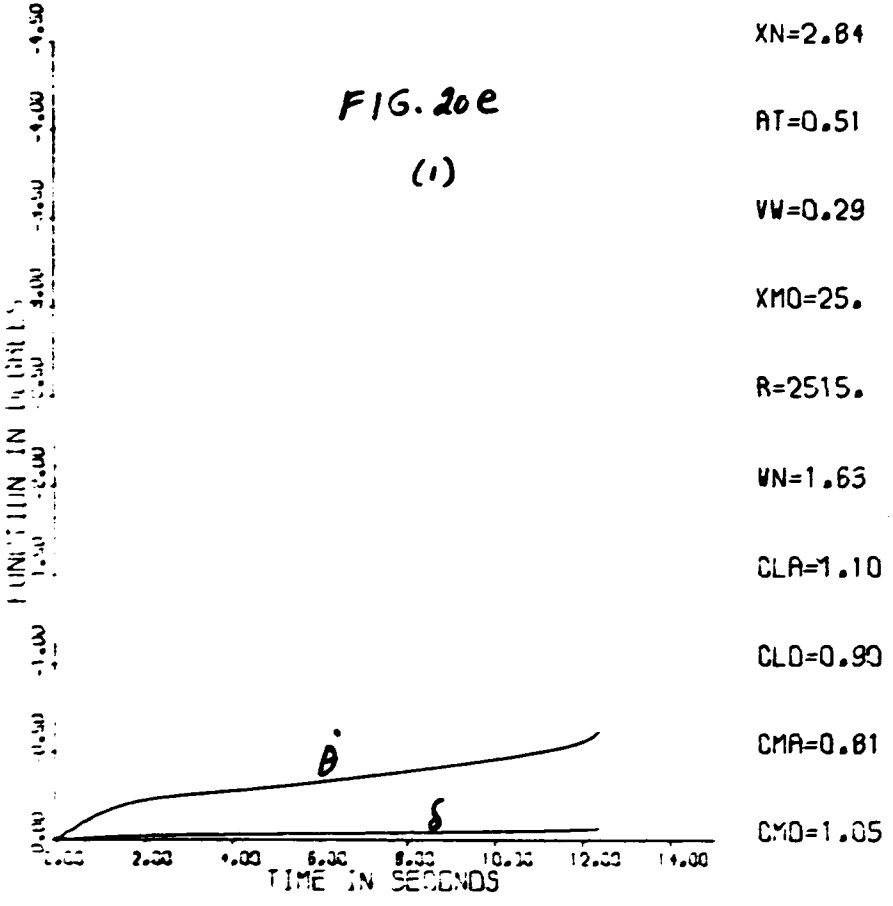

XN=2.84

AT=0.51

VW=0.29

XMO=25.

R=2515.

WN=1.63

CLA=1.10

CLO=0.90

CMA=0.81

CMO=1.05

LOCAL FEEDBACK SIMULATION

INPUT AND OUTPUT OF THE SYSTEM

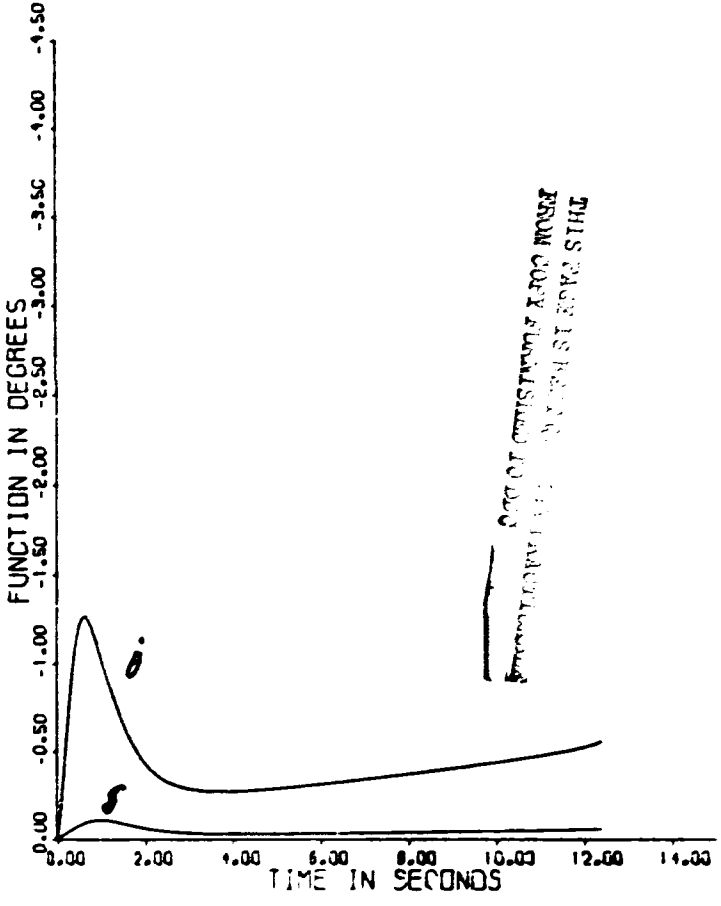

SECOND - ORDER SIMULATION

INPUT AND OUTPUT OF THE SYSTEM

FIG. 20c

(1)

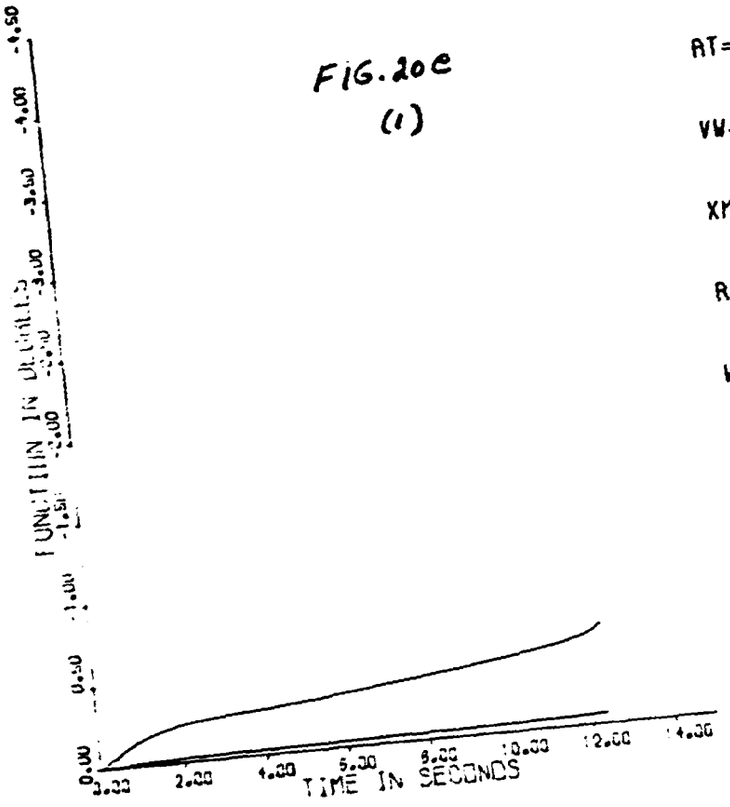

XN=2.84

AT=0.51

VW=0.29

XMO=25.

R=2515.

VN=1.63

CLA=1.10

CLO=0.90

CMA=0.81

CMO=1.05

GLOBAL FEEDBACK SIMULATION

INPUT AND OUTPUT OF THE SYSTEM

(3)

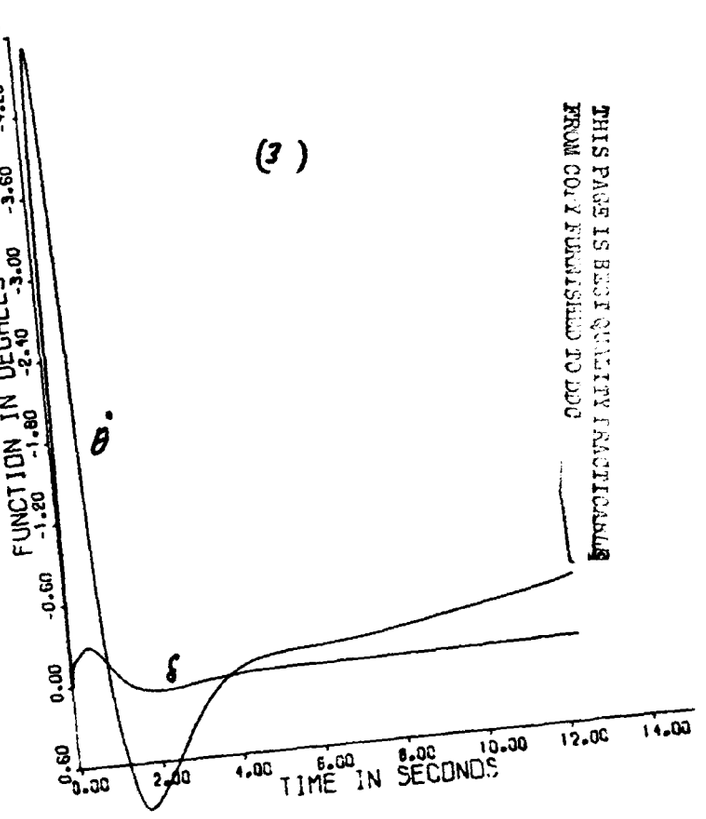

Figures (4a-q)). The second part uses the same input $\dot{\lambda}$ (to the autopilot) as in the first part and the outer loop is not closed. It is only a test of the autopilot and is therefore denoted as "local feedback simulation". In the third part the outer loop is closed, so the simulation is that of a "practical" system.

It is seen that in general the $\delta(t)$, $\dot{\theta}(t)$ values in the last two parts are larger in magnitude, but considerably smoother than in the first. But in considering the actual tracking, the outer loop was not found satisfactory. This is next treated.

3.7. Outer Loop Modification and Global Simulation

The above autopilot design was next imbedded into the over-all structure of Figure 2, and the tracking examined (y_T and y_m). In a sense it is an unfair comparison of the nonlinear design technique, because the latter was executed only for the autopilot part. In any case, when effected, the poorest results were the three shown in Figure 21, in which $y_T(t)$ represents the target trajectory and $y_m(t)$, the missile trajectory. The run is stopped precisely when $R = V_m t \cos\gamma$, i.e. when $\Delta x = 0$. A perfect hit requires $y_T = y_m$ precisely at this end-point. In Figure 21a, there is an error of 6 meters, and much smaller errors in 21b,c. Also, the $y_m(t)$ trajectories in Figures 21a,b are much too oscillatory.

The reson for the above is due to the fact that the design was, up to this point, completely a local one — of the autopilot alone, to achieve a specified response range for the autopilot. No overall global closed-loop response was considered at all. The logical procedure at this point would be to find the ℓti equivalent of the time-varying portion of the structure (i.e. of the $\lambda = \tan^{-1} \Delta y/\Delta x$ portion) and apply the design technique to the outer loop. The nonlinear design technique applies also to linear and nonlinear time-varying uncertain plants — see Reference 1. However, there was insufficient time left for effecting such a design. Therefore an ad-hoc modification of the prefilter $F(s)$ was made, with the new

$$F(s) = \frac{768(s+.5)}{(s+1)(s+4)(s+8)(s+12)} \qquad (21)$$

TRAJECTORY OF THE FLIGHT

GLOBAL SIMULATION
USING $F(A) = \frac{48}{(A+1.5)(A+4)(A+8)}$

FIG. 21

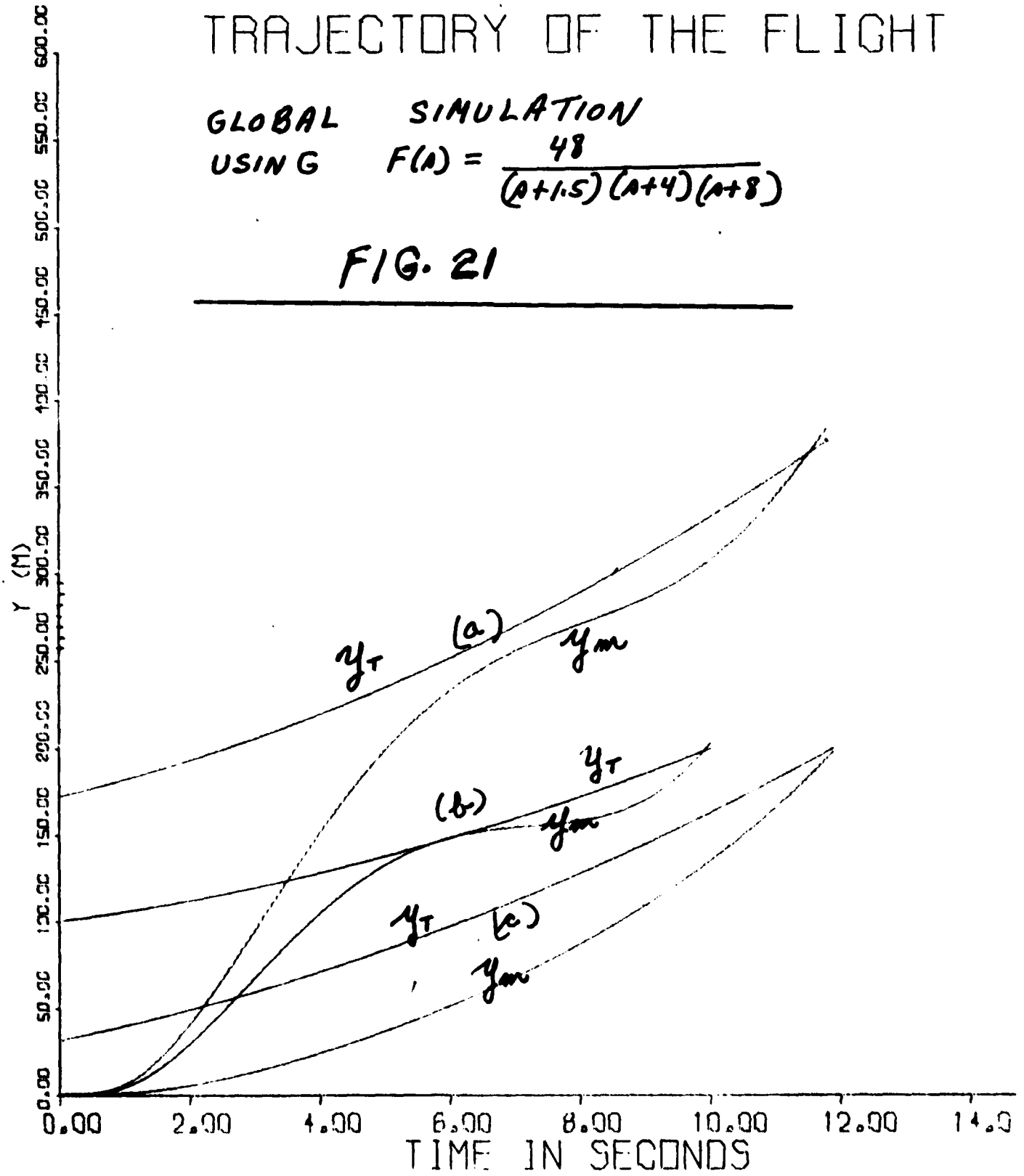

This gave much better results, shown in Figures 22a-t, whose interpretation is the same as of Figure 21. The star (explosion) indicates an "error" < 2 meters, interpreted as a "hit". Of all the runs made, there was only one case where the error ≈ 3 meters, in Figure 22s.

To complete the picture, a large number of runs of the variables δ , α , accel $\triangleq \dot{V_Y}/g$ are shown in Figures 23a-p.

TRAJECTORY OF THE FLIGHT

F16.22a

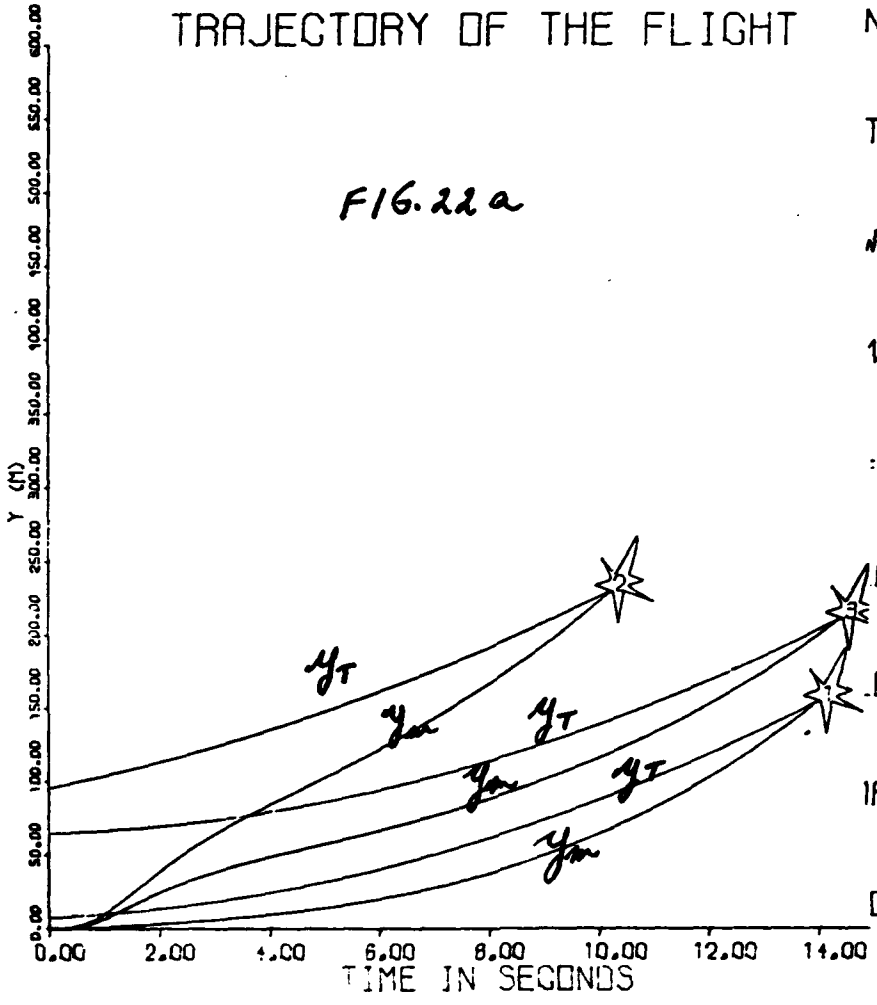

ASE 1	CASE 2	CASE 3
N=2.76	XN=2.25	XN=3.11
T=1.26	AT=1.05	AT=1.25
N=1.70	VW=7.87	VW=1.19
10=7.	XMO=95.	XMO=64.
:2799.	R=2042.	R=2881.
IA=1.01	CLA=0.91	CLA=0.89
.D=1.05	CLD=0.81	CLD=1.09
IA=1.04	CMA=1.04	CMA=0.93
D=0.95	CMD=1.01	CMD=1.12

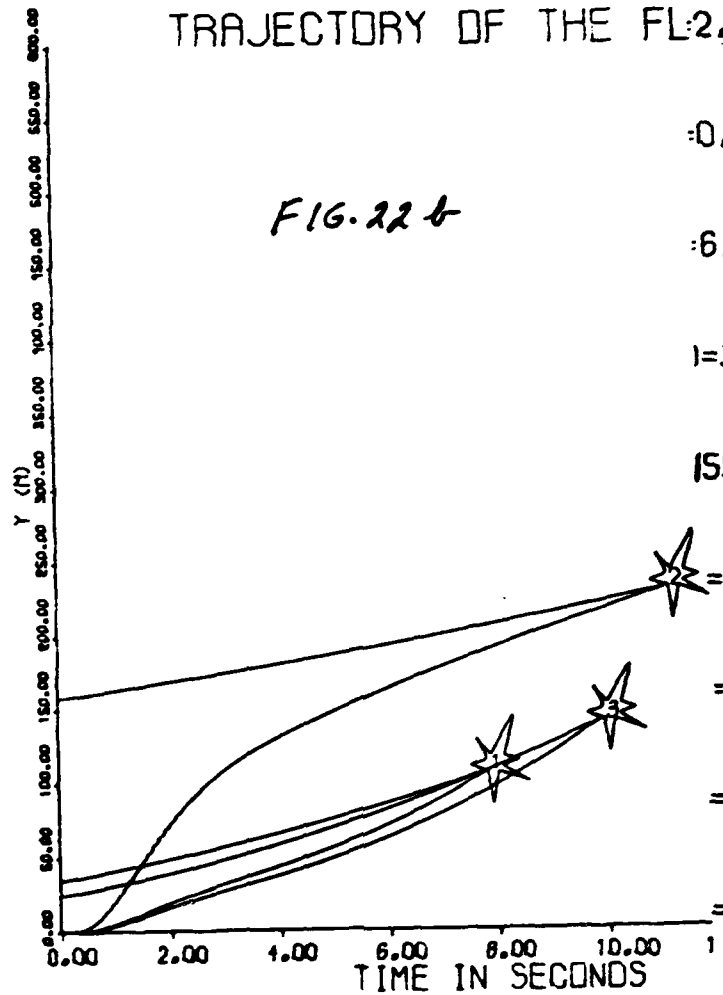

FIG. 22 b

E 1	CASE 2	CASE 3
2.03	XN=2.77	XN=3.07
=0.76	AT=0.25	AT=1.11
=6.32	VW=5.24	VW=6.26
)=34.	XMO=157.	XMO=24.
1554.	R=2213.	R=1981.
=1.18	CLA=1.09	CLA=1.15
=1.04	CLD=1.04	CLD=0.93
=1.01	CMA=0.91	CMA=0.89
=1.05	CMD=0.81	CMD=1.09

TRAJECTORY OF THE FLIGHT

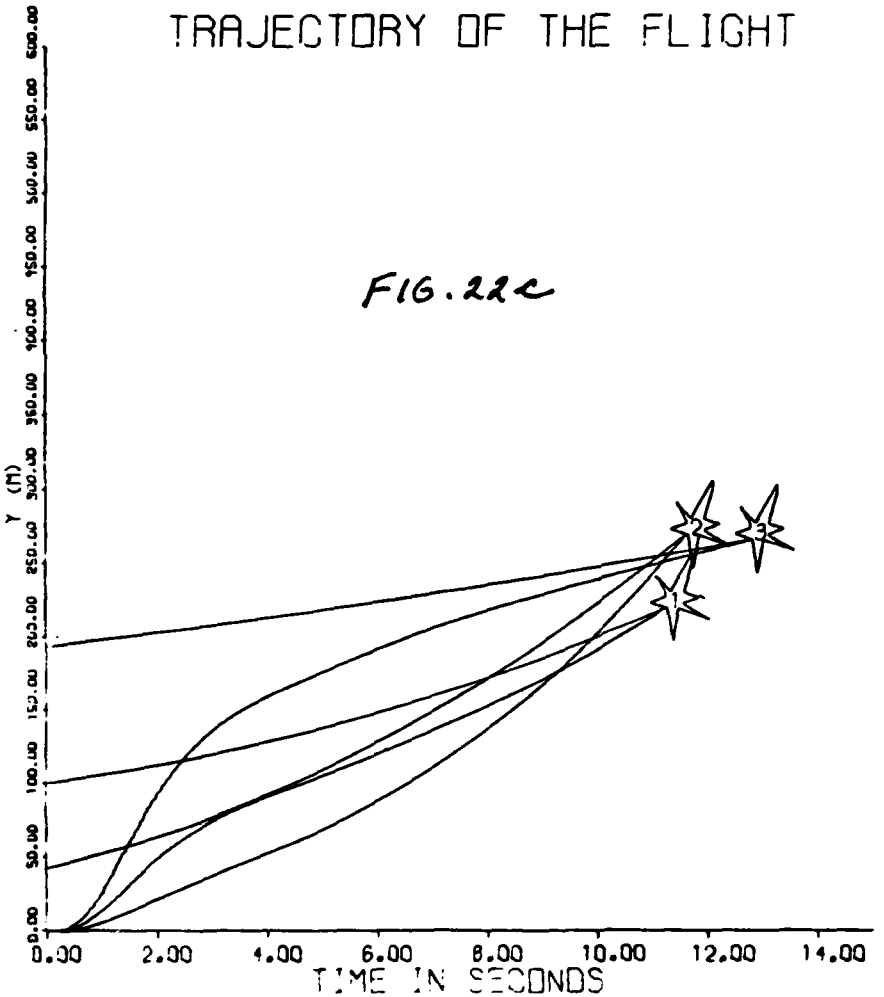

FIG. 22c

CASE 1	CASE 2	CASE 3
XN=3.00	XN=2.97	XN=3.42
AT=1.00	AT=1.88	AT=0.17
VW=5.00	VW=8.59	VW=4.58
XMO=100.	XMO=42.	XMO=193.
R=2250.	R=2324.	R=2559.
CLA=1.00	CLA=0.86	CLA=1.14
CLD=1.00	CLD=1.02	CLD=0.84
CMA=1.00	CMA=1.03	CMA=1.03
CMD=1.00	CMD=1.10	CMD=0.82

TRAJECTORY OF THE FLIGHT

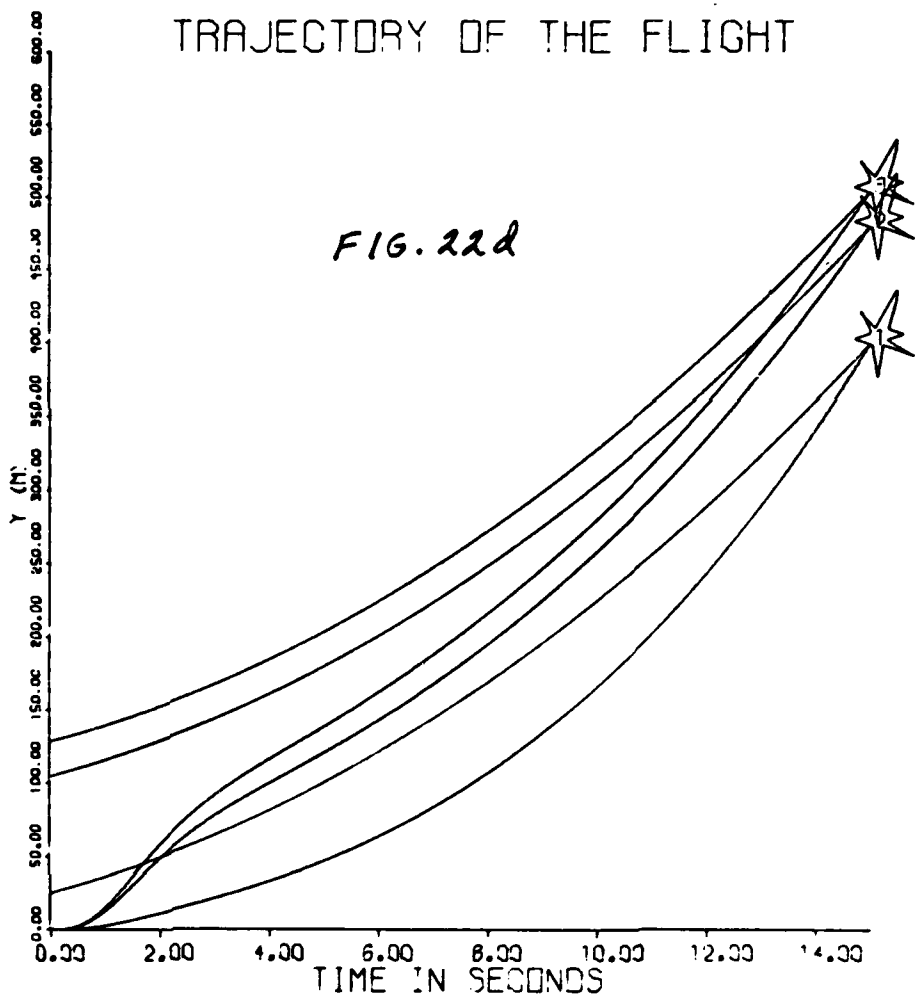

FIG. 22d

CASE 1	CASE 2	CASE 3
XN=2.84	XN=3.79	XN=3.71
AT=2.00	AT=2.00	AT=2.00
VW=10.00	VW=10.00	VW=10.00
XMO=25.	XMO=104.	XMO=128.
R=3000.	R=3000.	R=3000.
CLA=1.10	CLA=0.82	CLA=0.36
CLD=0.90	CLD=1.19	CLD=0.84
CMA=0.81	CMA=0.92	CMA=1.15
CMD=1.05	CMD=0.91	CMD=0.89

TRAJECTORY OF THE FLIGHT

FIG. 22e

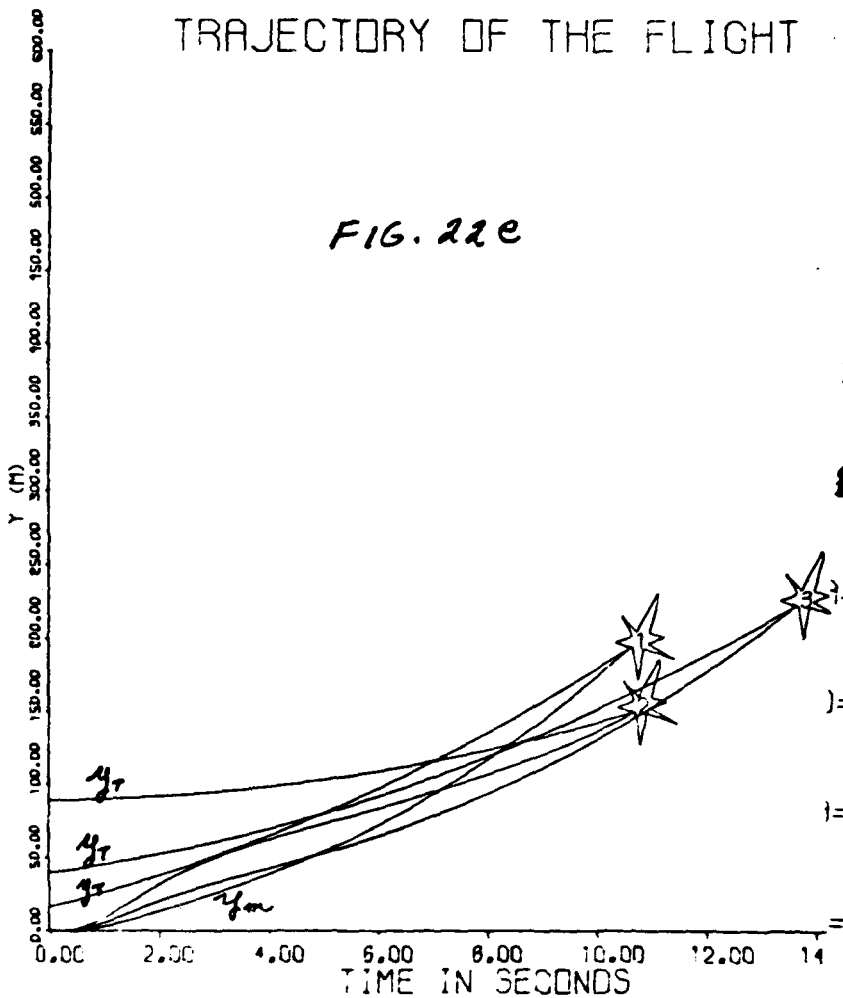

E 1	CASE 2	CASE 3
:3.58	XN=2.09	XN=3.64
:1.43	AT=1.00	AT=1.26
:9.10	VW=0.33	VW=4.85
)=16.	XMO=89.	XMO=40.
123.	R=2132.	R=2726.
)=0.88	CLA=1.02	CLA=1.01
)=0.86	CLD=0.96	CLD=0.95
)=1.00	CMA=1.03	CMA=0.86
=0.99	CMD=1.12	CMD=0.99

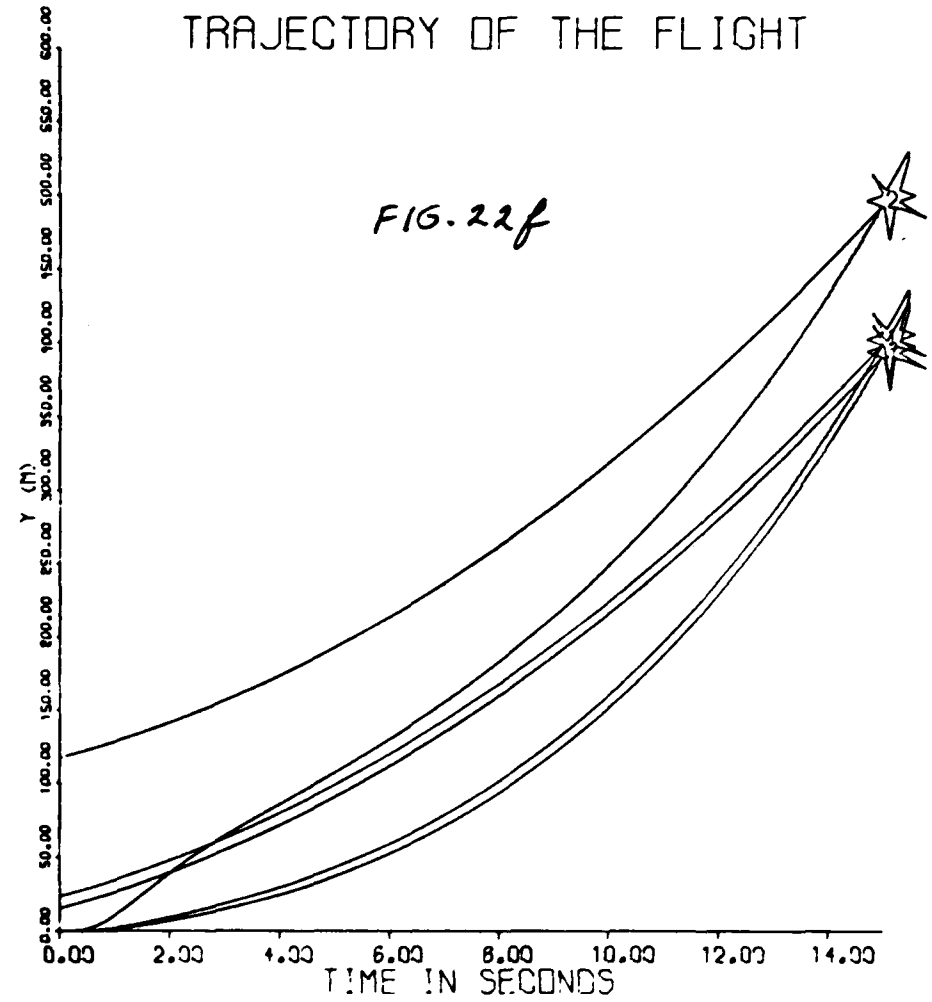

FIG. 22f

CASE 1	CASE 2	CASE 3
XN=2.67	XN=2.61	XN=2.60
AT=2.00	AT=2.00	AT=2.00
VW=10.00	VW=10.00	VW=10.00
XMO=24.	XMO=117.	XMO=15.
R=3000.	R=3000.	R=3000.
CLA=0.80	CLA=1.38	CLA=0.84
CLO=0.84	CLO=0.93	CLO=1.02
CMA=1.13	CMA=0.97	CMA=1.11
CMO=1.17	CMO=0.82	CMO=0.88

AD-A080 846 WEIZMANN INST OF SCIENCE REHOVOTH (ISRAEL) DEPT OF --ETC F/G 16/4
APPLICATION OF SYNTHESIS TECHNIQUE FOR NONLINEAR UNCERTAIN SYST--ETC(U)
JUN 79 B GOLUBEV, I HOROWITZ, Y KATZ DA-ERO-77-G-096

UNCLASSIFIED NL

2 OF 2
AD
A080646

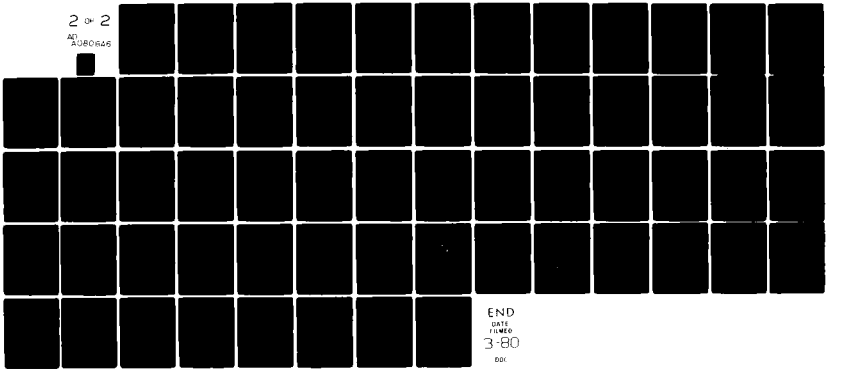

END
DATE FILMED
3-80
DDC

TRAJECTORY OF THE FLIGH

FIG.22g

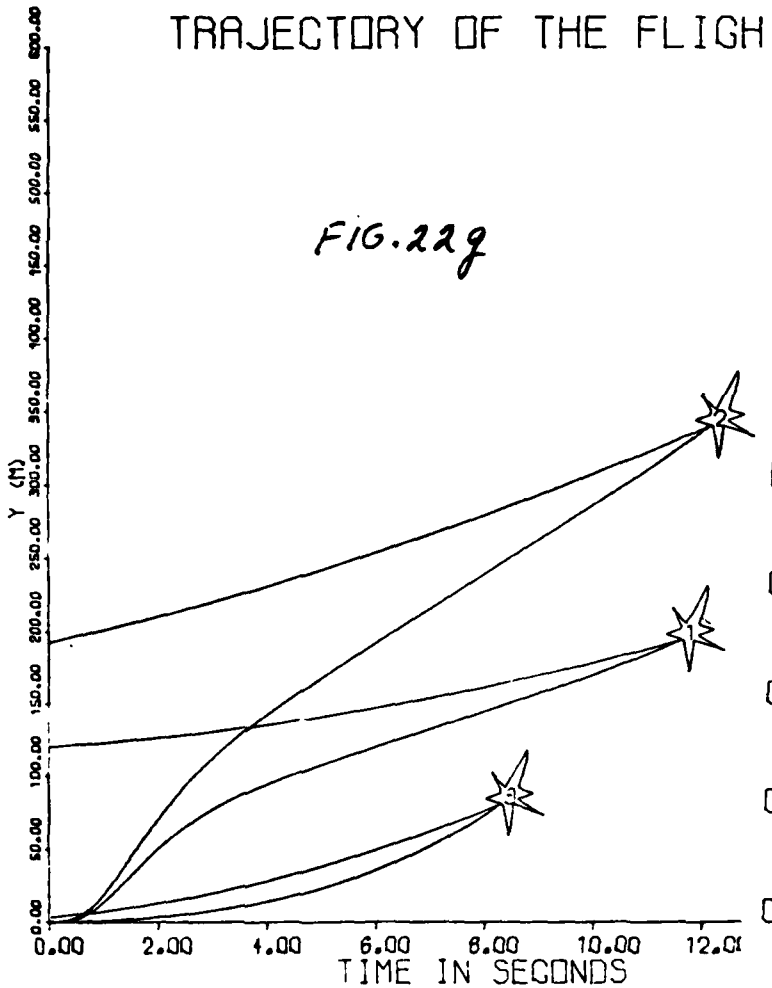

CASE 1	CASE 2	CASE 3
XN=2.74	XN=2.45	XN=2.42
AT=0.66	AT=0.64	AT=1.43
VW=2.59	VW=8.27	VW=3.37
XMO=120.	XMO=192.	XMO=3.
R=2327.	R=2439.	R=1662.
CLA=1.03	CLA=1.00	CLA=1.01
CLD=0.84	CLD=0.98	CLD=1.11
CMA=0.86	CMA=1.12	CMA=0.89
CMD=1.09	CMD=1.03	CMD=0.81

TRAJECTORY OF THE FLIGHT

FIG. 22 b

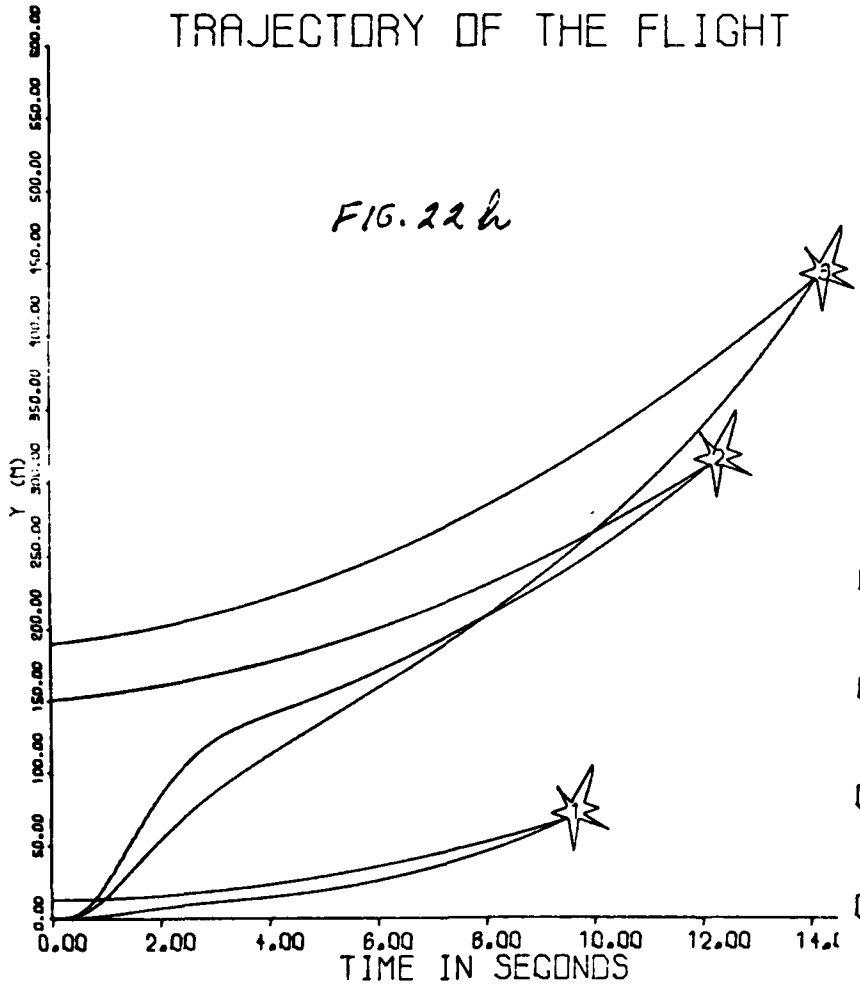

CASE 1	CASE 2	CASE 3
XN=2.82	XN=3.95	XN=2.18
AT=1.16	AT=1.65	AT=1.97
VW=0.33	VW=3.34	VW=3.85
XMO=13.	XMO=150.	XMO=190.
R=1895.	R=2427.	R=2817.
CLA=1.20	CLA=1.04	CLA=0.98
CLD=0.97	CLD=0.84	CLD=1.09
CMA=1.08	CMA=1.05	CMA=1.05
CMD=0.96	CMD=1.10	CMD=1.12

TRAJECTORY OF THE FLIGHT

FIG. 22i

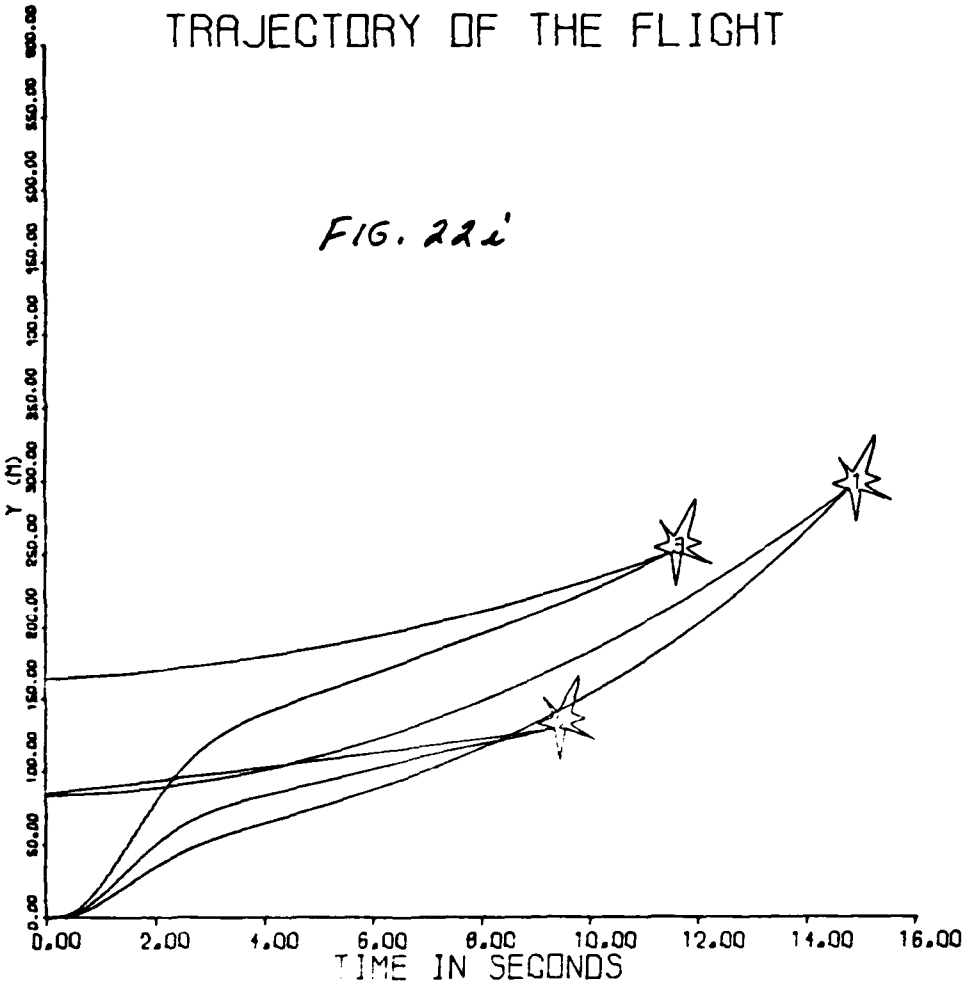

CASE 1	CASE 2	CASE 3
XN=3.43	XN=3.00	XN=3.26
RT=1.82	RT=0.07	RT=0.97
VW=0.82	VW=4.44	VW=1.98
XMO=83.	XMO=84.	XMO=[illegible]
R=2955.	R=1865.	R=2296.
CLA=1.00	CLA=1.03	CLA=0.86
CLD=0.99	CLD=1.12	CLD=0.93
CMA=0.86	CMA=0.96	CMA=0.95
CMD=0.82	CMD=1.13	CMD=0.89

TRAJECTORY OF THE FLIGHT

FIG. 22j

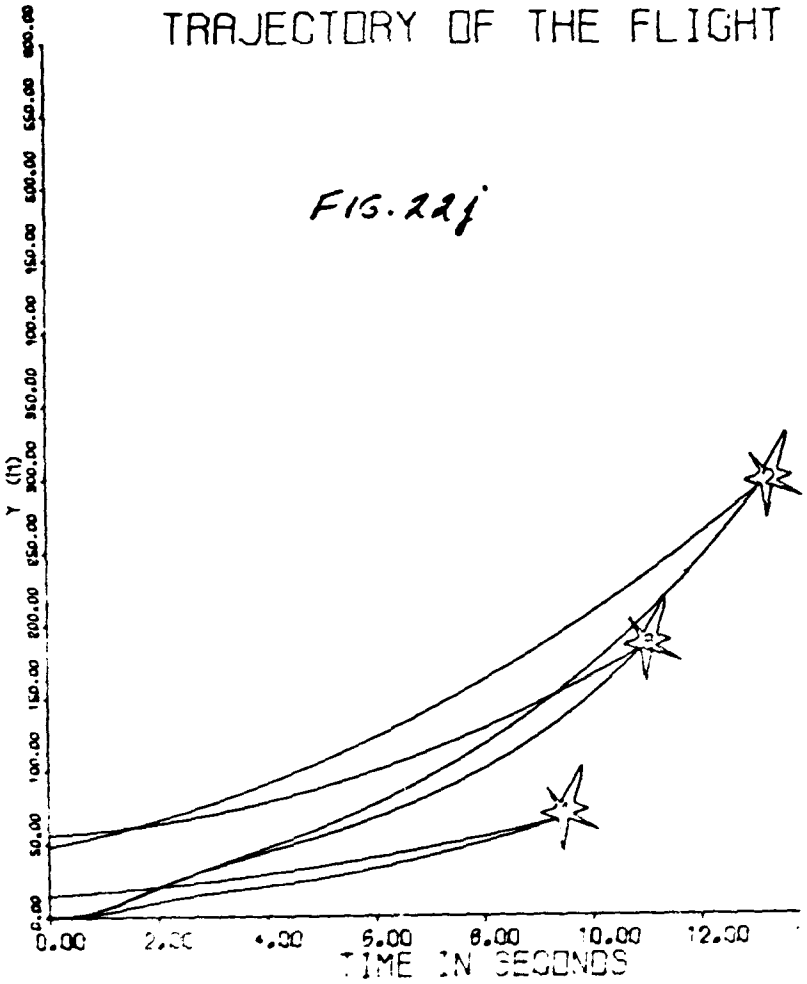

CASE 1	CASE 2	CASE 3
XN=3.39	XN=2.74	XN=2.15
AT=0.71	AT=1.78	AT=1.78
VW=2.07	VW=7.04	VW=1.90
XMO=15.	XMO=47.	XMO=55.
R=1863.	R=2624.	R=2175.
CLA=0.91	CLA=0.97	CLA=0.94
CLD=0.84	CLD=0.96	CLD=0.81
CMA=1.20	CMA=1.06	CMA=1.14
CMD=0.87	CMD=0.96	CMD=0.82

TRAJECTORY OF THE F

FIG.22k

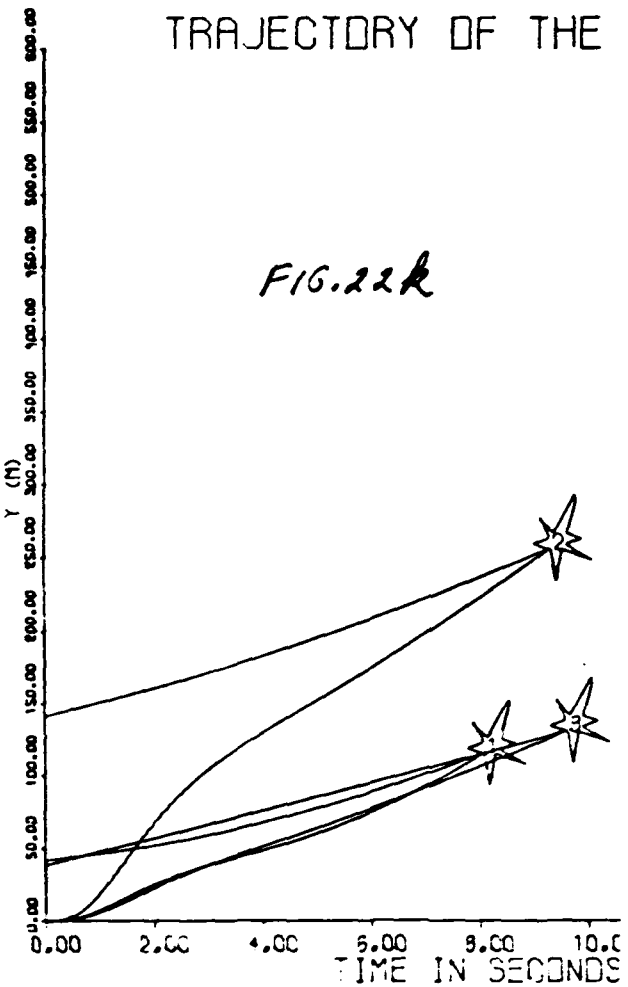

CASE 1	CASE 2	CASE 3
XN=2.43	XN=2.35	XN=2.81
AT=1.39	AT=0.74	AT=0.15
VW=3.53	VW=8.92	VW=8.92
XMO=41.	XMO=141.	XMO=38.
R=1609.	R=1856.	R=1916.
CLA=1.14	CLA=1.07	CLA=0.81
CLD=1.20	CLD=1.06	CLD=1.14
CMA=0.91	CMA=0.97	CMA=0.94
CMD=0.84	CMD=0.96	CMD=0.81

TRAJECTORY OF THE FLIGHT

FIG.22l

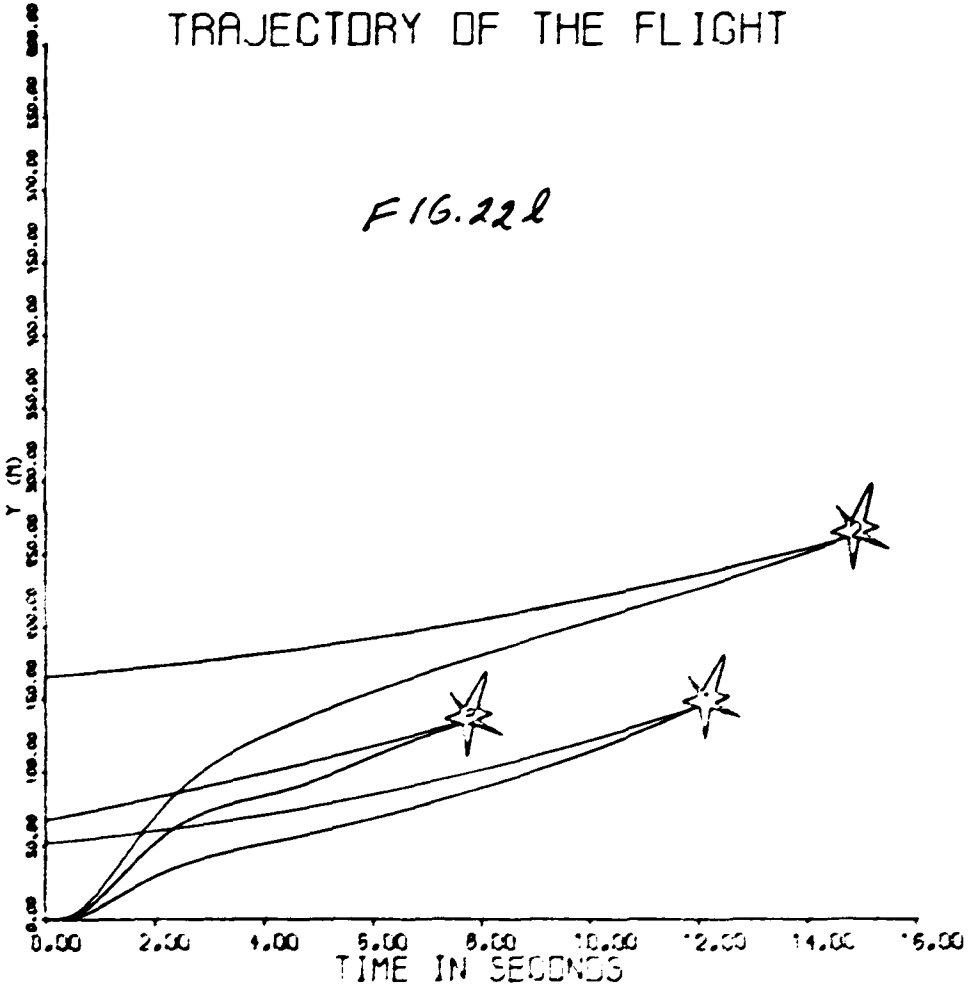

CASE 1	CASE 2	CASE 3
XN=3.62	XN=3.45	XN=3.13
AT=0.74	AT=0.45	AT=0.42
VW=3.28	VW=3.18	VW=7.15
XMO=52.	XMO=165.	XMO=67.
R=2398.	R=2942.	R=1523.
CLA=1.16	CLA=1.08	CLA=1.11
CLD=0.86	CLD=1.12	CLD=0.89
CMA=1.03	CMA=1.00	CMA=1.01
CMD=0.84	CMD=0.98	CMD=1.11

TRAJECTORY OF THE FLIGHT

FIG. 22 m.

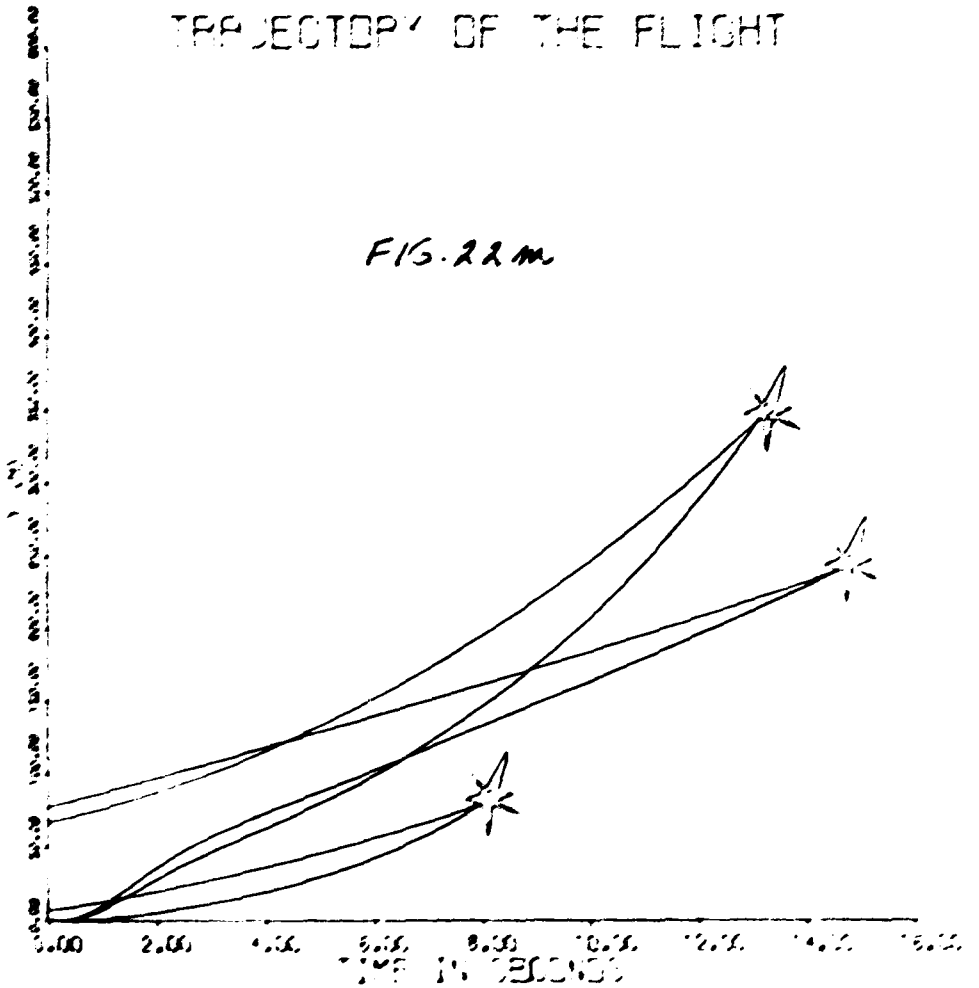

CASE 1	CASE 2	CASE 3
VN=2.12	VN=2.82	VN=3.32
AT=0.82	AT=1.35	AT=0.18
Vd=3.78	Vd=3.23	Vd=3.83
VMC=7.	VMC=67.	VMC=77.
R=1334.	R=2525.	R=2922.
CLA=0.91	CLA=0.37	CLA=1.03
CLD=1.08	CLD=1.05	CLD=1.05
CMA=1.20	CMA=1.04	CMA=0.38
CMD=0.37	CMD=0.84	CMD=1.03

TRAJECTORY OF THE FLIGHT

FIG. 22n

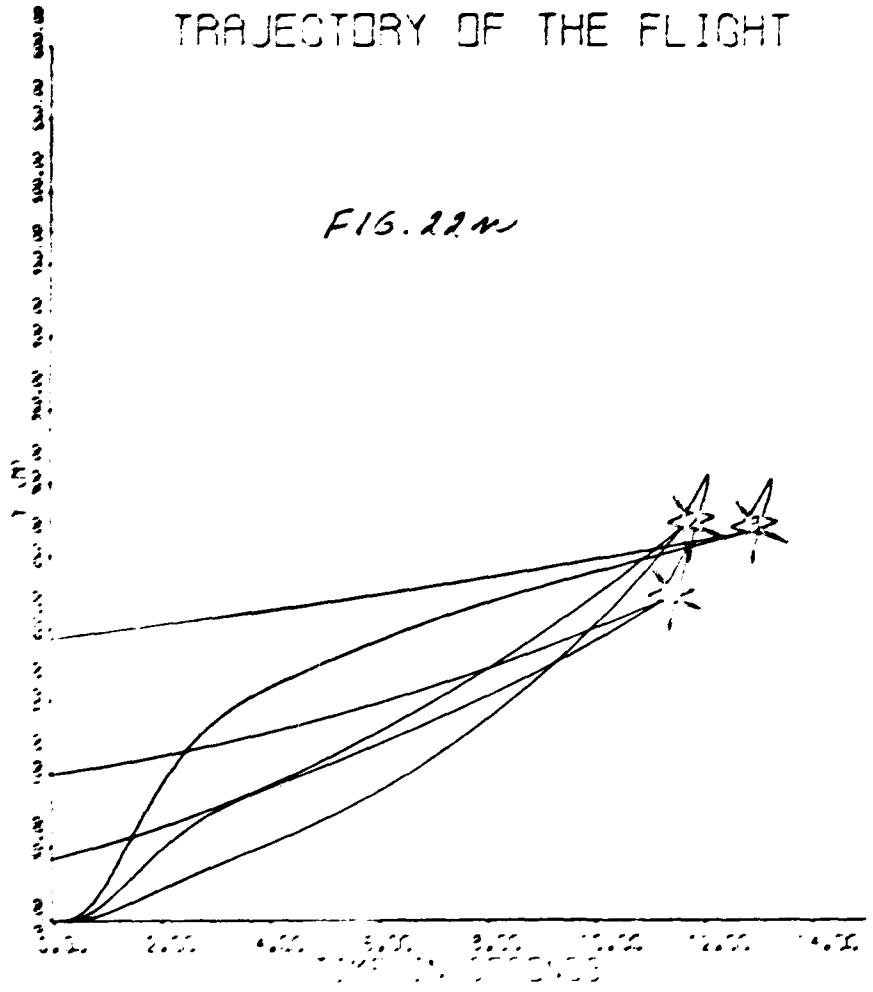

CASE 1	CASE 2	CASE 3
XN=3.00	XN=2.97	XN=3.42
AT=1.00	AT=1.88	AT=0.17
VW=5.00	VW=8.58	Vd=4.58
XMO=100.	XMO=42.	XMO=193.
R=2250.	R=2324.	R=2359.
CLA=1.00	CLA=0.86	CLA=1.14
CLD=1.00	CLD=1.02	CLD=0.84
CMA=1.00	CMA=1.03	CMA=1.03
CMD=1.00	CMD=1.10	CMD=0.82

TRAJECTORY OF THE FLIGHT

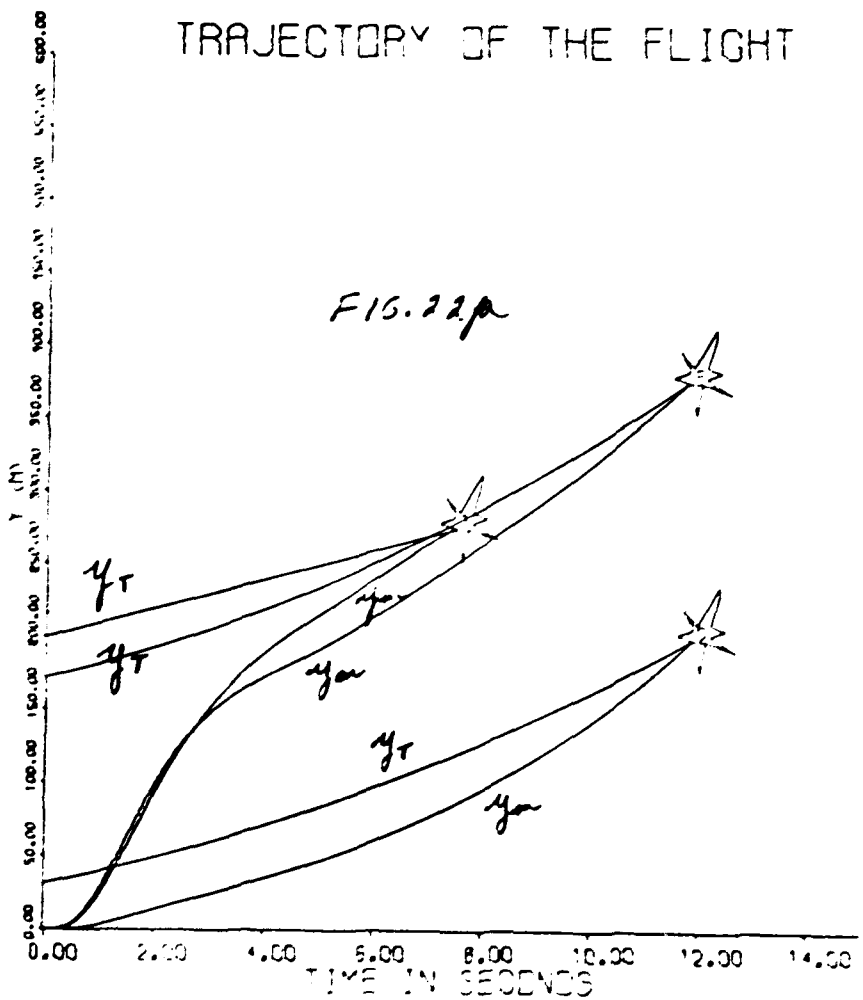

Fig. 22a

CASE 1	CASE 2	CASE 3
XN=2.00	XN=2.42	XN=3.93
AT=0.00	AT=1.10	AT=1.41
VW=10.00	VW=7.67	VW=8.99
XMO=200.	XMO=31.	XMO=172.
R=1500.	R=2378.	R=2356.
CLA=0.80	CLA=1.10	CLA=0.82
CLD=0.80	CLD=0.83	CLD=1.19
CMA=0.80	CMA=1.08	CMA=0.95
CMD=0.80	CMD=0.98	CMD=1.02

TRAJECTORY OF THE FLIGHT

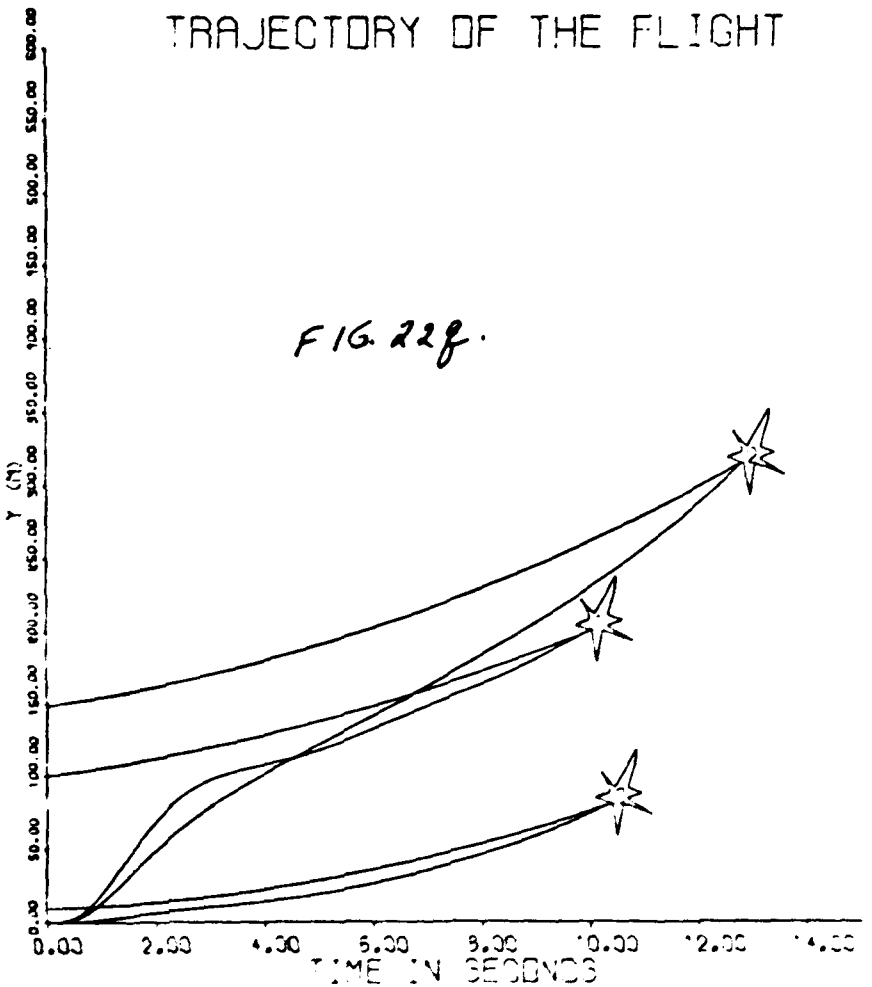

FIG. 22f.

CASE 1	CASE 2	CASE 3
XN=4.00	XN=2.31	XN=3.72
AT=1.00	AT=1.17	AT=1.14
VW=5.00	VW=5.42	VW=0.89
XMO=100.	XMO=149.	XMO=10.
R=2000.	R=2564.	R=2074.
CLA=0.80	CLA=0.98	CLA=1.02
CLD=1.20	CLD=1.08	CLD=0.94
CMA=1.20	CMA=1.19	CMA=1.05
CMD=0.60	CMD=1.16	CMD=1.01

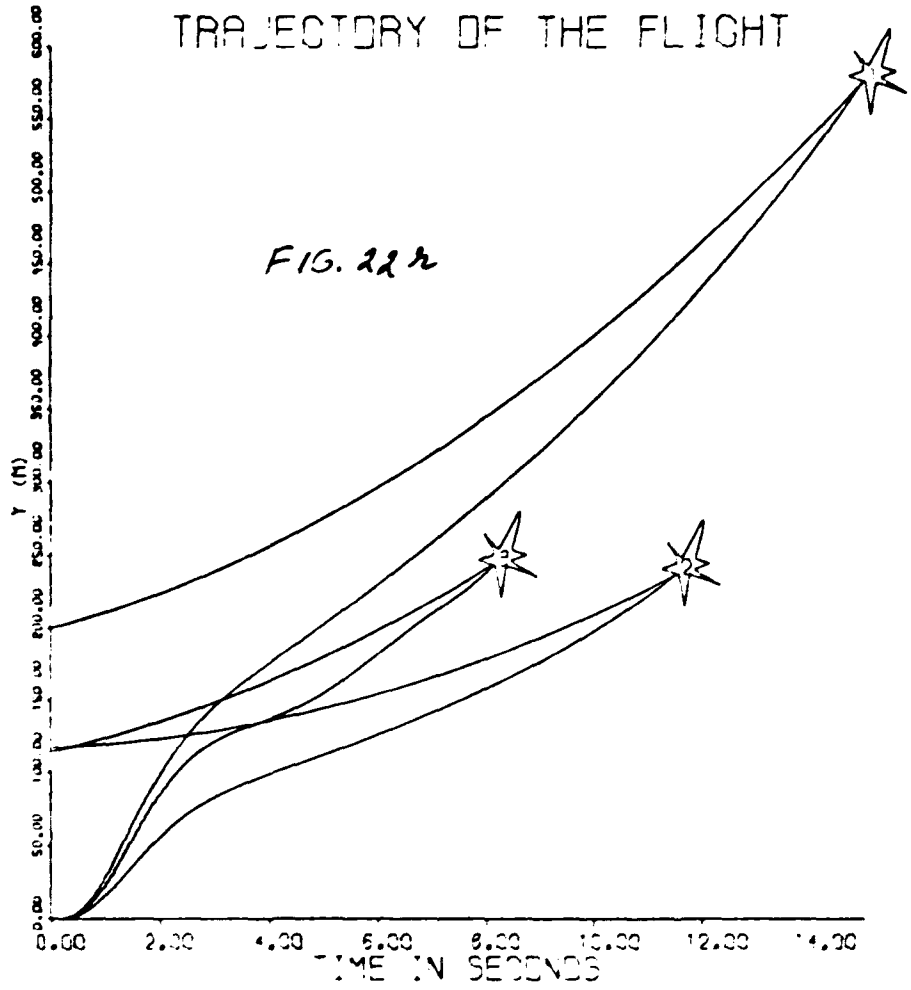

FIG. 22 a

CASE 1	CASE 2	CASE 3
XN=4.00	XN=3.10	XN=3.41
AT=2.00	AT=1.53	AT=1.80
VW=10.00	VW=1.56	VW=8.60
XMO=200.	XMO=117.	XMO=114.
R=3000.	R=2313.	R=1633.
CLA=1.20	CLA=1.08	CLA=0.95
CLD=1.20	CLD=0.98	CLD=1.02
CMA=1.20	CMA=0.83	CMA=1.19
CMD=1.20	CMD=1.19	CMD=1.05

TRAJECTORY OF THE FLIGHT

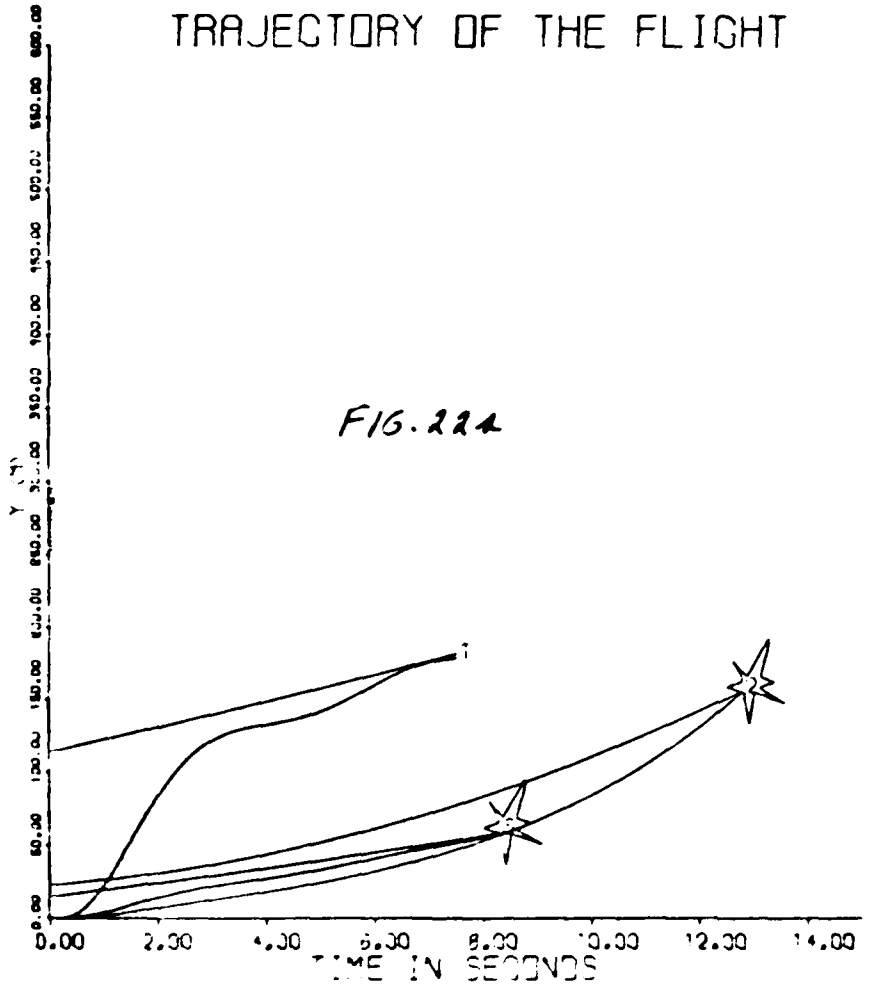

FIG. 22a

CASE 1	CASE 2	CASE 3
XN=3.23	XN=2.05	XN=3.85
AT=0.24	AT=1.17	AT=0.15
VW=8.15	VW=2.88	VW=4.59
XMO=114.	XMO=23.	XMO=14.
R=1503.	R=2558.	R=1658.
CLA=0.84	CLA=0.93	CLA=1.02
CLO=0.92	CLO=0.92	CLO=0.97
CMA=1.17	CMA=0.82	CMA=0.88
CMO=1.15	CMO=0.84	CMO=0.90

TRAJECTORY OF THE FLIGHT

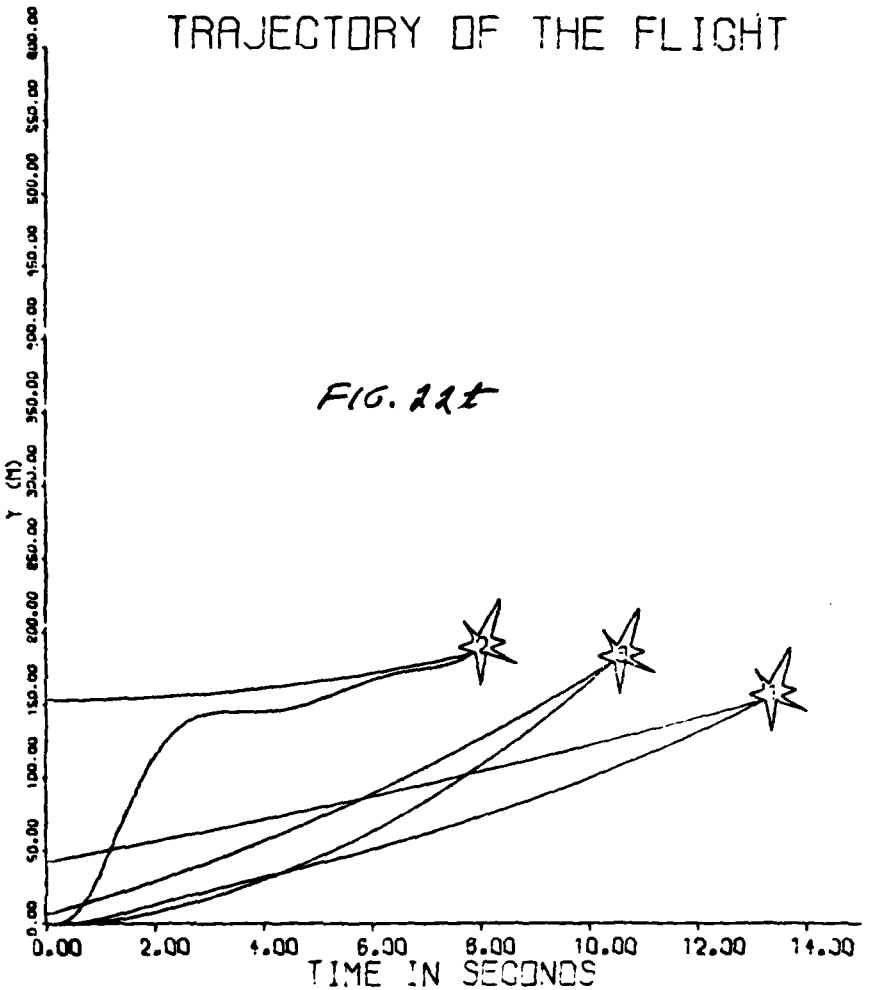

FIG. 22t

CASE 1	CASE 2	CASE 3
XN=2.06	XN=3.43	XN=3.32
AT=0.25	AT=1.04	AT=1.28
VW=6.77	VW=0.04	VW=9.93
XMO=42.	XMO=153.	XMO=6.
R=2642.	R=1571.	R=2084.
CLA=0.90	CLA=1.19	CLA=0.84
CLD=1.16	CLD=1.14	CLD=1.08
CMA=1.05	CMA=0.91	CMA=0.69
CMD=1.08	CMD=0.95	CMD=0.94

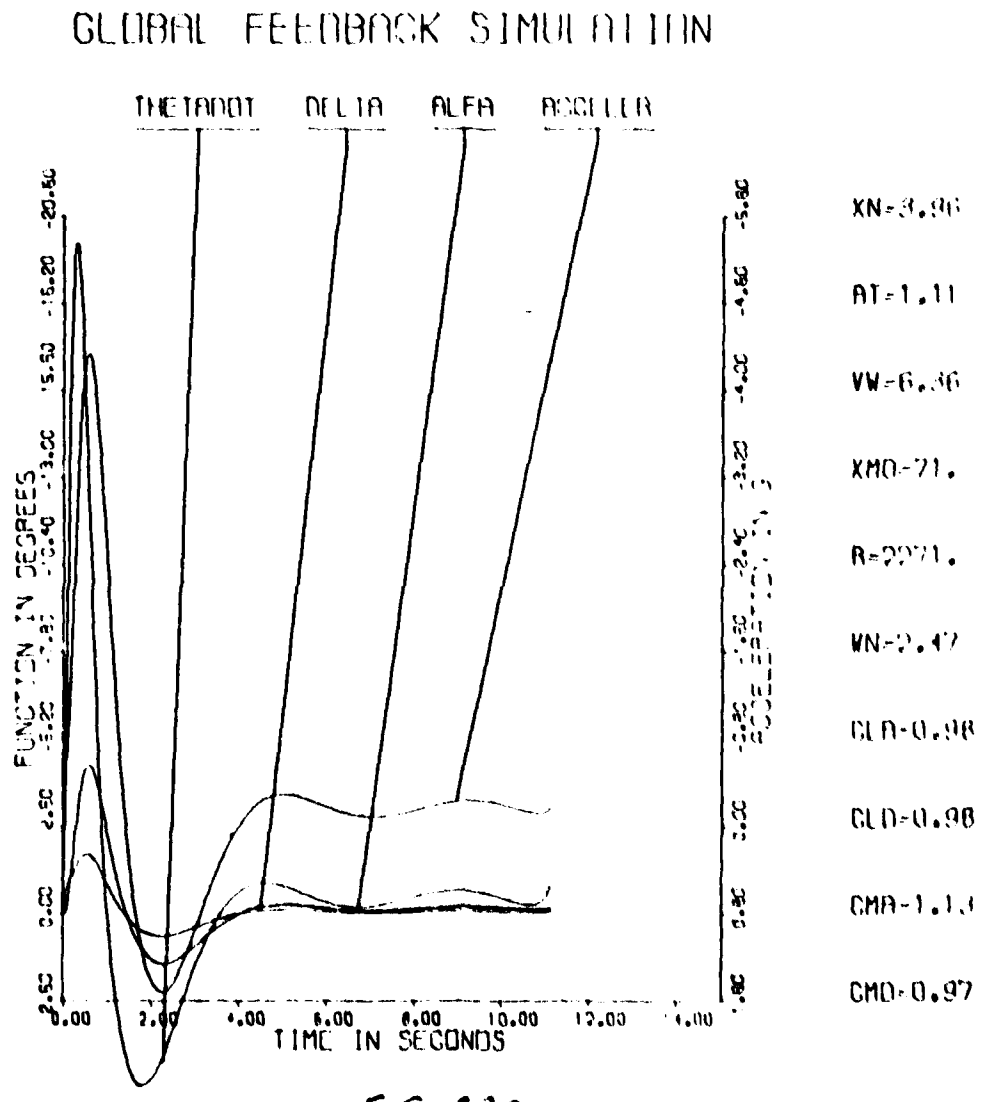
GLOBAL FEEDBACK SIMULATION
THETADOT
DELTA
ALFA
ACCELER
FUNCTION IN DEGREES
TIME IN SECONDS
XN=3.96
AT=1.11
VW=6.36
XMD=71.
R=2071.
WN=2.47
CLA=0.98
CLD=0.98
CMA=1.1
CMD=0.97

FIG. 23a

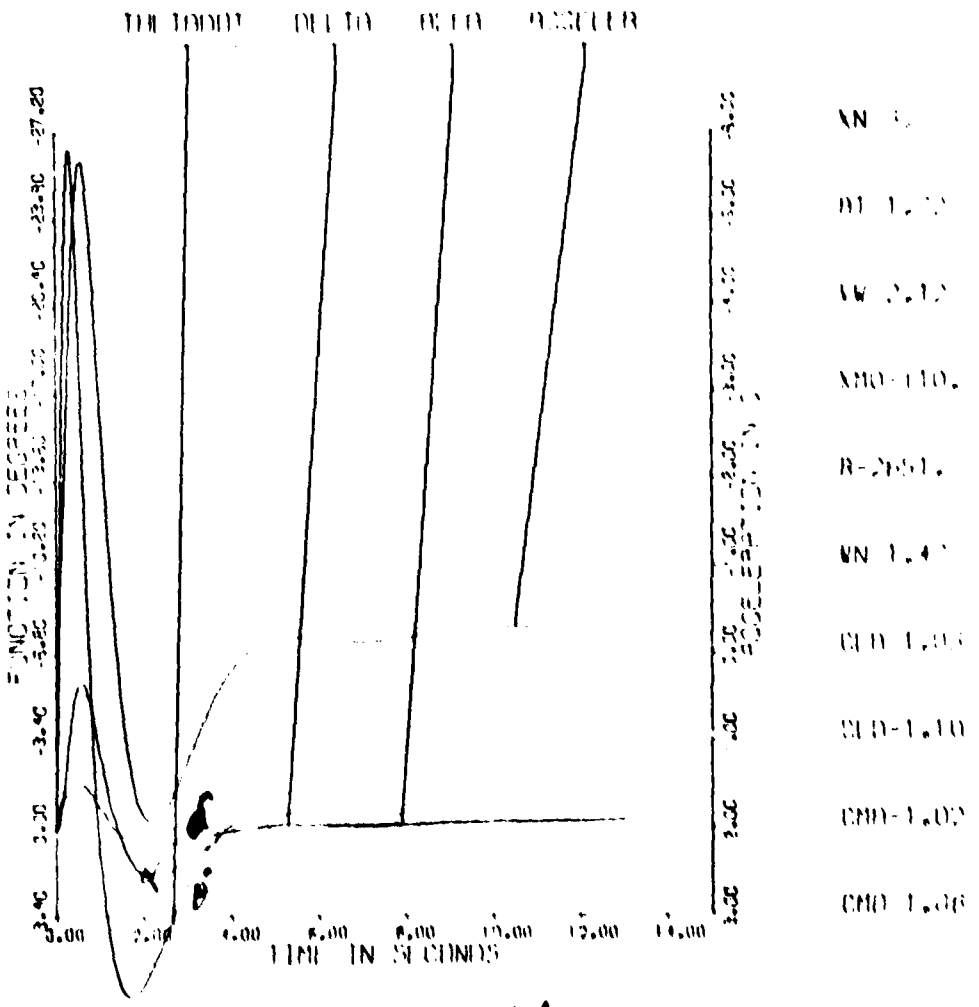

FIG. 23b

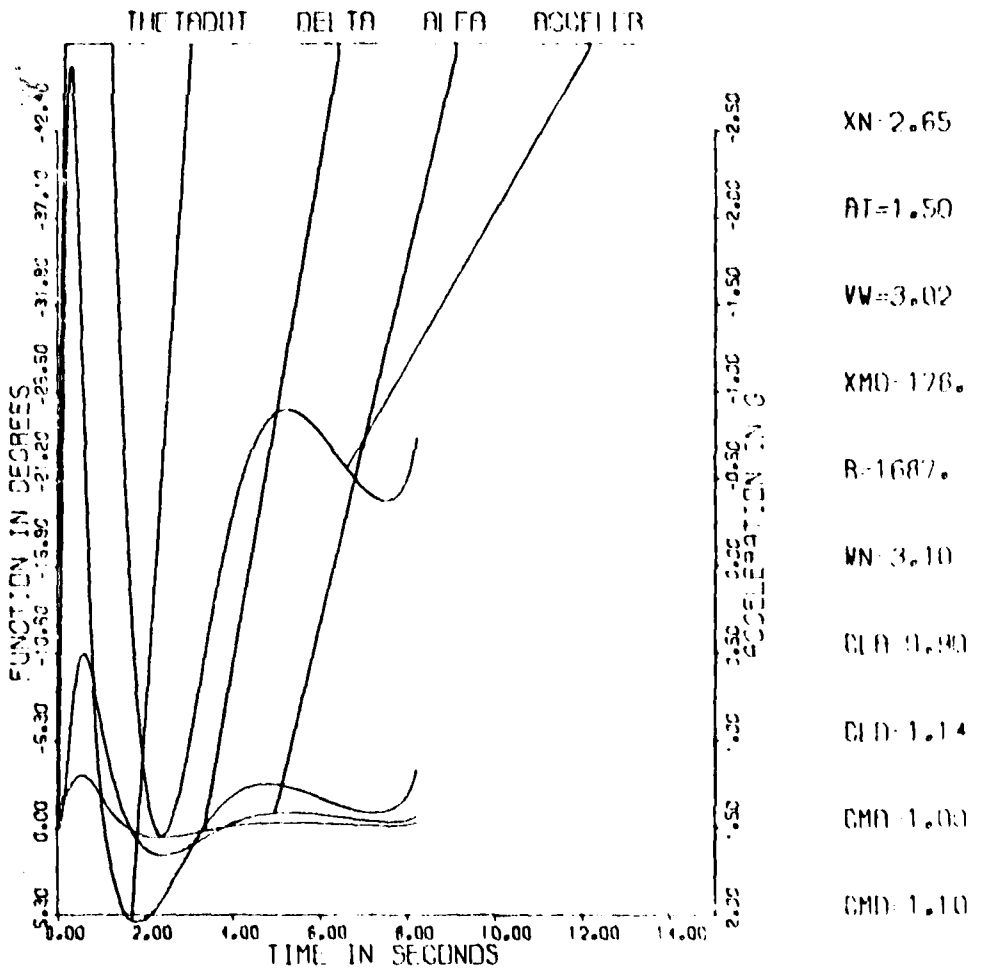
GLOBAL FEEDBACK SIMULATION
THETADOT
DELTA
ALFA
ACCELER
FUNCTION IN DEGREES
TIME IN SECONDS
0.00
2.00
4.00
6.00
8.00
10.00
12.00
14.00
XN=2.65
AT=1.50
VW=3.02
XMO=176.
R=1687.
WN=3.10
CLA=1.90
CLD=1.14
CMA=1.03
CMD=1.10

FIG. 23c

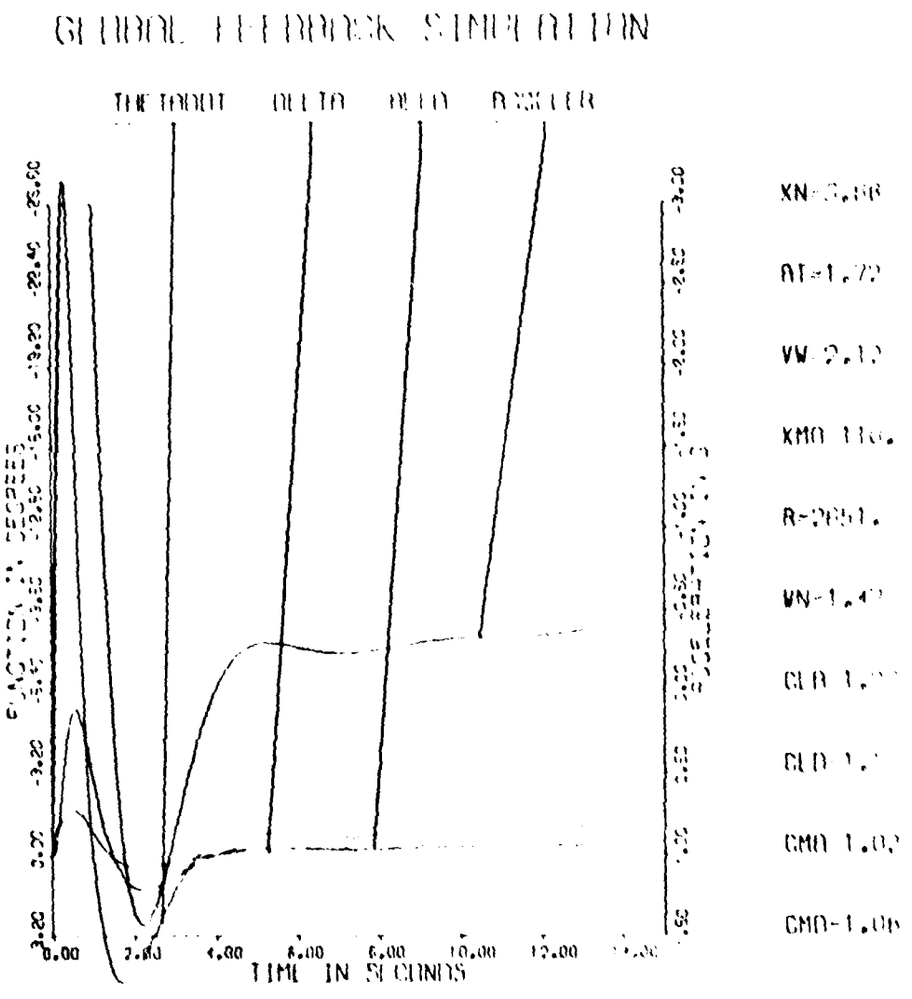
TIME IN SECONDS
0.00
2.00
4.00
6.00
8.00
10.00
12.00
XN=
AI=1.72
VW 2.12
KMO 116.
R=2851.
GMO 1.03
GMO=1.08

FIG. 23A

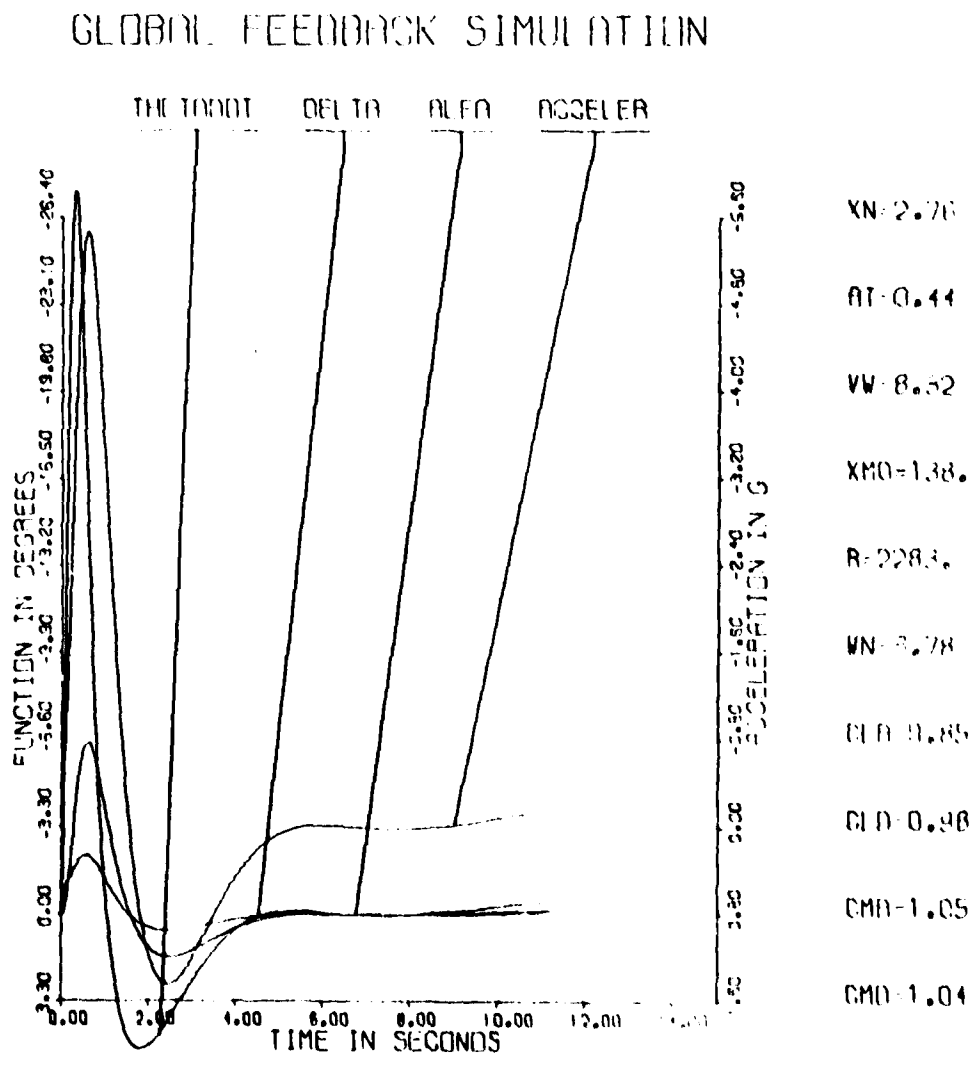
GLOBAL FEEDBACK SIMULATION
THETADOT
DELTA
ALFA
ACCELER
FUNCTION IN DEGREES
ACCELERATION IN G
TIME IN SECONDS
0.00
2.00
4.00
6.00
8.00
10.00
12.00
XN=2.76
AT=0.44
VW=8.52
XMO=138.
R=228.
GLD=0.98
GMO=1.05
GMO=1.04

FIG.23e

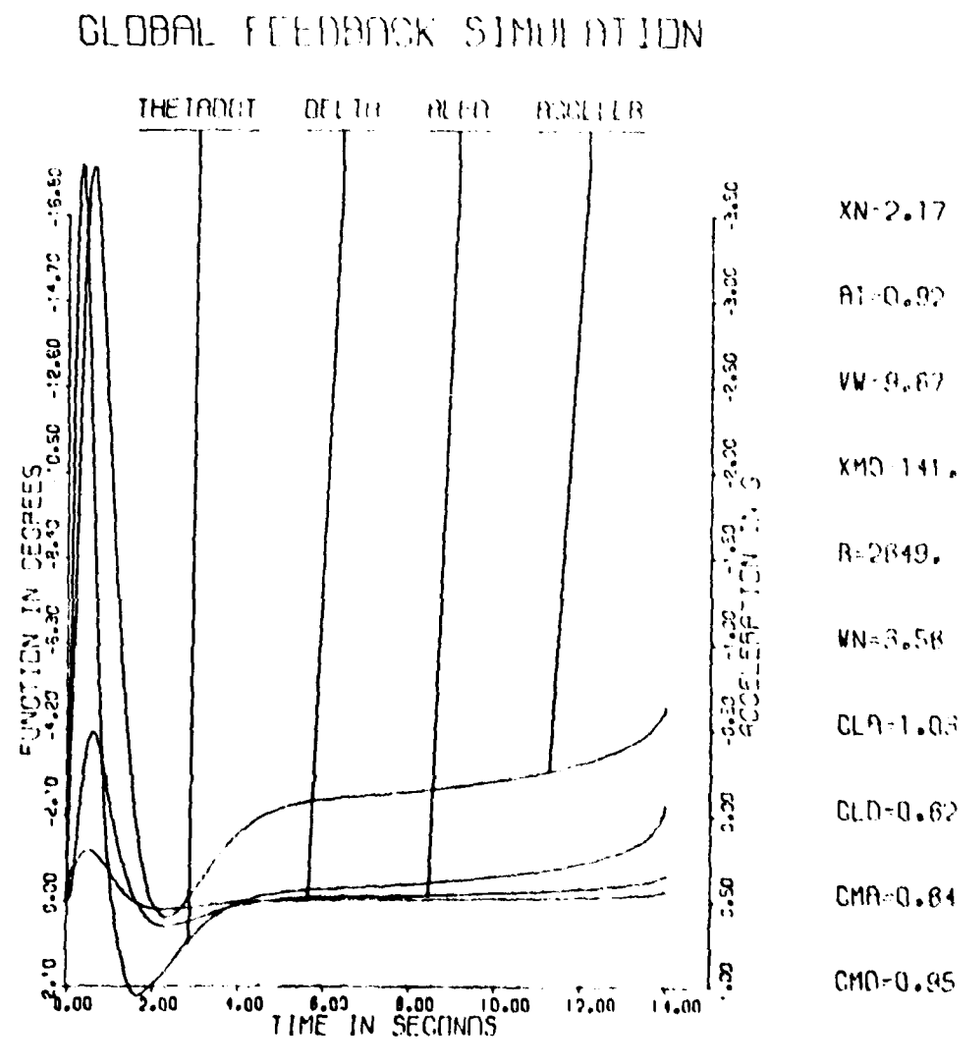
GLOBAL FEEDBACK SIMULATION
THETADOT
DELTA
ALPHA
ACCELER
FUNCTION IN DEGREES
ACCELERATION IN G'S
TIME IN SECONDS
0.00
2.00
4.00
6.00
8.00
10.00
12.00
14.00
XN=2.17
A1=0.92
VW=0.67
XMD=141.
B=2849.
WN=3.58
CLA=1.03
CLD=0.62
CMA=0.84
CMD=0.95

FIG. 23f

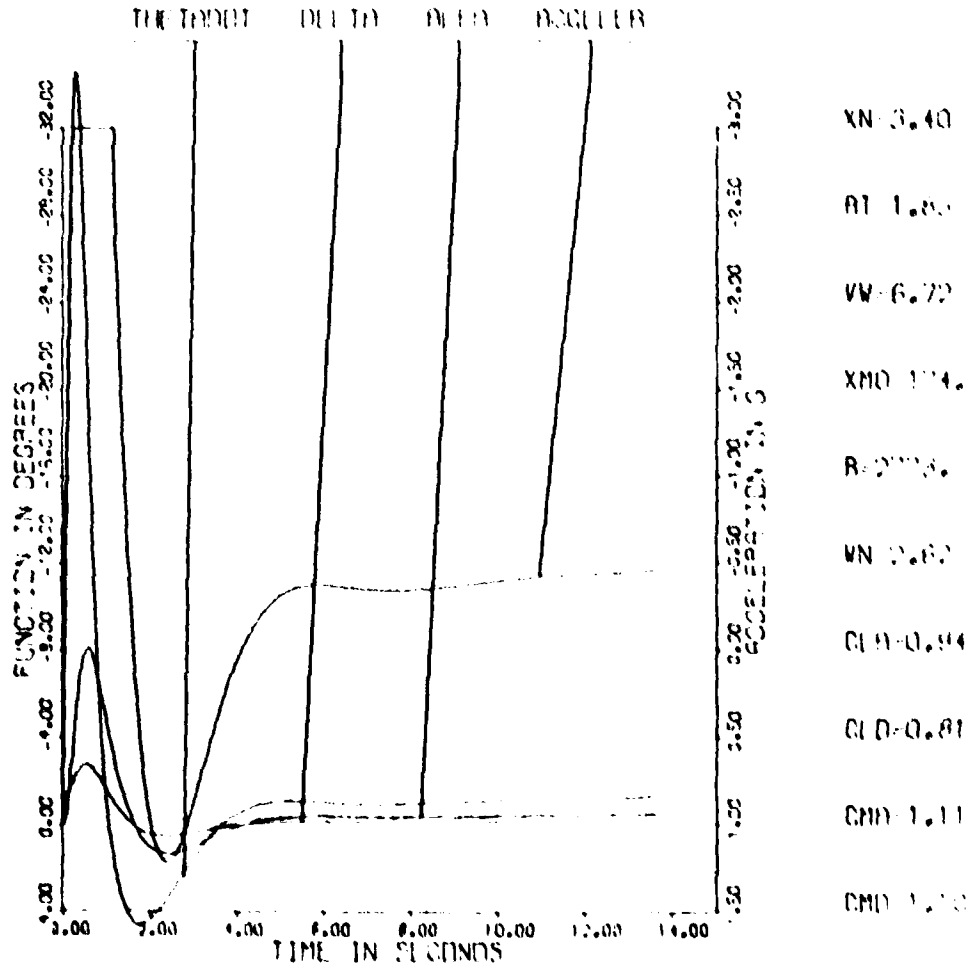
GLOBAL FEEDBACK SIMULATION
TIME IN SECONDS
XN 3.40
VW 6.72
GLD-0.81
GMD 1.11

FIG. 23g

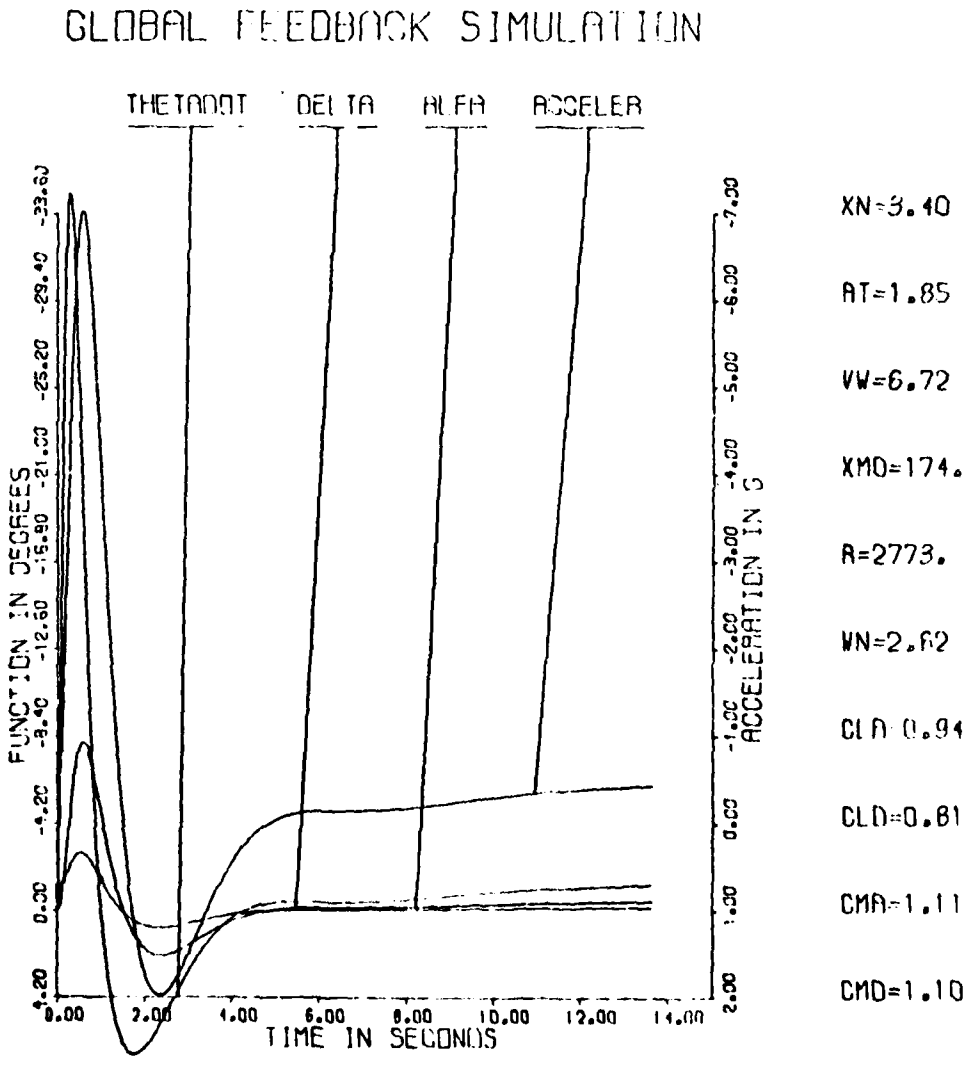
GLOBAL FEEDBACK SIMULATION
THETADOT
DELTA
ALFA
ACCELER
FUNCTION IN DEGREES
ACCELERATION IN G
TIME IN SECONDS
0.00
2.00
4.00
6.00
8.00
10.00
12.00
14.00
XN=3.40
AT=1.85
VW=6.72
XMD=174.
R=2773.
WN=2.62
CLA=0.94
CLD=0.81
CMA=1.11
CMD=1.10

FIG. 23 a

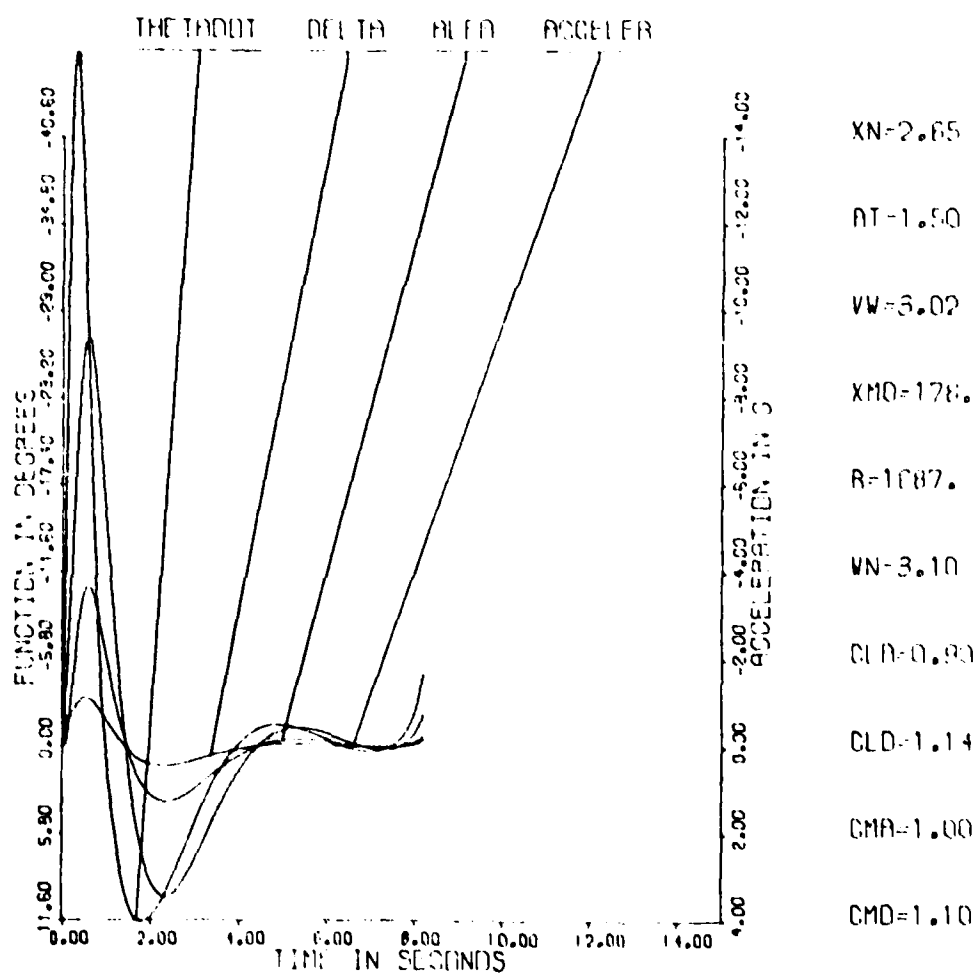
GLOBAL FEEDBACK SIMULATION
THETADOT
DELTA
ALFA
ACCELER
FUNCTION IN DEGREES
ACCELERATION IN G'S
TIME IN SECONDS
0.00
2.00
4.00
6.00
8.00
10.00
12.00
14.00
XN=2.65
AT=1.50
VW=3.02
XMD=178.
R=1087.
VN=3.10
CLD=0.93
CLD=1.14
CMA=1.00
CMD=1.10

FIG. 23i

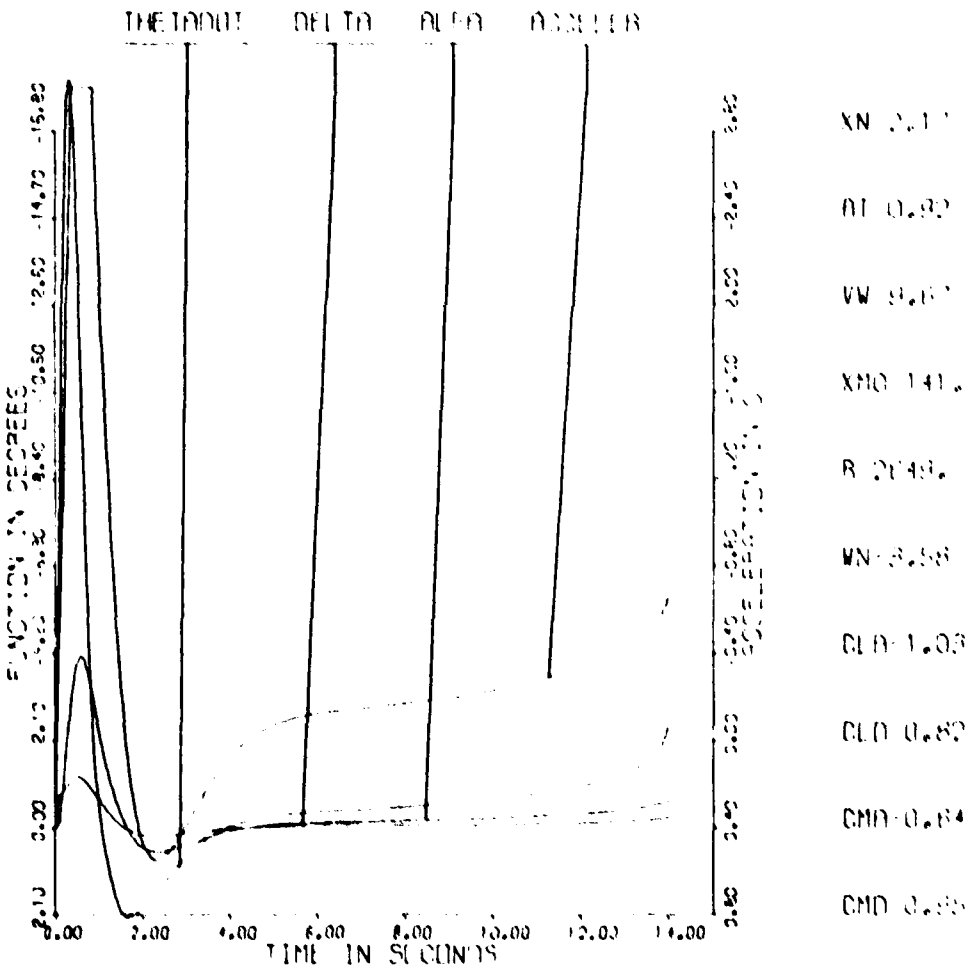
GLOBAL FEEDBACK SIMULATION
THETADOT
DELTA
ALPHA
ACCELER
FUNCTION IN DEGREES
TIME IN SECONDS
0.00
2.00
4.00
6.00
8.00
10.00
12.00
14.00
XN
DT
VW
XMO
R
MN
ALD
ALD
CMD
CMD

FIG. 23

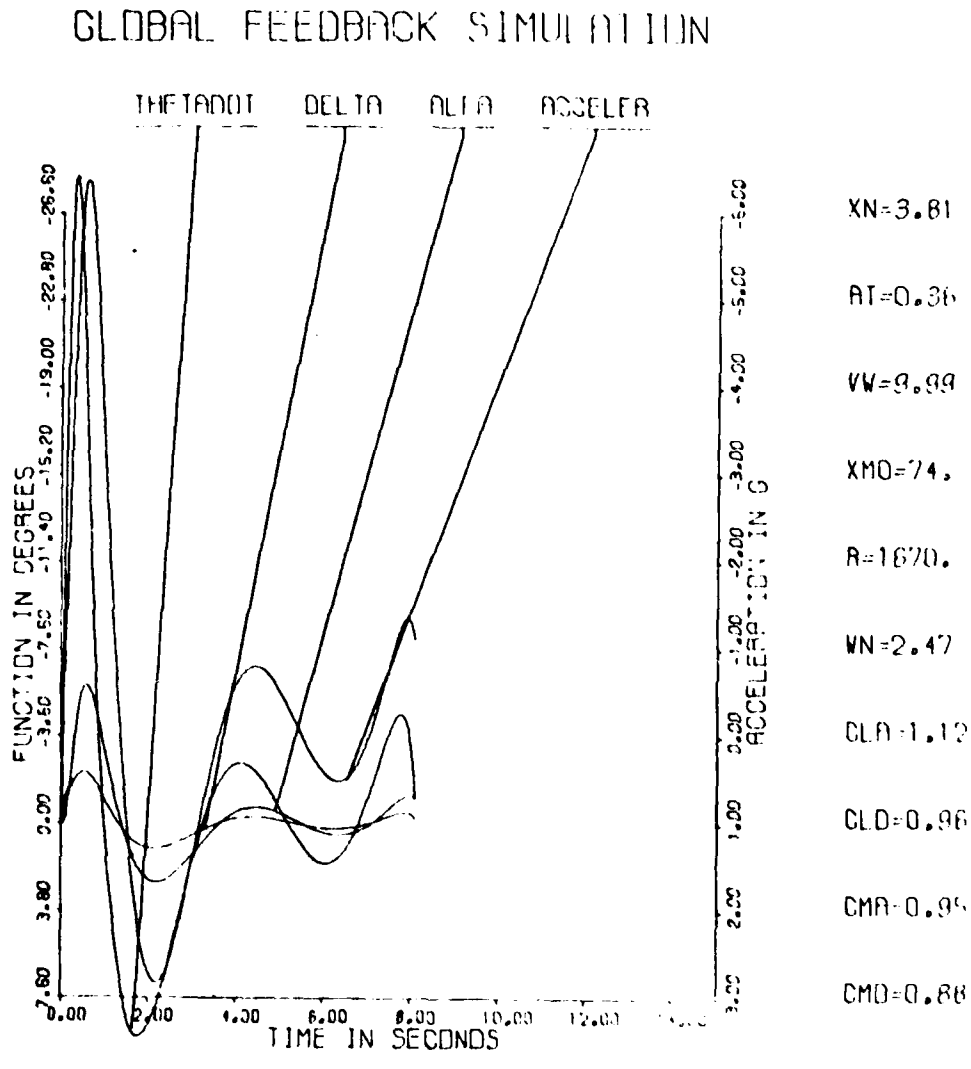
GLOBAL FEEDBACK SIMULATION
THETADOT
DELTA
ALFA
ACCELER
FUNCTION IN DEGREES
TIME IN SECONDS
XN=3.81
AT=0.36
VW=9.99
XMO=74.
R=1670.
WN=2.47
CLA=1.12
CLD=0.96
CMA=0.95
CMD=0.88

FIG. 23A

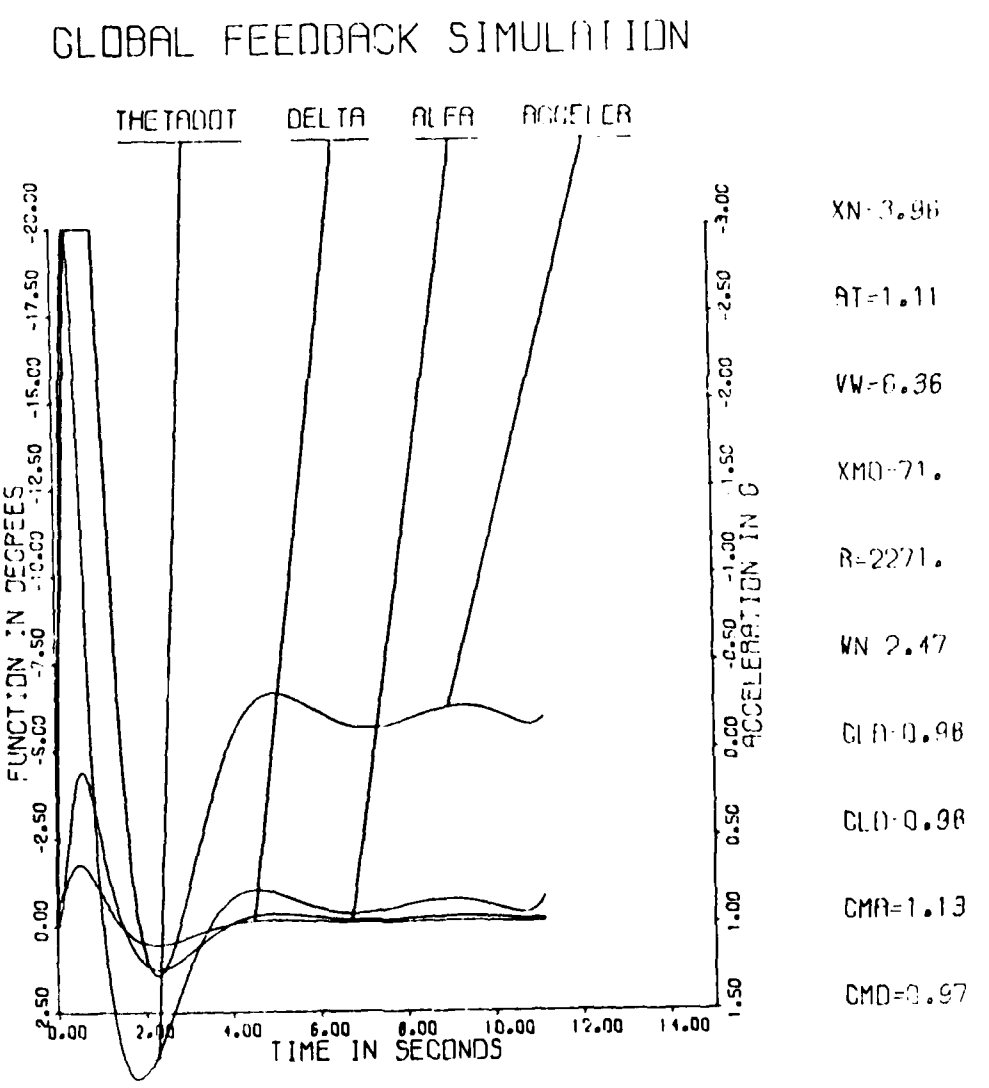
GLOBAL FEEDBACK SIMULATION
THETADOT
DELTA
ALFA
ACCELER
FUNCTION IN DEGREES
ACCELERATION IN G
TIME IN SECONDS
0.00
2.00
4.00
6.00
8.00
10.00
12.00
14.00
XN=3.96
AT=1.11
VW=6.36
XMD=71.
R=2271.
WN 2.47
CLA=0.98
CLD=0.98
CMA=1.13
CMD=0.97

Fig. 23l

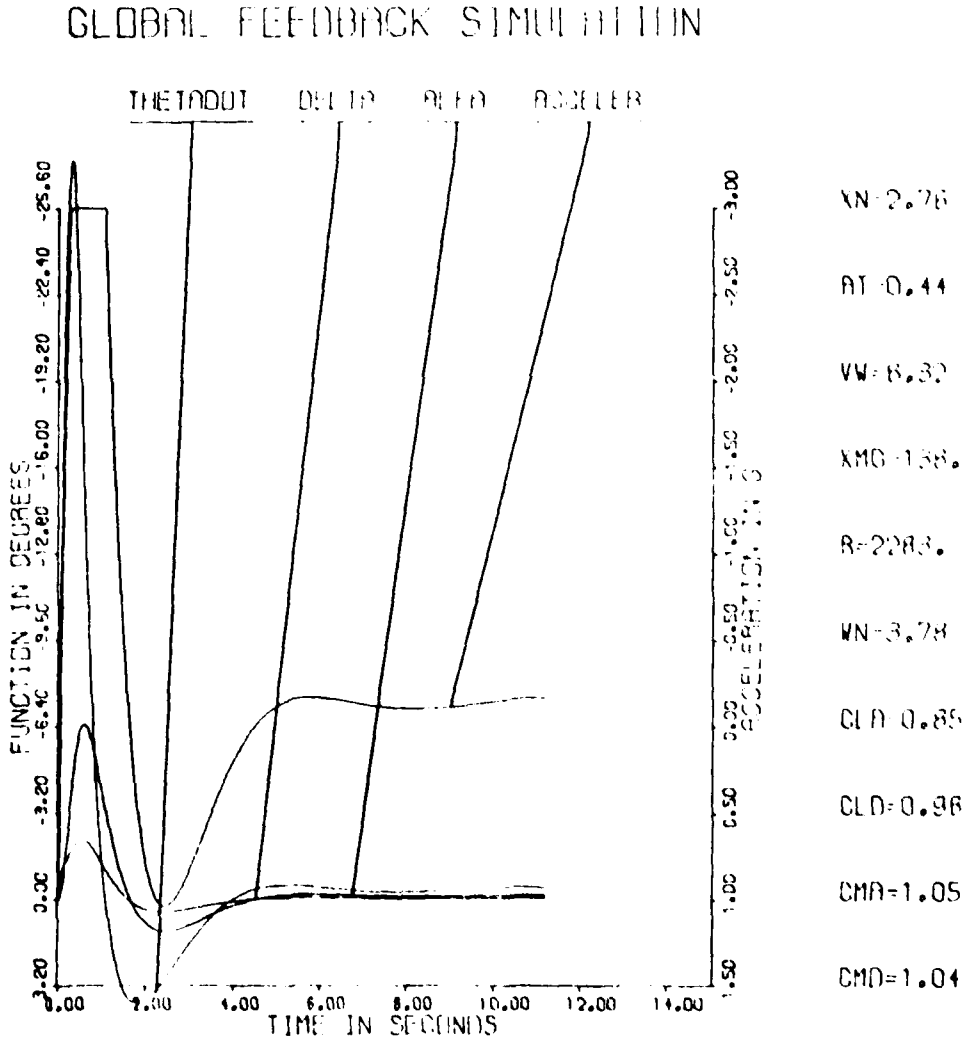
GLOBAL FEEDBACK SIMULATION
THETADOT
FUNCTION IN DEGREES
TIME IN SECONDS
XN=2.76
AT=0.44
VW=8.32
XMG=138.
R=2283.
WN=3.78
CLA 0.85
CLD=0.96
CMA=1.05
CMD=1.04

FIG. 23a

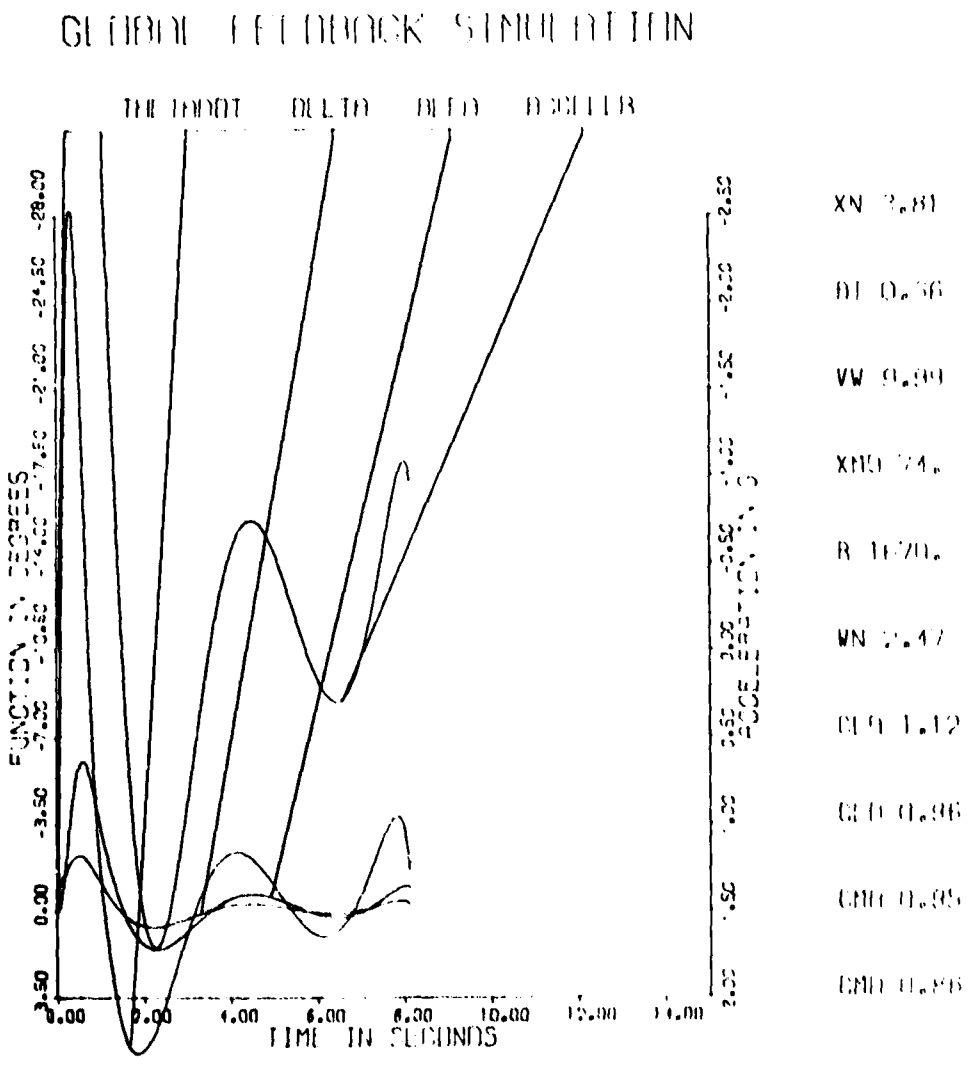
TIME IN SECONDS
0.00
2.00
4.00
6.00
8.00
10.00
12.00
14.00
-3.50
0.00
3.50
-28.00
-24.50
-21.00
-17.50
-14.00
-10.50
-7.00
-3.50
0.00
3.50
XN 2.81
AY 0.56
VW 0.00
XNO 24.
R 1570.
MN 2.47
GLO 1.12
GLO 0.96
GNO 0.85
GNO 0.96

FIG. 23a

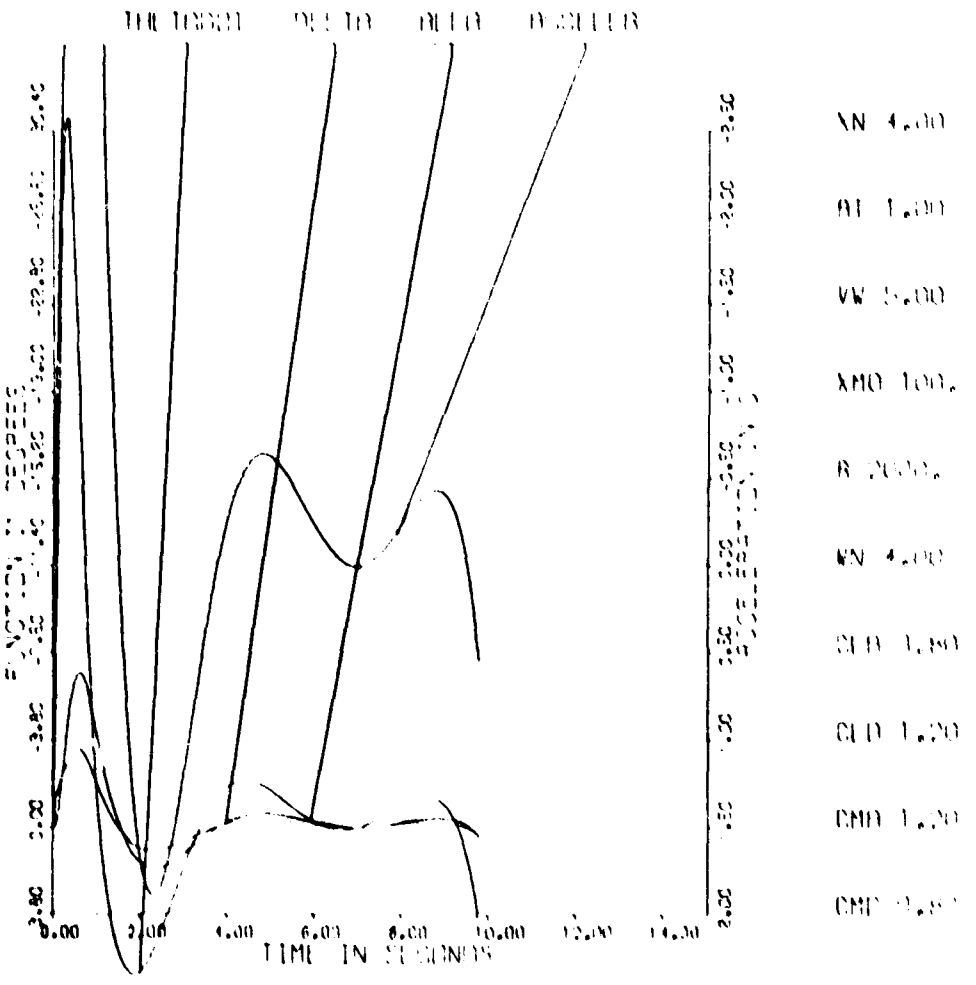

FIG. 23

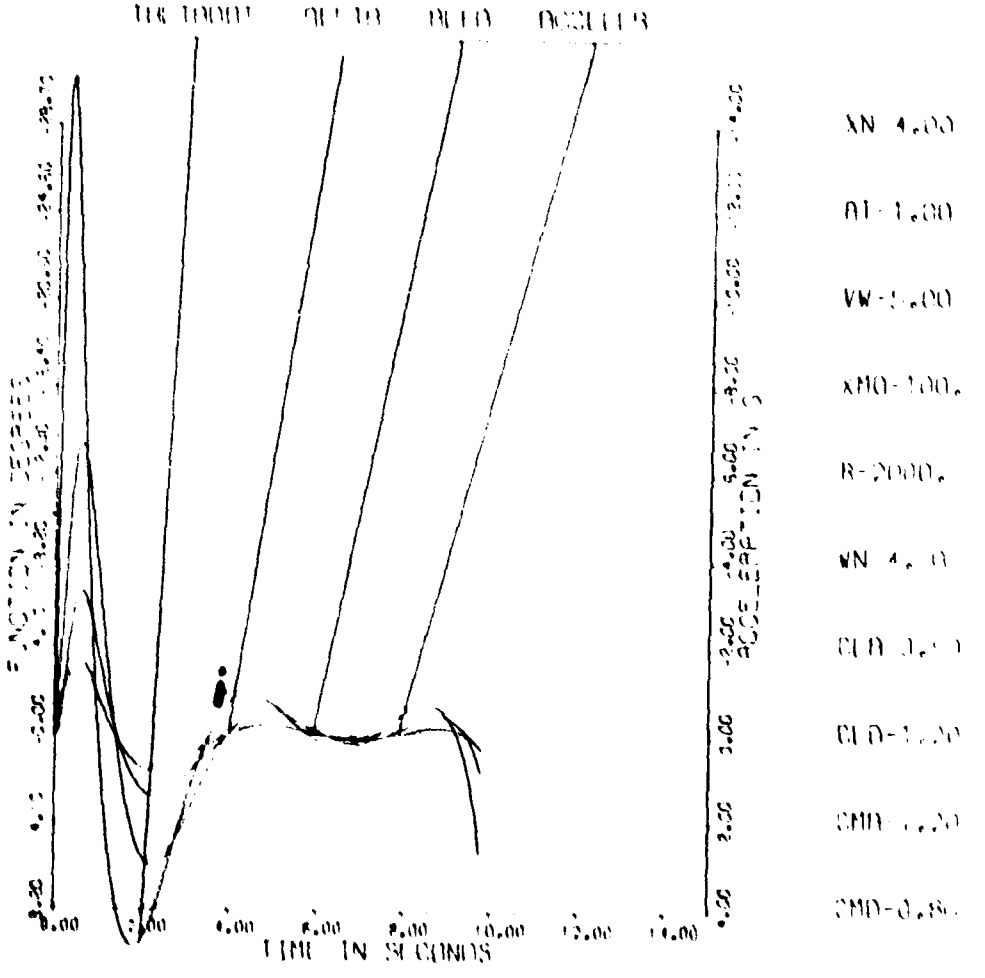
TIME IN SECONDS
XN 4.00
AI 1.00
VW 1.00
xMO 1.00
R 2000.
WN 4.0
CLO 1.0
CLO 1.50
CMO 1.20
CMO 0.80

FIG. 23 p.

APPENDIX 1

FLIGHT CONTROL DESIGN BASED ON NONLINEAR MODEL WITH UNCERTAIN PARAMETERS

Isaac Horowitz†, Boris Golubev*, Tzvi Kopelman*

Department of Applied Mathematics
The Weizmann Institute of Science
Rehovot, Israel

Abstract

A simplified but significantly nonlinear model is used for the short period longitudinal flight control problem, with c^* taken as the output. Uncertainty is included in the model by allowing for a large range in velocity and air-density, without any provision for their measurement. The output $c^*(t)$ is to lie within specified bounds in response to a range of step commands. A recent exact design technique for uncertain nonlinear systems is used. In this technique, the nonlinear plant set is replaced by a linear time-invariant plant set, which is precisely equivalent to the nonlinear set with respect to the problem tolerances. The design execution then involves frequency response concepts and techniques. For a large problem class, the resulting design is guaranteed to solve the problem, for the specific class of inputs posed. The design was simulated with excellent results.

Index Categories: Guidance and Control; Handling Qualities, Stability and Control.

---

† Cohen Professor of Applied Mathematics
* Students

Nomenclature

a - parameter in model of $T(s)$

$B(\omega)$ - bounds on $G(j\omega)$

C — mean aerodynamic chord, m .

$C_{ij}(\alpha)$ various aerodynamic coefficients

c^* -- output variable = a handling qualities criterion

$C^*(s)$ - $\mathcal{L}c^*(t)$

db -- decibels ($20 \log_{10}$)

e_G - excess of poles over zeros of $G(s)$

$F(s)$- prefilter transfer function

g -- gravity acceleration 9.8 m/sec^2

$G(s)$ - loop compensation function

I_y -- moment of interia in pitch, $kgm\text{-}m^2$

j -- $\sqrt{-1}$

k -- see R

lti - linear time-invariant

$L(s)$ = $G(s)P(s)$, loop transfer function

$\mathcal{L}$ - Laplace transform

m -- mass of vehicle, kgm

mp — minimum-phase

nmp - non minimum-phase

$p(t)$, p_i equivalent lti plant function

$P(s)$ $\mathcal{L}p(t)$

$\mathcal{P}$ set $\{p\}$ or $\{P(s)\}$

$q = \dot{\theta}$ - pitch angular velocity

$r(t)$ system command input

$R(s)$ $\mathcal{L}r(t) = k/s$

$\mathcal{R}$ set $\{r(t)\}$ or $\{R(s)\}$

s -- complex variable

S -- wing surface area, m^2

$T(s)$ closed loop transfer function

$\mathcal{J}$ -- set $\{T(s)\}$

$\mathcal{J}_P$ -- template of $P = P(j\omega)$

u -- vertical velocity, m/sec
v -- horizontal velocity = V_0 constant
w -- nonlinear plant function, $y = w(x)$

w^{-1} - inverse of w, $x = w^{-1}(y)$

$\mathcal{W}$ set $\{w\}$

x, x_i input to nonlinear plant

$X(s)$ - $\mathcal{L}\, x(t)$

y, y_i acceptable output of plant

$Y(s)$ $\mathcal{L}\, y(t)$

$\mathcal{Y}$ set $\{y\}$

α angle of attack

δ elevator deflection

$\Delta(s)$ $\mathcal{L}\, \delta(t)$

ζ parameter in model of $T(s)$

ρ air density, kgm/m^3

ω frequency, rps

FLIGHT CONTROL DESIGN BASED ON NONLINEAR MODEL WITH UNCERTAIN PARAMETERS

INTRODUCTION

In most flight control design techniques, the nonlinear differential equations are linearized about a trim condition. The resulting incremental linear time invariant (lti) model with its fixed aerodynamic coefficients, is reasonably valid for small excursions from trim. By using different trim points, there are obtained different sets of coefficient values. The model is then taken as lti , in which these sets are treated either

(1) as uncertain parameters in a lti design technique for securing specified performance over the uncertain parameter set, or

(2) as known functions of Mach and dynamic pressure. The latter are monitored, leading to a "Scheduling" design, or

(3) as uncertain parameters to be identified and compensated for in a so-called "Adaptive" design.

A combination of all three may also be used. However, in all of these approaches the model used is lti .

There have recently been attempts at incorporating the nonlinearities to some extent into the system model, the vehicle for doing so being optimal control theory. However, the calculations have been very laborious, requiring considerable approximations (see Ref. 1 and its references for discussion). This paper takes a far different approach and is based on a recent[2] synthesis technique for feedback aronnd a nonlinear uncertain plant, the latter denoting the constrained part of the system. This synthesis technique has the following important properties.

1. For a large class of practical nonlinear plants, the design is precise and direct with no approximations even for highly nonlinear (even nonlinear time-varying) models with large uncertainties in the plant parameters.
2. Design execution is in the frequency domain.

REVIEW OF NONLINEAR DESIGN TECHNIQUE

The key ingredient is the extension to sets of an idea often used by engineers: Given a specific nonlinear element w, it is usually possible to find an lti element p which is equivalent, in a certain sense, to w for a single specific output $y_1(t)$ (or input $x_1(t)$): Let $y_1(t) = w(x_1(t))$ be the (assumed) unique output of w due to input $x_1(t)$. Choose p so that its output is also y_1 when its input is $x_1(t)$. A simple way to do this is to find (Laplace transform) $\mathcal{L} y_1(t) \triangleq Y_1(s)$ and $\mathcal{L} x_1(t) \triangleq X_1(s)$. Then let $P(s) \triangleq Y_1(s)/X_1(s)$, giving $p(t) = \mathcal{L}^{-1} P(s)$ the lti equivalent of w, but only for the special case when the input is x_1. Hence, the two essential conditions are: (1) w has a unique inverse, thus excluding hard saturation etc. which, however, could be replaced by very low gain over the appropriate interval. (2) the desired plant output $y(t)$ and the resulting $x = w^{-1}(y)$, are Laplace transformable, a condition difficult to violate.

This eqivalence idea can be extended to a set of nonlinear plants $\mathcal{W} = \{w\}$ for which a lti set denoted by $\mathcal{P}_1$ can be found which is equivalent to $\mathcal{W}$, with respect to $y_1(t)$. Simply find p_1 the y_1-equivalent of w_1, for each $w_1 \in \mathcal{W}$ and let $\mathcal{P}_1 = \{p_1\}$. A further extension is to find a lti set $\mathcal{P}$ which is eqivalent to $\mathcal{W}$ with respect to a set of outputs $\mathcal{Y} = \{y_j\}$. To find $\mathcal{P}$, repeat the previous for each $y_j \in Y$ giving $\mathcal{P}_j$ and then

$\mathcal{P} = \{P_j\}$. If $\mathcal{W}$ has 10 elements and $\mathcal{Y}$ has 20, $\mathcal{P}$ has 200 members. But in general, both $\mathcal{W}$ and $\mathcal{Y}$ are uncountable and so is $\mathcal{P}$.

In Fig. 1, the closed-loop system is to behave like a lti one, with transfer function T(s), in response to any command input in a set $\mathcal{R} = \{r\}$ and for any $w = \mathcal{W}$, i.e. $\mathcal{L}y(t) \triangleq Y(s) = T(s)R(s)$, where $R(s) = \mathcal{L}r(t)$. However, due to the uncertainty, a set of acceptable $\{T(s)\} = \mathcal{T}$ must be specified, insomuch as dynamic invariant response for all w in $\mathcal{W}$ is impossible. The sets $\mathcal{R}, \mathcal{T}$ determine the set of desired acceptable system outputs $\mathcal{Y} = \{y(t)\}$, via $\mathcal{L}y(t) = Y(s) = T(s)R(s)$, or vice versa. The nonlinear set $\mathcal{W}$ is then replaced by the lti set $\mathcal{P}$ which is equivalent to $\mathcal{W}$ with respect to $\mathcal{Y}$. We say that $\mathcal{P}$ is mp (minimum-phase) with respect to $\mathcal{Y}$, if all $P(s) \in \mathcal{P}$ have no zeros in the right half-plane, and stable if they all have no such poles. In our specific problem $\mathcal{P}$ is mp, but not stable.

We now have a pure lti feedback problem: Find the lti compensation F(s), G(s) needed in FIg. 1, such that the system transfer function $T = FL/(1+L)$, $L = GP$, is a member of the set $\mathcal{T}$, no matter which $P \in \mathcal{P}$ is used. A frequency-response design technique for a very general problem class[3], is available for minimum-phase $\mathcal{P}$. $\mathcal{P}$ may have unstable elements. If this lti problem is solvable, then under quite general conditions the solution (i.e., the F(s), G(s) compensation pair used) is also precisely valid for the original nonlinear problem. The details and proof[2] involve functional analysis techniques. However, design execution involves frequency-response concepts, as next seen.

PROBLEM STATEMENT AND EXECUTION

Nonlinear Plant. The nonlinear plant is described by Eqs. 1-3 (see Nomenclature Section).

$$\dot{u} = qV_0 + g\cos\theta - \frac{\rho V_0 S}{2m}\left[C_{N\alpha}(\alpha) + C_{N\delta}(\alpha)\delta\right] \tag{1}$$

$$\ddot{\theta} = \dot{q} = \frac{\rho V_0 SC}{2I_y}\left[C_{m\delta}(\alpha)\delta + C_{M\alpha}(\alpha) + \frac{C}{2V_0}C_{mq}(\alpha)q\right] \ , \ \alpha = \tan^{-1}\frac{u}{V_0} \ . \tag{2,3}$$

$$c^* = 12.4\dot{\theta} + \frac{1}{9.8}\left(\dot{u} - V_0\dot{\theta} + 60\ddot{\theta}\right) \tag{4}$$

is the output[4] to be controlled, i.e. to be in $\mathcal{Y}$. The numbers used are[5,6] $I_y = 207{,}000$ kg m^2 , $m = 17{,}600$ kg , $C = 4.89$ meters , $S = 49.2$ m^2 . The $C_{ij}(\alpha)$ are nonlinear functions of α , see Fig. 2. Since α (Fig. 9) ranges in $[0,35°]$, there is strong nonlinear operation. The horizontal velocity v was taken as V_0 fixed, which is incorrect for some low-velocity cases, but the objective here is to demonstrate the validity of the design technique in a strongly nonlinear situation, which is achieved sufficiently by means of the nonlinear $C_{ij}(\alpha)$.

The bounds[4] on the acceptable $c^*(t)$ in response to a unit step command are included in Fig. 3, which also includes design simulation results. The set of command inputs $\mathcal{R}$ consists of steps 1 to 5 in magnitude. Parameter uncertainty is due to ρ ranging in $[.3,1.22]$ and V_0 in $[75,206]$. Initial conditions are $\dot{w}(0) = \dot{q}(0) = q(0) = 0$, $\alpha(0) = \theta(0)$, giving initial values for δ (as well as u , θ , α) which is substracted out so that the change in δ is used to find the lti equivalent $\mathcal{P}$ set . The detailed steps in the design implementation are next presented, with comments postponed to the end.

Step 1. The lti set $\mathcal{P}$. Let $\mathcal{L}c^*(t) \triangleq C^*(s) = T(s)R(s)$, $R(s) = k/s$ with $k \in [1,5]$ and $T(s) \in \mathcal{T}$, derived from the bounds in Fig. 3. A simple means for generating $\mathcal{T}$, taken from Ref. 5, is to let $T(s) = a^2(s + 2.9)/2.9(s^2 + 2\zeta as + a^2)$, ζ ranging in [3.7, 1.5], a in [3.14, 7.6], giving the bounds on $|T(j\omega)|$ in Fig. 4. Such bounds suffice[3] for mp (and obviously stable) T(s). Any T(s), R(s) pair thus generates an acceptable $c^*(t)$. A computer program solved Eqs. (1-4) backwards for $\delta(t)$ and then checked the result by solving Eqs. (1,4) forwards for $c^*(t)$ from $\delta(t)$. The program was considered adequate only when excellent agreement was obtained over the entire range considered. $C^*(s)$ was apriori available and $\Delta(j\omega) \triangleq \mathcal{L}\delta(t)]_{j\omega}$ was obtained by numerical integration. As c^* is a short-period criterion and for all the acceptable cases has definitely reached steady-state in 4 seconds (see Fig. 3), Eqs. (1,4) were solved only for $t \in [0,4$ seconds], and the constant $\delta(4)$ was used for $t > 4$.

Loci of six $P(j\omega)$ are shown in Fig. 5, two of them (e,f) unstable with a pair of right half-plane poles, which are zeros of $\Delta(s)$. The set includes a large number of such unstable lti P(s), which the lti design technique[3] can easily handle.

Plant templates. At any ω say $\omega = \omega_1$, the set $\{P(j\omega)\}$, $P \in \mathcal{P}$ consists of a region in the logarithmic complex plant (Nichols chart) denoted as the ω_1-plant template $\mathcal{T}_{P(\omega_1)}$. A number of $\mathcal{T}_{P(\omega)}$ are shown in Figs. 6a-c. At very small ω there are two almost constant angle sub-templates 360° apart. This is due the presence of both stable and unstable $P \in \mathcal{P}$, and the fact that Arg P near $\omega = 0$ is either $\doteq 0$ or $n\pi/2$ for some integer n. As ω increases, the two groups merge together and approach a single vertical line at large ω well beyond the plant "dynamics"

($\omega = 12$ is large enough in this case, see Fig. 6a-c). Note how this frequency response approach is indifferent to system order.

Step 2. Bounds $B(\omega)$ on $G(j\omega)$ Given the set $\mathcal{P} = \{P\}$, the problem is to find $F(s)$, $G(s)$ in Fig. 1 such that the system transfer function $T(j\omega) = FGP/(1+GP) \in \mathcal{T}$, for all $P \in \mathcal{P}$. One may program the computer to find the (unique) bounds $B(\omega)$ on $G(j\omega)$, so that as P ranges over $\mathcal{P}$, $\Delta \ln|T(j\omega)| = \Delta \ln \left|\frac{GP}{1+GP}\right| \leq [A_2(\omega) - A_1(\omega)]$ db of Fig. 4. Alternatively, this may be done by hand, giving useful insight: The template of $L(j\omega_1) = G(j\omega_1)P(j\omega_1)$ is that of P, shifted (in the Nichols chart) by Arg $G(j\omega_1)$ in the x axis and by $20 \log_{10}|G(j\omega_1)|$ in the y axis. Suppose $\mathcal{T}_{P(j2)}$ is given by ABCD in Fig. 7 and one tries positioning it at A'B'C'D', to give the template of $L(j2)$. From the contours of constant $|L/(1+L)|$ in the Nichols chart, it is seen that the maximum change in $|T(j2)|$ is then closely $(-.49) - (-5.7) = 5.2$ db, with maximum at C', minimum at A'. Suppose the $|T(j\omega)|$ tolerance permits a maximum change of 6.5 db at $\omega = 2$, so the above trial is conservative. The template may be shifted lower to A"B"C"D", at which the $|T(j\omega)|$ tolerances are precisely satisfied. Choose some specific P as nominal, e.g., point A giving $P_0(j2) = -13$ db $\angle -153.4°$. Since $L_0(j2)$ (A" in Fig. 7) $= -4.2$ db $\angle -60°$, the corresponding bound on $G(j2) = L_0(j2)/P_0(j2)$ is 8.8 db $\angle 93.4°$, i.e., if Arg $G(j2)$ is 93.4°, it is necessary for $|G(j2)| \geq 8.8$ db, in order that $\Delta|T(j2)| \leq 6.5$ db due to the uncertainty in $P(j2)$. This manipulation of $\mathcal{T}_{P(2)}$ is repeated along a new vertical line, giving another point on the boundary $B(2)$ of permissible $G(j2)$.

Fig. 8 shows the bounds so obtained on $G(j\omega)$, and the $G(j\omega)$ chosen to satisfy these bounds. Let e_G be the excess of poles over zeros assigned to $G(s)$, so that as $s \to \infty$, $G \to k_G/s^{e_G}$. It is reasonable to define the optimum G as that which satisfies its bounds with minimum k_G. It has been shown[7] that G_{opt} lies on $B(\omega)$ at all ω and that G_{opt} exists and is unique. The design of a practical $G(s)$ to satisfy the bounds is somewhat of an art[3]. For a given skill in the art, the greater the number of poles and zeros of G, the closer one can get to the optimum, so there is trade-off between complexity and bandwidth. Here, we chose simply by cut and try $G(s) = (1 + .2s/s(1 + .033s^2)(1 + .002s + 10^{-4}s^2)$ with very modest bandwidth, Figs. 4, 8. A much simpler $G(s)$ could have been chosen with larger bandwidth. The designer must make his own trade-off. Ref. 3 offers some advice on the shaping of a function to satisfy a set $\{B(\omega)\}$ in the Nichols chart.

Step 3. Design of $F(s)$. $G(s)$ only guarantees that $A|T(j\omega)| \leq A_2(\omega)-A_1(\omega)$ of Fig. 4, e.g., at $\omega = 10$, the actual change in $|L(j10)/(1+L(j10))|$ is from -7 db to 4 db, while from Fig. 4, the permitted change in $|T(j10)| = |FL/(1+L)|$ is from -15 to 2.8 db. Hence, any value of $|F(j10)| \in [-8, -1.2 \text{ db}]$ is acceptable. In this way, upper and lower bounds on $|F(j\omega)|$ are obtained and $F(s)$ is chosen to satisfy them, which is also somewhat of an art. In this example, a satisfactory $F(s) = (1+.33s)(1+.05s)/(1+.25s)(1+.2s)(1+.0125s)^2$, see Fig. 4.

Design Results. The nonlinear system was simulated and its response found for several hundred command inputs and gust disturbances, some of which are shown in Figs. 3, 9-12. Some typical responses to c^* step commands are shown in Fig. 3 for various V_0, ρ and step (k) values. The assigned bounds on c^* are also shown. The transient response of $\alpha(t)$, $\dot{\theta}(t)$ etc. depend, of course, on the values of k, ρ, V_0. Two sets of these are shown in Figs. 9a, b, with Fig. 9a depicting very large $\alpha(t)$ excursion, for which the $C_{ij}(\alpha)$ in Fig. 2 are in strongly nonlinear ranges. These are the inputs for which the system was designed, and for which guarantees can be made. In a very few cases there was very slight excursion out of the bounds. It is possible to include in the design other inputs and gust disturbances, with specified response tolerances - and then guarantees can be made for these as well. The response to other inputs is nevertheless found here to be also quite satisfactory. This is typical of the design, i.e., the system is not very sharply tuned to the class of inputs used in the design execution. There is reasonable response continuity to other inputs.

Some responses to very large c^* step commands causing hard δ saturation are shown in Fig. 10. Response to Gust Disturbances. The gust input was modelled by replacing α in (3) by $\alpha = \tan^{-1}\frac{u}{V_0} + \alpha_{gust}$. Two kinds of α_{gust} were used. In one α_{gust} is a half-sine wave of amplitude $20/V_0$ radians and half-period THALF $\in [.2,2]$ sec. Some results are shown inf Figs. 11a,b. In both, the gust begins precisely at the instant of application of simultaneous c^* step commands. The second kind, as in Fig. 11b, is stochastic guassian with power spectrum $k/(1+\omega^2)V_0^2$ and $(\alpha_{gust})_{rms} = 6/V_0$ radians. Examples of responses to a single square wave c^* command with equal positive and negative values k and total duration 2 THALF are shown in Fig. 12.

DISCUSSION AND CONCLUSIONS

A second-order model was used for $T(s)$ with excess of poles over zeros $e_T = 1$, in Step 1. This appears to be incompatible with G, F fifth order and excesses $e_G = 4$, $e_F = 2$, and P (no analytical expression but linearized (1-4) give second-order P) with $e_P = 0$. Strict design execution appears to require a $T(s)$ of complexity compatible with $T = F\,GP/(1 + GP)$. Note, however, that in Step 1, the model of $T(s)$ is used only to generate a set which covers the range of apriori specified acceptable outputs $\mathcal{Y}$. Any $T(s)$ model which achieves this is clearly satisfactory, and the simpler the better. The designer can later choose the complexity of $G(s)$, $F(s)$, with no regard for that of the $T(s)$ model used in Step 1.

The class of applicable nonlinearities has been defined implicitly in Ref. 2, but one very large class can be defined explicitly. Let $D_1\, y(t) = D_2\, x(t)$ with D_1, D_2 operators which may be nonlinear, uncertain and time-varying, e.g.

$$D_1\, y = M(\ddot{y})(\dot{y})^{.5}\operatorname{sgn}\dot{y} + \left(\frac{A + Bt\, e^{-\alpha t}}{E + Ft}\right)\dot{y}^2\,|y|^n + H\,y^2$$

$$E \in [1,5]\ ,\quad F \in [.5,4]\ ,\quad A \in [-3,6]\ ,\quad \alpha \in [.5,1.5]$$

$$B \in [-3,2]\ ,\quad H \in [-4,1]\ ,\quad n \in [.5,2]\ ,\quad M \in [1,5]\ .$$

The range of M must be of the same sign. All $y \in \mathcal{Y}$ and $D_1\, y$ must be bounded for all t in $[0,\infty]$ and $D_1\, y$ must exist. Hence y must be twice differentiable except, at most, at a countable number of points. Then $D_1\, y \triangleq \psi(t)$ is known and there must exist a unique solution for x in $D_2\, x = \psi(t)$. The solution must be bounded for all $t \in [0,\infty]$. Thus, $D_2\, x = \psi(t)$ must be "bounded-input, bounded-output" stable. However, $D_1\, z(t) = v(t)$ may be "unstable" in that a bounded $v(t)$ is allowed to result

in unbounded $z(t)$. It is only necessary that bounded $z(t)$ gives bounded $v(t)$.

It is possible that a simple linearization might do just as well in practice, but this is a matter of chance, whereas this design technique is guaranteed to work if the constraints are satisfied. It can be argued that the constraint of uniqueness may be waived in Sec. 2, if the set of inputs $\{x(t)\}$ which can give the single output $y(t)$, is "compact", i.e. if that set can be covered as accurately as desired by a finite number of elements. A single w , y pair then generates a set of lti P instead of only one. However, this has not been rigorously proven as yet.

The constraint on $\mathcal{H}$ that $\mathcal{B}$ is mp, is required because only then can one guarantee that <u>any</u> specifications no matter how narrow (A_2-A_1 arbitrarily small but nonzero in Fig. 4), may be satisfied for arbitrarily large but bounded parameter uncertainty (but some parameters must not change sign[7]). No such gurantee can be made for nmp $\mathcal{B}$, but the problem is still solvable if the specifications are not too narrow and $\mathcal{B}$ is not too large[8,9] a set.

Finally, a recent extension[7] is to linear and nonlinear multiple input-output systems, where the problem is transformed into the design of n^2 single-loop lti systems like Fig. 1.

Acknowledgement

This research was sponsored by the Air Force Flight Dynamics Laboratory/ AFFDL, Air Force Systems Command, United States Air Force under Grant AFOSR-77-3355 at the Weizmann Institute of Science.

REFERENCES

1. Garrard, W.L., and Jordan, J.M., "Design of Nonlinear Automatic Flight Control Systems", Automatica, Vol. 13, Sept. 1977, pp. 497-505.

2. Horowitz, I., "Synthesis of Feedback Systems with Nonlinear Time-Varying Plants to Satisfy Quantitative Performance Specifications", Proc. IEEE, Vol. 64, Jan. 1976, pp. 123-130.

3. Horowitz, I., and Sidi, M., "Synthesis of Feedback Systems with Large Plant Ignorance for Prescribed Time-Domain Tolerances", Int. J. Control, Vol. 16, Aug. 1972, pp. 287-309.

4. Toble, H., Elliott, E., and Malcolm, L., "A New Longitudinal Handling Qualities Criterion", Boeing Co. Commercial Airplane Division, Report TL 693.N3, May 1966.

5. Kisslinger, L., et al, "Survivable Flight Control System", Interim Report 1, McDonnell Douglas, May 1971, p. 12, Table 1.

6. Laacke, F., and Miller, C., "Comparison of the Basic F4E and the Slotted F4E Stall/Near Stall/Spin Characteristics", McDonnell Douglas Report MDC A 2181, December 18, 1969.

7. Horowitz, I., "Quantitative Synthesis of Uncertain Multiple Input-Output Feedback Systems", to appear in Int. J. Control. Preprint copies available from Dept. of Electrical Engineering, University of Colorado, Boulder, Co. 80309.

8. Horowitz, I., and Sidi, M., "Optimum Synthesis of Nonminimum-Phase Feedback Systems with Plant Uncertainty", Int. J. Control, Vol. 27, March 1978, pp. 361-386.

9. Horowitz, I., Synthesis of Feedback Systems, Academic Press, New York, 1963, Ch. 7.

FIGURE TITLES

Figure 1. System structure. $\mathcal{W} = \{w\}$ is replaced by $\mathcal{P} = \{p\}$.

Figure 2. Aerodynamic coefficients $C_{ij}(\alpha)$.

Figure 3. Normalized bounds on acceptable $c^*(t)$. Representative simulation results.

Figure 4. Bounds on $|T(j\omega)|$. Bode plots of designed $|F(j\omega)|$, $|G(j\omega)|$.

Figure 5. Loci of typical Iti $P(j\omega)$. Cases e,f are open-loop unstable.

	k	ζ	ω_n	V_0	ρ	δ_{max}	α_{max}
(a)	1	1.0	3.77	180	.36	6.3	16.4
(b)	2	1.0	3.77	100	1.05	11.0	23.5
(c)	4	.45	5.66	120	1.05	18.6	29.3
(d)	4	.45	5.66	117	1.05	22.4	31.3
(e)	4	1.0	3.77	230	.36	13.8	27.0
(f)	3	.92	7.54	180	.36	27.4	34.2

Figures 6a-c. Templates $\mathcal{T}_{p(\omega)}$ of $\{P(j\omega)\}$ at $\omega = .04, 1.9, 12$.

Figure 7. Hand derivation of bounds on $L(j\omega)$ in Nichols chart.

Figure 8. Bounds $B(\omega)$ on $G(j\omega)$, and $G(j\omega)$ chosen.

Figure 9 a,b. Representative responses of $\alpha(t)$, $\dot{\theta}$, δ, c*.

Figure 10. Responses for input causing hard δ saturation.

Figure 11. Responses to gusts and simultaneous c* step command (a) half-sine gust, (b) random gaussian.

Figure 12. Responses to square wave c* command.

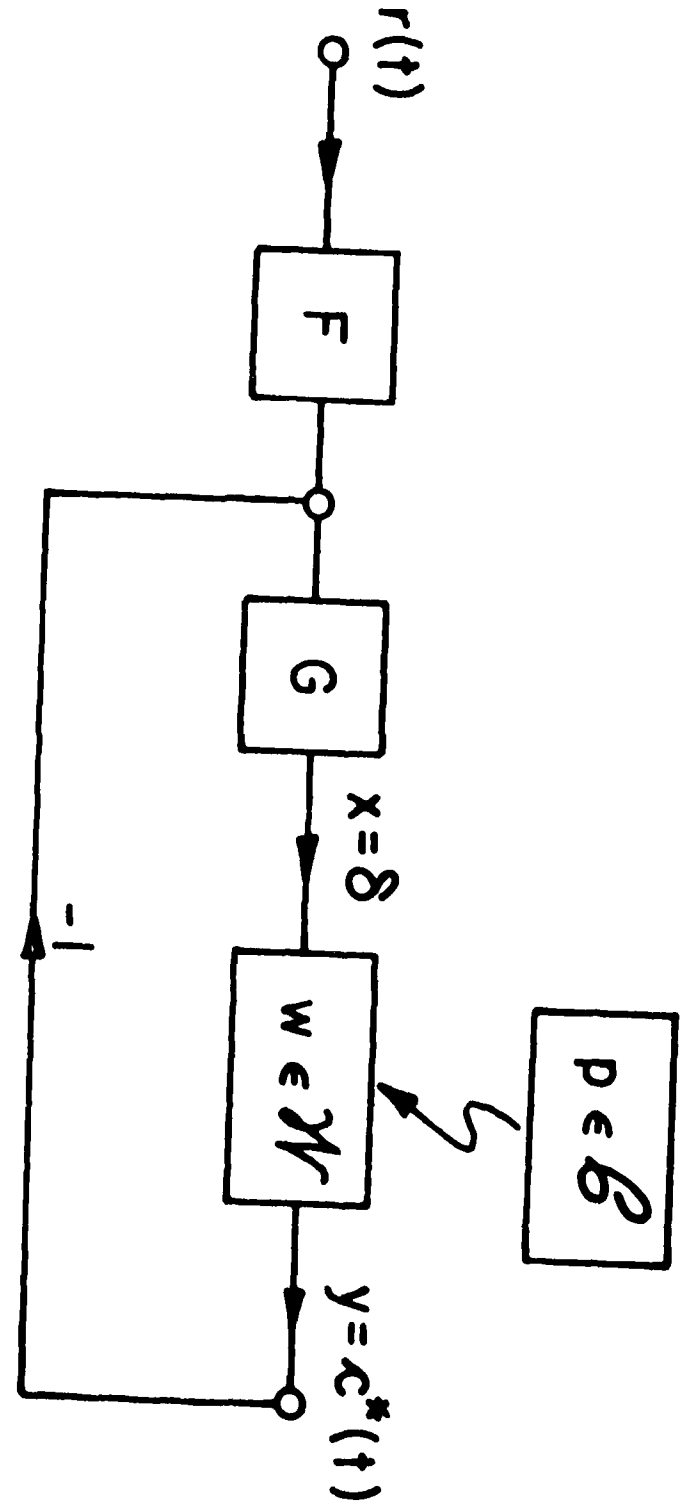

Fig. 1

Fig. 2

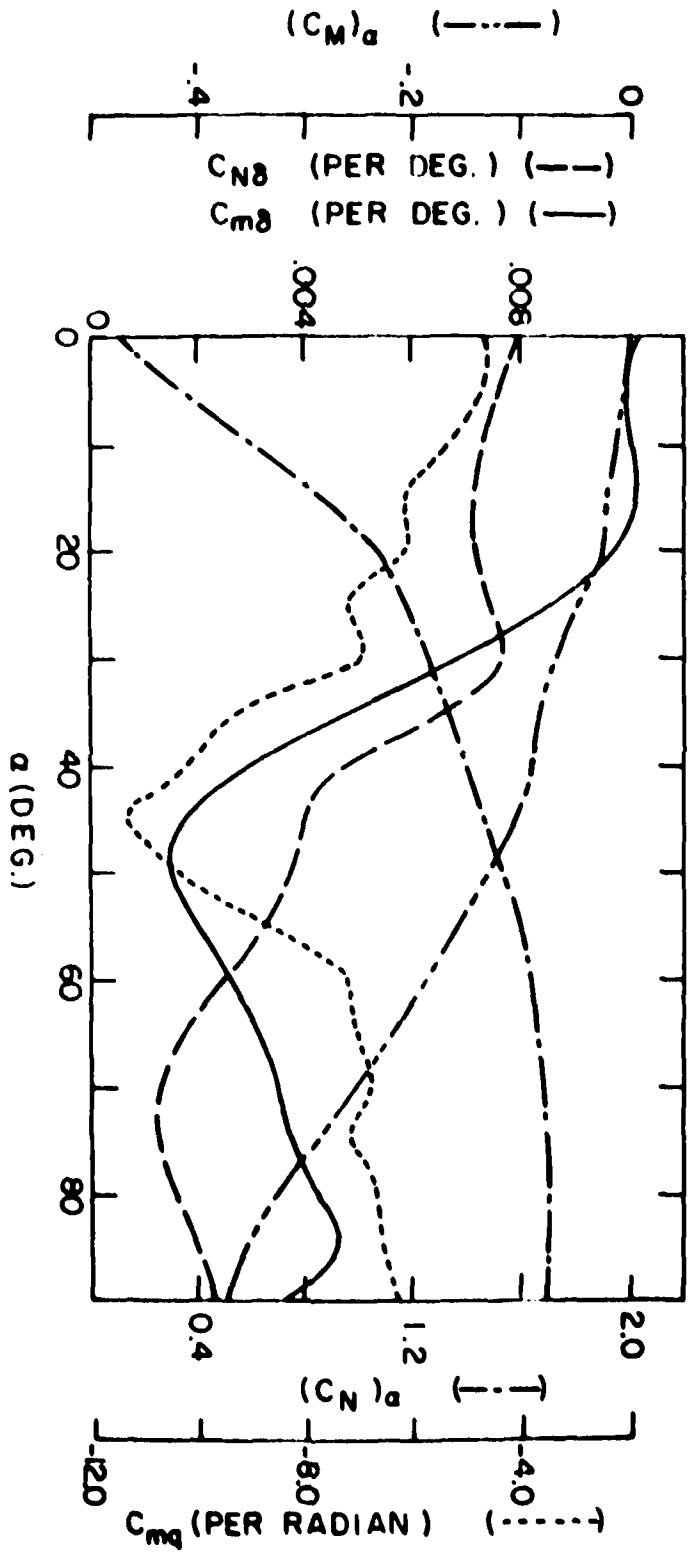
$(C_M)_\alpha$ (—·—)
-.4
-.2
0
$C_{N\delta}$ (PER DEG.) (——)
$C_{m\delta}$ (PER DEG.) (——)
.004
.006
0
0
20
40
60
80
α (DEG.)
0.4
1.2
2.0
$(C_N)_\alpha$ (——)
-12.0
-8.0
-4.0
C_{mq} (PER RADIAN) (-----)

Fig. 3

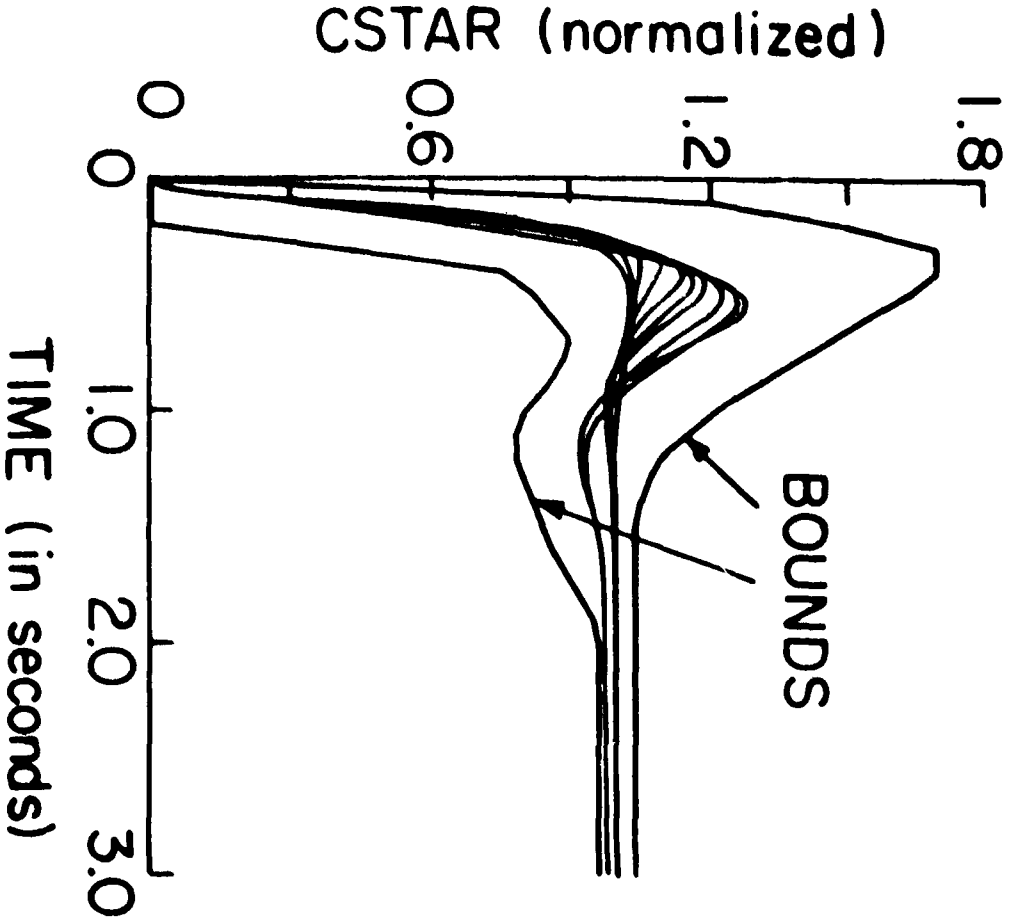

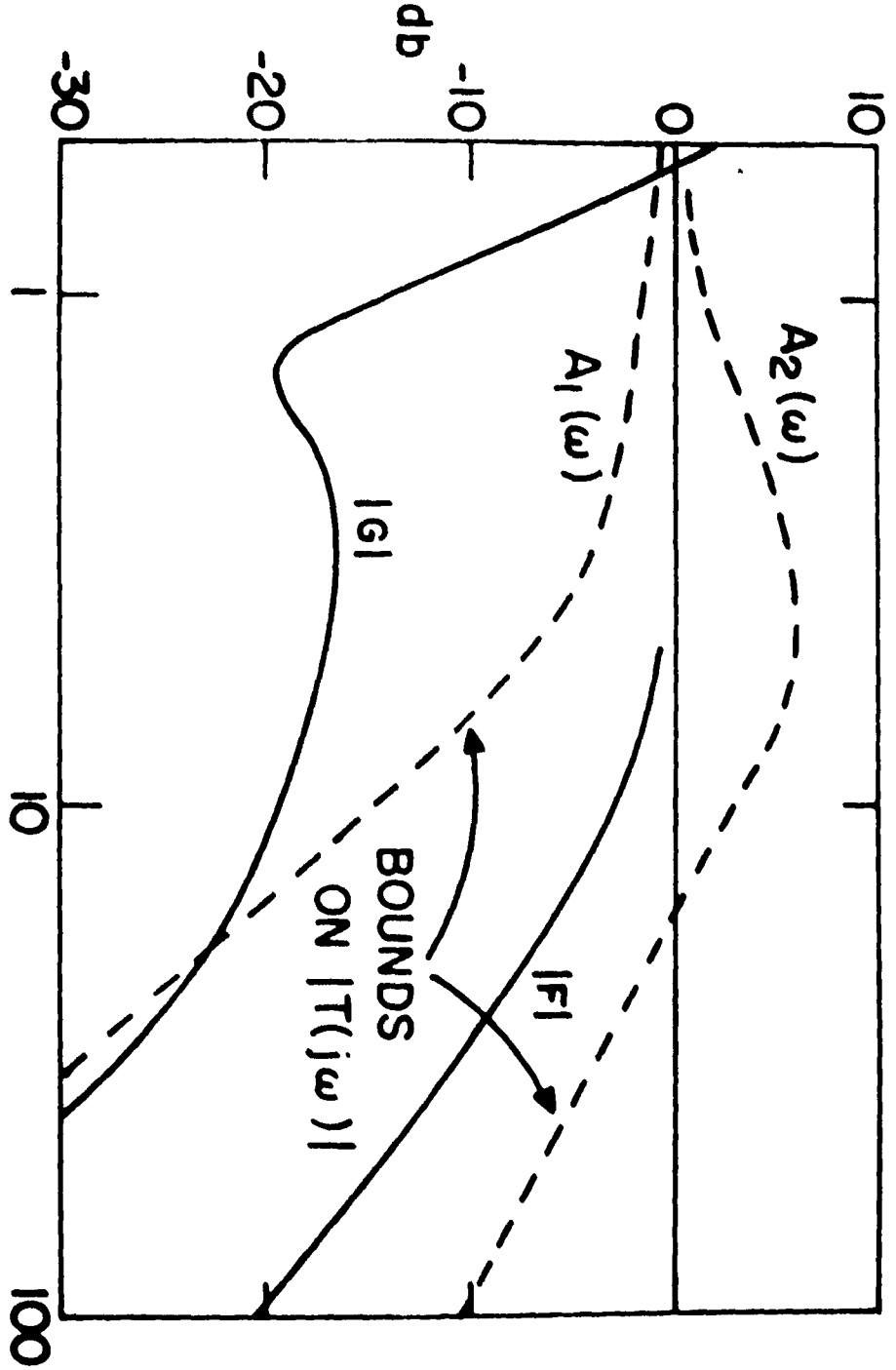

Fig. 4

Fig. 5

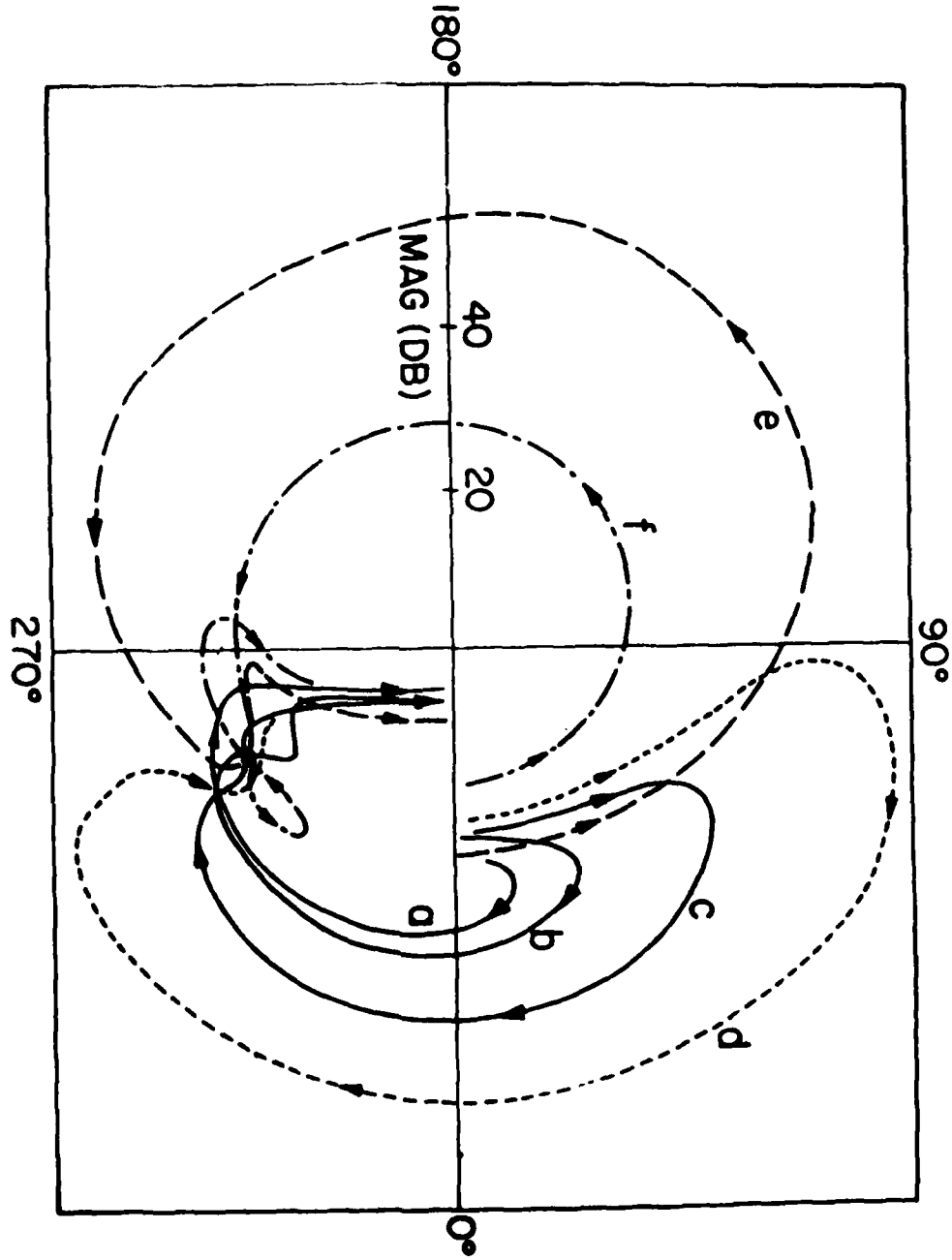

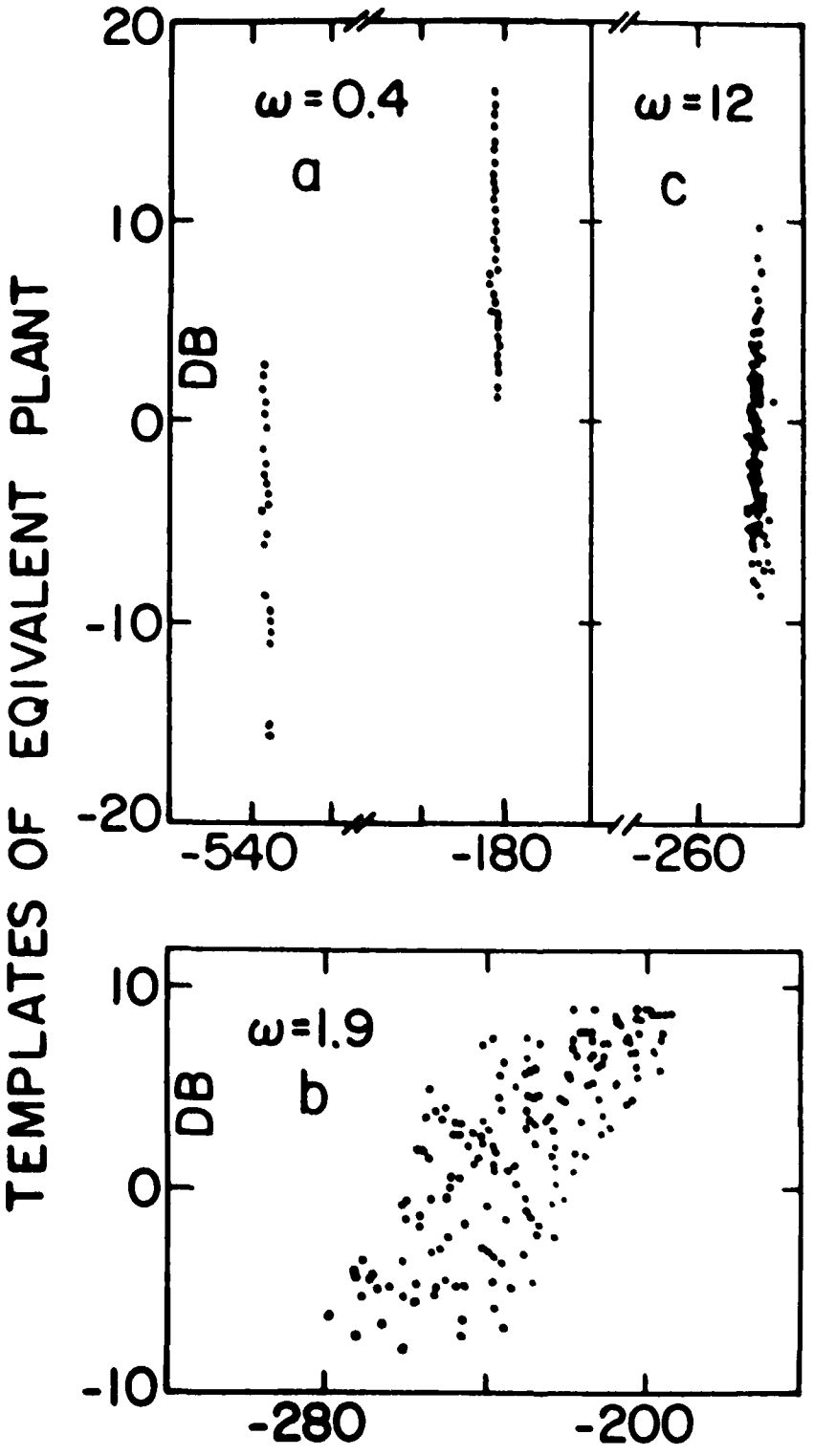
TEMPLATES OF EQIVALENT PLANT
20
10
0
-10
-20
DB
ω = 0.4
a
ω = 12
c
-540
-180
-260
10
0
-10
DB
ω = 1.9
b
-280
-200

6a-c

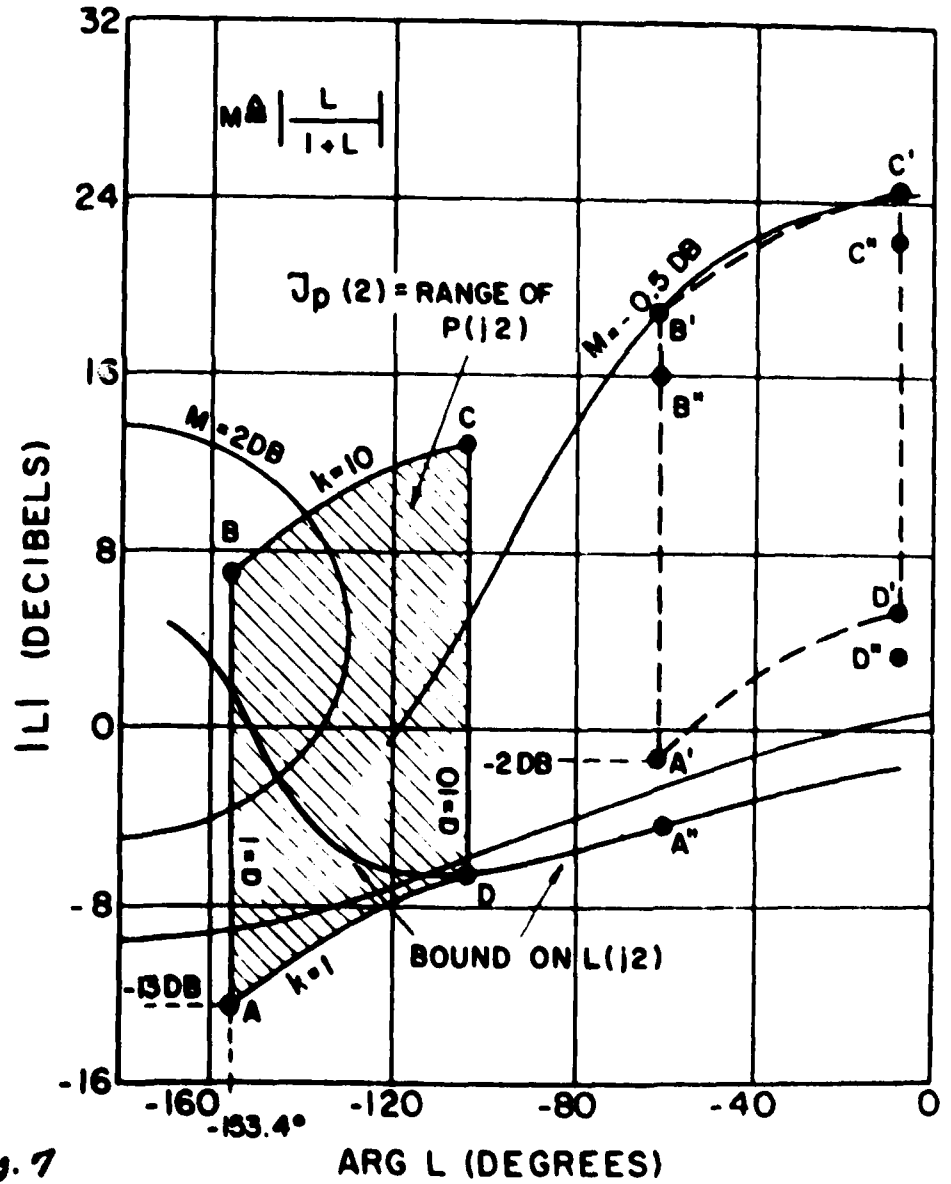
32
24
16
8
0
-8
-16
-160
-133.4°
-120
-80
-40
0
|L| (DECIBELS)
ARG L (DEGREES)
M = |L/(1+L)|
J_P (2) = RANGE OF P(|2)
M = 2 DB
k=10
k=1
k=0
k=-10
M = 0.5 DB
-2 DB
-13 DB
BOUND ON L(|2)
A
B
C
D
A'
B'
C'
D'
A"
B"
C"
D"

Fig. 1

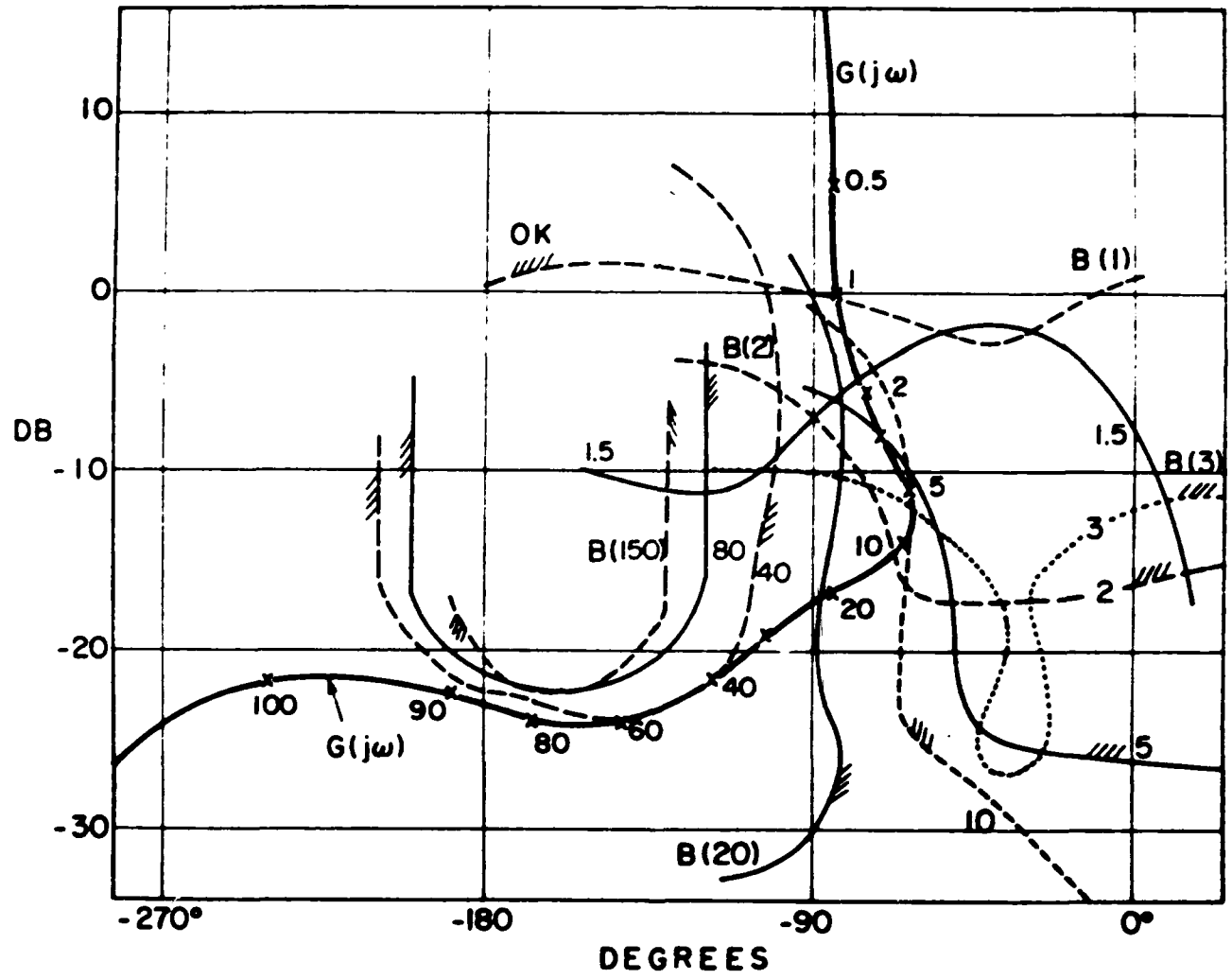
G(jω)
10
0.5
OK
0
1
B(1)
B(2)
2
DB
-10
1.5
1.5
B(3)
5
3
B(150)
80
40
10
2
20
-20
100
90
40
G(jω)
80
60
5
-30
10
B(20)
-270°
-180
-90
0°
DEGREES

Fig. 8

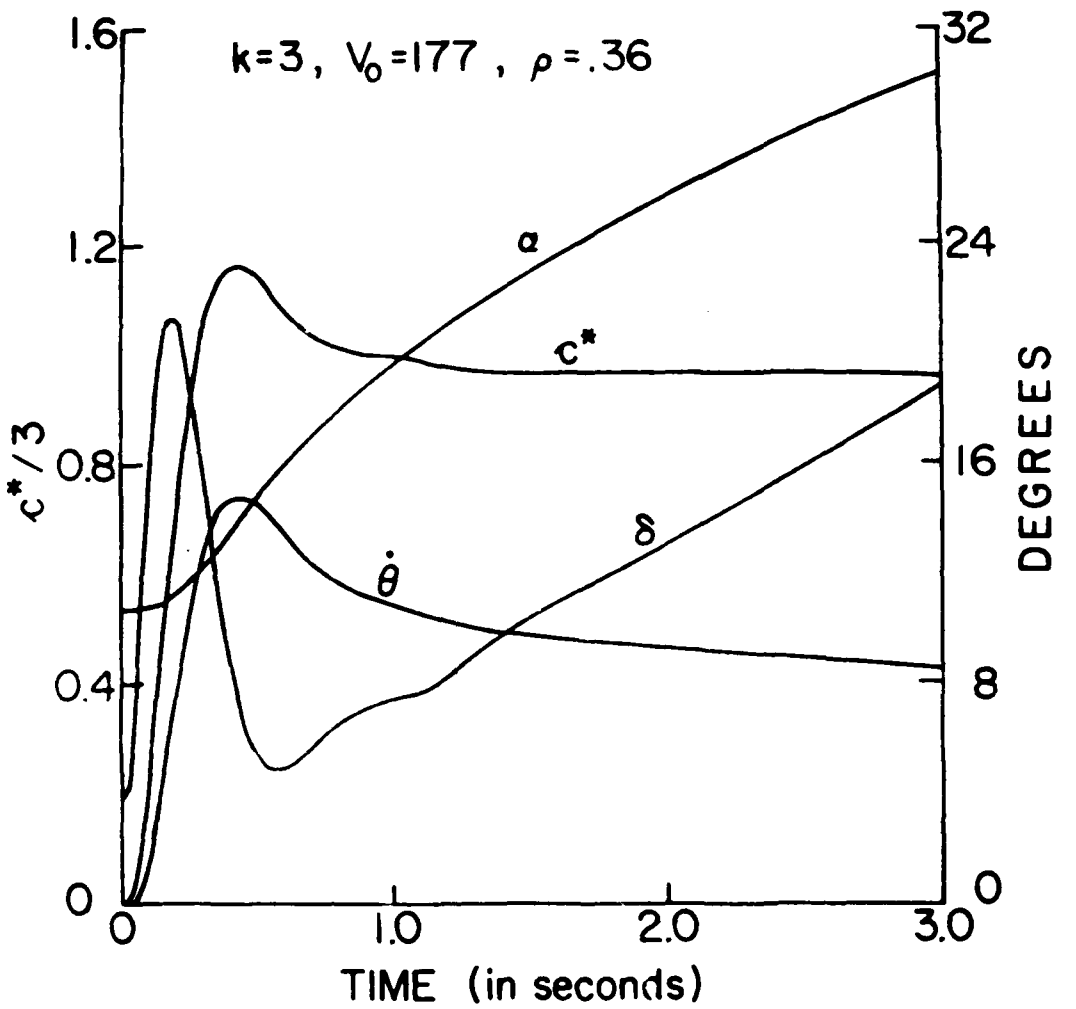
k=3, V_0=177, ρ=.36
1.6
1.2
0.8
0.4
0
$c^*/3$
32
24
16
8
0
DEGREES
α
c^*
δ
$\dot{\theta}$
0
1.0
2.0
3.0
TIME (in seconds)

Fig. 9a

Fig. 46

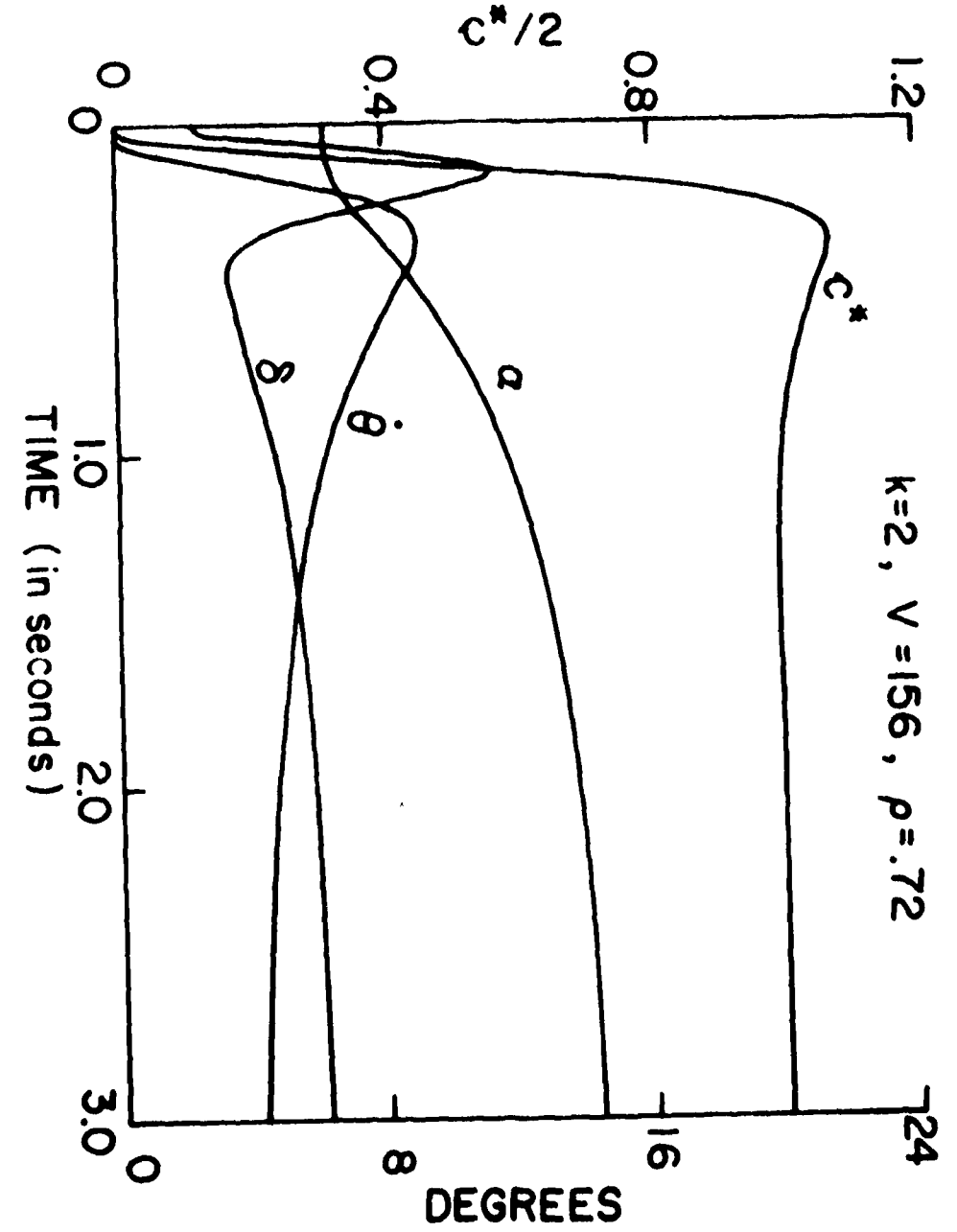
c*/2
0
0.4
0.8
1.2
0
c*
δ
α
θ̇
TIME (in seconds)
1.0
2.0
3.0
k=2, V=156, ρ=.72
0
8
16
24
DEGREES

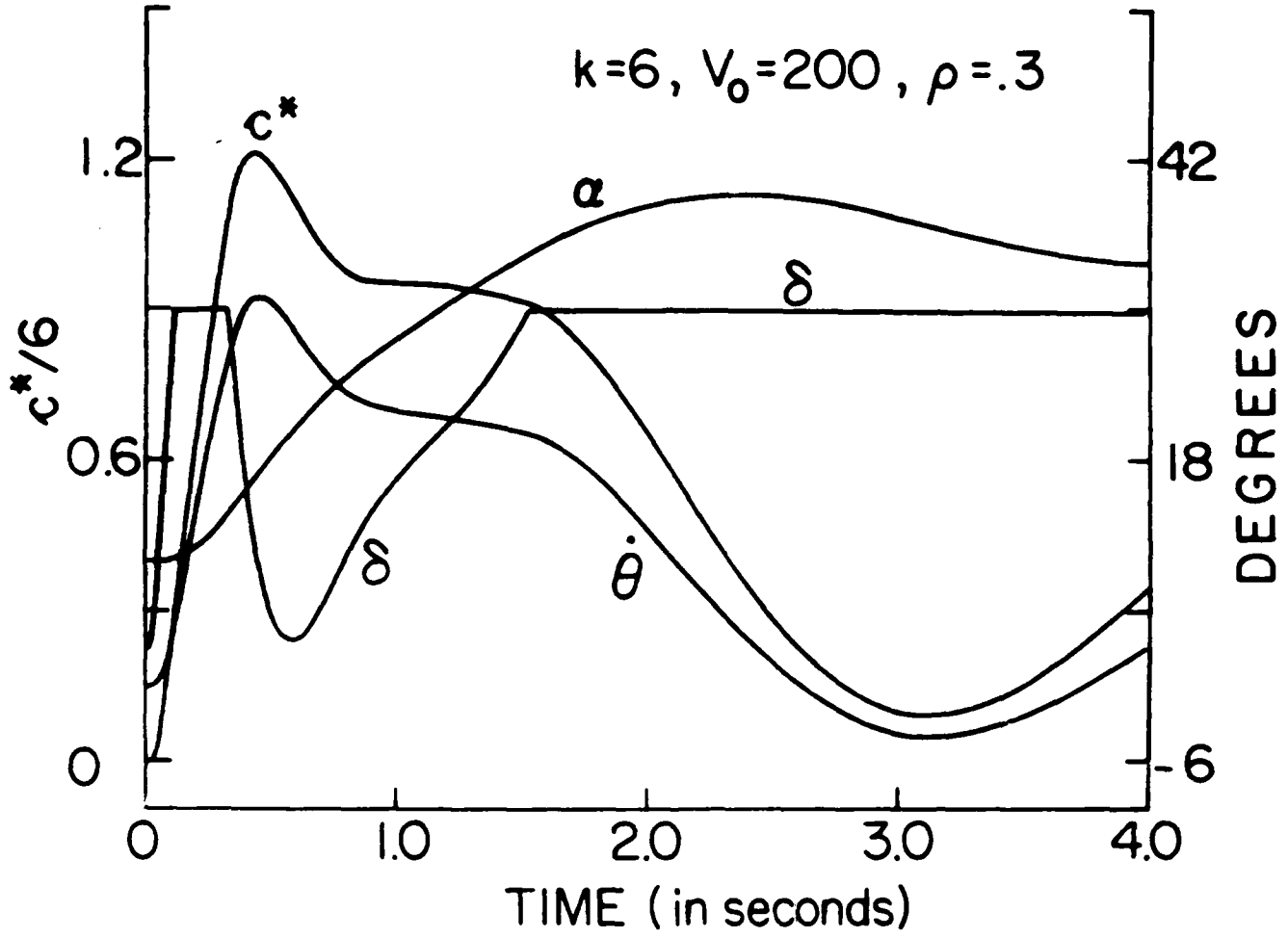
k=6, V_0=200, ρ=.3
c*
α
δ
δ
θ̇
1.2
0.6
0
c*/6
42
18
-6
DEGREES
0
1.0
2.0
3.0
4.0
TIME (in seconds)

Fig. 10

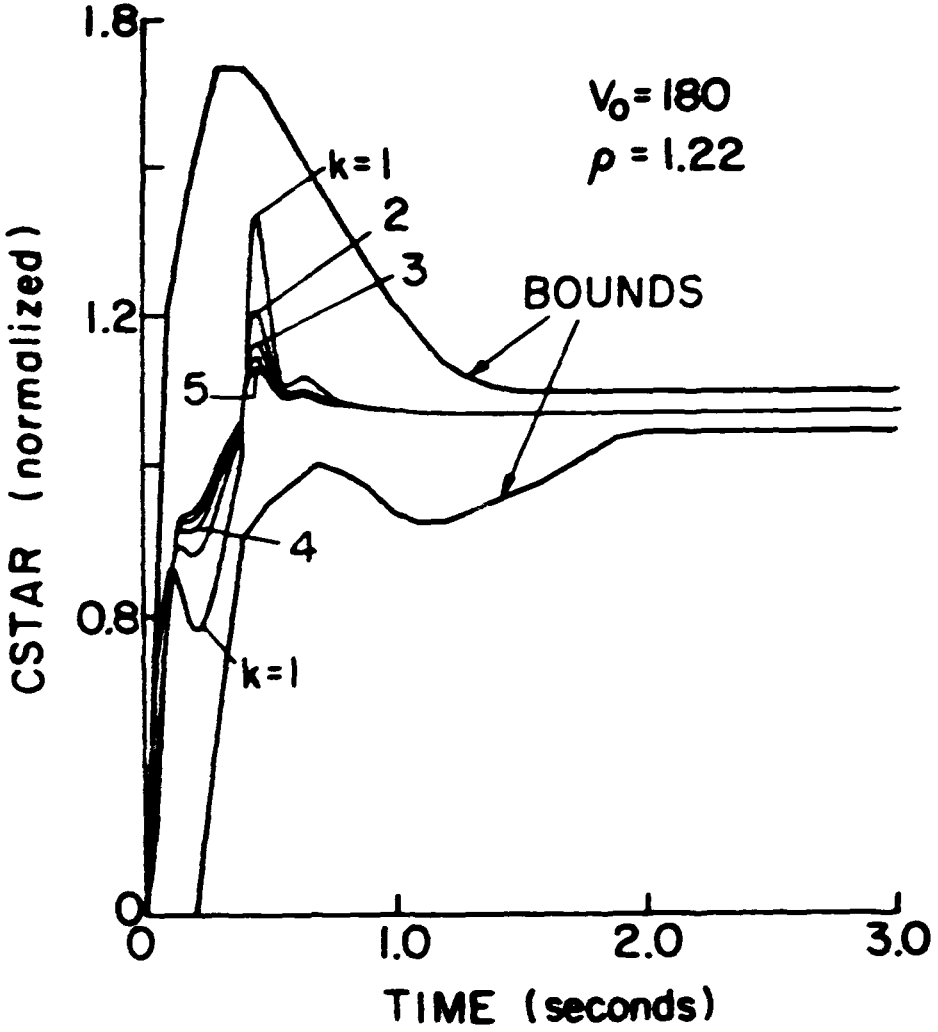
1.8
1.2
0.8
0
CSTAR (normalized)
V_0= 180
ρ = 1.22
k=1
2
3
BOUNDS
5
4
k=1
0
1.0
2.0
3.0
TIME (seconds)

Fig. 11a

Fig. 11b

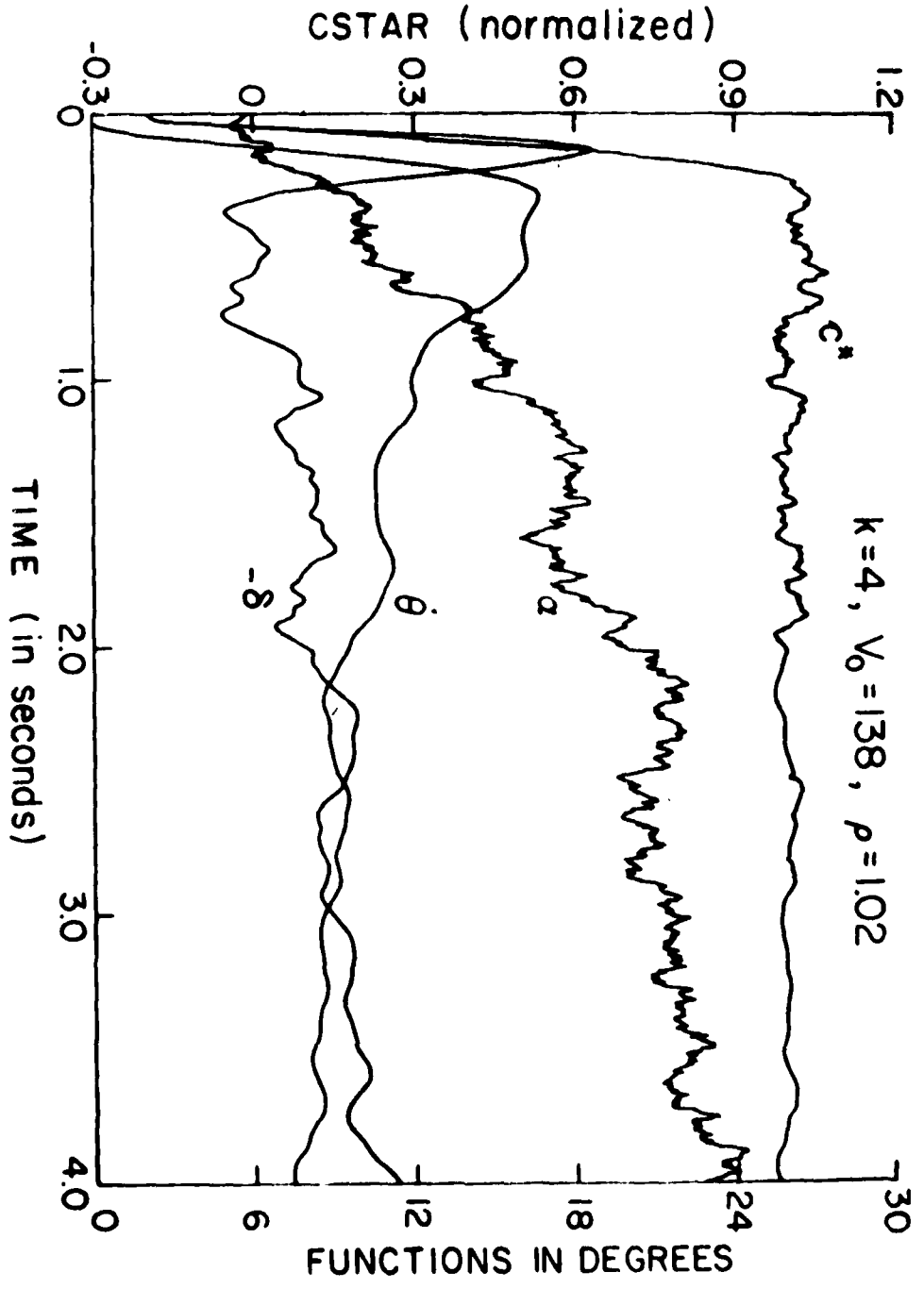
CSTAR (normalized)
-0.3
0
0.3
0.6
0.9
1.2
0
1.0
2.0
3.0
4.0
TIME (in seconds)
C*
α
θ
-δ
k=4, V0=138, ρ=1.02
0
6
12
18
24
30
FUNCTIONS IN DEGREES

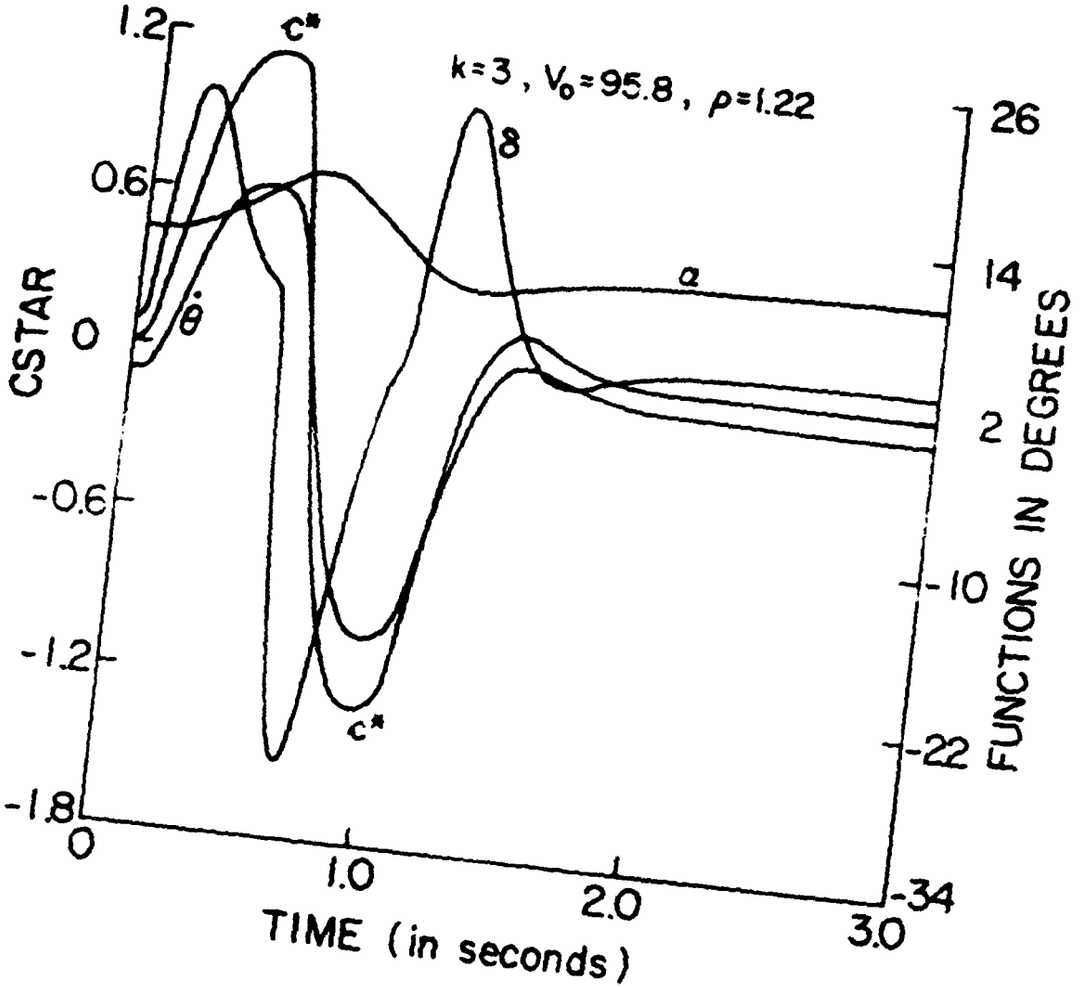
k=3 , V_0=95.8 , ρ=1.22
c*
δ
α
θ̇
c*
CSTAR
FUNCTIONS IN DEGREES
TIME (in seconds)
1.2
0.6
0
-0.6
-1.2
-1.8
26
14
2
-10
-22
-34
0
1.0
2.0
3.0

Fig. 12

APPENDIX 2

Derivation of the transfer function of a system, from an input-output pair

Let $x(t)$, $y(t)$ be the input and output of a system for $t \in [0,T]$. Find a transfer function $T(s) = Y(s)/X(s)$, where $Y(s) = Ly(t)$, etc. Actually, we seek a rational approximation of $T(s)$, $P(s)/Q(s)$, where P and Q are polynomials of degree m , n respectively. Let $P(s) = \sum_{k=0}^{m} p_k s^k$, $Q(s) = \sum_{k=0}^{n} q_k s^k$, $q_n = 1$,

$$\frac{Y(s)}{X(s)} - \frac{P(s)}{Q(s)} = \frac{Q(s)Y(s) - P(s)X(s)}{X(s)Q(s)} = \frac{\frac{Q(s)}{s^n}Y(s) - \frac{P(s)}{s^n}X(s)}{\frac{Q(s)X(s)}{s^n}} \quad . (1)$$

If $\frac{Y(s)}{X(s)}$ is a rational function then $\frac{Q(s)}{s^n}y(s) - \frac{P(s)}{s^n}x(s) = 0$ is an exact representation. We seek the coefficients p_k , q_k which minimize

$$J = \int_{-\infty}^{\infty} \left| \frac{Q(j\omega)Y(j\omega)}{(j\omega)^n} - \frac{P(j\omega)X(j\omega)}{(j\omega)^n} \right|^2 d\omega$$

$$= \int_{-\infty}^{\infty} \left| \sum_{k=0}^{n} \frac{q_k Y(j\omega)}{(j\omega)^{n-k}} - \sum_{k=0}^{m} \frac{p_k X(j\omega)}{(j\omega)^{n-k}} \right|^2 d\omega \quad . \qquad (2)$$

Parseval's formula gives $J = \int_{-\infty}^{\infty} |f(t)|^2 dt$, where

$$f(t) = \sum_{k=0}^{n} q_k y^{-(n-k)}(t) - \sum_{k=0}^{m} p_k x^{-(n-k)}(t) \quad , \qquad (3)$$

$y^{(-i)}(t)$, the i-times integral of $y(t)$, $\int_0^t \cdots \int_0^t y(t)dt^i$,

$J = \int_{-\infty}^{0} |f(t)|^2 dt + \int_0^T |f(t)|^2 dt + \int_T^{\infty} |f(t)|^2 dt$; $\int_{-\infty}^{0} |f(t)|^2 dt = 0$,

since $y(t) = 0$, $x(t) = 0$ for $t < 0$; $\int_T^{\infty} |f(t)|^2 dt = 0$, since $x(t)$, $y(t)$ for $t \geq T$ can be defined correspondingly for any p_k , q_k . Therefore

$$J = \int_0^T |f(t)|^2 \, dt \tag{4}$$

and the minimization of J determines p_k , q_k uniquely.

Let $x(t)$, $y(t)$ be given at the points $t = 0,h,2h,\ldots lh = T$. We construct the integral $y^{(-1)}(t)$ by the following formulae:

$$y^{(-1)}(0) = 0 \quad , \quad y^{(-1)}(ih) = y^{(-1)}(h(i-1)) + \frac{h}{2}\,[y(ih) + y(i-1)h)]$$

The multiple integrals $y^{(-k)}(t)$, $1 \leq k \leq n$ and $x^{(-u)}(t)$, $n-m \leq u \leq n$ are computed in the same manner. We replace the integral (4) by the corresponding sum:

$$J = h \sum_{i=0}^{\ell} \left[\sum_{k=0}^{n} q_k y^{(n-k)}(ih) - \sum_{k=0}^{m} p_k x^{(n-k)}(ih) \right]^2 \quad , \quad q_n = 1$$

and determine the coefficients p_k , q_k as coefficients of linear regression (by the least square method).

Remarks

(1) The degrees of the polynomials $P(s)$ and $Q(s)$ should be chosen from the apriori information about the system. If apriori information is lacking, different degree choices of P , Q may be tried and the best selected. Another kind of apriori information which could be used in this method is, for example, asymptotic behavior of the functions. The difference in degree of P , Q can be judged by the difference in smoothness, at $t = 0$, of $x(t)$ and $y(t)$, because of the initial value theorem in Laplace transforms.

(2) If the function $P(s)/Q(s)$ is stable, then the approximation can be checked by computation of $\tilde{y}(t) = \frac{P(s)}{Q(s)}\,[x(t)]$ and comparison of $\tilde{y}(t)$ with $y(t)$.

REFERENCES

1. I. Horowitz, A synthesis theory for linear time-varying feedback systems with plant uncertainty, IEEE Trans. AC-20, pp. 454-464, Aug. 1975.

2. I. Horowitz, Synthesis of feedback systems with nonlinear time-varying uncertain plants to satisfy quantitative performance specifications, Proc. IEEE, 64, Jan. 1976, pp. 123-130.

3. I. Horowitz and M. Sidi, Optimum synthesis of nonminimum-phase feedback systems with plant uncertainty, Int. J. Control, 27, 1978, pp. 361-386.

4. H.W. Bode, Network Analysis and Feedback Amplifier Design, Van Nostrand, N.Y., 1945.

5. B.C. Wang and I. Horowitz, Synthesis of Multiple-Loop Feedback Systems with Plant Modification, 1978. Dept. of Electrical Engineering, University of Colorado, Boulder, Co. 80309.